Synthesis of Novel CYP1 Activated Heterocyclic Anticancer Prodrugs

Avninder Singh Bhambra

Submitted in fulfilment of the requirements for the degree of Doctor of Philosophy

De Montfort University

April 2011

Acknowledgements

I would like to thank Kenneth J. M. Beresford for his supervision in the completion of this thesis and Gerry A. Potter for giving me the opportunity of working within the Cancer Drug Discovery Group, De Montfort University. Many thanks to my colleagues Ketan Ruparelia and Dyan Ankrett for their valuable input created towards this thesis. I am grateful to Mike Needham for his expertise in NMR spectroscopy, Graham Lawson, Geoff Hall and Martin Elliott for their support and guidance. I would like to express my sincere appreciation to the staff (past and present) of the Chemistry Stores for providing equipment and chemicals when required.

Finally, I would like to thank my family and friends for their encouragement and appreciation of my studies.

Abstract

The cytochrome P450 superfamily of enzymes are critical in the metabolism of endogenous and exogenous substrates. CYP1A1 and CYP1B1 have been found to be over-expressed in tumour cells whilst undetected or present in very low levels in corresponding normal tissue. This presented a novel target for the development of anti-cancer prodrugs, which would remain non-toxic until undergoing metabolism to toxic species by CYP1 enzymes over-expressed at tumour sites. The chalcones have been shown to exhibit effective anti-cancer prodrug activity, but are labile to photoisomerisation reactions converting the potent *trans* isomer to the less toxic *cis* isomer. Several heterocyclic ring systems were incorporated across the α,β-unsaturated moiety of the chalcones to produce rigid structures, eliminating the possibility of photoisomerisation occurring whilst maintaining the substituted phenyl groups in a *trans* like geometry. Lead compounds were identified using an *in vitro* MTT screening assay against a panel of tumour cell lines characterised for their constitutive or inducible CYP1 expression. These were the MDA 468, MCF7 and MDA 231 cell lines. The non-tumour MCF10A cell line which has no basal CYP1 expression was used as the control.

A library of eighteen 3,5-diarylpyrazoles were synthesised. The lead pyrazole DMU 10107 (3-(2,3,4-trimethoxyphenyl)-5-(3,4-methylenedioxyphenyl)pyrazole) gave an IC_{50} value of 8μM towards the MDA 468 cell line. The MCF7 cells, TCDD induced and non-induced gave IC_{50} values of 10μM each. Although the pyrazoles showed plausible tumour toxicity, an investigation into six membered pyrimidine heterocycles was undertaken in an attempt to obtain enhanced cytotoxicities than those observed from the five membered pyrazoles. Therefore, a library of fifteen 2-amino-4,6-diarylpyrimidines was synthesised. The lead amino-pyrimidine DMU 10212 (2-amino-4-(2,4-dimethoxyphenyl)-6-(3,4-methylenedioxyphenyl)pyrimidine) showed significant cytotoxicity towards the MDA 468 cell line with an IC_{50} value of 0.01μM. Notable IC_{50} values of 0.3μM and 0.07μM were also observed towards the MCF7 and MCF7 cells induced with TCDD. The important toxicity seen from the 2-amino-4,6-diarylpyrimidines prompted the investigation of the 2-position of the pyrimidine ring, and to assess the tumour toxicities of the synthesised compounds.

The 2-amino-4,6-diarylpyrimidines were converted to produce 4,6-diarylpyrimidones by a one-step conversion reaction using sodium nitrate. The pyrimidone DMU 10313 (4-(2-methoxyphenyl)-6-(3,4-methylenedioxyphenyl)pyrimidin-2-one) showed high toxicity with an IC_{50} value of 0.07μM towards the MDA 468 cells and IC_{50} values of 1.8μM and 0.5μM

towards the MCF7 and MCF7 cells induced with TCDD. A library of nine 2-morpholino-4,6-diarylpyrimidines was synthesised. The lead compound DMU 10405 (4-(2,4-dimethoxyphenyl)-6-(4-methoxyphenyl)-2-morpholinopyrimidine) gave an IC_{50} value of 10μM towards the MDA 468 cells. DMU 10600 (4-(2,4-dimethoxyphenyl)-6-(3,4-methylenedioxyphenyl)-2-dimethylethylenediaminopyrimidine), showed an IC_{50} value of 7μM towards the MDA 468 cells and an identical IC_{50} value of 10μM towards the MCF7 and MCF7 cells treated with TCDD. DMU 10700 (2-methyl-4-(2,4-dimethoxyphenyl)-6-(3,4-methylenedioxyphenyl)pyrimidine), a substituted pyrimidine based on the phenyl substitutions of DMU 10212 gave an IC_{50} value of 2.5μM towards the MDA 468 cells. DMU 10800 (4-(2,4-dimethoxyphenyl)-6-(3,4-methylenedioxyphenyl)pyrimidine), also based on the phenyl substitutions of DMU 10212 showed an IC_{50} value of 0.08μM towards the MDA 468 cells and equal IC_{50} values of 0.2μM against the MCF7 and MCF7 cells induced with TCDD. All lead compounds did not show toxicity towards the non-tumour MCF10A cell line.

DMU 10212 was selected as the overall lead compound due to the significant tumour toxicities recorded, and for the non-toxicity observed towards the MCF10A cells. Inhibition studies using the known CYP1 inhibitor α-naphthoflavone (α-NF) were conducted to show that DMU 10212 was a substrate of the CYP1 enzymes. The resulting data showed that the cytotoxicity of DMU 10212 was completely eliminated suggesting CYP1 enzymes play an activating role in the cytotoxic effect of DMU 10212. LCMS metabolism studies using isolated CYP1 isoforms were performed showing that DMU 10212 is metabolised to produce four metabolites (M1, M2, M3 and M4), determined from their individual retention times and molecular masses. The metabolites of DMU 10212 were also found to be generated at a greater rate with CYP1A1 than CYP1B1. Metabolite structures were proposed as CYP1 enzyme reactions are known. The metabolite M2 was synthesised and was identified to be an authentic metabolite of DMU 10212 via LCMS and co-elution studies. Screening of M2 against the tumour cells gave an IC_{50} value of 0.6μM towards the MDA 468 cells, and IC_{50} values of 0.6μM and 1μM against the MCF7 and MCF7 cells induced with TCDD. In conclusion, DMU 10212, a novel CYP1 activated anticancer prodrug with selective high toxicity towards tumour cells has been identified.

Contents

List of Figures

List of Tables

List of Schemes

Abbreviations

^{1}H NMR	Nuclear Magnetic Resonance
4-OHCPA	4-Hydroxycyclophosphamide
ADEPT	Antibody Directed Enzyme Prodrug Therapy
APH	Aldophosphamide
AQ4	1, 4-bis{[2-(dimethylamino)ethyl]amino}-5,8-dihydroxyanthracene-9,10-dione
AQ4N	1, 4-Bis-{[2-(dimethylamino-N-oxide)ethyl]amino}-5,8-dihydroxyanthracene-9,10-dione
ATP	Adenosine Triphosphate
BP	Benzo[*a*]pyrene
BPDE	(+)-*anti*-benzo[*a*]pyrene diol epoxide
CA4	Combretastatin A4
CDKs	Cyclin-Dependent Kinases
CML	Chronic Myelogenous Leukemia
CPA	Cyclophosphamide
CPG2	carboxypeptidase G2
CPR	Cytochrome P450 reductase
CSC	Claisen-Schmidt condensation
CYP	Cytochrome P450
DCM	Dichloromethane
DF 203	2-(4-amino-3-phenyl)benzothiazole
DHFR	Dihydrofolate Reductase
DMF	Dimethylformamide

DMSO	Dimethylsulfoxide
DNA	Deoxyribonucleic Acid
DNP	2,4-dinitrophenylhydrazine
DOX	Doxorubicin
ER	Estrogen Receptor
ER-	Oestrogen-Receptive Negative
ER+	Oestrogen-Receptive Positive
ERE	Estrogen Response Elements
EROD	Ethoxyresorufin-*O*-deethylase
FGFR	Fibroblast Growth Factor Receptor
GDEPT	Gene Directed Enzyme Therapy
HER-2	Human Epidermal Growth Factor Receptor 2
IBA	Infectious Biological Agent
IC_{50}	Concentration Causing 50% Growth Inhibition
IR	Infra-Red
LCMS	Liquid Chromatography Mass Spectrometry
MBr	4-morpholinylformamidine hydrobromide
MDSA	Microtubule Destabilising Agent
MOPP	Mechlorethamine, Oncovin, Procarbazine and Prednisone
mRNA	Messenger Ribonucleic Acid
MS	Mass spectrometry
MSA	Microtubule Stabilising Agent

MTT	3-[4,5-dimethylthiazol-2yl]-2,5-diphenyltetrazolium
NADPH	B-Nicotinamide Adenine Dinucleotide Phosphate Reduced
NTR	Nitroreductase
PAH	Polycyclic Aromatic Hydrocarbon
PDGFR	Platelet Derived Growth Factor Receptor
Rb	Retinoblastoma
RNA	Ribonucleic Acid
RT	Retention Time
SAM	S-adenosylmethionine
TCDD	2,3,7,8-tetrachlorodibenzodioxin
TGF-β_1	Transforming Growth Factor-β-$_1$
THF	Tetrahydrofuran
THFA	Tetrahydrofolate
THP	Tetrahydropyranyl
TIC	Total Ion Chromatogram
TK	Tyrosine Kinase
TLC	Thin Layer Chromatography
TMS	Tetramethylsilane
TSG	Tumour Suppressor Gene
UV	Ultra-Violet
VEGF	Vascular Endothelial Growth Factor
VEGFR	Vascular Endothelial Growth Factor Receptor

WHO	World Health Organisation
XRE	xenobiotic response element
α-NF	α-naphthoflavone

Chapter 1

Introduction

1.0 Cancer

Cancer is used to define the uncontrolled multiplication and spread of abnormal cells within the body.[1] Hallmark characteristics of cancer cells include uncontrolled proliferation, insensitivity to negative and positive growth regulation, evasion of apoptosis, invasiveness, metastasis and loss of normal function.[2]

A statistical report published by Cancer Research UK showed that 408,381 new cancer incidences and 156,723 cancer deaths occurred in the United Kingdom for the year 2008.[3] Breast cancer had the highest new incidence rate with 48,034 cases recorded, whilst the highest number of deaths were caused by lung cancer with 35,261 documented reports (Figure 1).

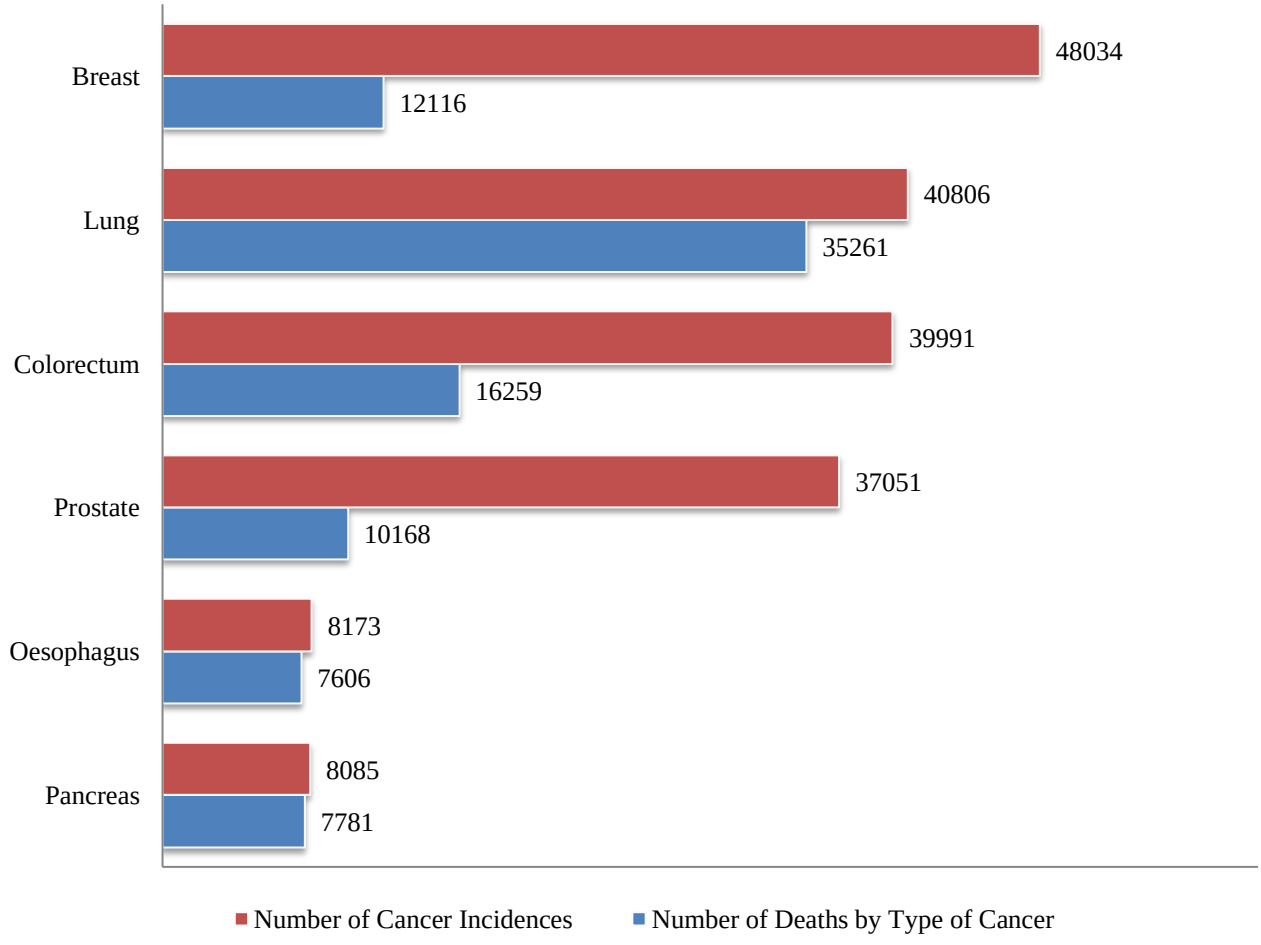

Figure 1. Types of cancer and their death rates reported in 2008

1.1 Cancer on a Cellular Level

1.1.1 The Cell Cycle

Normal cell proliferation can be illustrated by the cell cycle (Figure 2).1 Progression through the cell cycle is dependent on the balance of signalling pathways between positive growth factors and negative regulatory proteins. These are involved in the various phases of the cell cycle which are the G_0, G_1, S (DNA synthesis), G_2 and M (mitosis) phases. Vital checkpoints at the G_1/S and G_2/M transition stages also exist to regulate normal cell proliferation.

Figure 2. The cell cycle

Proto-oncogenes are responsible for positive growth factors such as cyclins and cyclin-dependent kinases (CDKs), which stimulate the cell to enter the cell cycle and the progression through it. Cyclins bind to the CDKs forming complexes which control and regulate important enzymatic functions of the cell. The cycle starts with the G_1 phase in which the cell synthesises components necessary for DNA replication. This is regulated by cyclins D1, D2 and D3 associating with CDKs 4 and 6.[4] In the later stages of G_1, cyclins A and E are expressed which form complexes with CDK2 promoting the cell through the G_1/S phase transition and the S phase itself.[5, 6] The G_2/M transition occurs with cyclins A1, A2, B1 and B2 associating with CDK1. This also takes the cells through the M phase, a complex

procedure divided into five stages consisting of the prophase, prometaphase, metaphase, anaphase and the telophase.[7] This is followed by cytokinesis, and the complete progression of the cell through these stages results in the formation of a new daughter cell. The G_0 phase is a resting period for cells. They exist in a quiescent state outside the cell cycle where they do not proliferate.[8]

However, opposing the positive growth factors are cell cycle inhibitory proteins called CDK inhibitors. These act as 'superbrakes' by binding with CDKs alone or regulate CDK activity by binding with CDK-cyclin complexes. Two important CDK inhibitors have been established, the INK4 and Cip/Kip families. The INK4 family includes p15 (INK4b), p16 (INK4a), p18 (INK4c) and p19 (INK4d). These specifically inactivate the G_1 phase of the cell cycle by binding to CDK 4 and 6 preventing their association with cyclin D. The Cip/Kip family of inhibitors includes p21 (Waf1, Cip1), p27 (Cip2) and p57 (Kip2). These function by binding to CDK-cyclin complexes, inactivating their function. CDK inhibitors are regulated by tumour suppressor genes (TSG) including the p53 and retinoblastoma (Rb) proteins. For instance, if damaged cells are detected at the G_2/M transition checkpoint the p21 and p27 CDK inhibitors are expressed. These prevent the CDK1-cyclin B1 complex forming and prevent damaged cells from entering the M phase. This also allows damaged cells to be repaired if possible.[9] If sufficient repairs to damaged DNA cannot be made the cell undergoes apoptosis, a cell-intrinsic programmed suicide mechanism that results in the controlled breakdown of the cell into apoptotic bodies. These bodies are recognised and engulfed by surrounding cells and subject to phagocytosis.[10] Two main protein families are involved in apoptosis, the Bcl-2 family of proteins which control mitochondrial integrity, and the cysteinyl aspartate specific proteases, or caspases, which mediate the execution phase of apoptosis. Morphological characteristics of a cell undergoing apoptosis include cell shrinkage, chromatid condensation and membrane blebbing (bulging).[11]

1.1.2 Carcinogenesis

Carcinogenesis is the term used to define the transformation of a normal cell into a cancer cell. Carcinogenesis proceeds in three stages which are determined and defined by their morphological and molecular characteristics (Figure 3).[12]

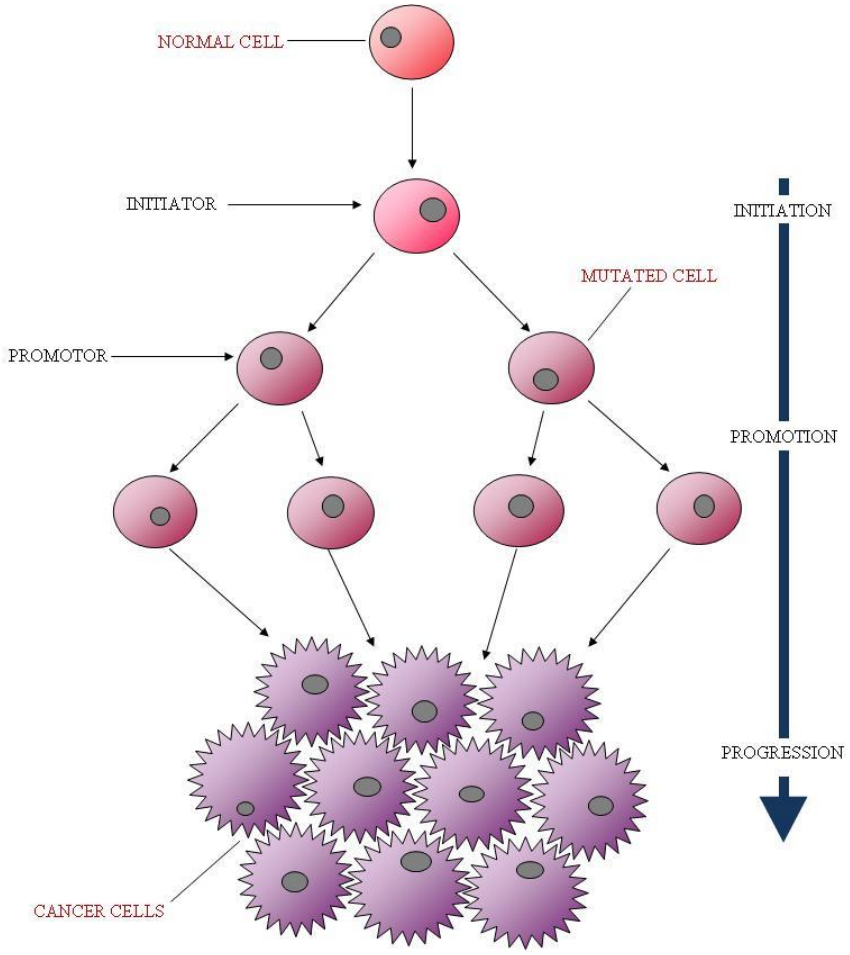

Figure 3. The three stages of carcinogenesis, initiation, promotion and progression

Initiation is the first stage of carcinogenesis and is characterised by permanent damage to DNA caused by a carcinogen. The formation of DNA-carcinogen adducts leads to mutations such as small deletions, transitions and transversions in the genome. The second stage is promotion, which involves the clonal replication of initiated cells in the presence of a promoting agent which can be either endogenous or exogenous. Promoting agents are generally non-mutagenic and are characterised by their ability to decrease the latency period of tumour formation once a cell has been exposed to an initiator. Progression is the final stage of carcinogenesis, established by an irreversible transition from the promotion stage. The tumour cells are formed and are characterised by the increasing aggressiveness and invasiveness of the cells.

The invasiveness of cancer cells occurs with the aid of angiogenesis.[13] This is the formation of new blood vessels, which provide the tumour with vital nutrients required for growth and replication. Angiogenesis is achieved by the stimulation of vascular endothelial cells through

the release of angiogenic peptides including the potent vascular endothelial growth factor (VEGF). Cancer cells also secrete proteases, such as matrix metalloproteinases (MMPs), which degrade basement membranes and surrounding stroma exposing vital nutrients and blood vessel access, thus allowing further growth and sustainability for the tumour. Following the invasion of surrounding tissue tumours may metastasise. This is when cancerous cells break away from the original tumour. These enter the blood stream and lymphatic system and can travel to distant sites in the body resulting in the formation of secondary tumours. On the contrary, tumours may remain in a benign state in which they do not metastasise.

1.2 Genetic Causes of Cancer

1.2.1 Inactivation of Tumour Suppressor Genes (TSGs)

TSGs are a critical part of the human body's natural defences in the prevention of cancer development. TSGs are regulated and activated in response to a wide variety of biological stresses such as DNA damage, oncogene activation, ultraviolet radiation, hypoxia, nutrient deprivation, nucleotide imbalances and heat shock.[14, 15]

The retinoblastoma (Rb) gene was the first tumour suppressor gene identified and is mutated in approximately 30% of all human cancers.[16, 17] During the early stages of the G_1 phase the Rb protein exists in an inhibiting hypo-phosphorylated state binding with E2F transcription factors such as E2F1, E2F2 and E2F3. The Rb-E2F complexes encode for products fundamental for the cell to enter the S phase.[18, 19, 20] When the cell is ready to enter the S phase, CDKs hyper-phosphorylate the Rb protein causing the Rb-E2F complexes to disassociate. Free E2Fs subsequently activate the transcription of genes necessary for DNA synthesis. The Rb protein remains in a hyper-phosphorylated state throughout both the S and M phases.[21] However, disruption of the Rb protein function is commonly linked with cancer originating from the over-expression of cyclin D1. This activates mutations in CDK-4 and the tumour suppressor p16Ink4a which becomes inactive in its role to prevent the association of CDKs and cyclins required for dephosphorylating Rb. This in turn prevents the Rb protein leaving the hyper-phosphorylated state allowing cells to replicate uncontrollably with the aid of free E2Fs.

The important p53 TSG has been found to be mutated in approximately 50% of cancers studied.[22] Normally, the p53 TSG responds to cell stress signals which are transduced into

transcribing genes such as the CDK inhibitor protein 21WAF1. This protein plays a part in controlling the G_1/S and G_2/M transition checkpoints, initiating growth arrest preventing damaged cells progressing further.[16, 23] In addition, p53 also stimulates expression of genes involved in the apoptotic receptor pathway including KILLER/DR5, FAS and PIDD.

In normal cells p53 is tightly regulated by the MDM2 protein. This pair function in an auto-regulatory loop as MDM2 is itself a p53 target. The p53 positively regulates MDM2 expression while MDM2 negatively regulates p53 levels and activity. However, p53 mutation prevents normal regulatory function at the vital transition checkpoints, inactivating the 'superbrake' function of the cell. Approximately 90% of mutated p53 proteins in cancers are accredited to missense (single point) mutations of residues in the p53s genes.

1.2.2 Activation of Proto-oncogenes to Oncogenes

Oncogenes are altered versions of their normal cellular genes (proto-oncogenes), which are involved in the regulation of normal cell growth.[24] Proto-oncogenes are converted to oncogenes by various processes such as structural or regulatory alterations, mutations, chromosomal rearrangements or gene amplification. These are usually somatic events but germ line mutations of proto-oncogenes can arise leading to predisposition to inheritable cancers. When proto-oncogenes involved in the proliferation of cells become activated to their oncogenes carcinogenesis is induced. The two essential G_1/S and G_2/M transition checkpoints in the cell cycle become ineffective leading to the formation of cancerous growths.[25] The K-ras gene of the Ras super family of proteins involved in cellular signalling transduction is thought to be the most mutated gene to be detected in cancers, present in up to 40% of colorectal adenomas and carcinomas.[26]

1.2.3 Inherited Cancer Risk

Cancers such as ovarian and breast cancers have been linked to occur due to the inheritance of mutated genes.[27, 28] The BRCA1 and BRCA2 genes play an essential role in DNA repair, but the inheritance of these genes in their mutated forms have been linked to a higher chance of cancer occurring. This has been shown by family based linkage studies where strong variances have been discovered in the BRCA genes, with BRCA1 reported to be mutated in an estimated 52% and BRCA2 in 32% of breast cancer families.

1.3 Environmental Causes of Cancer

1.3.1 Genotoxic Carcinogens

Genotoxins are DNA damaging toxins such as polycyclic aromatic hydrocarbons (PAH), aromatic amines and heterocyclic amines.[29] Genotoxic compounds are present in cigarette smoke, as by-products of burning fossil fuels and from the high temperature cooking of meats.[30] It has been found that genotoxins have been directly associated with cancers of the lung, upper respiratory tract, pancreas, colon, breast and prostate.[31] Genotoxins are metabolised by the cytochrome P450 system, converting them into electrophilic intermediates which then bind covalently with DNA forming carcinogen-DNA adducts. The carcinogen-DNA adducts have also been identified as biomarkers for the prediction of cancer, especially in hepatocellular carcinomas. If the adducts are not repaired appropriately, DNA becomes damaged leading to mutations and eventually cancer formation. For example, benzo[*a*]pyrene

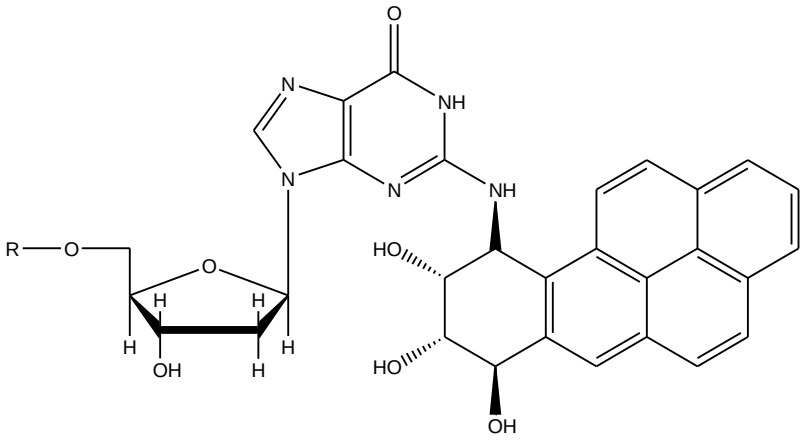

Figure 4. (+)-*ta*-[BP]G adduct

(BP) is a commonly known PAH.[32] BP is metabolically activated into several highly reactive intermediates including (+)-*anti*-benzo[*a*]pyrene diol epoxide (BPDE). The reaction of BPDE with DNA produces the (+)-*trans*-*anti*-N^2-benzo[*a*]pyrene deoxyguanosine adduct ((+)-*ta*-[BP]G), the most mutagenic BP-DNA adduct that can form. The (+)-*ta*-[BP]G is regarded as a major initiator in the pathway of cancer (Figure 4).[33]

1.3.2 Infectious Biological Agents (IBAs)

Currently, six human viruses (Table 1) deemed carcinogenic to humans have been identified which are the Epstein-Barr, hepatitis B, human T-cell lymphotropic type 1, human papilloma,

hepatitis C and Kaposi's sarcoma associated herpes viruses.[34] Although the direct mechanism of virus induced carcinogenesis is not completely known, two pathways have suggested which may operate either simultaneously or independently.[35] Direct oncogenesis can lead to malignancy as the IBAs infect the cell directly causing DNA damage. Indirect oncogenesis can occur in which the IBAs wield a circuitous effect on cell replication by affecting precursors involved in normal cell proliferation.

Table 1. Carcinogenic human viruses

Virus	Year of Discovery	Cancers Caused
Epstein-Barr	1965	Burkitt's lymphoma, Nasopharyngeal carcinoma, Hodgkin's lymphoma, immunosuppression-related non-Hodgkin lymphoma, extranodal NK/T-cell lymphoma
Hepatitis B	1967	Hepatocellular carcinoma
Human T-cell lymphotropic type 1	1980	Adult T-cell leukemia and lymphoma
Human papilloma	1983	Carcinoma of the cervix, oral cavity and tonsil
Hepatitis C	1989	Hepatocellular carcinoma, non-Hodgkin lymphoma
Kaposi's sarcoma associated herpes	1994	Kaposi's sarcoma, primary effusion lymphoma

1.4 The Beginnings of Cancer Chemotherapy

Research into the development of anti-cancer agents has been ongoing since the First World War where it was observed that soldiers being treated for exposure to sulfur mustard gas exhibited massive damage to the haematopoietic system, including lymphoid aplasia.[36, 37, 38] This is thought to have occurred due to the low activity of critical DNA repair enzymes combined with the high proliferation rates in bone marrow increasing susceptibility to alkylating agent based mutations.[39, 40] The observed lymphoid and myeloid suppression indicated the potential use of alkylating agents as treatment for lymphomas and leukemias. Related nitrogen mustards were the first chemical agents to be clinically tested for the treatment of cancer. Resulting data showed successful regression of lymphomas in patients, through mustards forming covalent bonds with nucleophilic groups in DNA. This leads to single-strand or double-strand DNA breaks which subsequently causes inter-strand and intra-strand DNA cross-linking halting DNA proliferation.[41] Further advances came with compounds such as methotrexate and chlorambucil in the 1960's which showed effectiveness against germ cell tumours, and cisplatin in 1965 which demonstrated the ability to inhibit cellular division.[42, 43] The 1990's produced two further important groups of anti-cancer agents; the taxanes and topoisomerase inhibitors. Drugs included the taxane paclitaxel and the topoisomerase I inhibitor camptothecin (Figure 5).

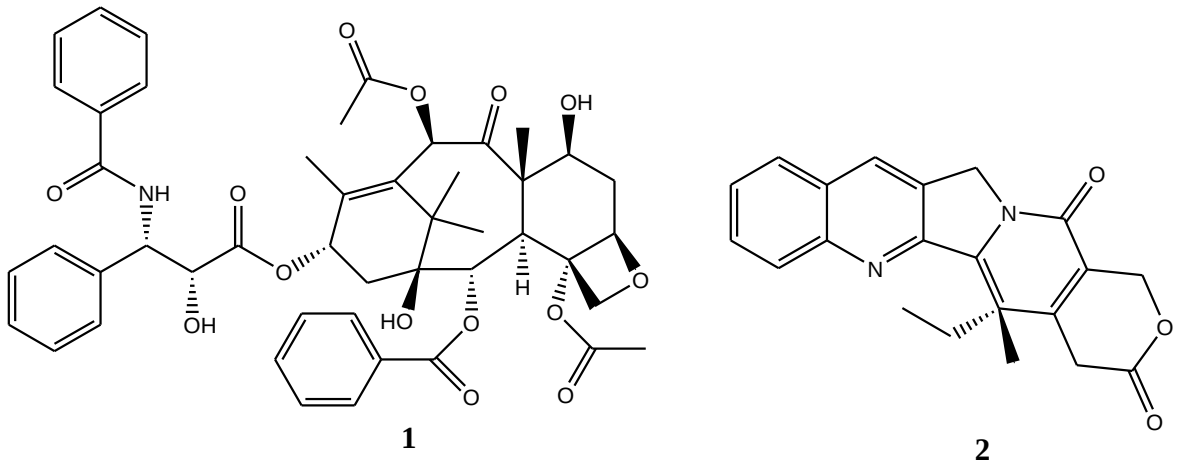

Figure 5. Structures of paclitaxel (1) and camptothecin (2)

1.5 Current Cancer Chemotherapy

Several groups of chemotherapeutic drugs exist which are used to treat a wide range of cancers. These are categorised according to their mode of action and structural similarities. Selectivity of chemotherapeutic drugs is thought to occur due to the highly proliferative nature of tumour cells relative to normal cells, therefore the metabolism of drugs interacting with the tumour cells will be greater than normal.[44]

1.5.1 Alkylating Agents

Alkylating agents act by forming covalent bonds with DNA. This causes various lesions including mono-adducts formed through single bonds to DNA and bi-adducts in which the alkylating agent forms either interstrand or intrastrand DNA cross-links with DNA.[45, 46, 47] Mono-adducts constitute the major portion (approximately 90%) of total DNA lesions inflicted by alkylating agents. However, bi-adduct cross-links are more cytotoxic as these are associated with the anti-tumour ability of alkylating agents by blocking DNA replication. DNA alkylation has been shown to occur preferentially at the endocyclic nitrogen atoms including the N7 atom of guanine and the N1, N3, N6 and N7 atoms of adenine. N7-N7 cross-linking of opposing guanine bases has been well documented.[48]

Mechlorethamine was the first alkylating agent commonly used in chemotherapy.[49] It is administered with other anti-cancer drugs in the MOPP (Mechlorethamine, Oncovin, Procarbazine and Prednisone) chemotherapy combination used to treat Hodgkins disease, and has been reported to be particularly effective against cutaneous T-cell lymphoma when administered topically. Mechlorethamine exerts its anti-cancer effects through the formation of aziridinium ion intermediates. These are formed by the sequential loss of the electron withdrawing chlorine atoms (Scheme 1). The aziridinium intermediates are highly reactive species which continue to alkylate multiple sites of DNA upon interaction.[45] It has been shown experimentally that mechlorethamine reacts faster with nucleic acids and proteins than its aromatic nitrogen mustard analogues.

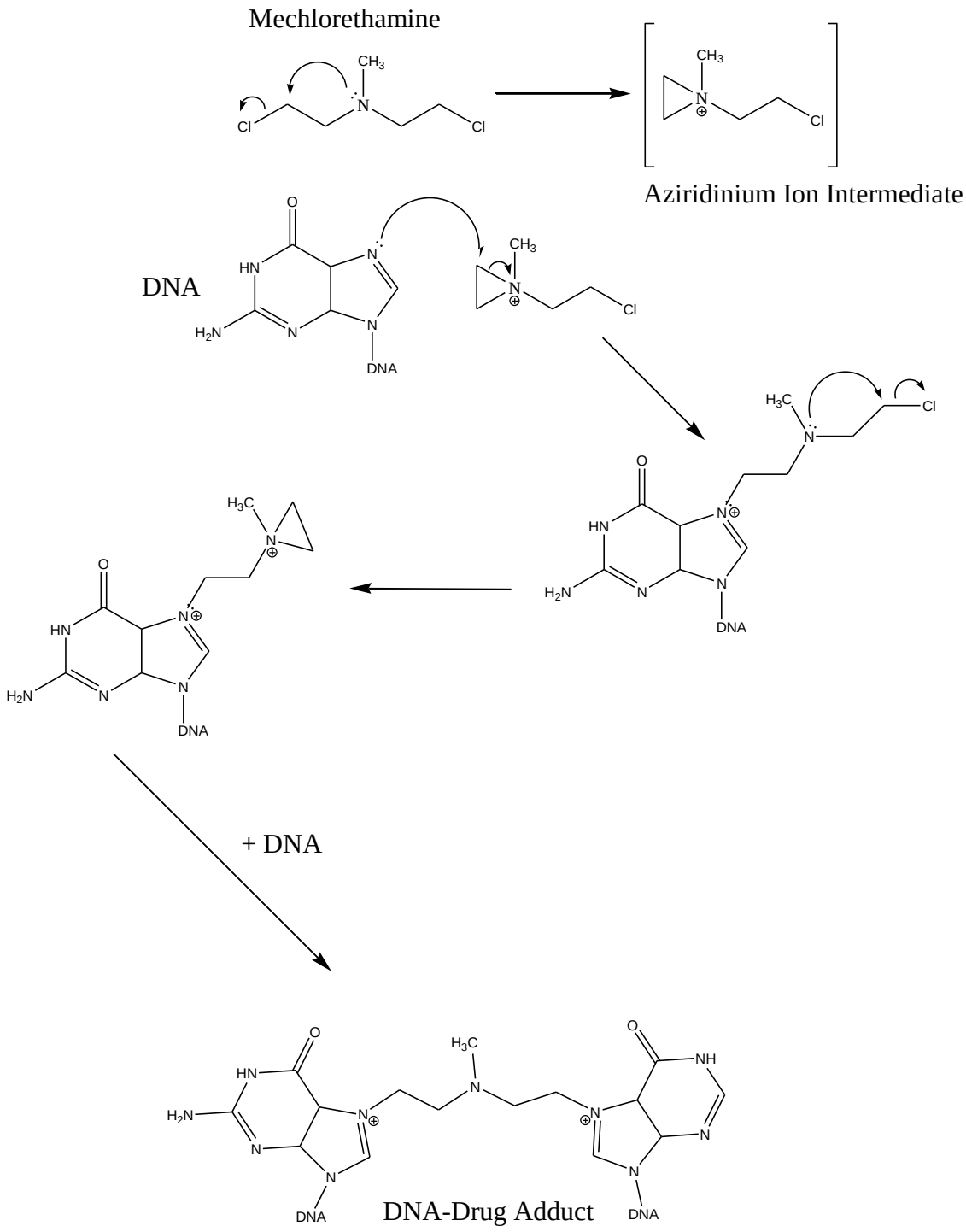

Scheme 1. Alkylating mechanism of mechlorethamine

1.5.2 Platinum Containing Compounds

Platinum compounds are widely used in chemotherapy to treat various cancers such as ovarian, lung, oesophageal, cervical and testicular cancers.[50, 51] The anti-tumour mechanism of platinum based drugs mirrors that of the alkylating agents in that intrastrand adducts and interstrand cross-links are formed with DNA (Scheme 1). The major binding sites for platinum based agents on DNA are the N7 positions in guanine and adenine. Currently three platinum based anti-tumour drugs are in clinical use; cisplatin, carboplatin and oxaliplatin (Figure 6).[41]

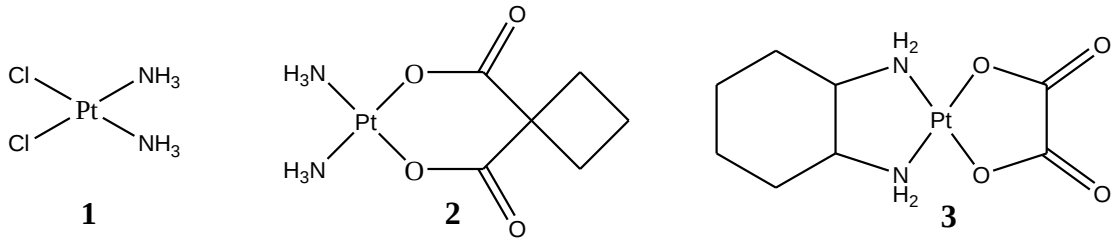

Figure 6. Structures of cisplatin (1), carboplatin (2) and oxaliplatin (3)

Cisplatin, introduced in the late 1970's, was the first platinum based anti-cancer drug to be used clinically.[52] The anti-tumour activity of cisplatin was discovered inadvertently when the inhibition of cell replication was observed during investigations into the effects of electric fields on the growth of *Escherichia coli*.[53] This occurred as a result of platinum electrodes reacting with the chemical solution in which they were immersed (containing ammonium and chloride salts) forming the cisplatin complex through electrolysis. Cisplatin is now responsible for the cure of over 90% of testicular cancers, and is an important agent in the treatment of bladder, cervical, head, neck and ovarian cancers. The molecular anti-tumour mechanism of cisplatin occurs through numerous chemical reactions once it enters the body. Prior to DNA attack cisplatin undergoes activation through rapid aquation where the two chloride molecules are replaced by two water molecules. This occurs in intracellular regions where concentrations of chloride ions are significantly lower than in the blood plasma were the cisplatin complex remains stable. Once activated, the cisplatin complex forms DNA cross-links as the water molecules are displaced by the favourable N7 nitrogen atoms in the guanidine region of the DNA (Figure 7). The chelation of cisplatin and DNA causes the DNA to bend, and this abnormal shape is considered to be the critical lesion triggering the pathway to cell death.

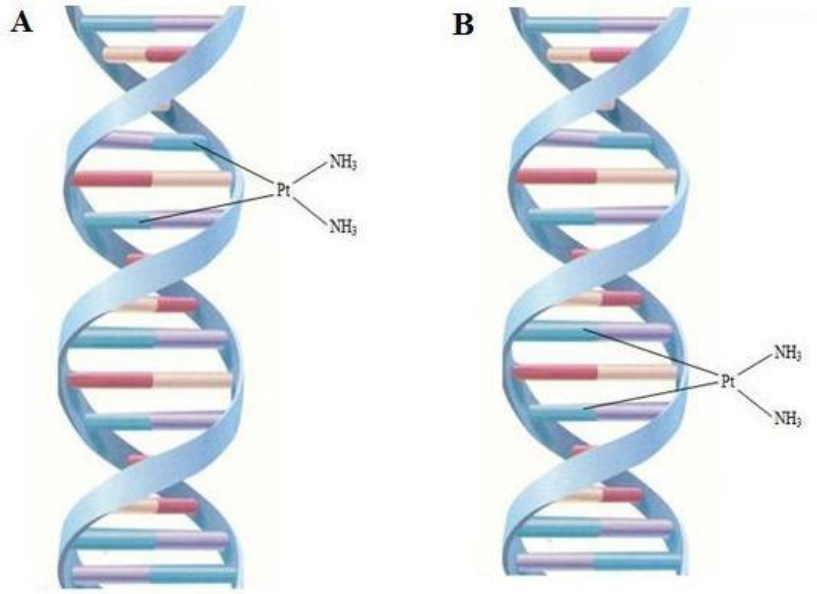

Figure 7. A) Interstrand binding of DNA with cisplatin B) Intrastrand binding of DNA with cisplatin

1.5.3 Antimetabolites

Antimetabolites are cytotoxic agents that structurally resemble naturally occurring purines and pyrimidines essential in the replication of DNA.[41, 54] Their anti-cancer activity comes from both their ability to inhibit key enzymes involved in DNA synthesis, and their capability of incorporating into DNA and RNA. These properties of the antimetabolites cause strand breaks and the termination of cell proliferation (usually during the S phase of the cell cycle). Methotrexate the most commonly used antimetabolite in clinical use which is structurally similar to folic acid (Figure 8).

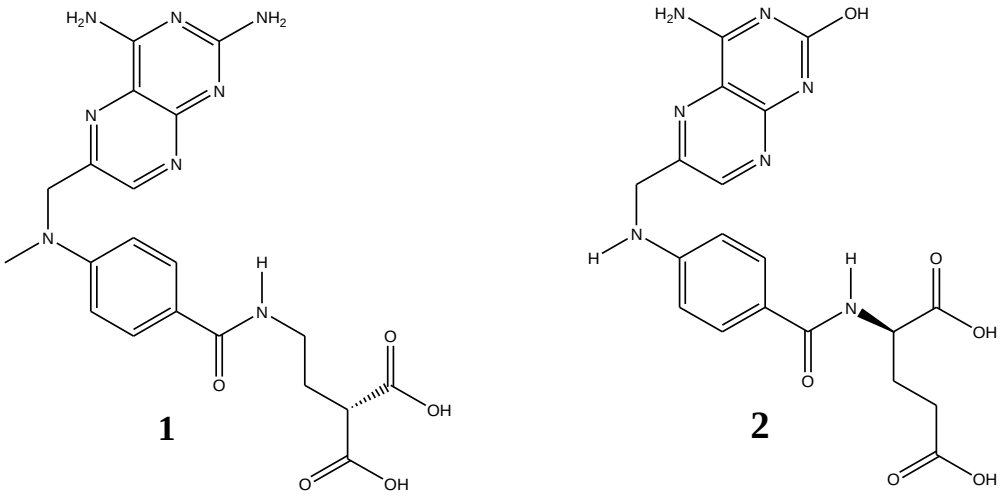

Figure 8. Structures of methotrexate (1) and folic acid (2)

Methotrexate acts by inhibiting the enzyme dihydrofolate reductase (DHFR), which is responsible for the regeneration of oxidised folates into their reduced forms of tetrahydrofolates (THFA).[35] Folate in the form of N^5-methyltetrahydrofolate is essential for the conversion of homocysteine into methionine via methylation, which then undergoes further biological modification to become S-adenosylmethionine (SAM). This is an important universal methyl donor in a variety of biochemical reactions, especially methylating specific cytosines in DNA which regulate genome stability and gene transcription.[55, 56] Depletion of SAM induces DNA hypomethylation and studies have shown abnormal methylation plays an integral role in carcinogenesis through various pathways including altered expression of TSG's and proto-oncogene expression.

N^5, N^{10}-methylenetetrahydrofolate is another important folate which methylates uracil to form thymine essential for DNA synthesis and repair. Deficient folate levels result in the disincorporation of thymine into DNA, leading to mutagenic effects and eventually cancer. Methotrexate usually causes cells to arrest in the G_1 and/or the S phases of the cell cycle.[57, 58]

1.5.4 Anthracyclines

The anthracyclines are broad-spectrum anti-cancer drugs which were originally isolated from the pigment producing *Streptomyces peucetius*.[59, 60] Since the 1960's, more than 200 naturally occurring anthracyclines have been identified. Daunorubicin was the first anthracycline to be successfully isolated in 1963, but more important was the development of doxorubicin (DOX) in 1968 which is commonly used in the treatment of breast cancer and various other solid tumours (Figure 9).[61]

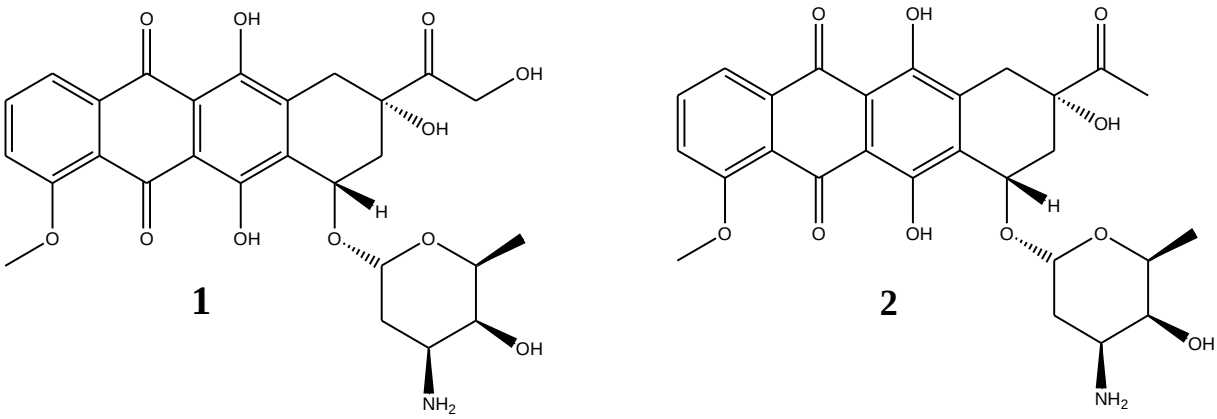

Figure 9. Structures of doxorubicin (1) and daunorubicin (2)

The anthracyclines generally target the S phase of the cell cycle. They intercalate into the chromophore between DNA strands in a longitudinal orientation. This together with binding of the amino sugar with the DNA backbone causes DNA topoisomerase II malfunction. DNA topoisomerase II is a critical enzyme involved in breaking and re-joining DNA during cell proliferation.[62] The disruption of this enzyme results in irregular DNA assembly leading to cell death. An alternative mechanism of action involves transfer of an electron from NADPH to the anthracycline. This results in a free radical intermediate of the anthracycline, which can readily transfer an electron to molecular oxygen forming free radicals capable of causing damage to DNA.[63] In addition, anthracyclines can exert direct effects on cell membranes including the disruption of ion and electron transportation systems vital for cell proliferation.

1.5.5 Tubulin Binding Drugs (TBDs)

Tubulin is the basic sub-unit of microtubules which play an important and diverse role in the normal function of cells including mitosis, meiosis, intracellular transport and axonal function.[41] Microtubules are hollow polymeric protein complexes built up of α and β tubulin heterodimers which consist of three domains; the N-terminal, the central and the C-terminal domain.[64, 65] The dynamic nature of their ability to polymerise and depolymerise is critical in the formation of the mitotic spindle which is essential for cellular division and chromosome segregation during mitosis.[66] Drugs which target tubulin act by suppressing the kinetics of the spindle microtubule dynamics, inhibiting the metaphase/anaphase transition which inhibits mitosis and induces apoptosis of tumour cells. Three binding sites have been categorised which are named after the ligands that occupy them; these are the taxane, vinca alkaloid and colchicine binding sites.[67] TBDs are categorised according to the mechanism by which they affect the microtubules and to which site that they bind.

The first category comprises of microtubule destabilising agents (MDSAs). These inhibit the assembly of microtubules by binding to the vinca alkaloid or colchicine binding sites preventing the formation of tubulin dimers. Drugs in this class include vincristine, a vinca alkaloid isolated from the periwinkle plant *Catharanthus roseus*, which is used in the treatment of leukemias, lymphomas and sarcomas (Figure 10).[68]

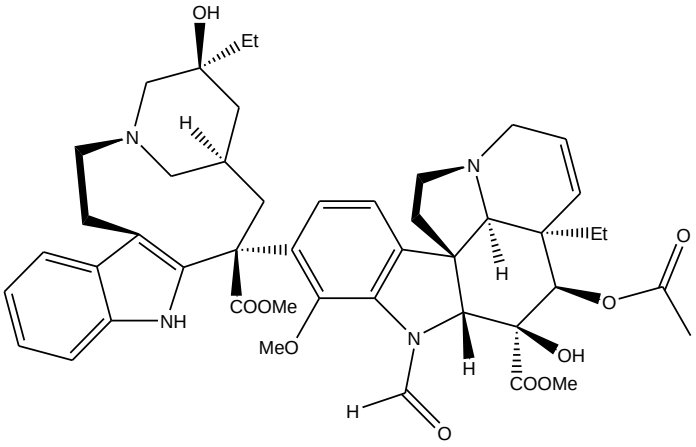

Figure 10. Chemical Structure of Vincristine

The second category of tubulin binding drugs is made up of microtubule stabilising agents (MSAs). These stabilise microtubules by binding to the taxane binding sites on polymeric tubulin, preventing its disassembly into α and β tubulin dimers. The taxane paclitaxel (Taxol) (Figure 11) was first isolated from the bark of the pacific yew tree (*Taxus Brevifolia*). Its ability to cause cell cycle arrest has subsequently gained clinical success in the treatment of ovarian, head, neck, lung and metastatic breast cancers.[69, 70] Taxol inhibits cell proliferation by binding to the microtubule surface, especially to the β sub unit of tubulin heterodimers and preventing microtubule disassociation. It has also been accredited to induce the microtubule assembly which further disrupts the microtubule dynamics.[71] However, unavailable ionisable functional groups make this drug extremely insoluble (<0.03 mg/mL) in aqueous environments which is responsible for its low bioavailability.[72]

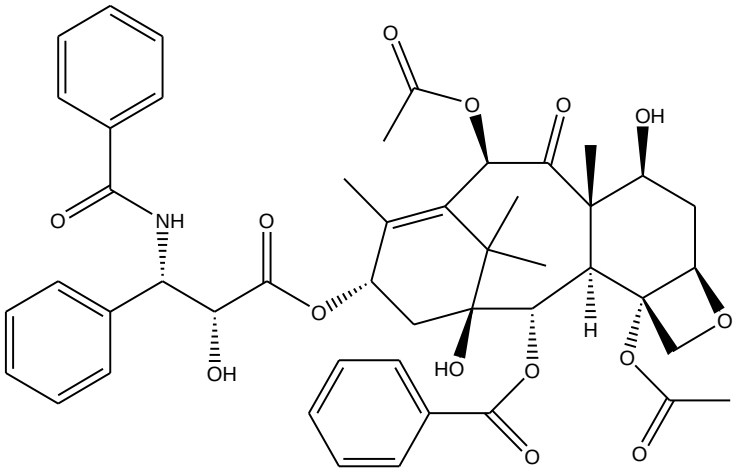

Figure 11. Paclitaxel

Ixabepilone, an epothilone MSA received clinical approval in October 2007. It is used for the treatment of metastatic or locally advanced breast cancer that progresses after anthracycline and taxane therapy, or in patients with taxane-resistant cancer with contraindication to further

anthracycline therapy. Ixabepilone has also been approved as monotherapy in patients with metastatic and locally advanced breast cancer refractory to taxanes, anthracyclines, and capecitabine.[73, 74]

The combretastatins are a group of antimitotic agents isolated from the bark of the South African tree *Combretum caffrum.*[75] The most important of these, Combretastatin A4 (CA4) (Figure 12A), is a potent cytotoxic compound which strongly inhibits the polymerisation of tubulin by binding to the colchicine-binding site of the β-tubulin subunits.[76] CA4 also displays powerful vascular disrupting and anti-angiogenesis properties leading to a significant reduction in tumour blood flow. However, CA4 showed poor bioavailability and low aqueous solubility but this was overcome by the development of a water soluble disodium-phosphate prodrug (Figure 12B), currently in clinical trials. This derivative is inactive as the phosphate but highly cytotoxic following *in vivo* hydrolysation to CA4.[77]

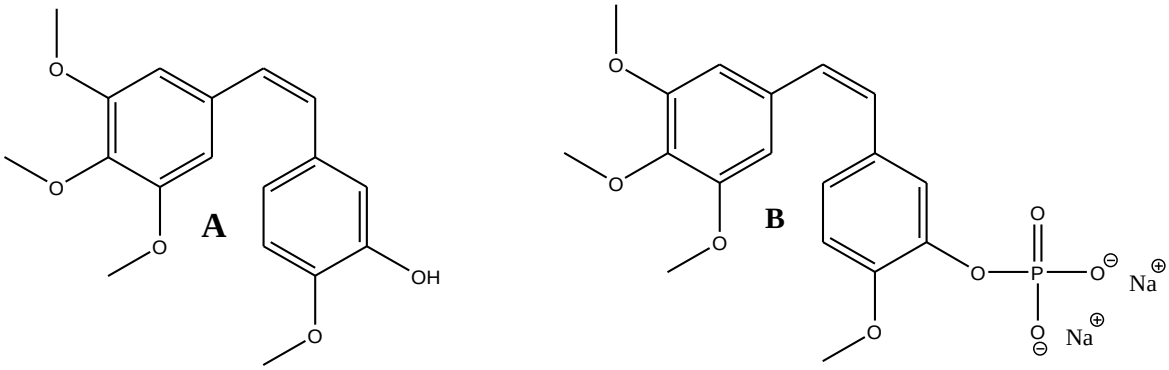

Figure 12. CA4 (A) and the disodium-phosphate prodrug of CA4 (B)

1.5.6 Tyrosine Kinase Inhibitors

Tyrosine kinases (TKs) are key components within the cellular communication network and function as "master switches" regulating signalling pathways pivotal to normal cell development and survival.[78] Examples include the epidermal growth factor receptor (EGFR/ErbR), platelet derived growth factor receptor (PDGFR), vascular endothelial growth factor receptor (VEGFR), fibroblast growth factor receptor (FGFR) and the hepatocyte growth factor receptor (MET).

In certain cancers, mutations causing the over-expression of TK's appear to be the source of the disease causing carcinogenesis by altering normal downstream signalling which controls normal cell functions.[79, 80] An example of mutated genes causing abnormal TK expression are

fusion proteins. These are the combination of two or more genes which originally coded for separate proteins, resulting in increased abnormal kinase activity and eventually cancer. Fusion proteins are observed in chronic myeloid leukemia, and mutations or deletions directly in TK's are seen in solid tumours.

The human epidermal growth factor receptor 2 (HER-2) belongs to a family of receptor tyrosine kinases. Amplification of the HER-2 gene and consequent over-expression of the cell-surface receptor have been implicated in the pathogenesis in one out of four cases of breast cancer.[81, 82] Herceptin was the first commercially available TK inhibiting antibody.[83] It acts by down regulating HER2 expression (also known as ErbB2) by acting as a partial ligand for this receptor. This accelerates receptor endocytosis and degradation causing rapid de-phosphorylation of ErbB2. This prevents downstream signalling proteins initiating signal transduction cascades responsible for DNA synthesis and cell proliferation resulting in the inhibition of cell cycle progression.[84, 85] Experimental evidence suggests that herceptin may also affect the regulation of genes related to angiogenesis such as the vascular endothelial growth factor (VEGF) and angiopoietin-1.[86]

Gleevec (Figure 13) is an inhibitor of the Abl protein-tyrosine kinases which are important in normal cell proliferation. Gleevec was clinically approved for the treatment of chronic myelogenous leukemia (CML) in May 2001. CML is usually detected and diagnosed by the presence of the Philadelphia chromosome, a fusion gene formed by the translocation of chromosomes 9 and 22.[87]

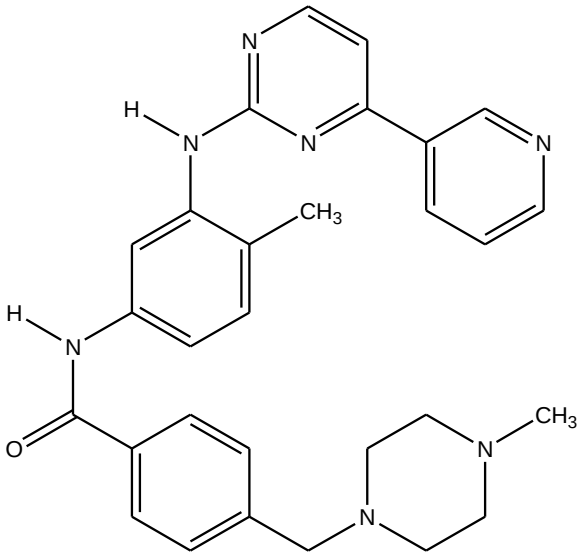

Figure 13. Gleevec

1.6 The Side-effects of Chemotherapy

Advances in chemotherapy have successfully provided remissive treatments for some types of cancers. For example, cisplatin provides testicular cancer patients with up to a 95% cure rate if the cancer is detected in its early stages.[88] Unfortunately, chemotherapy comes with the cost of unwanted side-effects often as a result of the relatively narrow therapeutic index of anticancer agents. This is due to their poor selectivity and inability to differentiate between cancer cells and normal cells.[89]

Cisplatin has been associated with the formation of new primary malignancies, infertility, renal toxicity and nephrotoxicity. These have been attributed to the direct toxic effects of secreted platinum species in the excretive system and reactive platinum species which have reached non target sites. Another common side-effect of cisplatin is bone marrow suppression, also observed in patients treated with anthracyclines and alkylating agents which cause white cell and platelet depletion and anaemia.[90] Nausea and vomiting are observed in 70-80% of patients receiving chemotherapy, alongside diarrhoea.[91] The unfortunate apoptotic effect of chemotherapy on healthy hair follicles induces alopecia, which has been described as one of the most distressing side-effects observed in patients.[92]

The administration of ifosfamide (Figure 14) to treat childhood tumours results in nephrotoxicity. This is severe in approximately 30% of cases where it is characterised by the Fanconi Syndrome. This is when damage to renal tubule cells occurs preventing the reabsorption of vital nutrients such as glucose, proteins, sodium, potassium and phosphates. The nephrotoxicity is caused by chloroacetaldehyde, the hepatic metabolite of ifosfamide.[93, 94]

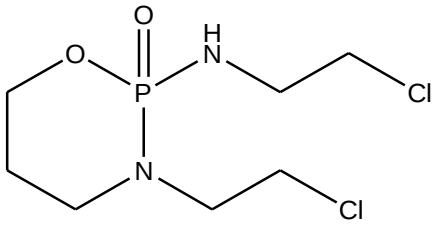

Figure 14. Chemical Structure of ifosfamide

Cardiomyopathies, including heart failure and arrhythmia have been induced by anthracyclines (especially DOX) during chemotherapy and have been reported many years after a course of treatment has finished.[95, 96] Endomyocardial biopsy specimens suggest that DOX depletes cytosolic ATP crucial in supplying energy to the heart resulting in myocardial damage.[97]

Herceptin based chemotherapy was found to produce congestive heart failure in patients, especially when pre-treated with anthracyclines. This is due to ErbB receptors in the heart important for maintenance and survival interacting with the cytotoxic herceptin drug.[98]

Other side-effects suffered by patients treated with chemotherapy include central nervous system toxicity resulting in seizures, cerebella dysfunction, inflammation, retinopathy, cerebral venous thrombosis, cognitive impairment and psychiatric symptoms.[99, 100] Chemotherapy is often combined with drugs such as prednisone, an anti-inflammatory agent which also reduces nausea in patients. Another protecting agent is dexrazoxane, administered alongside doxorubicin to protect heart damage occurring. However, with the combination of chemoprotective drugs the problem of unwanted side-effects is still a large problem amongst cancer patients.[101, 102]

1.7 Prodrug Strategies in Chemotherapy

The prodrug concept in chemotherapy was first introduced by Albert and Harper in the late 1950's to try and achieve a safer systemic approach for the treatment of cancer.[103] A prodrug is a chemical with little or no pharmacological activity until it undergoes biotransformation *in vivo* into a therapeutically active metabolite.[104] The aims of using the prodrug approach in chemotherapy are to produce compounds with improved pharmaceutical, pharmacokinetic and pharmacodynamic properties compared to existing drugs.[105] In order to achieve this, the prodrug must reach and distribute efficiently across the tumour and undergo selective biotransformation to its cytotoxic form, without harming normal healthy cells.[106] This in turn will reduce unwanted side-effects commonly observed with chemotherapy. Successful prodrug development relies in exploiting tumour properties which make cancer cells distinguishable from normal cells. Possible prodrug targets include hypoxic conditions observed in cancer cells due to the lack of vascular network development, specific or over-expressed enzymes, pH differences, tumour specific antigens and the excretion of tumour specific enzymes.[107]

1.7.1 Antibody Directed Enzyme Prodrug Therapy (ADEPT)

ADEPT is an approach where tumour selectivity is achieved by using an antibody (non-mammalian or mammalian) which is specific to an antigen on the tumour surface.[108] Enzymes which are essential for the biotransformation of the prodrug are attached to the

antibody and this conjugate is administered to the patient. Sufficient time is then allowed for this conjugate to accumulate at the site of the tumour and for it to clear from the blood supply and normal tissues.[109] This is followed by the administration of the prodrug, which is stable under non-activating conditions but quickly activated to its cytotoxic form once it interacts with the target conjugate (Scheme 2).[110]

Ideal prodrugs for use with ADEPT should be relatively small molecules which can easily diffuse within tumour tissues, including both antigen positive and antigen negative, and have the capability of producing the "bystander effect" (see GDEPT).[111] The target antigen should be either expressed on the tumour cell membrane or be secreted into the extracellular matrix of the tumour. Conjugated enzymes should have no human homologue to prevent prodrug activation and cytotoxicity outside of the tumour site.

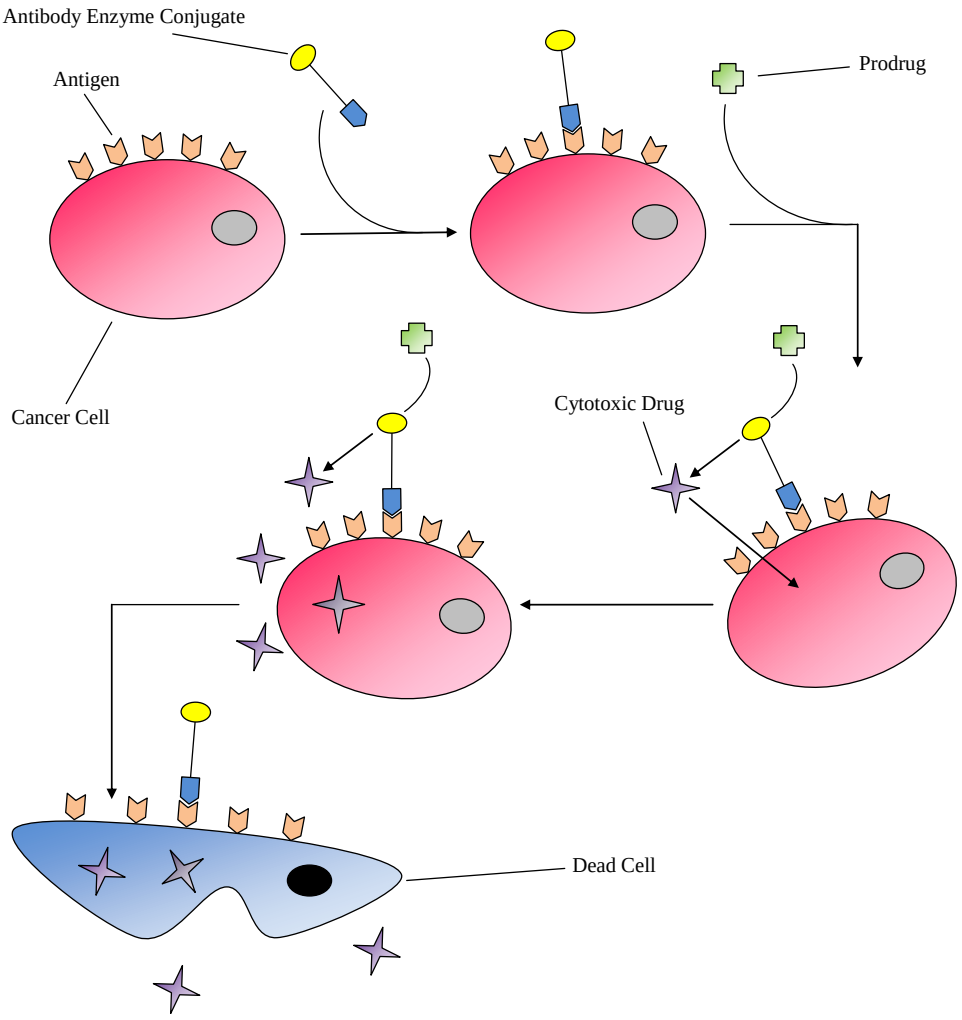

Scheme 2. Schematic representation of ADEPT.

The first pilot study of ADEPT was carried out at Charing Cross Hospital in London on patients with advanced colorectal cancers. An anti-CEAF(ab')2 antibody conjugated to the bacterial enzyme carboxypeptidase G2 (CPG2) was used to target a benzoic acid mustard prodrug. The enzyme converted the prodrug to its toxic metabolite by cleavage of its glutamate terminal. Using this system, reduction in tumour masses of 50% were observed.

Other systems used in ADEPT include the enzyme aminopeptidase which converts the prodrug 2-L-pyroglutamylmethotrexate to the toxic methotrexate, and the enzyme cytosine deaminase which converts 5-fluorocytosine into 5-fluorouracil. Disadvantages with ADEPT include the high cost and difficulties associated with the development and purification of antibodies, and unwanted immunogenic responses from the antibodies and antibody-enzyme conjugates.

1.7.2 Gene Directed Enzyme Therapy (GDEPT)

GDEPT requires the integration of a non-mammalian enzyme gene into the tumour of interest.[112] This allows the tumour to express enzymes which will convert a specific prodrug into its cytotoxic metabolite, killing cells inside the tumour and by the "bystander" effect.[113] The "bystander effect" is observed as the cytotoxic drug leaves the tumour cells and kills surrounding cancerous tissue which may not have received the non-mammalian enzyme gene.[114] Critical requirements for GDEPT are that the integrated non-mammalian enzyme gene is absent from the human genome or expressed in very low levels in healthy tissue. It must also have a high rate of catalytic activity in the biotransformation of the prodrug once expressed. The prodrug is also required to have an exceptionally high affinity for the targeted enzyme, be able to penetrate into tumours, exhibit virtually no toxicity in its prodrug form and have a half-life of the active metabolite sufficient to enable the "bystander" effect to occur.[115]

Systems used in GDEPT include the enzyme nitroreductase (NTR), encoded for by the *nfs*B gene of *Escherichia coli*.[116] NTR reduces the prodrug CB1954 to 2-HX and 4-HX, bifunctional alkylating agents which form interstrand cross-links with DNA resulting in cell death (Figure 15).

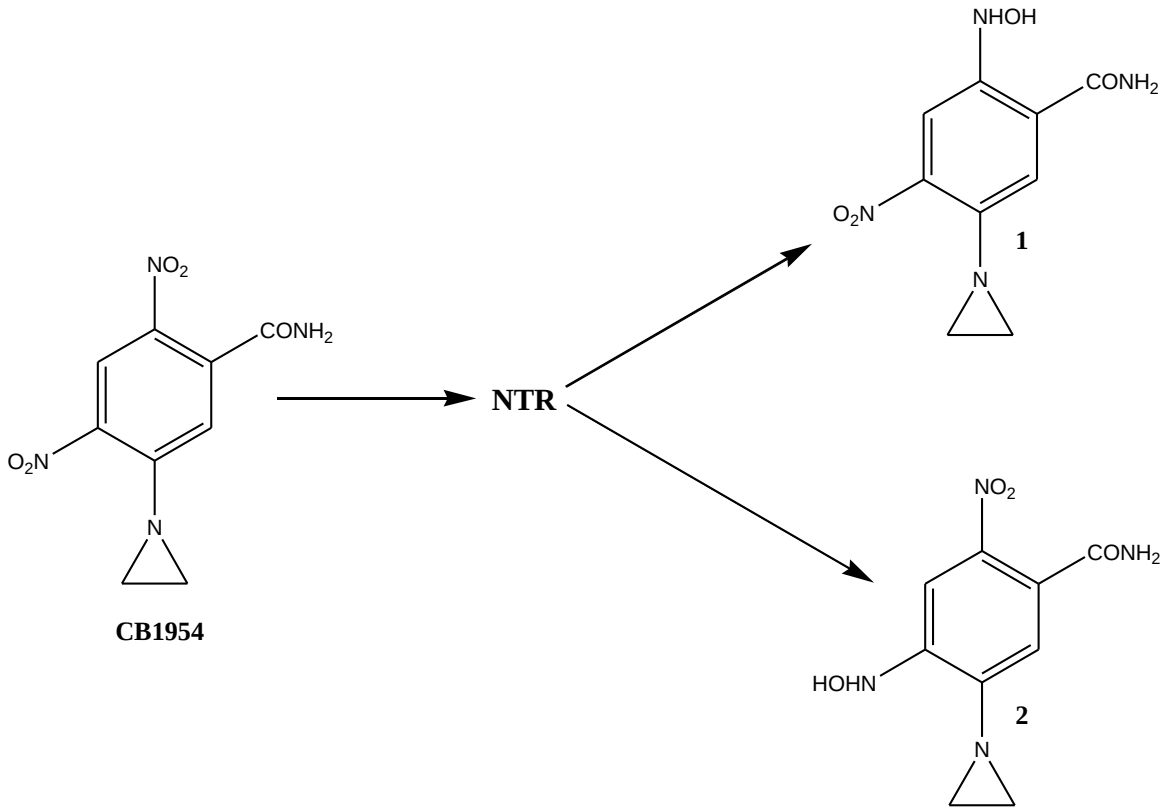

Figure 15. Metabolism of CB1954 to 2-HX (1) and 4-HX (2) by NTR

Also, Purine nucleoside phosphorylase has been used to convert 6-methylpurine 2-deoxyriboside to the antimetabolite 6-methylpurine, currently in clinical trials (Figure 16).[117, 118, 119]

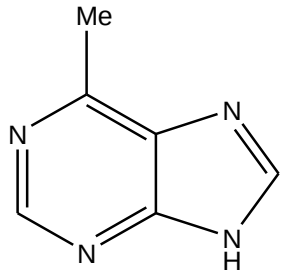

Figure 16. 6-Methylpurine

One of the major advantages of GDEPT is the higher concentrations of metabolised toxic species produced inside and surrounding the tumour. This increases the therapeutic index

significantly in comparison with standard chemotherapeutic agents.[114] However, disadvantages associated with this approach include the unwanted killing of normal neighbouring tissue via the bystander effect and systematic diffusion of the activated prodrug causing cytotoxicity to unwanted regions.[111]

1.8 The Cytochrome P450s

The cytochrome P450 enzymes (CYPs) are haem containing proteins originating from a gene super-family with over 1000 members found in humans, plants and bacteria.[120] The name cytochrome P450 was given during investigations into the spectrophotometric properties of pigments in a microsomal fraction containing these proteins prepared from rat livers. The addition of the reducing agent sodium dithionite to the microsomal fraction which was previously gassed with carbon monoxide gave a unique absorbance band at 450 nm. This was due to the 5th cysteine thiolate anion ligand of the cytochrome enzymes.[121, 122] Generally CYPs contain 500 amino acids with iron-protoporphoryrin IX as the prosthetic group, providing the electronic centre for the important activation of molecular oxygen. CYPs are bound to the endoplasmic reticulum or mitochondria in eukaryotic organisms.[123]

In humans, 40 CYPs have so far been identified but research continues in the discovery and identification of further examples.[120] A critical role played by CYPs in the human body is in the metabolism of xenobiotics, such as drugs and environmental pollutants. They are also important in the biosynthesis of cholesterol, endogenous steroidal hormones, bile acids and the metabolism of vitamin D_3.

Reactions catalysed by CYP enzymes include carbon hydroxylation, heteroatom oxygenation, dealkylation, epoxide formation and group migration.[124] Substrates bind to CYPs when the iron containing haem is in its oxidised state (Fe^{3+}).1 Donation of an electron from NADPH mediated by NADPH-cytochrome P450 reductase (CPR) reduces the iron haem to Fe^{2+} which then combines with molecular oxygen.[125, 126] CPR is an electron transfer diflavoprotein and is widely expressed in all tissues but is most abundant in the endoplasmic reticulum of the liver.[127] Donation of a second electron from NADPH activates the haem bound molecular oxygen, inserting one atom into the substrate and converting the other atom into water.[128] Regio and stereo selectivity of the oxygenation depend on the spatial orientation of the bound substrate relative to the position of the activated oxygen molecule on the haem. Hydrophobic substrates are preferred for a majority of CYPs, but some catalyse the oxygenation reactions of hydrophilic compounds such as ethanol and acetone.[129] A prime example of CYP

hydroxylation is that of tamoxifen, which undergoes biotransformation to 4-hydroxytamoxifen, a 100 times more potent than its parent compound.[130]

Phase I drug metabolism involves the bio-transformation of xenobiotics by oxidative or reductive reactions carried out by CYPs in the liver.[131] The CYP1, CYP2 and CYP3 families are responsible for over 90% of drug bio-transformations in humans and determine the elimination, systemic clearance and bioavailability of therapeutic compounds. CYP3A4 is the most abundant of the hepatic metabolising enzymes taking part in the metabolism of 50% of xenobiotics. The other CYPs involved in drug bio-transformations are CYP1A2 (4%), CYP2A6 (2%), CYP2C9 (10%), CYP2C19 (2%), CYP2E1 (2%), CYP2D6 (30%).[132, 133]

1.8.1 The Over-Expression of CYPs in Tumours

The identification of a novel subfamily of CYPs was made by *Sutter et al* in 1994.[134] Using the P450 nomenclature system, the novel mRNA sequence was named CYP1B1. Since its discovery, it has been identified as a vital enzyme in the metabolism of 17β-estradiol.[135]

Research into identifying xenobiotic metabolising enzymes in tumours has been ongoing for numerous years.[136] *Murray et al* found that CYP1B1 was over-expressed in a wide range of tumour cells including lung, breast and bladder, whilst remaining undetected in the corresponding normal tissue.[137] Specific monoclonial antibodies designed to detect CYP1B1 in immunohistochemical studies were developed by *Morag et al* and used in the determination of the over-expression of CYP1B1 in breast tumours.[138] It was found that 77% of breast tumours contained the over-expression of CYP1B1 enzymes, and were specifically localised to tumour cells. Colorectal tumours were found to over-express CYP1B1 enzymes by *Gibson et al*.[139] However, they also detected the presence of CYP1B1 in normal colorectal tissue, but this was expressed to a far lesser degree than that observed in the tumour cell lines. It has also been reported that CYP1B1 expression is differential between tumours of different types.[140] *Pinpin et al* elucidated that CYP1B1 was over-expressed in lung tumours, but to a higher degree in lung adenocarcinomas than in lung squamous cell carcinomas.

However, contrary to the above finding it has been claimed that the over-expression of CYP1B1 occurs in normal tissue as well as tumour tissues. *Leclerc et al* studied non-tumour and tumour samples of lung tissue and found that the expression of CYP1B1 was to approximately the same extent in both tissue types.[141] However, discrepancies in the finding of CYP1B1 expression in normal and tumour tissue may be attributed to the detection techniques used. It has been documented that CYP1B1 mRNA is commonly detected in

normal tissue but this does not necessarily indicate the expression of the enzyme protein.[142] For example, CYP1B1coded mRNA has been found in normal liver cells but the CYP1B1 protein is undetectable.

Interestingly, the CYP1A1 gene has been found to be amplified in tumour cells in contrast to its corresponding normal tissue.[143] Studies conducted with ovarian cancers showed significant CYP1A1 over-expression.[144]

Contrary theories suggesting the role of the CYP1 family of enzymes in tumour development exist. One theory is that the over-expression of CYP1 enzymes contributes towards tumour development, as the greater enzyme concentration produces a higher turnover of possible carcinogenic metabolites.[145] Polymorphisms in CYP1A1 and CYP1B1 proteins have also been accredited to an increased risk of cancer.[146, 147] The polymorphisms produce variant species of the CYP enzymes which have abnormal functionality, in turn displaying uncharacteristic metabolism of its substrates.[148]

on the other hand, the over-expression of CYPs in tumours has generated an area of great interest for chemotherapeutic drug design and novel therapies to be developed.[149, 150] CYPs have been categorised as targets for anti-cancer prodrugs as the over expression of these enzymes in tumours is still a legitimate concept. CYP based prodrugs have been designed to undergo selective metabolism by the over-expressed enzymes, producing cytotoxic metabolites killing the cancer cells. This allows for toxic differentiation between normal and tumour cells, which will give the drugs a greater therapeutic window and reduce problematic side-effects observed with current chemotherapy. Patents for CYP1B1 activated prodrugs, inhibitors and immunotherapies have already been issued and some are pending further investigation.[151]

1.8.2 CYP Activated Prodrugs

1.8.2.1 Cyclophosphamide

The prodrug cyclophosphamide (CPA) belongs the oxazaphosphorine class of anti-cancer agents, and is used in the treatment of breast and ovarian cancers, certain leukemias and lymphomas (Figure 17).[152, 153] CPA becomes biologically active after it undergoes hepatic biotransformation to 4-hydroxycyclophosphamide (4-OHCPA). This process is catalysed by several CYPs including CYP2A6, CYP2B6, CYP2C8, CYP2C9, CYP2C19 and CYP3A4. The 4-OHCPA exists in equilibrium with its ring opened tautomer aldophosphamide

(APH).[154, 155] The equilibrium mixture diffuses from the hepatocytes into the blood plasma and is distributed throughout the body.[156] At physiological pH the equilibrium lies in favour of 4-OHCPA and since it is relatively non-polar it readily enters cells via diffusion. APH undergoes further chemical transformations to yield the highly electrophilic aziridinium phosphoramide species which is the key cytotoxic entity as it forms DNA cross-links halting cell proliferation.

In comparison to other alkylating agents, CPA produces less gastrointestinal and hematopoietic toxicity due to the enzyme aldehyde dehydrogenase which is responsible for the oxidation of APH to carboxyphosphamide, an inactive metabolite of CPA which is excreted in the urine and accounts for 80% of administered CPA. Aldehyde dehydrogenase is found in high concentrations in the hepatic cytosol, primitive hematopoietic cells, and in stem and mucosal absorptive cells in the intestine.

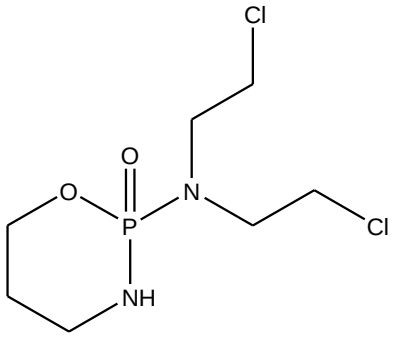

Figure 17. Cyclophosphamide

1.8.2.2 Tamoxifen

The anti-oestrogen tamoxifen (Figure 19, A) was first synthesised in 1963. It is a commonly used chemotherapeutic agent for the treatment of estrogen-receptive positive (ER+) breast cancers and has significantly decreased the mortality rate from this disease over the last decade.[157]

It first began clinical trials in 1969 with patients diagnosed with advanced breast cancer. Tamoxifen undergoes hepatic phase I and II metabolisation by CYP2B6, CYP3A4 and CYP3A5 to produce the metabolites 4-hydroxytamoxifen (Figure 18, D), N-desmethyltamoxifen (Figure 18, C) and to a lesser extent, α-hydroxytamoxifen (Figure 18, B).

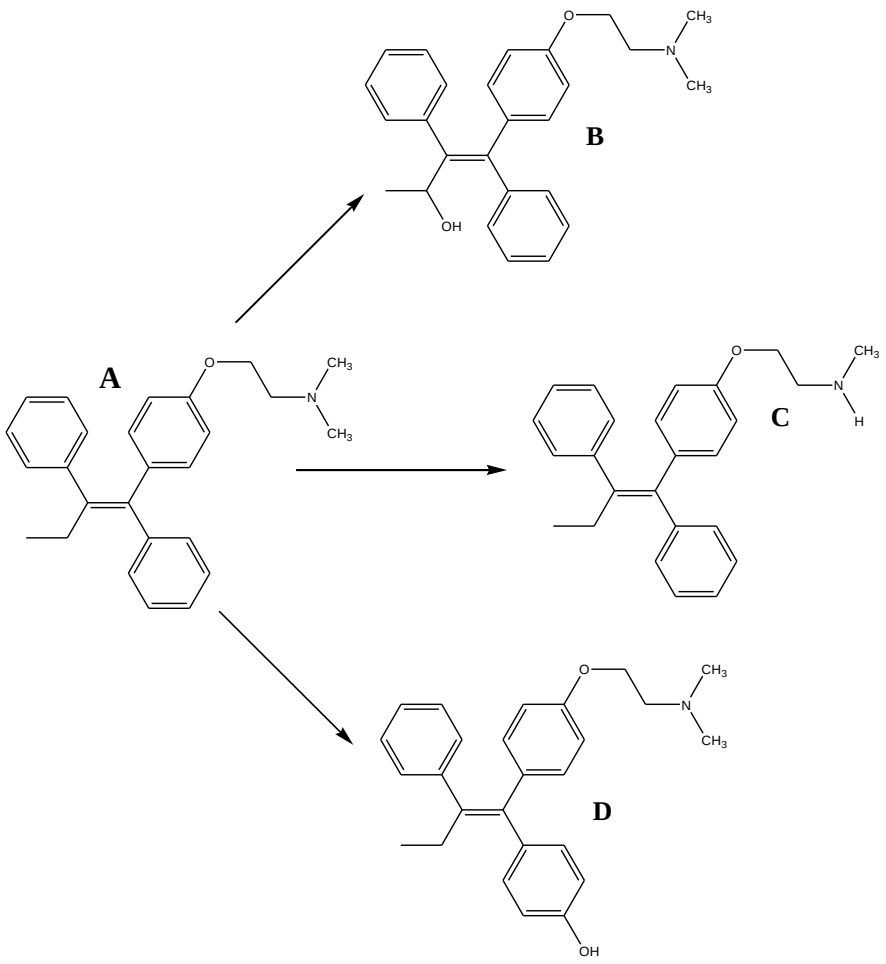

Figure 18. Tamoxifen (A) and its metabolites α-hydroxytamoxifen (B), N-desmethyltamoxifen (C) and 4-hydroxytamoxifen (D)

The mechanism of action of tamoxifen and its most important metabolite 4-hydroxytamoxifen occurs through the competitive inhibition of the ER.[158] Normally, estrogen binds with the ER and the estrogen–ER complex homodimerizes and binds to specific DNA sequences, known as estrogen response elements (ERE) in the regulatory regions of estrogen sensitive genes. Two transcriptional activation functions AF1 and AF2 located on the ER of the estrogen–ER complex interact with transcriptional co-activators to stimulate the activity of RNA polymerase II which catalyses the transcription of DNA precursors, thereby regulating gene activity and cell proliferation.[159] Tamoxifen binds to the ER forming a tamoxifen–ER complex which homodimerizes and binds to the ERE of estrogen sensitive genes. However, only AF1 is active and the inactivity of AF2 results in reduced transcription of DNA precursors blocking the G1 phase of the cell cycle. This reduces the growth of estrogen dependent cancers.[160] Another mode of action of tamoxifen is the promotion of

Transforming Growth Factor-β_1 (TGF-β_1), a cytokine which inhibits mammary cell proliferation, induces apoptosis and influences morphogenesis (cell shape and spatial arrangement).[161, 162, 163] Although blood plasma and tumour concentrations of 4-hydroxytamoxifen are only 2% in relation to tamoxifen, it is 100 times more potent as an estrogen receptor antagonist.[130]

Although tamoxifen is effective in the treatment of breast cancer, some tumours do not respond to tamoxifen treatment or become resistant to tamoxifen. This can be due to the absence of ER receptors in some breast cancers (known as ER- tumours), loss of ER expression, or mutations in ER genes and co-factors.[157] A change in tamoxifen pharmacology may occur too, as cells can start to recognise tamoxifen as an agonist when previously acting as an antagonist.[164]

1.8.8.3 AQ4N

1,4-bis{[2-(dimethylamino)ethyl]amino}-5,8-dihydroxyanthracene-9,10-dione (AQ4), is a potent topoisomerase II and DNA binding agent.[107] In solid tumours, poorly defined vascular network usually exist which result in disrupted oxygen delivery creating cell subpopulations which are chronically or acutely hypoxic.[165] Therefore, 1,4-Bis-{[2-(dimethylamino-N-oxide)ethyl]amino}-5,8-dihydroxyanthracene-9,10-dione (AQ4N), the bioreductively activated prodrug of AQ4 was specifically designed to target hypoxic tumour cells.[166] The mechanism of action of AQ4N relies on a four electron reduction to generate 1,4-bis{[2-(dimethylamino)ethyl]amino}-5,8-dihydroxyanthracene-9,10-dione (AQ4), an active cytotoxic metabolite.[167, 168] Under hypoxic conditions this process is catalysed by the

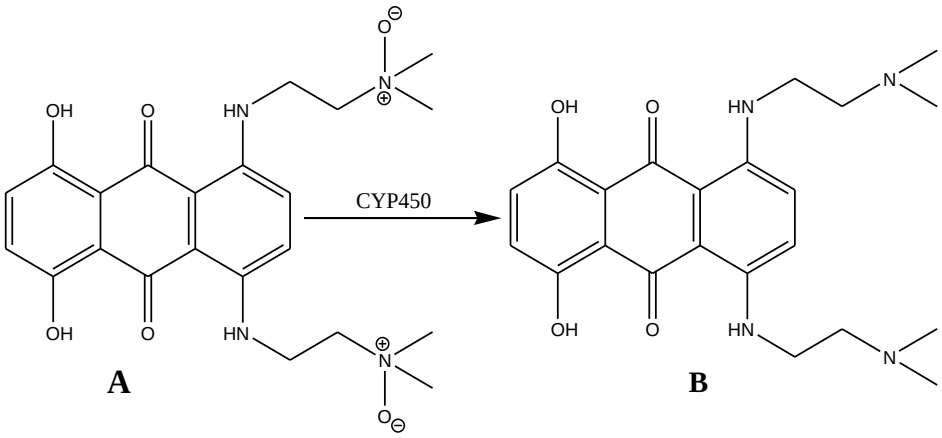

Figure 19. CYP450 reduction of AQ4N (A) to its toxic metabolite AQ4 (B)

cytochrome P450 enzymes CYP3A4, CYP1A1, CYP1A2 and CYP2B6 which are present in the tumour (Figure 19).

Importantly, AQ4N has shown selective tumour cytotoxicity as the AQ4N prodrug itself has a very low or un-measurable anti-proliferative effect on human tumour cell lines. This is due to the N-oxide groups preventing the interaction of the molecule with the sugar phosphate backbone of DNA, until converted to AQ4, the active cytotoxic metabolite.[169] The selective cytotoxicity of AQ4N towards the tumour cells provides this compound with a high therapeutic index, a valuable quality required for the reduction of unwanted side-effects.
It has also been reported that AQ4N, when administered alongside radiotherapy, significantly slows tumour growth by up to 40% when compared to treatment with radiation alone.[170, 171] This has been accredited to the active metabolite AQ4 killing hypoxic cells recruited into the cell cycle after being damaged by radiotherapy and chemotherapy.[172] Other studies have shown that AQ4N enhances the anti-tumour effects of cisplatin and cyclophosphamide when administered in combination. This has been supported by human tumour xenograft studies with radio and chemotherapy.
However, a contradicting report has stated that AQ4N acts as a DNA protecting agent and does not mediate enhanced DNA damage when administered alongside radiation therapy. The major destructive aspect of radiation is generated through DNA damage from hydroxy radicals formed through the dissociation of water. These cause damage to DNA by abstracting protons from DNA. The protective mechanism has been suggested to occur through AQ4N and AQ4 interacting with the hydroxy radicals forming drug radicals. This reduces the concentration of DNA damaging hydroxy radicals in cells. Although opposing reports exist, AQ4N still continues through clinical trials and further results are yet to be published.

1.8.8.4 Phortress

A series of 2-(4-aminophenyl)benzothiazole's were synthesised in the early 1990's which showed promising antitumour activity.[173] These were found to function as prodrugs which were metabolised to cytotoxic species by the cytochrome P450 enzyme CYP1A1. Of particular interest was 2-(4-amino-3-phenyl)benzothiazole (DF 203 or NSC 674495) (Figure 20) due to is its ability to induce its own metabolism.

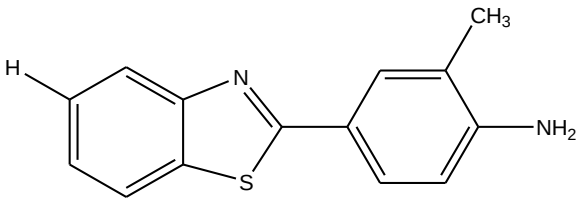

Figure 20. Structure of DF 203

DF 203 acts antagonistically on the aryl hydrocarbon receptor (AhR) which is directly involved in the expression of CYP1A1.[174, 175] Once DF 203 binds to the AhR, activated AhR translocates to the nucleus, dimerises with the arylhydrocarbon receptor nuclear transporter (Arnt) and activates transcription of target genes by binding to specific enhancer sequences (xenobiotic response elements or XREs) in the regulatory region of the CYP1A1 gene. These influence the transcription of genes they are located on, and binding with the AhR/Arnt complex induces the transcription and expression of the CYP1A1 protein.[176] Tumour cells which have shown a decrease in growth when treated with DF 203 have an increased level of CYP1A1 mRNA and enzymatic protein expression. The CYP1A1 mediated metabolites of DF 203 form adducts with DNA leading to irreparable single and double strand breaks triggering apoptosis when administered in doses greater than 100 nM. The binding of DF 203 metabolites have been shown to occur on nuclear fractions, mitochondria, microsomal and cytosolic regions of the tumour cell. To validate DF 203 as a CYP1A1 substrate, inhibition studies using the CYP1 inhibitor α-naphthoflavone were conducted. The results showed that a decreased anti-tumour effect was observed, confirming that DF 203 does require CYP1A1 metabolism to exhibit cytotoxicity. However, CYP1A1 has also shown to hydroxylate DF 203, forming an inactive metabolite. Therefore, modifications to DF 203 were made to enhance the activity of this prodrug. The first step was to fluorinate the 5 position of the phenyl moiety to give the new drug 5F 203 (NSC 703786) (Figure 21, A), as fluorination of compounds has shown to inhibit their susceptibility to hydroxylation occurring. Overall, 5F 203 showed improved cytotoxic activity in comparison to DF 203. The poor aqueous solubility of 5F 203 was overcome by conjugation of a lysyl-amide hydrochloride salt to the exocyclic primary amine function (Figure 21, B). The resulting lysyl prodrug Phortress (NSC 710305) is both water soluble and chemically stable but undergoes rapid bioreversion *in vitro* to 5F 203.[177]

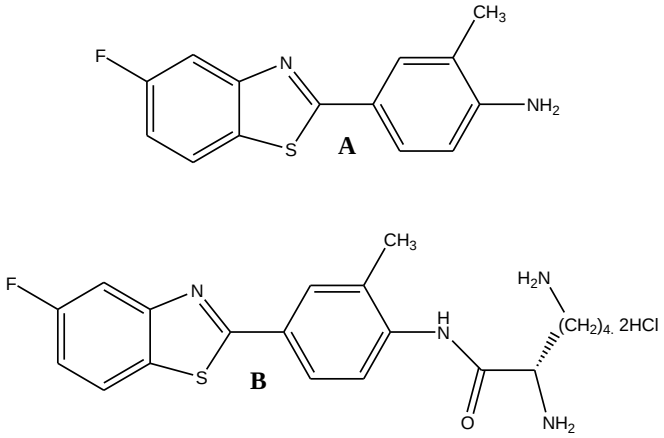

Figure 21. Structures of 5F 203 (A) and NSC 710305 (B)

The exact structures of the metabolites of phortress produced by CYP1A1 are yet to be established but the results of frontier molecular orbital studies have suggested the possible generation of nitrenium species. These structures suggest that nucleophilic centres in DNA bases might form adducts at the exocyclic nitrogen (via 1), or at carbon atoms in the 2-aryl group (via 2) or the benzothiazole moiety (via 3) (Figure 22).[178] Phortress (NSC 710305) is currently in clinical trials and further reports are awaiting publication.

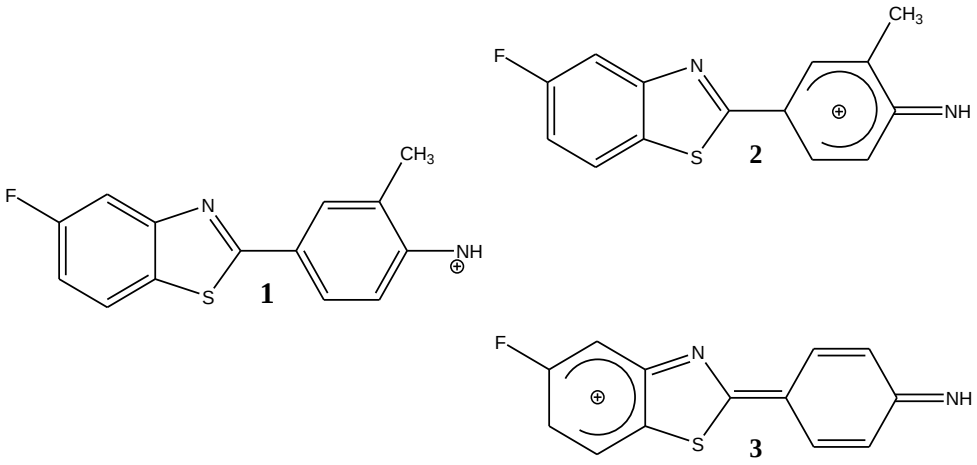

Figure 22. Possible DNA binding sites with DF 203 metabolites

1.9 Endogenous Steroids and the Development of Anticancer Prodrugs

17β-estradiol is an endogenous human steroid which is metabolised by both CYP1A1 and CYP1B1, which have also shown to be over-expressed in tumours.[179] CYP1A1 hydroxylates 17β-estradiol at the C-2, C-6 and C-15 positions. CYP1B1 hydroxylates 17β-estradiol at the

C-4 position, and to a lesser extent at C-2. CYP1B1 is the most catalytically efficient of the estradiol hydroxylases as indicated by its low K_m for 17β-estradiol, as a lower K_m value indicates a higher affinity of the substrate for the enzyme.[180, 181, 182]

Many naturally occurring phytoestrogens such as flavonoids, isoflavonoids, stilbenes, coumestans and lignans can be mapped on to the steroidal framework of estradiol.[183, 184]

Compounds which share structural similarities to estradiol may in fact possess potential anti-tumour ability. This can be an important tool in finding potential anti-cancer prodrugs which may be able to undergo CYP1 metabolism to toxic metabolites when reaching tumour sites. This can be determined by screening probable compounds against tumour cells and their corresponding normal tissues. Toxicity exclusive to tumour cells may be due to CYP1 metabolism of the compound. Metabolite structures can also be predicted as the CYP1 mediated metabolites of estradiol are known.

1.9.1 Resveratrol

Resveratrol (3,5,4'-trihydroxystilbene) (Figure 23 B) was first isolated from the roots of the White Hellebore (*Veratrum album*) plant. It is also present in red wine, grapes, peanuts and mulberries. In 1997 *Jang et al* published a paper showing resveratrol to be an effective agent for blocking the initiation, promotion and progression of carcinogenesis.[185] Since then, the anti-cancer properties of resveratrol have been established on a range of cancers, including breast, prostate, colon, pancreatic, ovarian and thyroid cancers. It has been suggested that the anti-cancer ability of resveratrol occurs through the initiation of apoptosis and cell cycle arrest in the S and G_2 phases of the cell cycle.[186, 187] The topical application of resveratrol was found to significantly reduce 7,12-dimethylbenz[*a*]anthracene (DMBA) initiated and 12-*O*-teradecanoylphorbol-13-acetate (TPA) promoted skin tumours in female mice. Growth arrest in human epidermoid carcinoma (A431) cells was observed when these were treated with resveratrol. A down-regulation in the expression of cyclins D1, D2 and D3 was detected together with the inhibition in the expression and activities of CDKs 2, 4 and 6 and an up-regulation of p21WAF/CIPI. A reduction in hyperphosphorylated Rb protein and decrease in E2F transcription factor expression were also observed. A number of other benefits have been reported for resveratrol. These include cardio-protective, anti-oxidant, anti-inflammatory and anti-infective properties.[188, 189]

Potter et al of the Cancer Drug Discovery Group (CDDG) studied the CYP1B1 metabolism of resveratrol and proposed that it is hydroxylated ortho to the 4'-hydroxyl group by CYP1B1 generating piceatannol (Figure 23, D).[190] This was achieved by mapping resveratrol on to estradiol (Figure 23, A), for which the CYP1B1 mediated metabolism is known to produce 4-hydroxyestradiol (Figure 23, B).

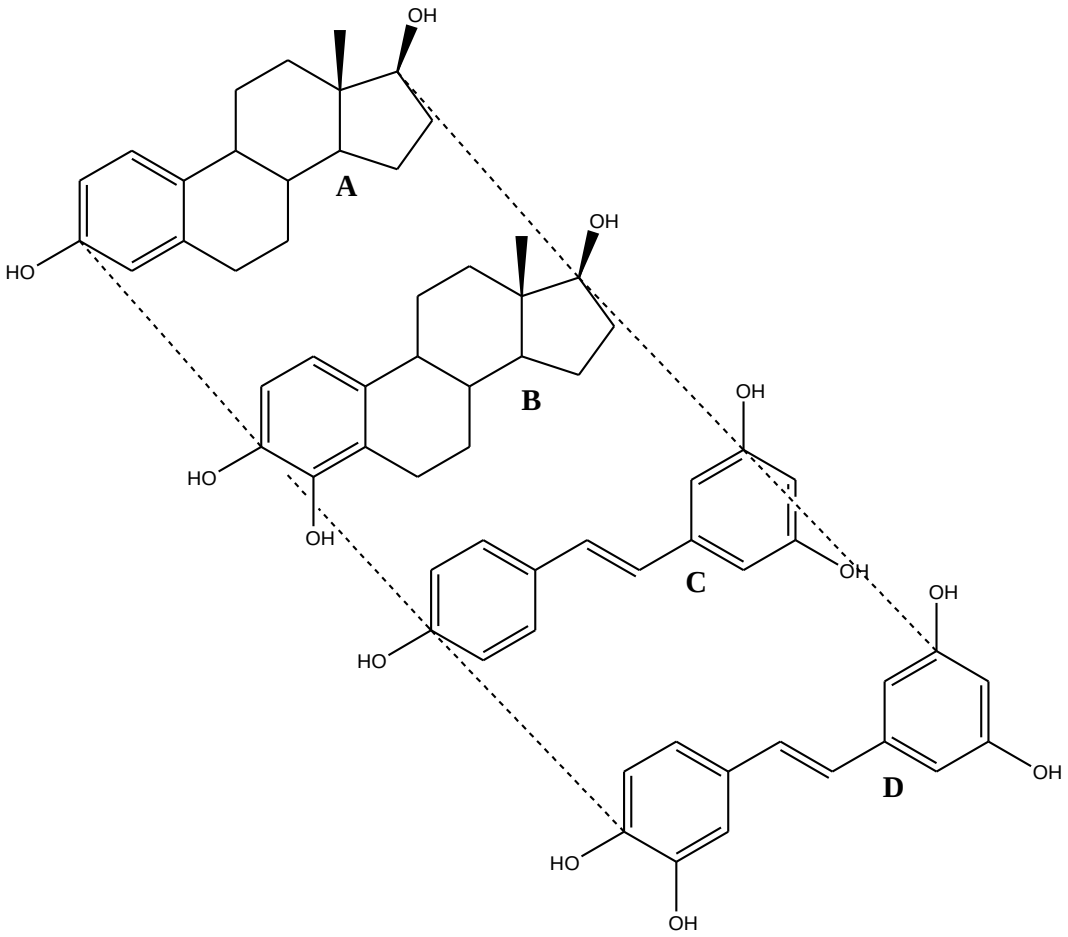

Figure 23. Estradiol (A) mapped with 4-hydroxyestradiol (B), resveratrol (C) and piceatannol (D)

To prove the hypothesis, the metabolism of resveratrol by CYP1B1 was carried out using a microsomal preparation of the human CYP1B1 enzyme. Using HPLC analysis with fluorescence detection the formation of two major metabolites (M1 and M2) and one minor metabolite M3 were observed. M1 has been suggested to be 3,4,5,4'-tetrahydroxystilbene formed through the hydroxylation of the other aromatic ring and M3 is thought to be 3,4,5,3',4'-pentahydroxystilbene. Most importantly, the major metabolite M2 was identified as piceatannol 3,4,5’,4'-tetrahydroxystilbene.

Piceatannol is a known naturally occurring compound and has exhibited anti-leukemic properties, demonstrating an ability to inhibit a variety of tyrosine kinases involved in cell proliferation; including those involved in the phosphorylation of DNA transcription factors and tubulin. Due to their findings, *Potter et al* proposed that CYP1B1 functions as a "rescue enzyme" due to its over-expression in tumours and ability to metabolise resveratrol to the anti-tumour piceatannol. Therefore, CYP1B1 can be targeted by potential prodrugs which would only become toxic once present in tumour cells over-expressing the CYP1B1 enzymes. Another relevant finding is that CYP1B1 is expressed in skin cells exposed to mutagenic UV light. The skin tumour reduction observed in mice by the topical application of resveratrol may be due to the formation of the CYP1B1 metabolite piceatannol, backing the theory for the role of this enzyme as a "rescue enzyme".

Contrary to the findings of *Potter et al*, it has been suggested that resveratrol is an inhibitor of CYP1A1, CYP1B1 and CYP1A2, and is also an antagonist of the AhR receptor. This theory implies that CYP1 enzymes help promote tumour development via the metabolism of PAHs to carcinogenic species. However, it is also known that carcinogens are metabolised by CYPs to make them into excretable species and the inhibition of these enzymes would cause the bioaccumulation of toxic species.

Nonetheless, resveratrol is currently in phase I clinical trials being tested against colon cancer in the USA.

1.10 Stilbenes and Chalcones as CYP1 Activated Prodrugs

The Cancer Drug Discovery Group (CDDG) of the Leicester School of Pharmacy has developed and patented a number of low molecular weight anti-cancer prodrugs.[191] They were designed to be metabolised by CYP1B1 as this is enzyme is a particularly attractive target for anticancer prodrugs, as it is often over expressed in tumours but rarely found in normal tissue.

The stilbene DMU 212 (Stilserine) was found to overlay the structure of estradiol by structural mapping, in the same fashion as resveratrol and its metabolites were investigated (Figure 24). Exciting cytotoxicity was observed for DMU 212, which was screened against tumour cell lines characterised for their CYP1 enzyme expression. Included was an IC_{50} value of 0.001μM observed against the MDA 468 cells, which constitutively expresses CYP1A1 and CYP1B1. DMU 212 is currently undergoing evaluation prior to clinical trials.

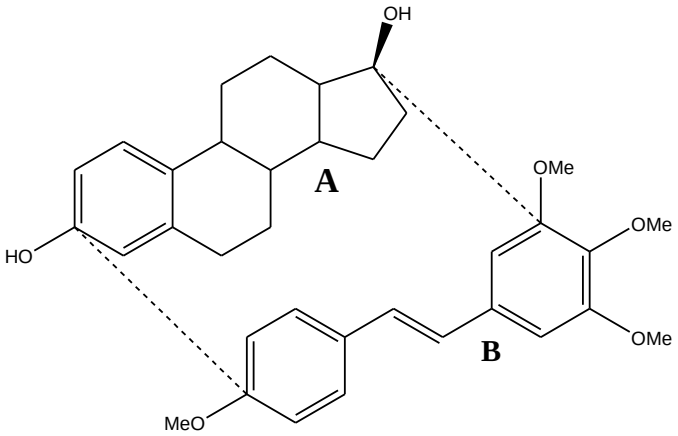

Figure 24. Estradiol (A) mapped with DMU 212 (B)

Chalcones exhibiting anti-tumour abilities have also been investigated by the CDDG. Numerous chalcones have been shown to occur naturally and have been of interest since the establishment of their many benefits, including anti-cancer, anti-malarial, and anti-inflammatory properties.[192] They consist of two phenyl rings connected by a three carbon link which is α, β-unsaturated. The chalcone DMU 135 was designed to be activated by CYP1B1, over-expressed in tumour sites. The non toxic prodrug DMU 135 is activated to the catechol DMU 117 (Figure 25), a broad spectrum potent tyrosine kinase inhibitor that has been shown to shut down greater than 30% of all cellular tyrosine kinase activity.[193]

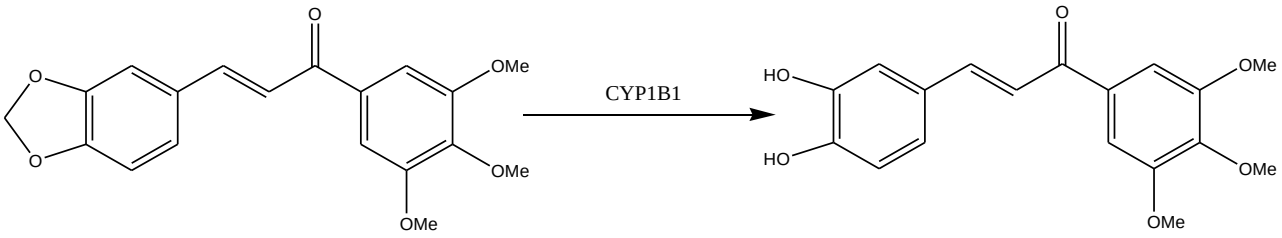

Figure 25. Bio-activation of DMU 135 to DMU 117

Studies on $Apc^{Min/+}$ mouse gastrointestinal adenoma, an effective model for colorectal cancer showed that DMU 135 considerably reduced multiplication of tumours by 18.3% and showed no systematic side-effects. It has been reported that tyrosine kinase activity is essential for adenoma development in the $Apc^{Min/+}$ mouse.

1.11 Heterocyclic Analogues of Chalcone Prodrugs

1.11.1 *Cis* and *Trans* Isomerisation of Chalcones

Chalcones can exist as either *cis* or *trans* isomers as the α,β-double bond is labile for photoisomerisation.[194] In general, the *trans* isomer is thermodynamically more stable and chalcones are usually isolated in this isomeric form. Photoisomerisation occurs as *trans* isomers absorb ultra-violet (UV) or visible light exciting an electron in the pi bonding molecular orbital to a pi-star anti-bonding orbital, yielding the *cis* isomer.[195,196]

It has been shown that the rate of isomerisation and the equilibrium ratio depend on the substitutions on the aromatic rings and the solvents employed. It is also suggested that electron withdrawing groups and the chelating properties of the substituents in the 2-position have a significant effect on the degree of isomerisation. However, this theory is countered by researchers who have stated it is not possible to predict chalcone isomerisation. It was accepted that both these isomers were equipotent in their toxicities, but this was investigated by locking known anti-plasmoidal chalcones in *cis* and *trans* isomers and evaluating their activity. It was found that the *trans* locked isomer was the more active isomer, and the *cis* locked compounds showed virtually no activity.

The cytotoxicities of the *cis* and *trans* isomers of DMU 407 and DMU 102 were investigated by the CDDG (Figure 26).[197] They were screened against the CYP1 enzyme expressing MDA 468 tumour cell line and the non-tumour control cell line of MCF10A which has no basal CYP1 expression. It was found that the cytotoxicities of the *trans* isomers were greater than that for the *cis* chalcones for both DMU 407 and DMU 102 when screened against the MDA 468 tumour cell line.

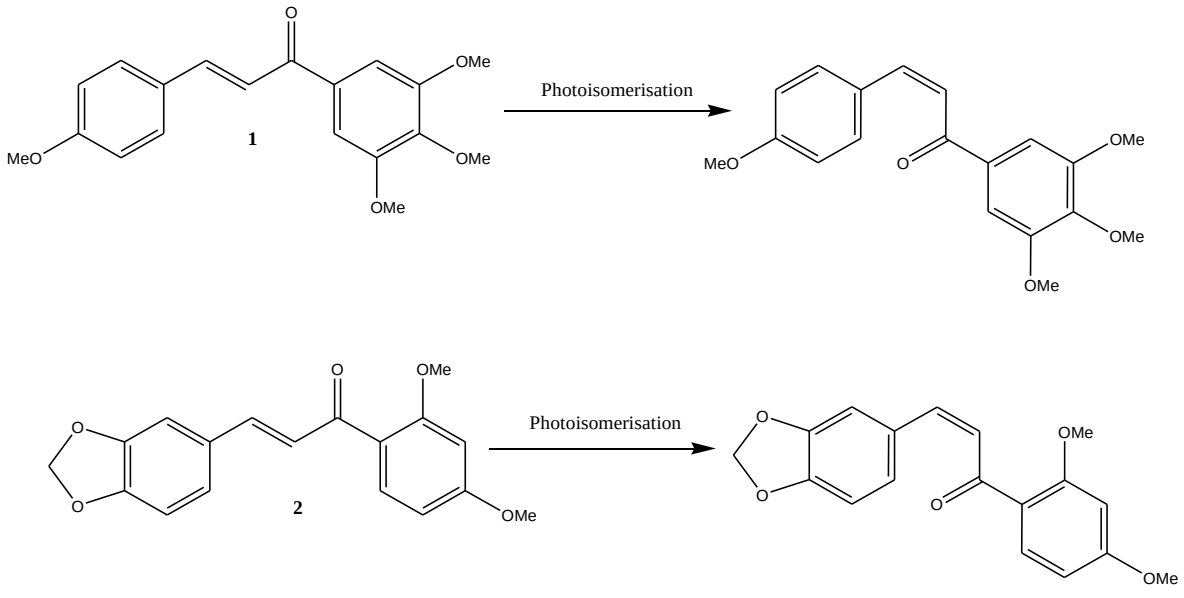

Figure 26. Photoisomerisation of DMU 102 (1) and DMU 407 (2)

To eradicate the problem of *cis* isomerisation occurring, heterocyclic ring systems can be incorporated into chalcone prodrugs (Figure 27). This can be achieved by modifying the α,β-double bond moiety of the chalcones, as this region is susceptible to nucleophilic attack by suitable nucleophilic reagents. The ring system would result in a more rigid compound maintaining the key functionalities of the chalcones by keeping the substituted phenyl groups in a *trans* like geometry.

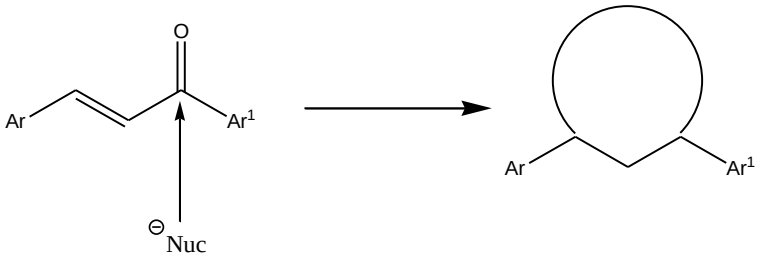

Figure 27. Integration of ring systems across the chalcone

1.12 Aims

The primary aim of this project will be to modify chalcones to prevent the problematic factor of photoisomerisation occurring. This will be achieved by incorporating heterocycles across the α,β-double bond of the chalcones which will lock the phenyl groups in a *trans* like geometry. Heterocycles will be synthesised by reacting chalcones with selected heteroatom nucleophiles, to generate variant libraries of heterocyclic compounds. This approach is favourable as the carbonyl of the chalcone is a receptive nucleophilic attack site, which in turn will provide the foundation for the heterocyclic ring construction.

The synthesised heterocyclic compounds will be screened against tumour cell lines characterised for their constitutive or inducible CYP1 expression. Cytotoxicity data will be compared throughout the libraries of compounds with the development of structure activity relationships being formulated. Resultant compounds with encouraging or significant toxicities will be investigated further to determine whether they are genuine CYP1 substrates. If successfully identified as CYP1 substrates, further studies involving the determination of possible metabolites formed will be made, from which proposed metabolites will be synthesised. Verification of the authenticity of the proposed metabolites will be investigated using LCMS techniques.

Chapter 2

Synthesis and Biological Evaluation of 3,5-Diarylpyrazoles

2.0 Synthesis of 3,5-Diarylpyrazoles via Chalcones and EpoxyChalcones

To overcome the problem of chalcones undergoing photoisomerisation reactions, pyrazole heterocycles were introduced across the α,β-unsaturated region of chalcones locking the phenyl groups in a *trans* like geometry (Figure 28). Pyrazoles are five membered heterocyclic rings consisting of three carbon atoms and two adjacent positioned nitrogen atoms.

LeBlanc et al synthesised a library of pyrazoles from chalcones in good yields which were screened against B16 melanoma and L1210 leukemia cells.[198]

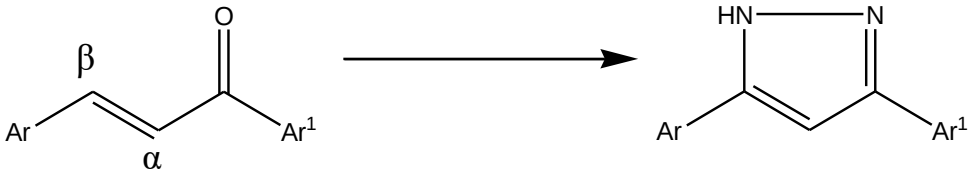

Figure 28. Incorporation of a pyrazole heterocycle across the α,β-unsaturated region of the chalcone

Bhat et al also synthesised pyrazole analogues from chalcones which were shown to exhibit anti-tumour activity on a number of cancer cell lines including colon, lung, liver, ovary, cervix and prostate.[192] Results from cytotoxicity assays of these compounds were encouraging, with IC_{50} values including 0.48μM observed from the lead compound 4n (Figure 29) when screened against the colon tumour cell line HCT-15. This was a 25 fold increase in toxicity when compared to its chalcone derivative.

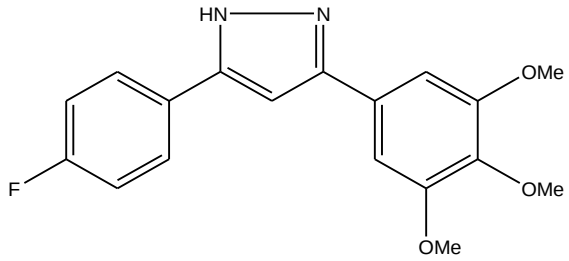

Figure 29. Structure of compound 4n synthesised by *Bhat et al*

Another route available for the synthesis of pyrazoles includes the conversion of diketones (Figure 30), which are treated with hydrazine hydrate in a one step reaction which forms the pyrazole heterocycle.[76, 199]

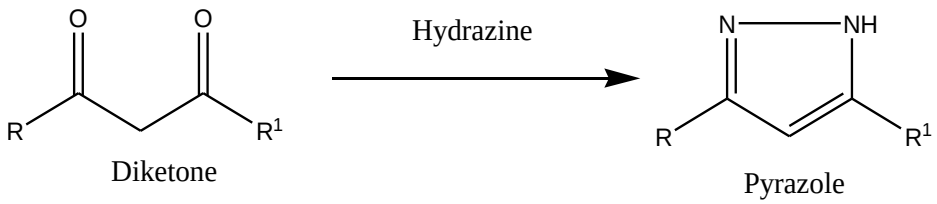

Figure 30. Formation of a pyrazole from a diketone

The diketone conversion has been demonstrated by *Shaw et al*, who cyclised diketones with hydrazine to afford a range of substituted pyrazoles. They screened their library of compounds against four tumour cell lines, which were ovarian carcinoma cells (OVCA), colorectal adenocarcinoma cells (SW620), large lung carcinoma cells (H460) and gastric carcinoma cells (AGS). From the cytotoxicity results observed, they established compound 26 (Figure 31) to be their lead compound as it displayed the most potent activity against the OVCA, SW620, H460 and AGS cells, with IC_{50} values of 0.67, 0.89, 0.73 and 0.79 µM respectively.

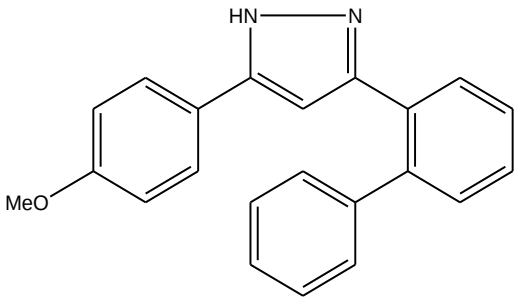

Figure 31. Structure of the lead pyrazole 26 synthesised by *Shaw et al*

Pyrazoles have also been shown to be synthesised from intermediary epoxychalcones formed through the treatment of chalcones with hydrogen peroxide.[198] Epoxychalcones are then reacted with hydrazine to form the pyrazole heterocycle (Figure 32).

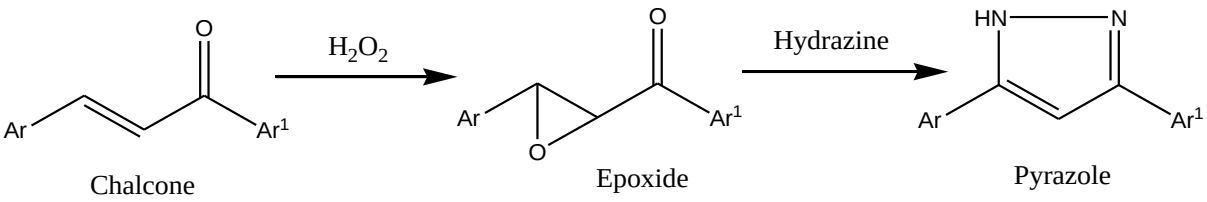

Figure 32. Pyrazole synthesis from a chalcone via an epoxide

Two separate reaction conditions have been reported for the synthesis of pyrazoles via epoxychalcones, one by *LeBlanc et al* and the other by *Bhat et al*. For the synthesis of pyrazoles in this project, the method by *LeBlanc et al* will be used as yields of up to 94% were reported in their synthesis.

2.1 The Synthesis of Chalcones

The chalcones synthesised were selected based on their cytotoxicity results obtained by the CDDG in previous experimentations. DMU 135 was included in the selected chalcones which gave an IC_{50} value of 0.09µM when screened against the MDA 468 cell line which constitutively expresses CYP1A1 and CYP1B1. IC_{50} values of 0.2µM and 0.03µM were recorded against the MCF7 cells which show no basal CYP1 expression and MCF7 cells induced with TCDD expressing CYP1A1.

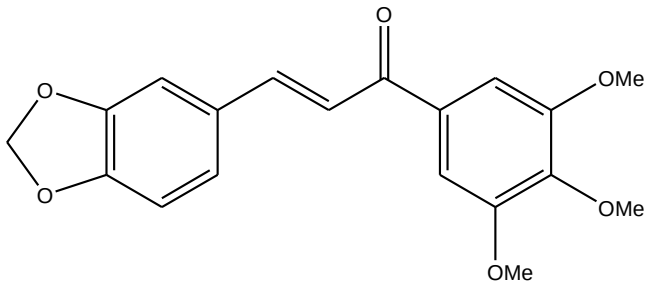

Figure 33. Structure of DMU 135

A number of reactions have been used to synthesise chalcones, but the most common approach is the Claisen-Schmidt condensation (CSC) reaction (Figure 33).[200] This generally involves the reaction of equimolar quantities of benzaldehydes and acetophenones in alcoholic basic conditions. Common bases used for this reaction are sodium and potassium hydroxide, added either as solids or as aqueous solutions.[201] Typically the reaction is carried out at room temperature with either methanol or ethanol as the solvent. When a phenolic group is present the CSC reaction is often slow and may require heating to proceed. Protecting the phenolic group as a tetrahydropyranyl (THP) ether using a 3,4-dihydro-2H-pyran protecting group eliminates this problem, and has been shown to prepare several polyphenolic chalcones using barium hydroxide as a base.[202]

An acid catalysed version of the CSC reaction also exists.[203, 204] Several acids, and lewis acids, have been used including hydrogen chloride, sulfuric acid and aluminium trichloride. Solvent free reactions using metal oxide catalysts impregnated onto zeolites and alumina have also been reported.[205, 206]

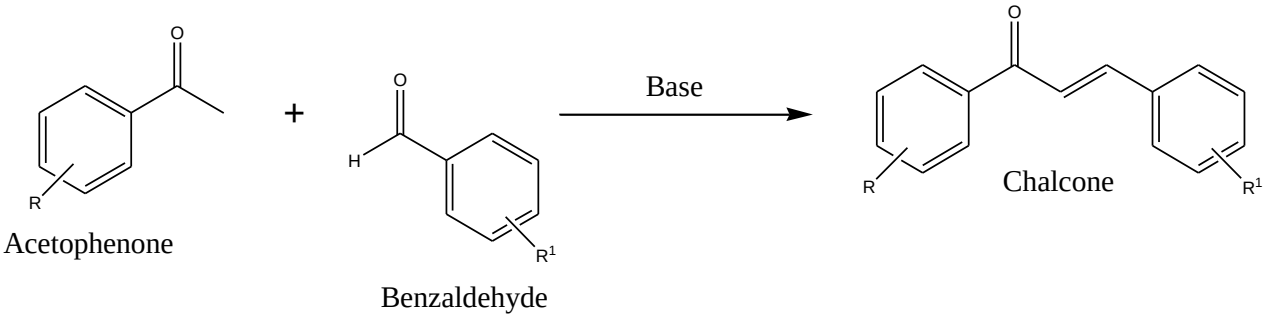

Figure 34. The Claisen-Schmidt condensation reaction

The mechanism for the chalcone formation via the CSC reaction begins with the formation of an enolate ion of the acetophenone (Scheme 3). This occurs as the base abstracts an α proton from the acetophenone forming a resonance stabilised enolate. With bases such as sodium hydroxide, this equilibrium process lies very much towards the acetophenone side, however, sufficient enolate is generated for the reaction to proceed. The benzaldehyde cannot undergo enolisation as it does not have α protons. The nucleophilic enolate attacks the carbonyl of the benzaldehyde forming an intermediate β-hydroxy ketone or aldol. Although this intermediate can be isolated the reaction is generally allowed to proceed. The abstraction of an α-proton from the aldol generates another enolate which undergoes dehydration, via a conjugate base elimination mechanism to yield the chalcone. This elimination occurs in a regio-specific manner forming the *trans* or *(E)*-isomer of the chalcone exclusively.

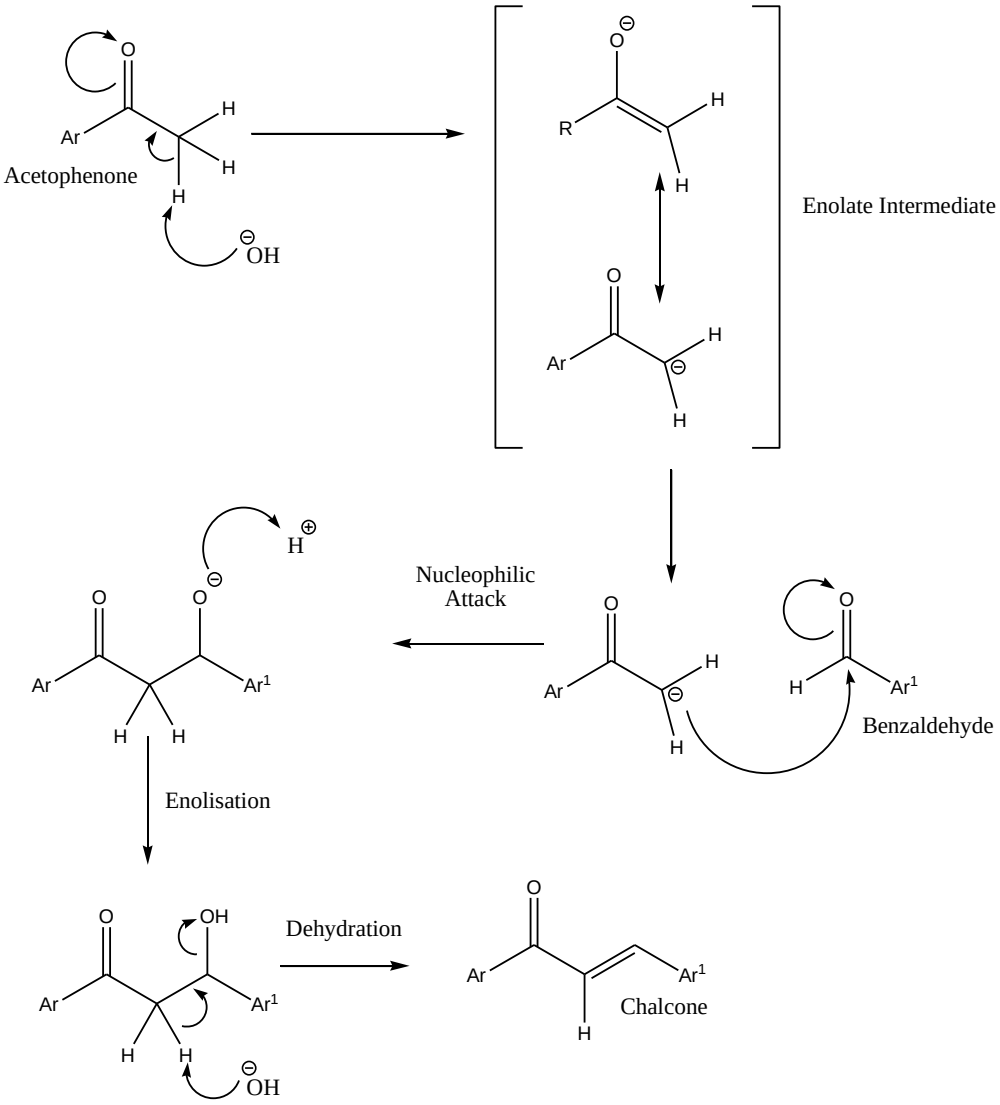

Scheme 3. Mechanism for the base catalysed CSC reaction to produce chalcones

Table 2. Synthesised chalcones

Entry	DMU No.	Structure	% Yield	mp °C	Appearance
1	2210	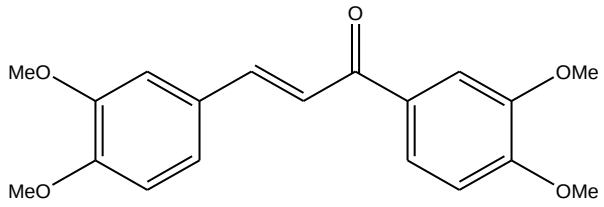	74	111-113	Yellow Crystals
2	1113	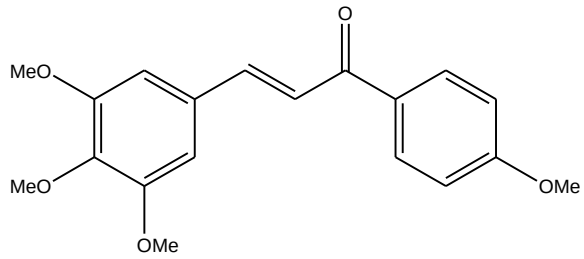	75	133-135	Yellow Crystals
3	2300	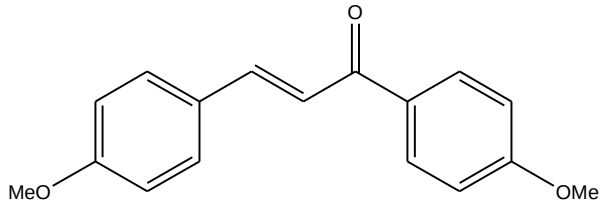	68	107-109	Yellow Crystals
4	135	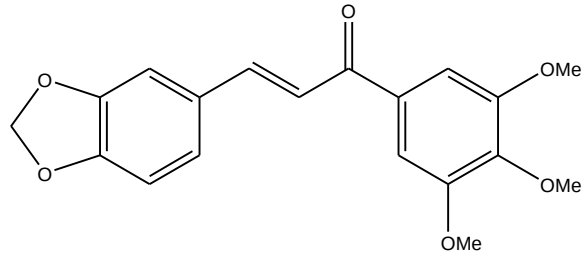	65	133-135	Yellow Crystals
5	2301	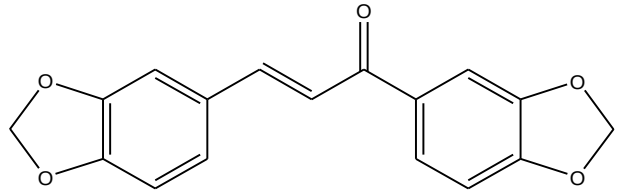	69	132-134	Yellow Crystals

6	160	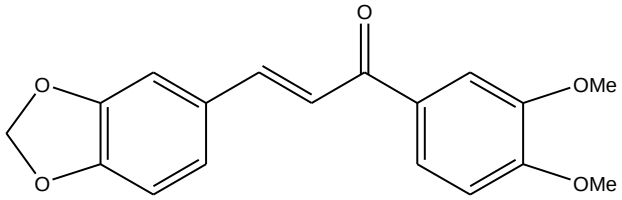	68	137-139	Yellow Crystals
7	419	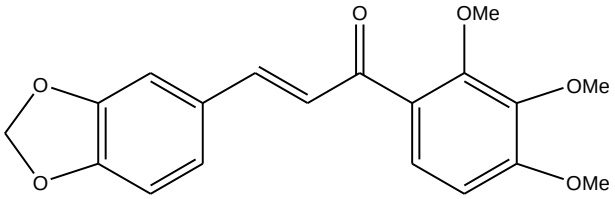	65	101-103	Yellow Crystals
8	407	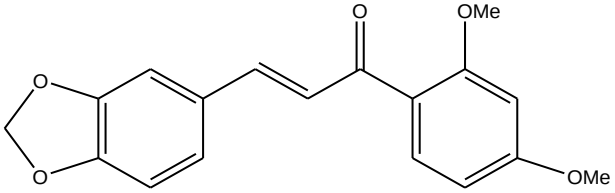	88	121-123	Yellow Crystals
9	423	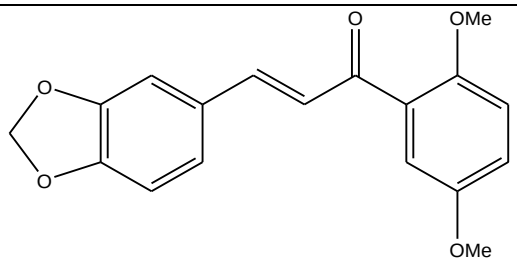	83	111-113	Yellow Crystals
10	2302	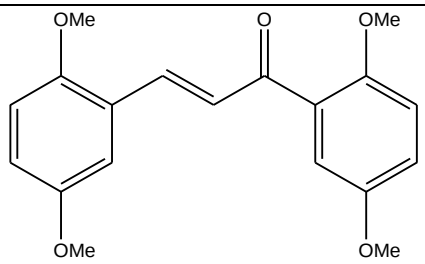	92	-	Oil
11	2303	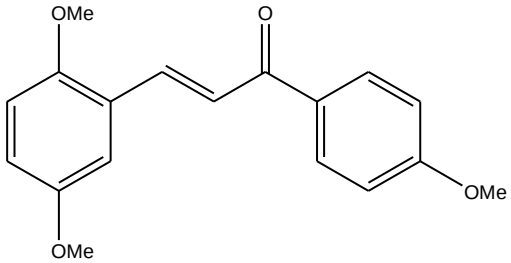	94	-	Oil

12	2304	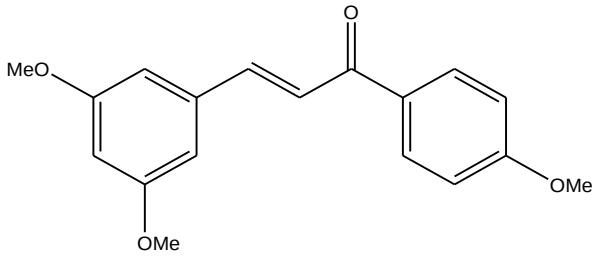	94	79-81	Yellow Crystals
13	2265	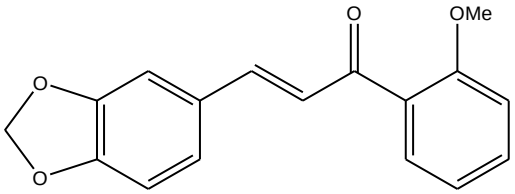	77	121-123	Yellow Crystals
14	2305	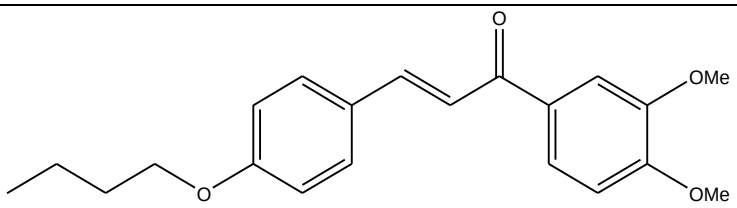	65	125-127	Yellow Crystals
15	2306	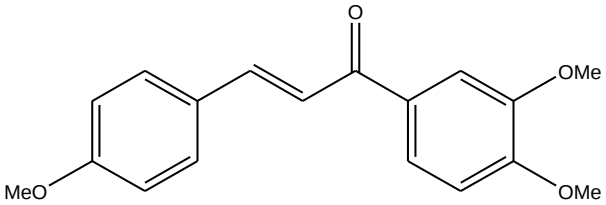	66	89-91	Yellow Crystals
16	2307	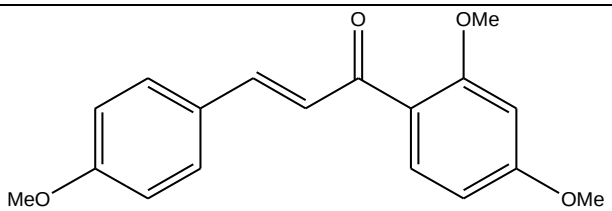	76	101-103	Yellow Crystals
17	102	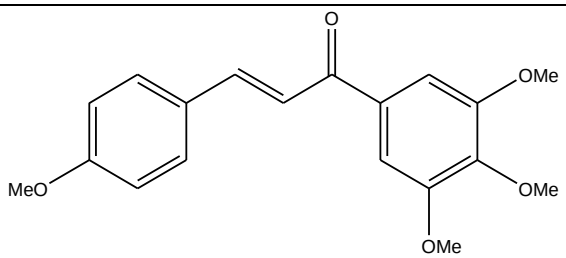	70	65-67	Yellow Crystals

18	2222	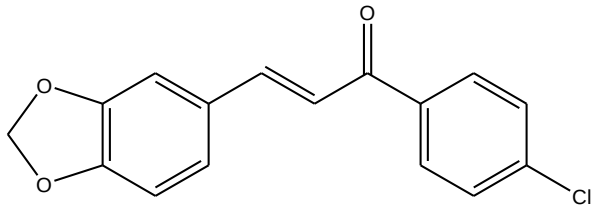	90	126-128	Yellow Crystals
19	2308	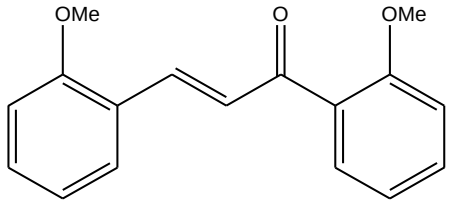	88	-	Oil
20	2309	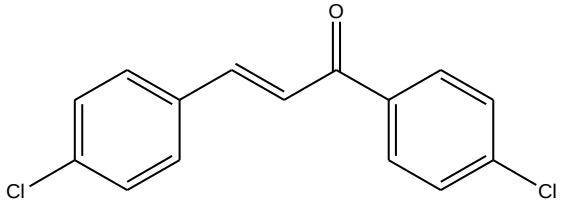	81	147-149	Yellow Crystals
21	2216	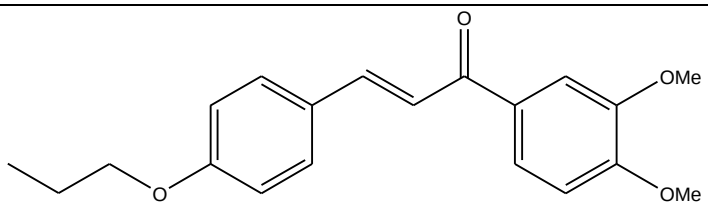	72	103-105	Yellow Crystals
22		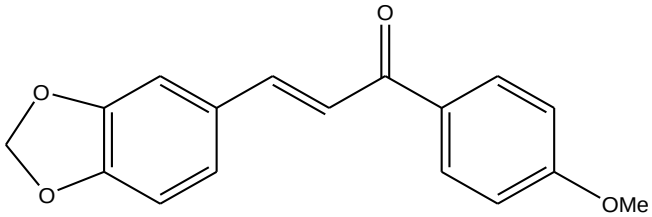	84	126-128	Yellow Crystals
23		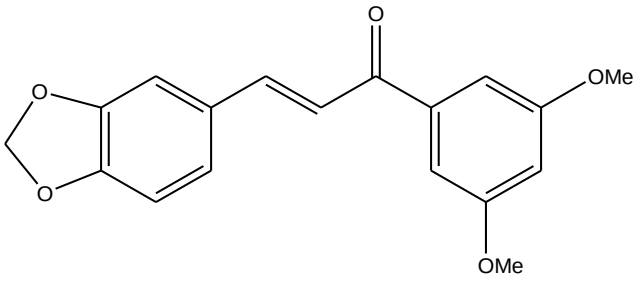	79	104-106	Yellow Crystals

24		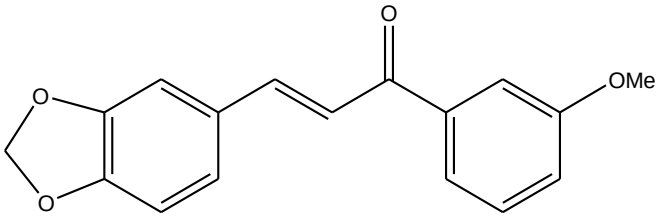	77	81-83	Yellow Crystals

All chalcones in Table 2 were synthesised in this project, using the base catalysed CSC reaction. Equimolar amounts of appropriate benzaldehydes and acetophenones were stirred in methanol at room temperature until fully dissolved. A twenty fold excess of aqueous NaOH (50% w/v) was added to the solution resulting in an instant colour change from colourless to yellow. Reactions were closely monitored by thin layer chromatography (TLC), and the chalcone was identified as a new bright orange spot when stained with 2, 4-dinitrophenylhydrazine (2,4-DNP). Reactions usually reached completion in less than four hours, as indicated by the disappearance of starting materials upon TLC analysis. Water was added to quench the reaction and the resulting mixture was extracted with dichloromethane (DCM). The organic extracts were combined and dried over $MgSO_4$. The solvent was removed *in vacuo* resulting in the crude chalcone. Solids were recrystallised from either ethanol or methanol depending on the solubility of the chalcone. In three cases (Table 2, entries 9, 10 and 18), oils were obtained on removal of the solvent. These products were purified by flash chromatography on silica gel using a mixture of ethyl acetate and hexane (4:6) as eluent.

Twenty four chalcones were synthesised in good yields ranging from 65% to 94%. In each case analytical data was consistent with the proposed structures. Nuclear magnetic resonance (^{1}H NMR) confirmed the *trans* nature of the alkene double bonds which appeared as doublets between 7.40 and 7.60 ppm. Coupling constants were measured between 11-19Hz, typical for *trans* alkene protons as they range between 12-18Hz, whereas *cis* isomers range between 0-12Hz.[207] In accordance, no *cis* isomers were detected in any of the spectra analysed. Mass spectrometry (MS) gave either M^+ or $(M+1)^+$ ion peaks of correct mass, and infra-red (IR) spectra showed strong absorptions in the 1690-1750 cm^{-1} region consistent with the α,β-unsaturated carbonyl group of a chalcone. All chalcones, apart from the three yellow oils, produced yellow crystals with melting points in the range of 66-148^{o}C.

2.2 The Synthesis of Epoxychalcones

The next stage in the synthetic route to the pyrazoles required the synthesis of epoxychalcones. Epoxides are important and versatile building blocks in organic synthesis commonly used as intermediate reagents for the synthesis of natural products.[208] Epoxychalcones are prepared by reacting hydrogen peroxide with chalcones, as shown in Scheme 4. Electrophilic epoxidising agents, such as *m*-chloroperbenzoic acid (MCPBA) give poor oxidising results with electron deficient double bonds such as those in chalcones, therefore making hydrogen peroxide the best reagent in this case.[209]

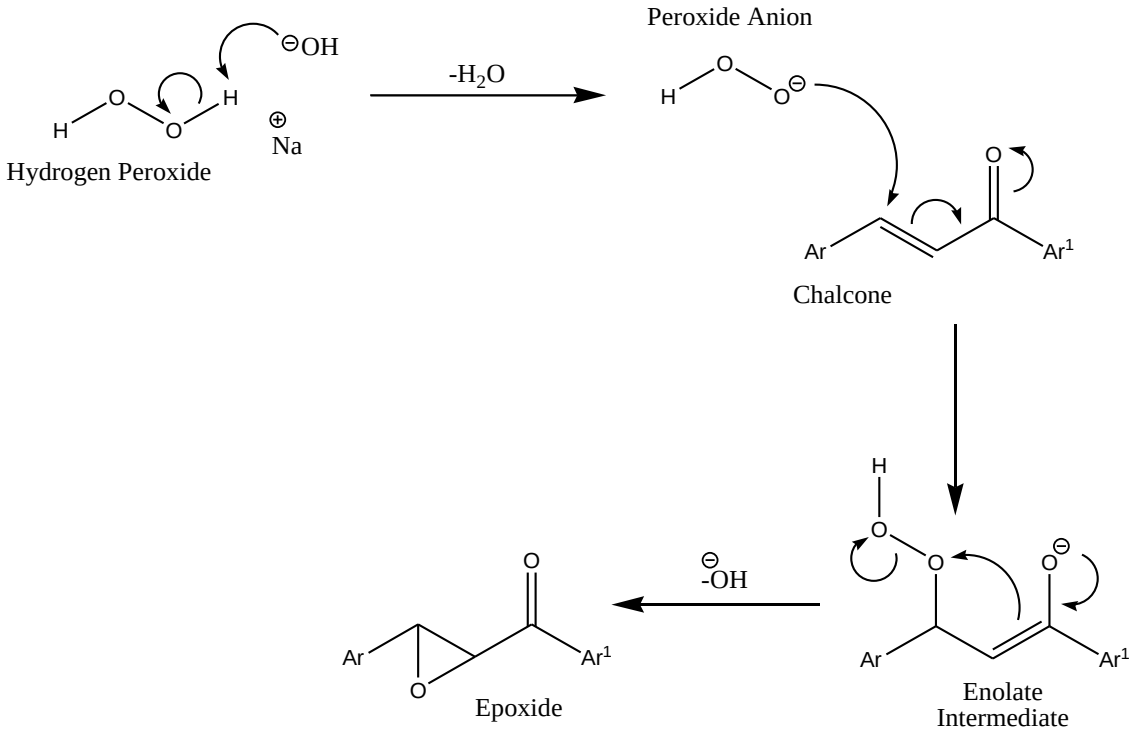

Scheme 4. Mechanism for the epoxidation of chalcones using alkaline hydrogen peroxide

The mechanism for the chalcone epoxidation (Scheme 4) initiates with the abstraction of a proton from hydrogen peroxide by NaOH, forming a hydroperoxide anion. The soft hydroperoxide nucleophile then undergoes conjugate addition to the chalcone generating an unstable enolate. The enolate intermediate undergoes intramolecular cyclisation to form the epoxychalcone with the loss of an OH group.

The procedure used to synthesise compounds shown in Table 3 was the same as that used by *LeBlanc et al* in their synthesis of heterocyclic analogues of the combretastatins.[198] Potassium carbonate (3 equivalents) and hydrogen peroxide (40 equivalents, 50% w/v) were added to a

stirred solution of the chalcone in methanol. As the epoxidation progressed a visible colour change from the characteristic chalcone yellow to off-white was observed. The reactions generally took 3 hours for completion as indicated by TLC analysis. Water was added to quench the reaction, followed by the addition DCM to extract the organic phase. The combined organic extracts were dried over $MgSO_4$ and the solvent removed *in vacuo* producing the crude epoxychalcones. Solids were recrystallised from either methanol or ethanol, resulting in white crystals. However, three compounds (Table 3, entries 4, 10 and 16) did not form solids but oils prior to and after recrystallisation.

Table 3. Synthesised epoxychalcones.

Entry	**DMU No.**	**Structure**	**% Yield**	**M.P ºC**	**Appearance**
1	10001	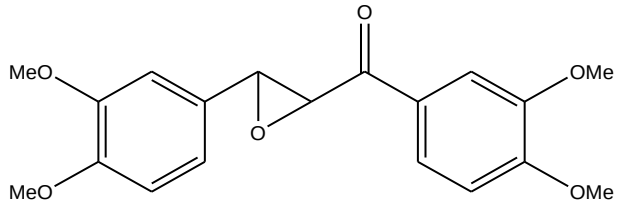	76	119-121	White Crystals
2	10002	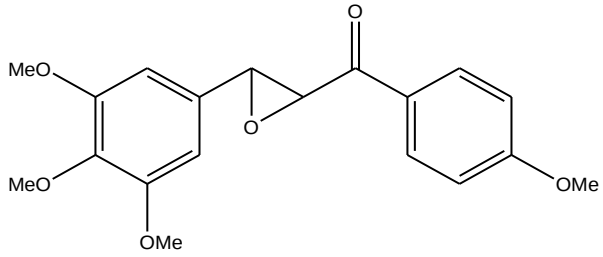	76	118-120	White Crystals
3	10003	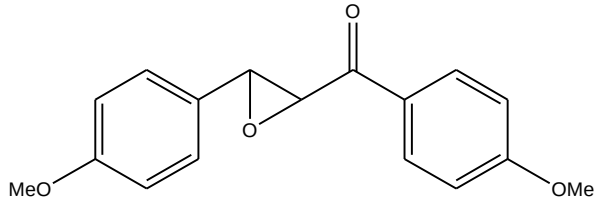	85	116-118	White Crystals

4	10004	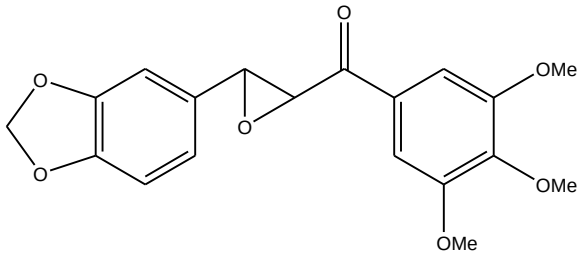	68	-	Oil
5	10006	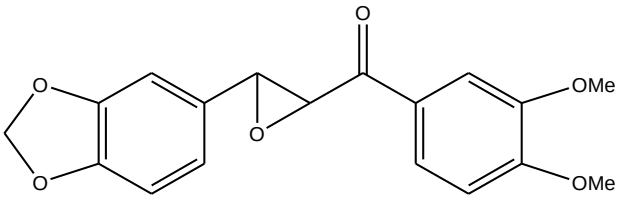	68	161-163	White Crystals
6	10007	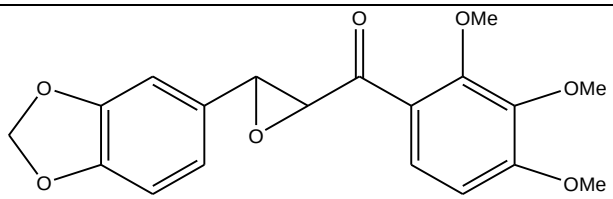	87	123-125	White Crystals
7	10008	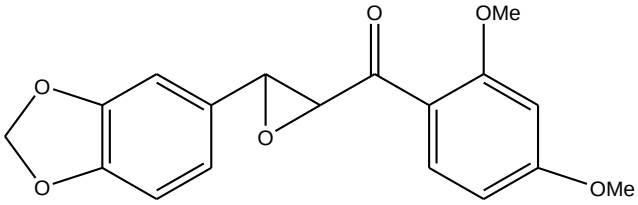	86	158-160	White Crystals
8	10009	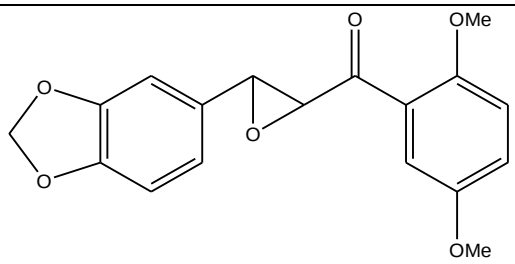	82	124-126	White Crystals
9	10010	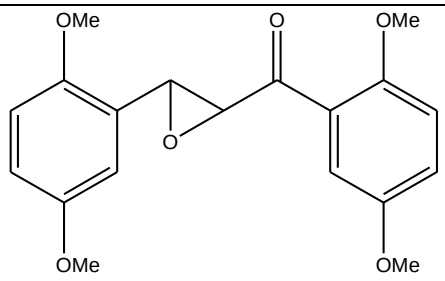	86	113-115	White Crystals

10	10011	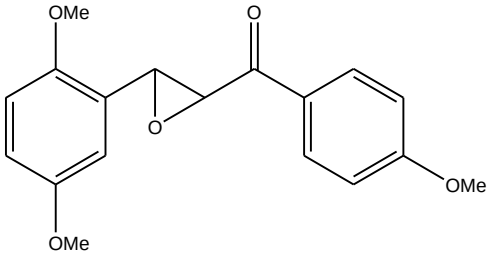	81	-	Oil
11	10012	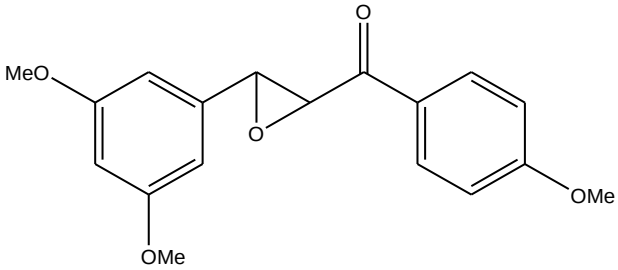	69	100-102	White Crystals
12	10013	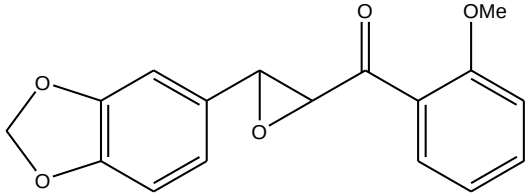	70	136-138	White Crystals
13	10014	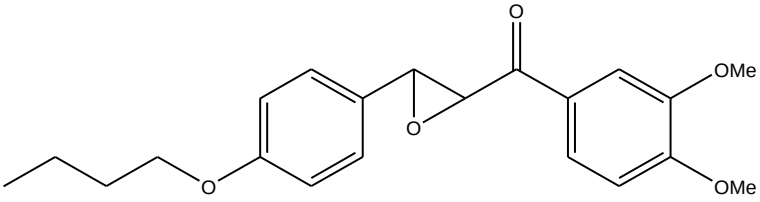	66	153-155	White Crystals
14	10016	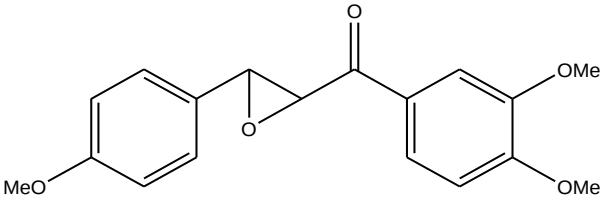	77	112-114	White Crystals
15	10017	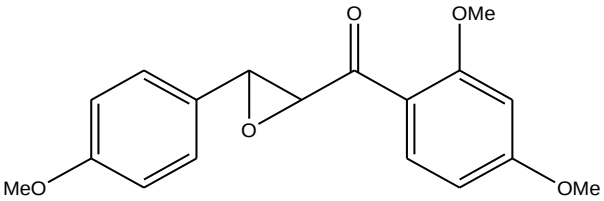	83	99-101	White Crystals

16	10020	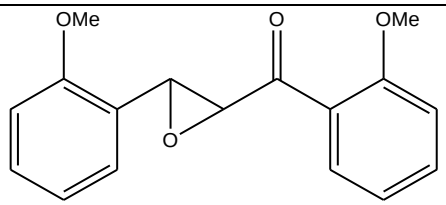	88	-	Oil
17	10021	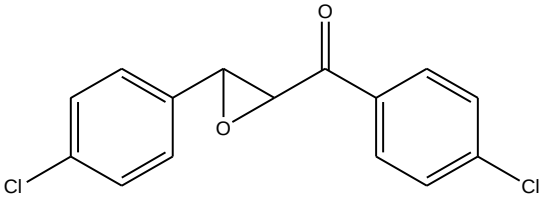	78	129-131	White Crystals
18	10023	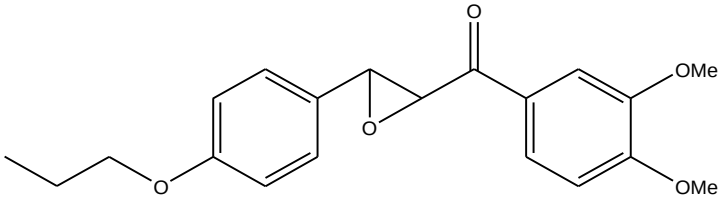	65	123-125	White Crystals

The epoxychalcones were synthesised with good yields ranging from 66 to 88%. The ^{1}H NMR spectra showed the epoxide ring protons appearing as doublets between 3.8 and 4.4 ppm. Coupling constants measured 3Hz, typical of *trans* epoxide protons (*cis* 4.5Hz).[210] MS showed $(M+1)^{+}$ peaks of correct ion masses, and IR spectra showed strong absorptions in the 1690-1750 cm^{-1} region corresponding to the presence of the carbonyl group. However, three chalcones (Table 2, entries 5, 17 and 18) proved to be unsuccessful in the epoxidation reaction. TLC analysis showed that the starting material was still present, demonstrating that the chalcones had not reacted with the peroxide. As there was no obvious explanation for these results the reactions were repeated but in each case gave the same unsuccessful outcome. *Zheng et al* synthesised epoxychalcones via chalcones using *t*-butyl-hydroperoxide as the oxidising agent. Problems encountered showed that the presence of an isopropyl group on the β-side of the chalcone did not allow epoxidation to occur, accrediting this problem to the bulkiness of the isopropyl group. [211] It was also found that electron donating groups decreased reaction activity and electron withdrawing groups had the opposing effect. Also,

para positioned substituent's on β-phenyl rings showed to influence yields as NO_2>Cl>Me, indicating electron withdrawing groups favour greater yields than electron donating groups.

The methoxy substituted A and B-rings of DMU 102 are electron donating by nature. As stated by *Zheng et al*, these groups have a negative effect on the epoxidation reaction which may be attributed by the resonance intermediates formed by DMU 102. The β-phenyl ring (A-ring) of DMU 102 also has the methoxy group in the *para* position, which can theoretically add to the negative reaction outcome based on the work of *Zheng et al* (Figure 35). These combined factors may act by lowering the reactivity of the α,β-unsaturated attack site of the peroxide.

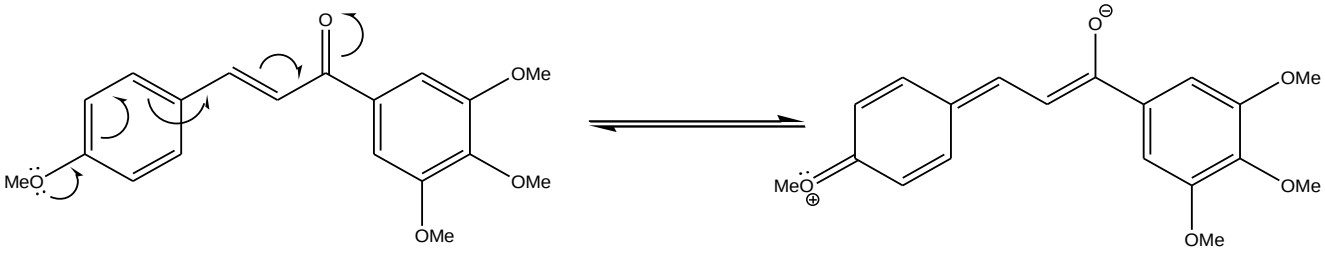

Figure 35. Possible intermediate formation by the para electron donating group of the A-ring

However, contrary to the above possible explanation for the non epoxidation of DMU 102, chalcones with *para* substituted electron donating groups on the B-rings have undergone successful epoxidation reactions (Table 2, DMU 2300 and DMU 2307). Therefore, the epoxidation reactions of DMU 2301, DMU 102 and DMU 2222 warrant further investigation to deduce the failing factor responsible for the unsuccessful reactions observed.

2.3 Synthesis of 3, 5-Diarylpyrazoles

The 3,5-diarylpyrazoles were designed to lock *trans* chalcone isomers in place by incorporating a pyrazole heterocycle across the α,β-unsaturated moiety of the chalcone. This reaction proceeded through epoxychalcone intermediates synthesised through the reaction of chalcones and hydrogen peroxide. It was anticipated that the conversion of the epoxychalcones to the desired 3,5-diarylpyrazoles could be achieved using the method of *LeBlanc et al* (Figure 36).

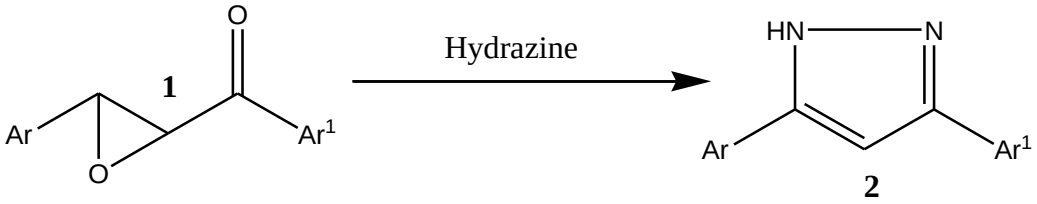

Figure 36. Epoxide conversion to the pyrazole

The method of *LeBlanc et al* required heating a solution of the epoxychalcone, hydrazine hydrate and *p*-toluenesulfonic acid in xylenes at reflux for 3h. The xylenes were removed *in vacuo* and the obtained solid was washed with hexanes. The mechanism for this reaction is shown below (Scheme 5). Under weak acidic conditions the hydrazine reacts with the carbonyl group of the ketone to form a hydrozone. Intramolecular cyclisation then occurs with the primary amine group of the hydrazone opening the epoxide ring to generate a pyrazoline. Protonation of the alcohol group is followed by elimination of water to generate the pyrazole ring.

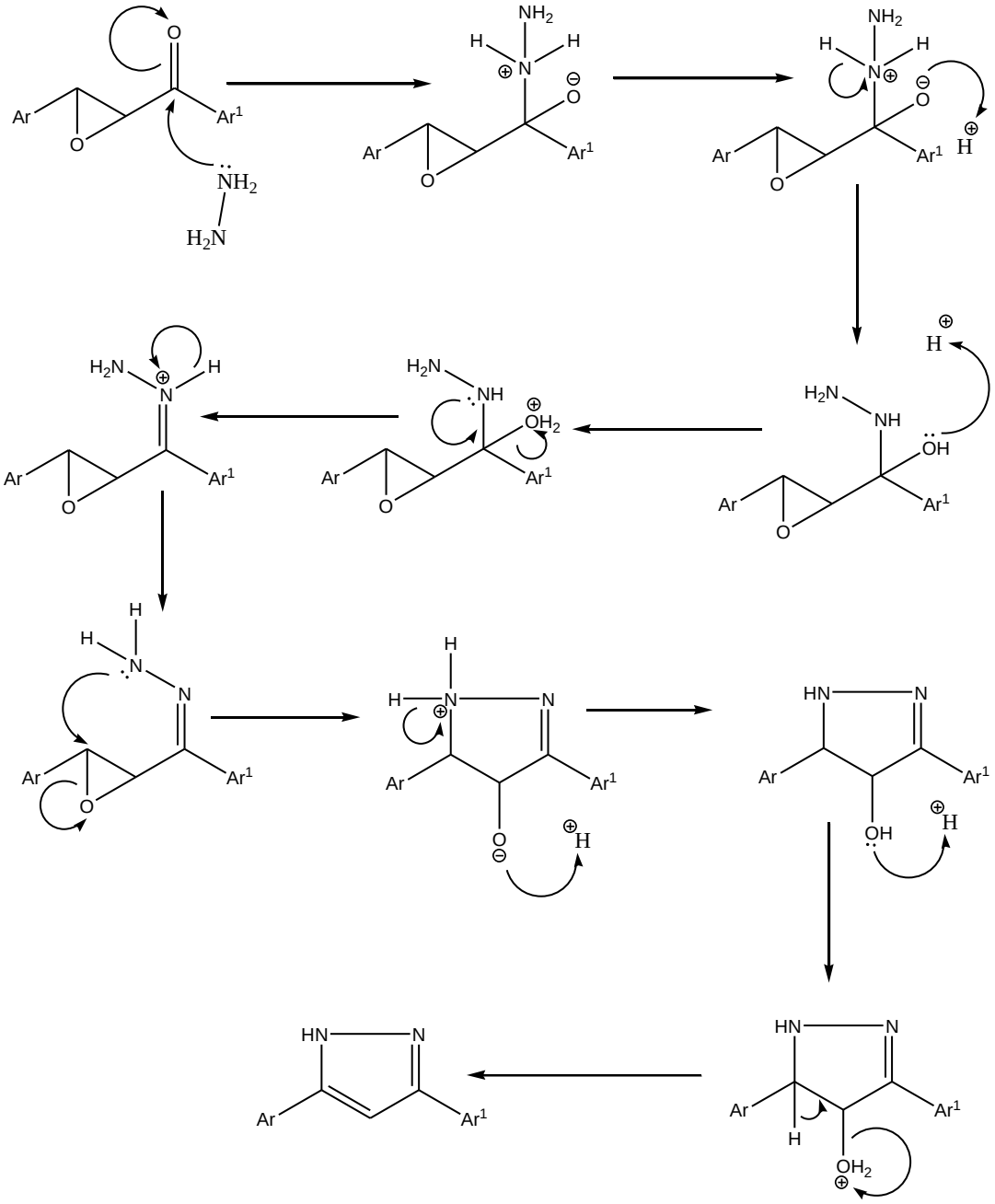

Scheme 5. Mechanism for conversion of the epoxide into the pyrazole

Therefore, the epoxychalcone DMU 10006 (Table 3, entry 5) was stirred in a mixture of DCM and xylenes until the epoxychalcone fully dissolved. The addition of DCM was required to fully dissolve the solid epoxychalcone which was insoluble otherwise. Hydrazine hydrate (3 equivalents) and a catalytic quantity of *p*-toluenesulfonic acid monohydrate were added to the solution which was heated at reflux for 3h. The solvent was removed *in vacuo* yielding a brown oil. Attempts to solidify this product by trituration with hexanes were unsuccessful. TLC analysis of the obtained oil showed the presence of the starting

epoxychalcone, therefore the reaction time was increased. After several attempts at synthesising the pyrazoles the reaction time was optimised at 6h. The pyrazole DMU 10106 was eventually isolated by flash chromatography using ethyl acetate and hexane (6:4) as eluent in variable yields of up to 63%. In view of these inconsistent results, a two-step approach based on the method of *Bhat et al* was investigated. This required stirring a solution of the epoxychalcone DMU 10006 with hydrazine hydrate (1.5 equivalents) in ethanol at reflux for 6h. TLC analysis showed the formation of the pyrazoline which appeared as a new fluorescent blue spot when viewed under ultra-violet (UV) light. The solvent was removed *in vacuo* and a brown residue was obtained which was dissolved in glacial acetic acid. Concentrated sulphuric (30 ml) acid was added to the solution which was then heated at reflux for 0.5h. After cooling, the reaction was neutralised by dropwise addition of concentrated ammonia solution resulting in the formation of a dark brown precipitate. Recrystalisation from ethanol gave DMU 10106 as brown crystals with a yield of 66%. Although this reaction gave a similar yield to the one pot method of *LeBlanc et al*, the two-step synthesis provided consistent results and avoided the need for purification via flash chromatography. It was thus decided to use this method to prepare the library of compounds shown in Table 4.

Table 4. Library of pyrazoles synthesised

Entry	**DMU No.**	**Structure**	**% Yield**	**M.P °C**	**Appearance**
1	10101	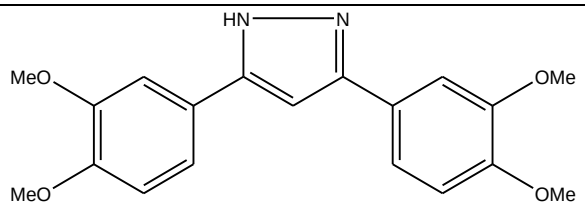	87	84-86	Brown Crystals
2	10102	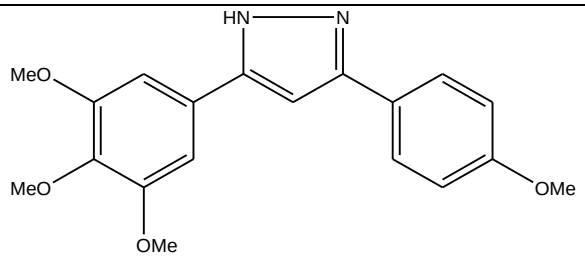	81	80-82	Brown Crystals

3	10103	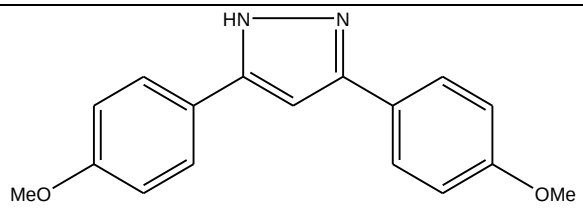	93	77-79	Brown Crystals
4	10104	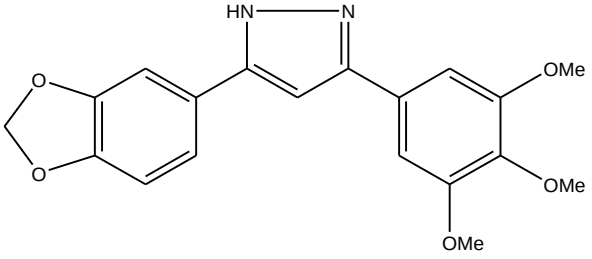	73	101-103	Brown Crystals
5	10106	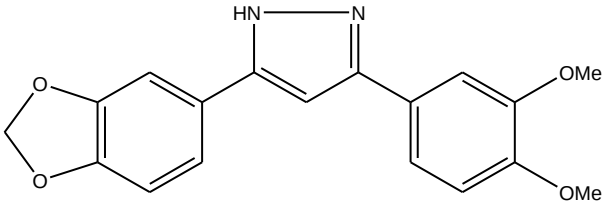	66	101-103	Brown Crystals
6	10107	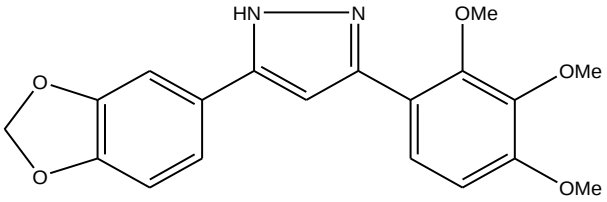	70	140-142	Brown Crystals
7	10108	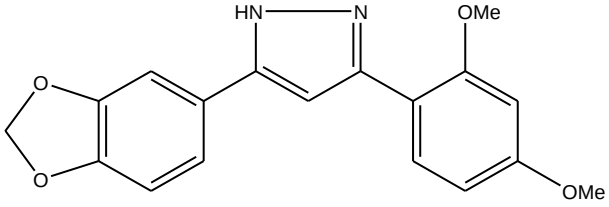	72	169-171	Brown Crystals
8	10109	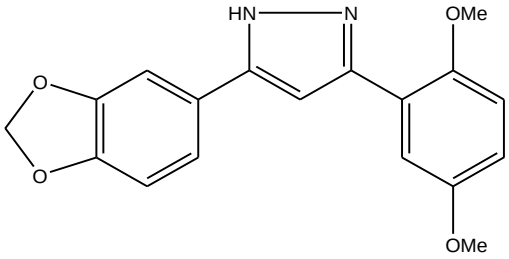	73	154-156	Brown Crystals
9	10110	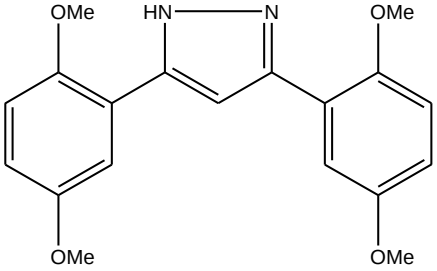	70	135-137	Brown Crystals

10	10111	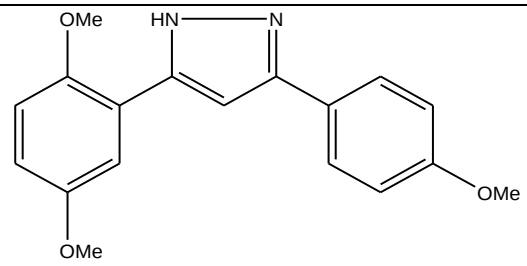	67	-	Oil
11	10112	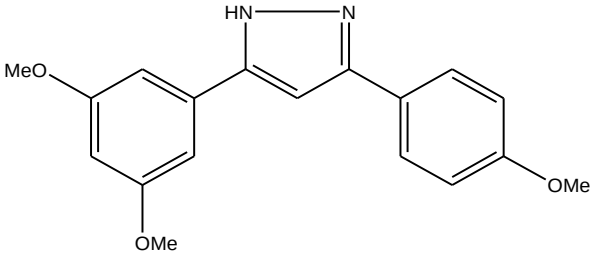	87	71-73	Brown Crystals
12	10113	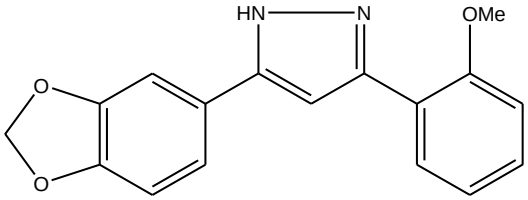	70	136-138	Brown Crystals
13	10114	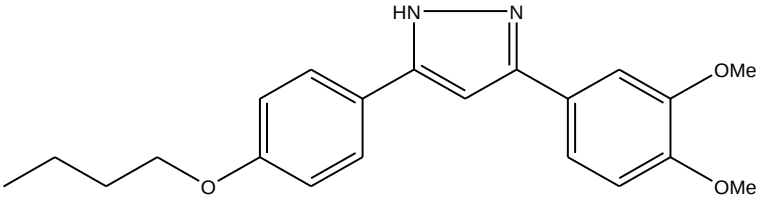	65	74-76	Brown Crystals
14	10116	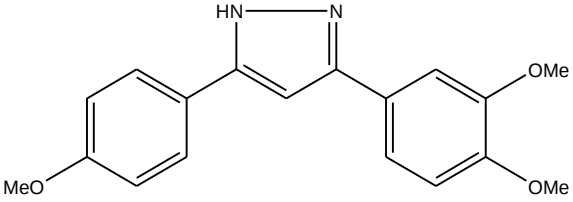	66	75-77	Brown Crystals
15	10117	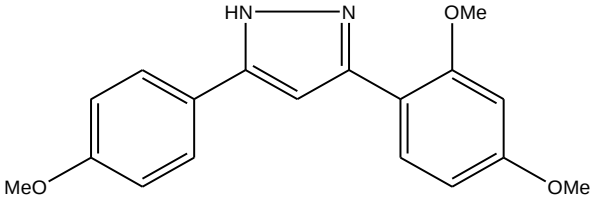	90	126-128	Brown Crystals
16	10120	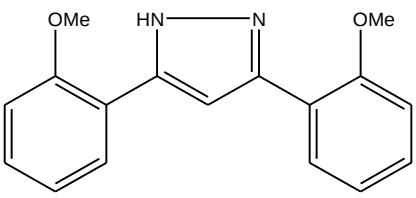	73	-	Oil

17	10121	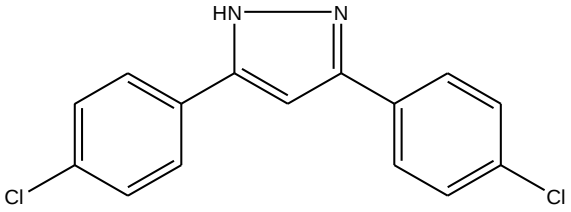	73	240-242	Light Brown Crystals
18	10123	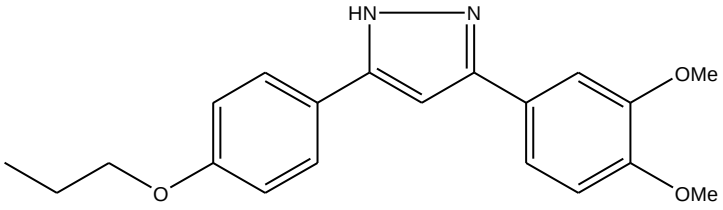	63	-	Oil

A library of eighteen 3,5-diarylpyrazoles was synthesised in yields ranging from 63-93%. With the exception of three compounds which produced oils (Table 4, entries 10, 16 and 23), the pyrazoles were obtained as brown crystals on recrystallisation from ethanol with melting points in the range of 71-242^{o}C. The ^{1}H NMR spectra were consistent with the expected structures, with the pyrazole ring proton at C4 (Figure 37) appearing as a broad singlet between 6-7.3ppm. The NH of the pyrazole ring was not apparent in the spectra as the pyrazole can undergo tautomerisation in which the NH proton can migrate between the two nitrogens in the heterocycle. This occurs at a rapid pace undetectable by the conditions used to conduct the ^{1}H NMR analysis. Figure 38 shows the ^{1}H NMR spectrum and Figure 39 shows the MS spectrum of DMU 10112.

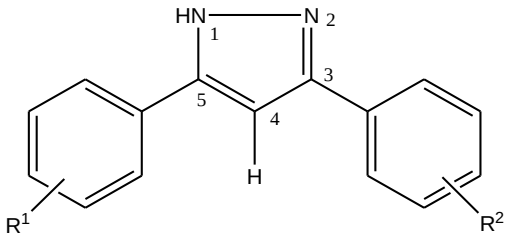

Figure 37. Numbering of atoms of the pyrazole heterocycle

IR spectroscopy showed weak absorptions between 3300 and 3400cm^{-1} characteristic of the NH of the pyrazole heterocycle. MS spectra were consistent with the proposed structures showing the $(M+1)^{+}$ ion peaks of correct mass.

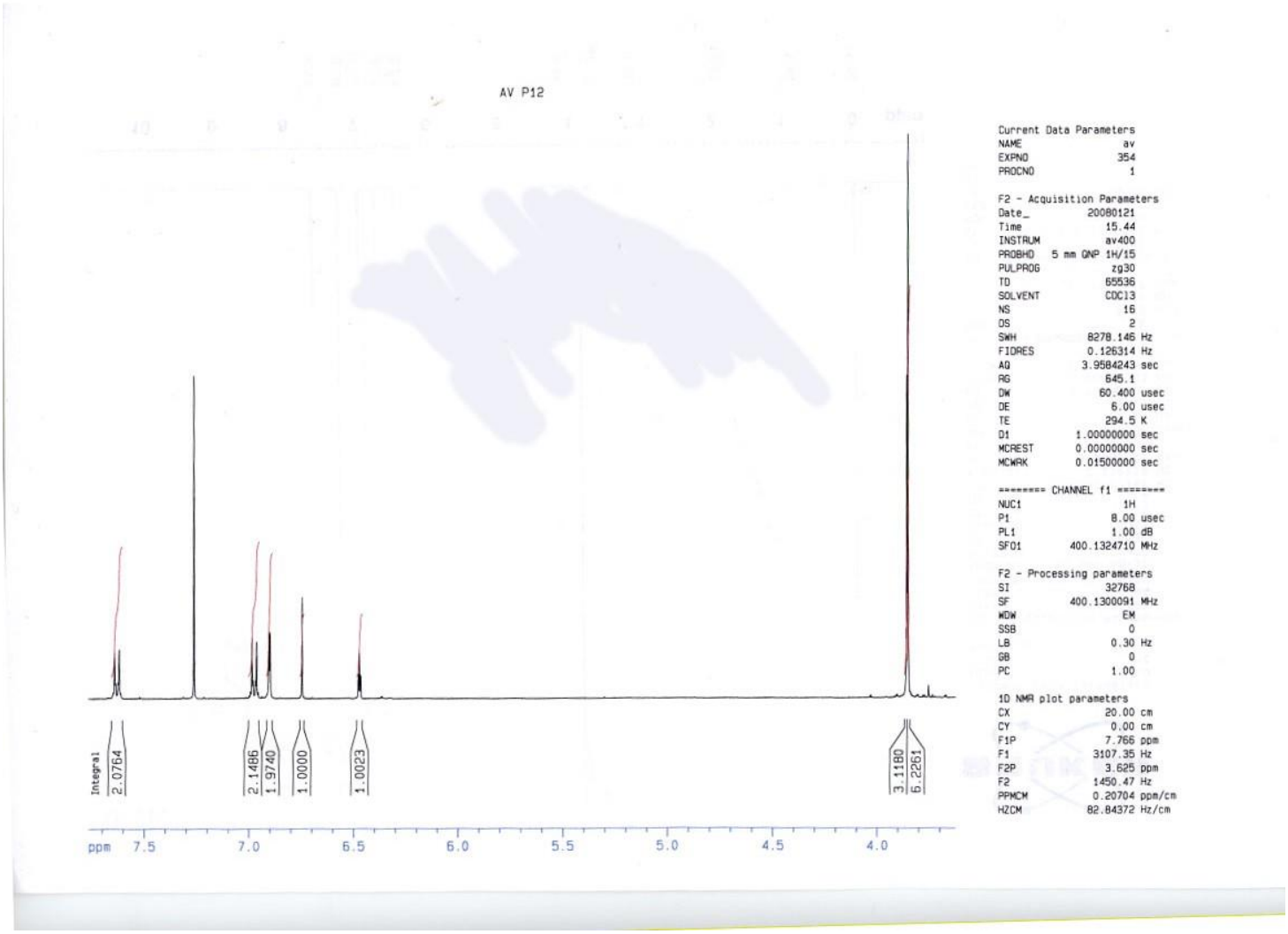

Figure 38. ^{1}H NMR spectrum of DMU 10112

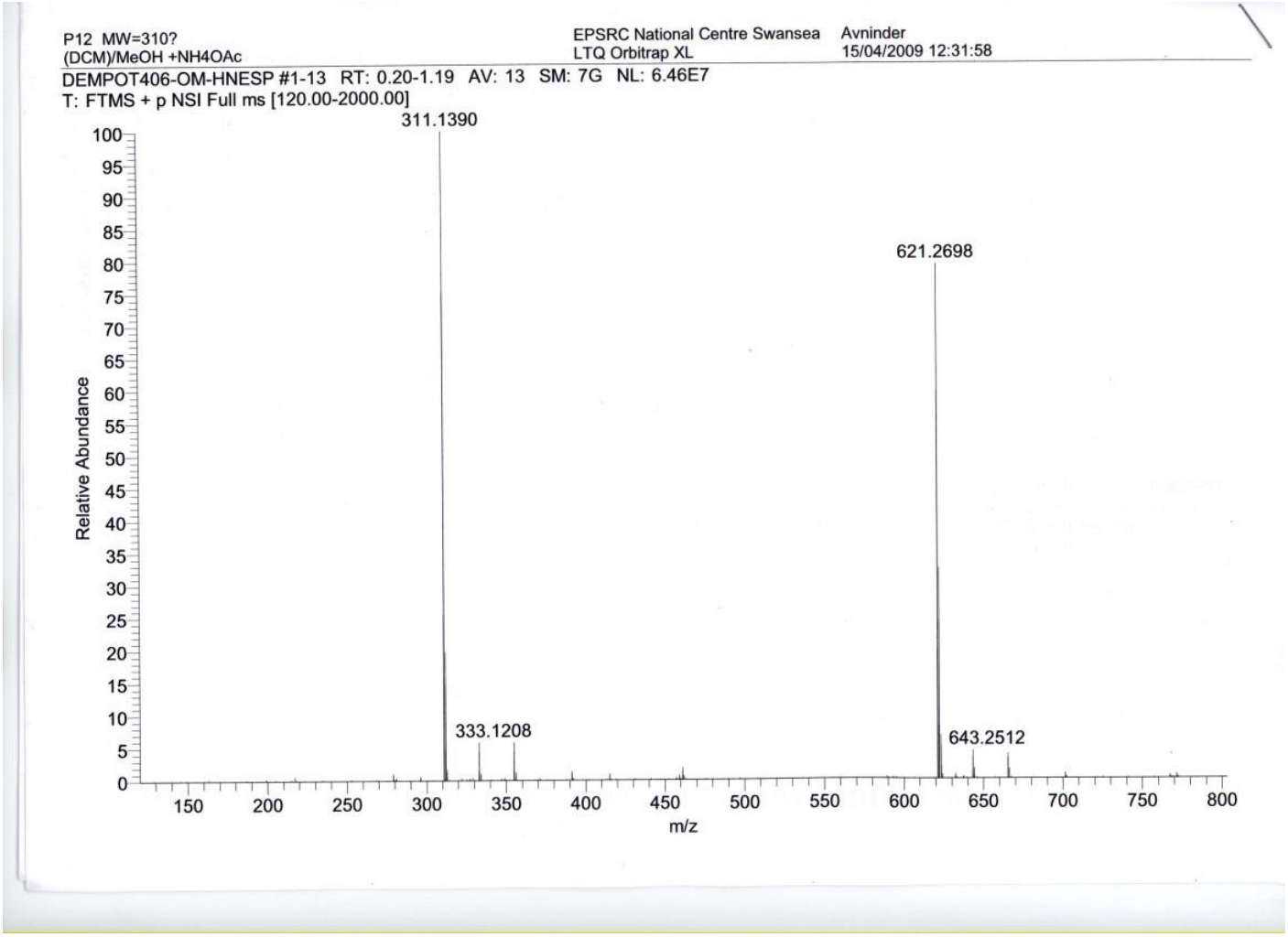

Figure 39. MS spectrum of DMU 10112

2.4 Cytotoxicity Screening

2.4.1 MTT Assay

The cytotoxicity of the compounds synthesised in this project were screened using the MTT assay by Dr. D. Ankrett of the CDDG (Appendix, 10.0). The MTT assay is a quantitative colorimetric assay based on the cleavage of the yellow water-soluble 3-[4,5-dimethylthiazol-2yl]-2,5-diphenyltetrazolium salt (MTT) to form water-insoluble, dark blue formazan crystals (Figure 40).[212] MTT cleavage occurs only in living cells by the mitochondrial enzyme succinate dehydrogenase. The formazan crystals are solubilised in organic solvent and the absorbance of the resulting solution is measured using a spectrophotometer. The absorbance is directly proportional to the concentration of the blue formazan solution, which is directly proportional to the number of metabolically active cells.

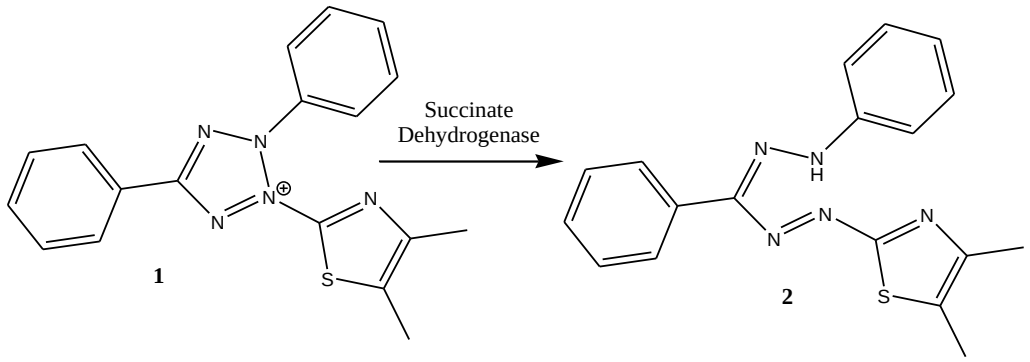

Figure 40. Cleavage of MTT (1) to Formazan (2) by succinate dehydrogenase

2.4.2 Cell Lines Chosen for MTT Screening

The human breast tumour cell lines MDA-MB-468 (MDA 468), MCF7 and MDA-MB-231 (MDA 231) were selected for screening compounds synthesised in this project for their anti-cancer prodrug ability. This was due to their capacity to express functioning CYP1 proteins, either constitutively or after exposure to 2,3,7,8-tetrachlorodibenzodioxin (TCDD), an agonist for the AhR widely used to induce CYP1 enzymes.[213, 214] Experimentation techniques including western blotting were conducted by Dr. S. Surichan of the CDDG to determine the CYP1 expression in the MDA 468 and MCF7 cell lines.

The MDA 468 cell line is estrogen receptor negative (ER-) as the levels of detection of the estrogen receptor are below 1 fmol/mg. The growth of this tumour is not dependent on the hormone estrogen, and this type of tumour cannot be treated with anti-estrogen drugs like tamoxifen, which exhibit their anti-tumour function by inhibiting the ER.[215] MDA 468 cells have been shown through EROD (ethoxyresorufin-*O*-deethylase) assaying and western immunoblotting to constitutively express both CYP1A1 and CYP1B1 enzymes, with the latter at a lower concentration in comparison to CYP1A1.[216] TCDD treatment amplifies the expression for both CYP1A1 and CYP1B1 with the ratio of CYP1A1 still remaining higher than that of CYP1B1.

The MCF7 cell line is ER+ and is the most widely used breast cancer cell line in research.[217] This cell line does not constitutively expresses CYP1 enzymes, but treatment with TCDD induces the expression of CYP1A1.

The MDA231 cell line is an ER- tumour cell line which constitutively expresses low levels of CYP1s. Treatment with TCDD primarily induces CYP1B1 but CYP1A1 is also expressed to a lesser extent.[214, 218]

The control used in the MTT assay consisted of the non-tumourigenic MCF10A cell line. CYP1A1 or CYP1B1 enzymes are not constitutively expressed in this cell line, but it has been reported that MDA 468 exposure to TCDD induces the expression of CYP1A1 and CYP1B1.[219, 220]

2.4.3 Biological Evaluation of the 2,4-Diarylpyrazoles

A problematic factor associated with chalcones is their susceptibility to undergo photoisomerisation reactions producing both *cis* and *trans* isomers. However, it has been shown that the *trans* isomers are more potent in their biological activities compared to the *cis*

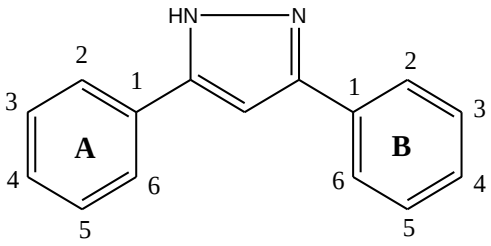

Figure 41. The pyrazole structure indicating A and B rings

isomers. To eliminate this problem, pyrazole heterocycles were incorporated across the α,β-double bond moiety of the chalcones to produce rigid structures invulnerable to photoisomerisation. The synthesised pyrazoles (Table 4) were screened for their prodrug activity against a panel of tumour cell lines including the MDA 468, MCF7 and MDA 231 cells. To enable discussion of the cytotoxicity data observed, the phenyl groups at the 3 and 5 positions have been assigned as A and B-rings (Figure 41), and compounds with similar substitutions have been grouped together.

2.4.3.1 Methylenedioxy Substituted A-Ring

Five compounds with constant 3,4-methylenedioxy substituted A-rings were synthesised (Figure 42).

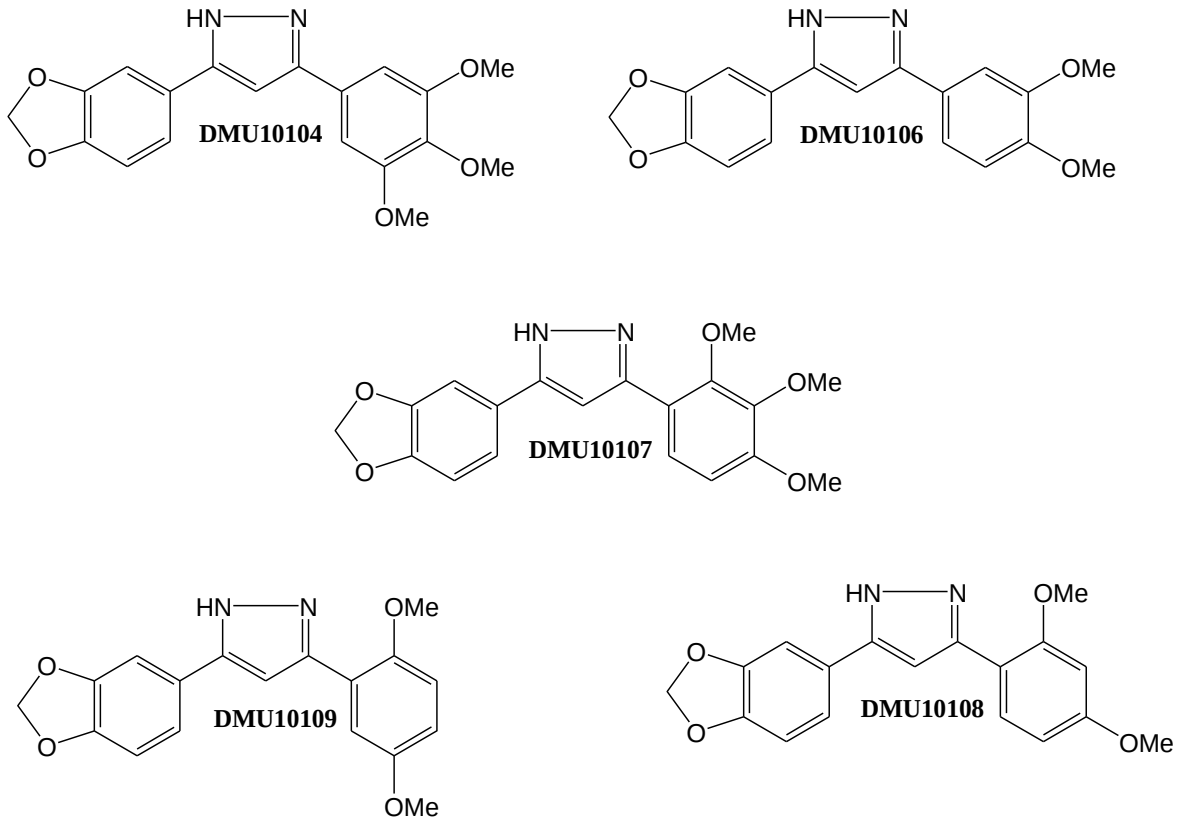

Figure 42. Methylenedioxy substituted A-ring pyrazoles

Table 5. Cytotoxicity data for the A-ring methylenedioxy substituted pyrazoles

Entry	DMU No.	IC_{50} (μM)		IC_{50} (μM)		IC_{50} (μM)	
		MCF10A	MDA468	MCF7	MCF7 + TCDD	MDA231	MDA231 + TCDD
1	10104	>100	25	8	5	20	20

2	10106	>100	>100	80	80	50	50
3	10107	>100	8	10	10	>100	>100
4	10108	>100	55	>100	>100	>100	>100
5	10109	100	50	50	30	ND	ND

n=1, ND=No data

DMU10104, with a 3,4,5-trimethoxy substituted B-ring (Table 5, entry 1) did not show toxicity towards the non-tumour MCF10A cells. In the MDA468 cancer cell line which constitutively expresses both CYP1A1 and CYP1B1, a relatively high IC_{50} value of 25μM was obtained. In the MCF7 cell line, which expresses very low levels of CYP1 enzymes, a lower IC_{50} of 8μM was achieved. Treatment of the MCF7 cells with TCDD to induce CYP1A1 expression made no significant difference to this value suggesting that CYP1 prodrug activation does not play a role in the mode of action of this derivative. The MDA231 cell line which principally expresses CY1B1 on induction with TCDD, gave an IC_{50} of 20μM. No change in cytotoxicity was observed on treatment of these cells with TCDD, again suggesting no prodrug action was occurring. DMU 10107, substituted with a 2,3,4-trimethoxy B-ring (Table 5, entry 3) did not show toxicity towards the non-tumour MCF10A cells. Results from the MCF7 cell line gave IC_{50} values of 10μM each for both the TCDD induced and non-induced cells. Unlike DMU 10104, DMU 10107 showed slight activity in the MDA 468 cell line with an IC_{50} value of 8μM being recorded. No activity was seen in the MDA231 assays as IC_{50} values were greater than 100μM. DMU 10106 (Table 5, entry 2), synthesised with a 2,3-dimethoxy substituted B-ring did not show toxicity towards the tumour cell lines as all IC_{50} values were above 50μM. DMU 10108 and DMU 10109 (Table

5, entries 4 and 5) gave similarly disappointing results, with IC_{50} values of 30μM and greater for each tumour cell line tested against.

The pyrazoles DMU 10104, DMU 10107 and DMU 10108 were synthesised based on lead chalcones investigated in previous experimentations by the CDDG. DMU 135 (Table 6, entry 1) showed significant cytotoxicity towards the MDA 468 cell line giving an IC_{50} value of 0.09μM whilst having no toxic effect on the MCF10A cell line. However, the pyrazole analogue DMU 10104 (Table 6, entry 2) was approximately 280 times less toxic to the MDA 468 cell line giving an IC_{50} value of 25μM, but showed the same non-toxic result towards the MCF10A cell line as DMU 135. A similar outcome was also apparent with the MCF7 and MDA 231 cells as DMU 135 showed greater toxicity towards these in comparison to DMU 10104.

Table 6. Cytotoxicity comparison of pyrazole and chalcone analogues bearing the same substituted A and B-rings

			IC_{50} (μM)					
Entry	**DMU No.**	**Structure**	**MCF 10A**	**MDA 468**	**MCF7**	**MCF7 + TCDD**	**MDA 231**	**MDA 231 + TCDD**
1	135	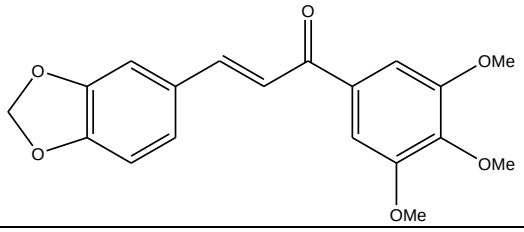	>100	0.09	0.2	0.03	11	11
2	10104	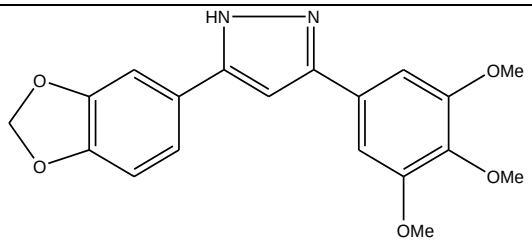	>100	25	8	5	20	20
3	419	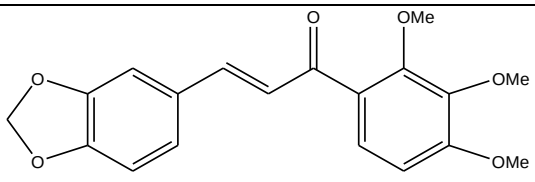	>100	3	2	2	6	6

4	10107	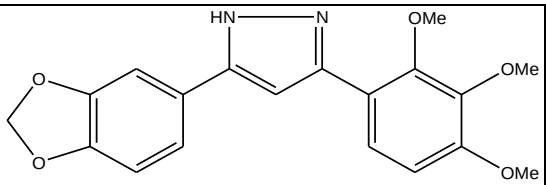	>100	8	10	10	>100	>100
5	407	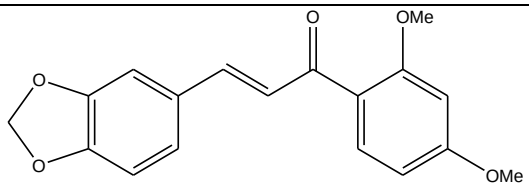	>100	10	11	11	5	8
6	10108	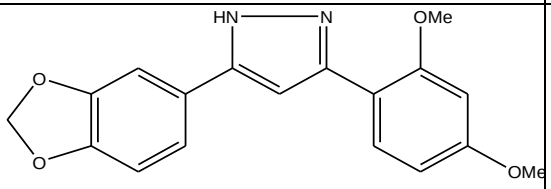	>100	55	>100	>100	>100	>100

The chalcone DMU 419 (Table 6, entry 3) also gave greater toxicities across the cancer cell line panel in contrast to its pyrazole analogue of DMU 10107 (Table 6, entry 4). This was significantly more noticeable towards the MDA 231 cells as DMU 419 gave identical IC_{50} values of 6µM for both the TCDD induced and non-induced cells but DMU 10107 did not show toxicity towards the MDA 231 cells in comparison. The chalcone DMU 407 (Table 6, entry 5) was far more toxic towards the MCF7 and MDA 231 cell lines in contrast to its pyrazole analogue of DMU 10108 (Table 6, entry 6), and over five times more toxic towards the MDA 468 cell line.

2.4.3.2 4-Methoxy Substituted Pyrazoles

Six 4-methoxy substituted pyrazoles were synthesised as shown in Figure 43. DMU 10103, DMU 10116 and DMU 10117 were synthesised from chalcones with 4-methoxy substituted B-rings, whilst DMU 10122, DMU 10112 and DMU 10111 were synthesised from chalcones substituted with 4-methoxy substituted A-rings. However, as pyrazoles are liable to undergo tautomerisation, a line of symmetry can be drawn through the centre of the pyrazole heterocycle making the A and B-rings interchangeable as long as all remaining substituents remain equal. Hence, the 4-methoxy substituted pyrazoles can be considered together for the discussion of the biological data observed.

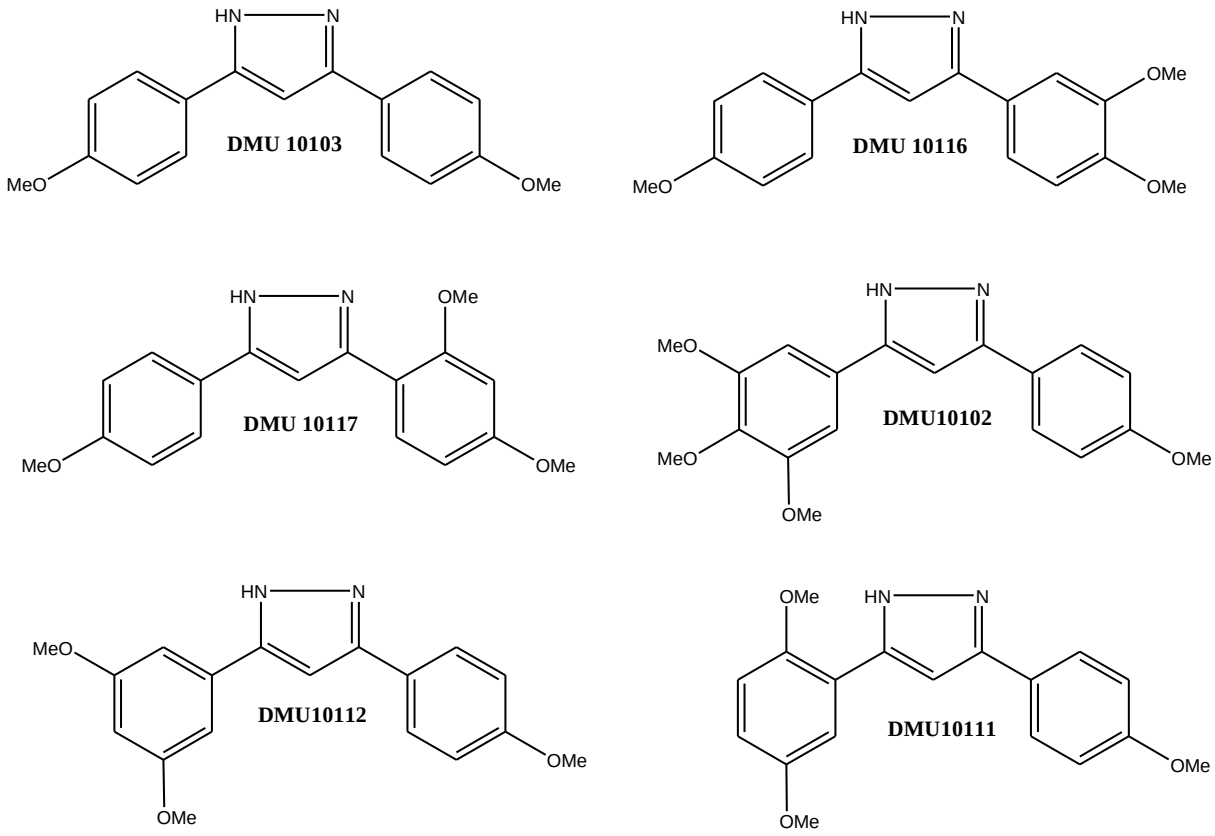

Figure 43. 4-methoxy substituted pyrazoles

Table 7. 4-methoxy substituted pyrazoles

Entry	DMU No.	IC_{50} (μM)		IC_{50} (μM)		IC_{50} (μM)	
		MCF10A	**MDA468**	**MCF7**	**MCF7 + TCDD**	**MDA231**	**MDA231 + TCDD**
1	10102	>100	50	30	40	38	21
2	10103	>100	>100	>100	>100	>100	>100

3	10111	70	40	55	40	ND	ND
4	10112	>100	45	45	55	60	90
5	10116	ND	ND	55	70	65	50
6	10117	>100	>100	100	70	>100	>100

n=1, ND=No data

The 4-methoxy substituted pyrazoles showed little toxicity towards the non-tumour MCF10A cell line with IC_{50} values of 70μM or above being observed. Cytotoxicity was seen towards the tumour cell lines but not to a degree that would be considered noteworthy, as IC_{50} values were above 20μM. DMU 102 (Table 8, entry 1), the chalcone analogue of DMU 10102 was another lead chalcone synthesised and investigated by the CDDG. An IC_{50} of 0.5μM was observed when DMU 102 was screened against the MDA 468 cell line, ten times more toxic in contrast to DMU 10102 (Table 8, entry 2). The chalcone analogue was also 15 times more toxic towards the MCF7 cell line, but interestingly 670 times more toxic against the MCF7 cells induced with TCDD.

Table 8. Toxicity comparison of DMU 102 and DMU 10102

			IC_{50} (µM)					
Entry	**DMU No.**	**Structure**	**MCF 10A**	**MDA 468**	**MCF7**	**MCF7 + TCDD**	**MDA 231**	**MDA 231 + TCDD**
1	102	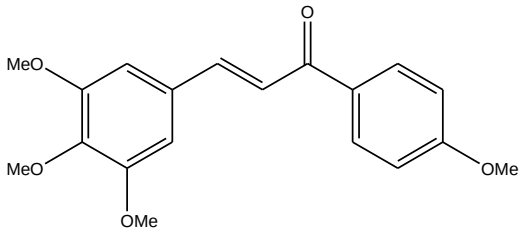	>100	0.5	0.5	0.06	ND	ND
2	10102	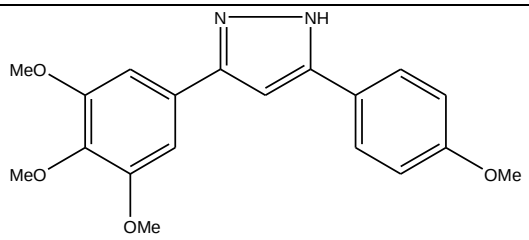	>100	50	30	40	38	21

The remainder of the chalcone analogues of the above 4-methoxy substituted pyrazoles were greater in toxicities than their pyrazole derivatives, but not to a degree of substantial interest. As the pyrazoles did not enhance their activity, further discussion of these compounds will not be undertaken.

2.4.3.3 4-Propoxy and 4-Butoxy Substituted A-Ring

The chalcone DMU 2216, substituted with a 4-propoxy A-ring and 3,4-dimethoxy substituted B-ring showed significant cytotoxicity towards the MDA 468 cell line. An IC_{50} value of 0.6µM was observed whilst no toxicity was seen towards the non-tumour MCF10A cells. Hence, DMU 10123 was designed and synthesised based on DMU 2216 in an attempt to obtain comparable or better cytotoxic behaviour. Also, DMU 10114 (Figure 44) was synthesised with a 4-butoxy substituted A-ring and 3,4-dimethoxy substituted B-ring in order

to investigate whether an increase in the alkyl chain length influenced the cytotoxicity of the pyrazole.

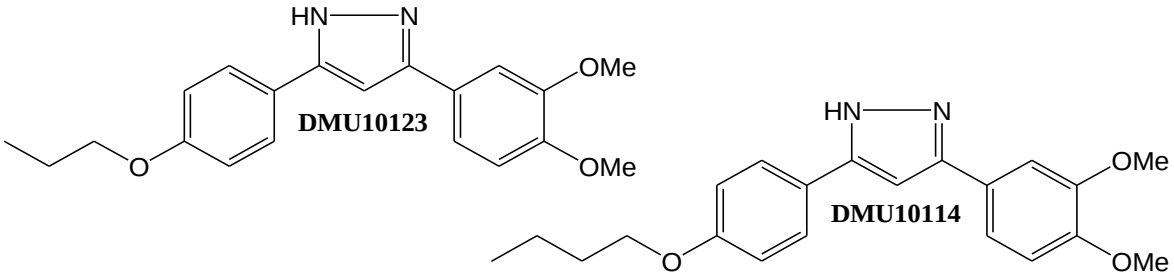

Figure 44. Alkyl-ether substituted pyrazoles

Table 9. Alkyl-ether substituted pyrazoles

Entry	DMU No.	IC_{50} (µM)		IC_{50} (µM)		IC_{50} (µM)	
		MCF10A	MDA468	MCF7	MCF7 + TCDD	MDA231	MDA231 + TCDD
1	10114	>100	20	8	8	25	25
2	10123	25	18	21	21	19	19

n=1, ND=No data

The results obtained from screening DMU 10123 against the tumour cells did not show to be more potent in comparison to DMU 2216 against the MDA 468 cell line, as DMU 10123 was 30 times less toxic than DMU 2216 (Table 10, entry 1). DMU 10123 (Table 10, entry 2) also showed toxicity towards the non-tumour MCF10A cells unlike DMU 2216 and although it was not to a great degree the toxicity was undesirable nonetheless. DMU 10114 (Table 9, entry 1) exhibited less toxicity towards the MCF10A cell, but a similar toxicity towards the MDA 468 cells as DMU 10123 was recorded. DMU 10114 also proved to be more potent towards the MCF7 cells in contrast to DMU 10123, but not to an extent requiring further investigation.

Table 10. Comparison of cytotoxicities observed from DMU 2216 and DMU 10123

			IC_{50} (µM)					
Entry	**DMU No.**	**Structure**	**MCF 10A**	**MDA 468**	**MCF7**	**MCF7 + TCDD**	**MDA 231**	**MDA 231 + TCDD**
1	2216	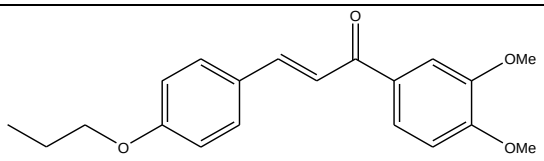	>100	0.6	60	20	ND	ND
2	10123	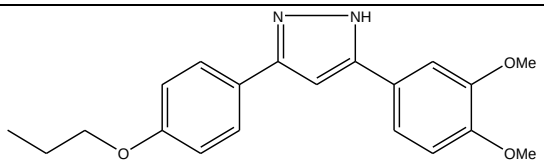	25	18	21	21	19	19

2.4.3.4 Other Substituted Pyrazoles

Four pyrazoles with identical substitutions on the A and B-rings were synthesised (Figure 45).

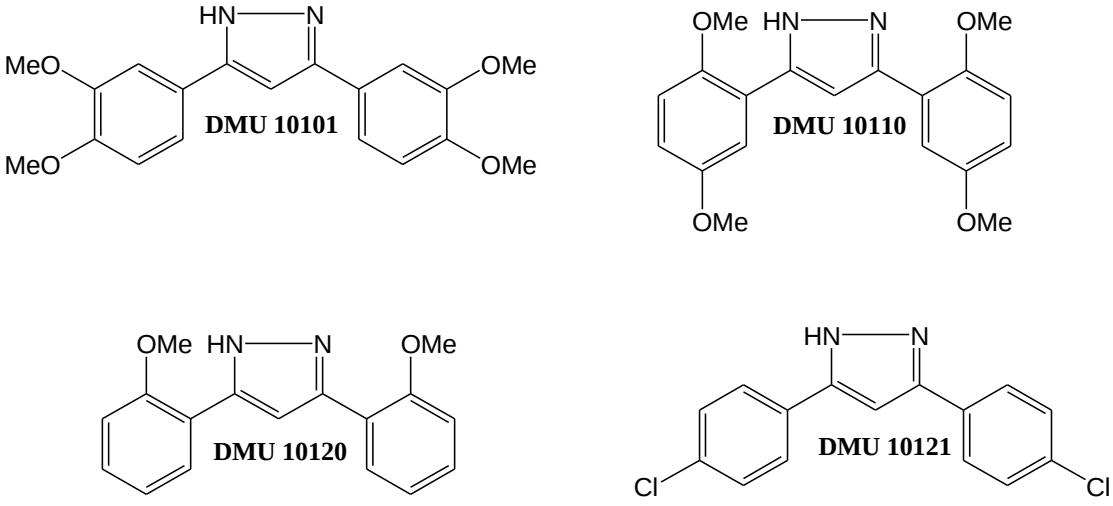

Figure 45. Symmetrically designed pyrazoles

It was deduced from structure activity relationship analysis of the lead chalcones that the occupancy of the 2, 3 and 4-positions on the A and B-rings have shown to be valuable for anti-cancer cytotoxicity. To further investigate this, methoxy groups were strategically placed in these positions on both the A and B-rings to see if any link or further enhancements of cytotoxicities could be seen. A chlorine substituted analogue was also synthesised, which would be a direct comparison to the methoxy substituted analogue of DMU 10103.

Table 11. Cytotoxicity data from the symmetrically synthesised pyrazoles

Entry	DMU No.	IC_{50} (μM)		IC_{50} (μM)		IC_{50} (μM)	
		MCF10A	MDA468	MCF7	MCF7 + TCDD	MDA231	MDA231 + TCDD
1	10101	>100	80	80	80	70	70
2	10110	>100	50	ND	ND	ND	ND
3	10120	>100	60	60	60	ND	ND
4	10121	>100	65	>100	>100	>100	>100

n=1, ND=No data

The pyrazoles shown in Table 11 did not show significant cytotoxicities against the panel of tumour cell lines screened against. However, an interesting result was obtained with DMU10121 (Table 11, entry 4) which was 4-chloro substituted on both of the A and B-rings. This derivative, although having an IC_{50} value of 65μM against the MDA468 cell line, showed activity at a much lower concentration with an IC_{25} value of 0.7μM being obtained (Figure 46). This was not observed with other pyrazoles screened.

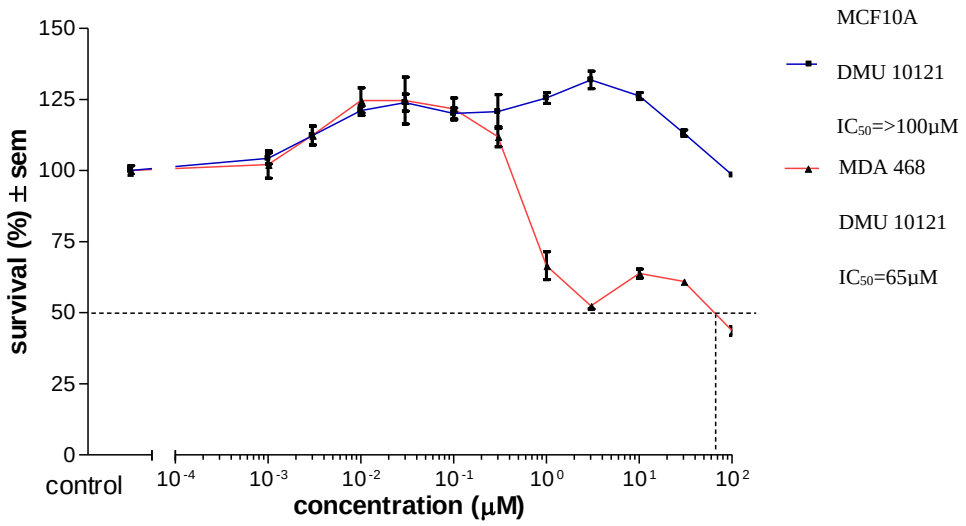

Figure 46. Cytotoxicity plot for DMU 10121

In comparison to its methoxy analogue of DMU 10103, the chloro substituted DMU 10121 only showed a slight increase in cytotoxicity towards the MDA 468 cell line but remained non-toxic towards the remaining cell lines alongside DMU 10103.

2.5 Summary and Conclusions

A library of eighteen pyrazoles were designed and synthesised using a two step method taken from *Bhat et al*, with yields of up to 93% being obtained. The rationale behind the synthesis was to lock the biologically active *trans* chalcone isomers in a rigid structure, preventing the problematic photoisomerisation reaction from occurring which produces the non-active *cis* isomers. The pyrazole heterocycle was incorporated across the α,β-unsaturated moiety of selected chalcones, including the lead compounds DMU 135 and DMU 102 via epoxychalcone intermediates.

The synthesised pyrazoles were screened for their prodrug activity against a panel of tumour cell lines, consisting of the MDA 468, MCF7 and MDA 231 cells. DMU 10107, synthesised with a 3,4-methylenedioxy substituted A-ring and 2,3,4-trimethoxy substituted B-ring was concluded as the most toxic compound out of the pyrazoles synthesised. An IC_{50} value of 8µM was recorded from screening DMU 10107 against the MDA 468 cell line, whilst no toxicity was observed towards the non-tumour MCF10A cell line. The MCF7 cells, TCDD

induced and non-induced gave IC_{50} values of 10µM each. However, the cytotoxicities observed from DMU 10107 were not as potent as the cytotoxicities seen from the chalcone analogue of DMU 419, which was twice as toxic towards the MDA 468 cell line and five times as toxic towards the MCF7 cell lines. DMU 10107 did not show toxicity towards the MDA 231 cells whereas DMU 419 exhibited a noticeable toxicity of 6µM towards the TCDD induced and non-induced cells.

It was generally observed that the chalcone analogues of the pyrazoles synthesised were more cytotoxic across the tumour cell lines screened against, making the incorporation of the pyrazole heterocycle across the α,β-unsaturated moiety of the chalcones unfavourable in this case.

The next stage of investigation would require the exploration of other heterocyclic ring systems which could be incorporated across the α,β-unsaturated moiety of the chalcones, resulting in rigid structures unable to photoisomerise. Also, comparable or increased cytotoxicities towards the tumour cell lines should be observed from modified compounds compared with the chalcone analogues they were synthesised from.

Chapter 3

Synthesis and Biological Evaluation of 2-Amino-4,6-Diarylpyrimidines

3.0 Synthesis of 2-Amino-4,6-Diarylpyrimidines

Photoisomerisation reactions occurring in chalcones are problematic as they convert biologically active *trans* isomers to the less potent *cis* isomer. To overcome this, pyrazole rings were incorporated across the chalcone α,β-double bond to lock the substituted phenyl groups in a *trans* like geometry. The pyrazole library was screened against a selected panel of tumour cell lines where it was experimentally concluded that DMU 10107 was the most effective cytotoxic compound synthesised. However, the cytotoxicity of DMU 10107 was not as potent as its chalcone analogue of DMU 419. Therefore, the investigation into alternative heterocyclic rings was required to achieve rigid, non-photoisomerisable structures with comparable or greater cytotoxicities towards the tumour cell lines in contrast to the parent chalcones.

The incorporation of a pyrimidine heterocycle into the chalcones was investigated. Pyrimidines are 6-membered heterocycles with nitrogen atoms at positions 1 and 3 of the ring (Figure 47).

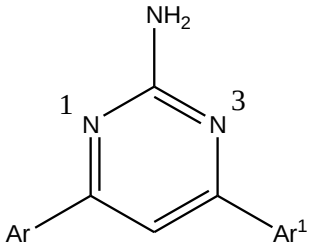

Figure 47. Nitrogen positions within the pyrimidine heterocycle

Pyrimidines have been shown to be important for the treatment of malaria, cancer, inflammation and tuberculosis.[221] For example, 5-fluorouracil is a pyrimidine based anti-cancer drug used to treat various cancers including breast and stomach cancers. A widely known synthetic route for the preparation of pyrimidines is via the *Biginelli* reaction which was discovered in 1893 (Figure 48).[222] It involves the acid catalysed cyclo-condensation of ethylacetoacetate, benzaldehyde and urea in ethanol under reflux which affords dihydropyrimidin-2-one as the product.[223]

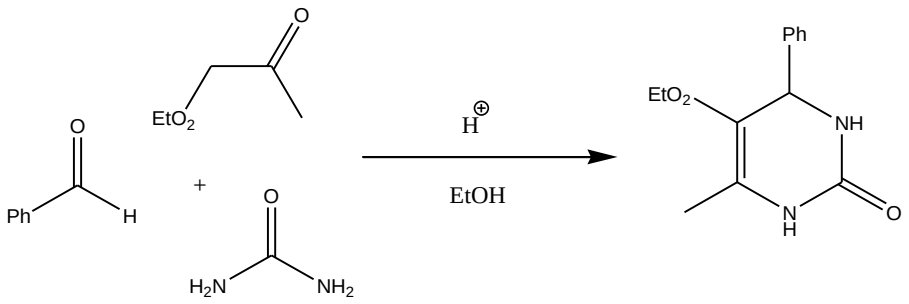

Figure 48. General reaction for the Biginelli synthesis

More importantly, a synthetic route using chalcones to yield pyrimidines has been reported by *Varga et al*, applied in experimentations investigating the oxidation of dihydro-pyrimidine intermediates to aromatised pyrimidines (Figure 49).[224] Chalcones were stirred with guanidine in a basic alcoholic solution under refluxing conditions, followed by the subsequent addition of hydrogen peroxide solution. The synthesis of pyrimidines from chalcones occurs via dihydro-pyrimidine intermediates which require oxidation in order to form the aromatised pyrimidine heterocycle. The oxidation step can be achieved by stirring the dihydro-pyrimidines in the open air, but it has been reported that air alone is not sufficient enough for aromatisation to occur in larger scale reactions which require the addition of oxidative reagents. It was concluded by *Varga et al* that hydrogen peroxide was found to be the most efficient oxidising reagent, as it is cheap, clean and easily accessible.

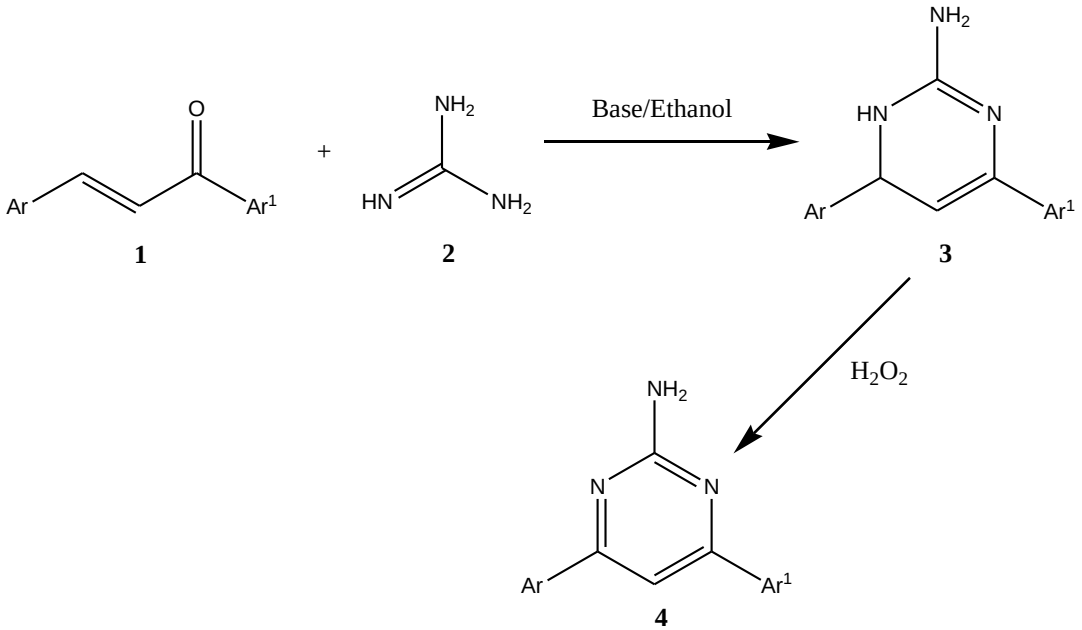

Figure 49. General reaction of the synthesis of pyrimidines (4) through the dihydro-pyrimidine (3) by reacting chalcones (1) and guanidine (2)

The mechanism for the pyrimidine synthesis is illustrated in scheme 6. Under basic conditions the guanidine reacts with the chalcone via 1,2-nucleophilic addition which forms an imine. Intramolecular cyclisation then follows forming the dihydro-pyrimidine which then undergoes further deprotonation by the peroxide, forming the aromatised pyrimidine.

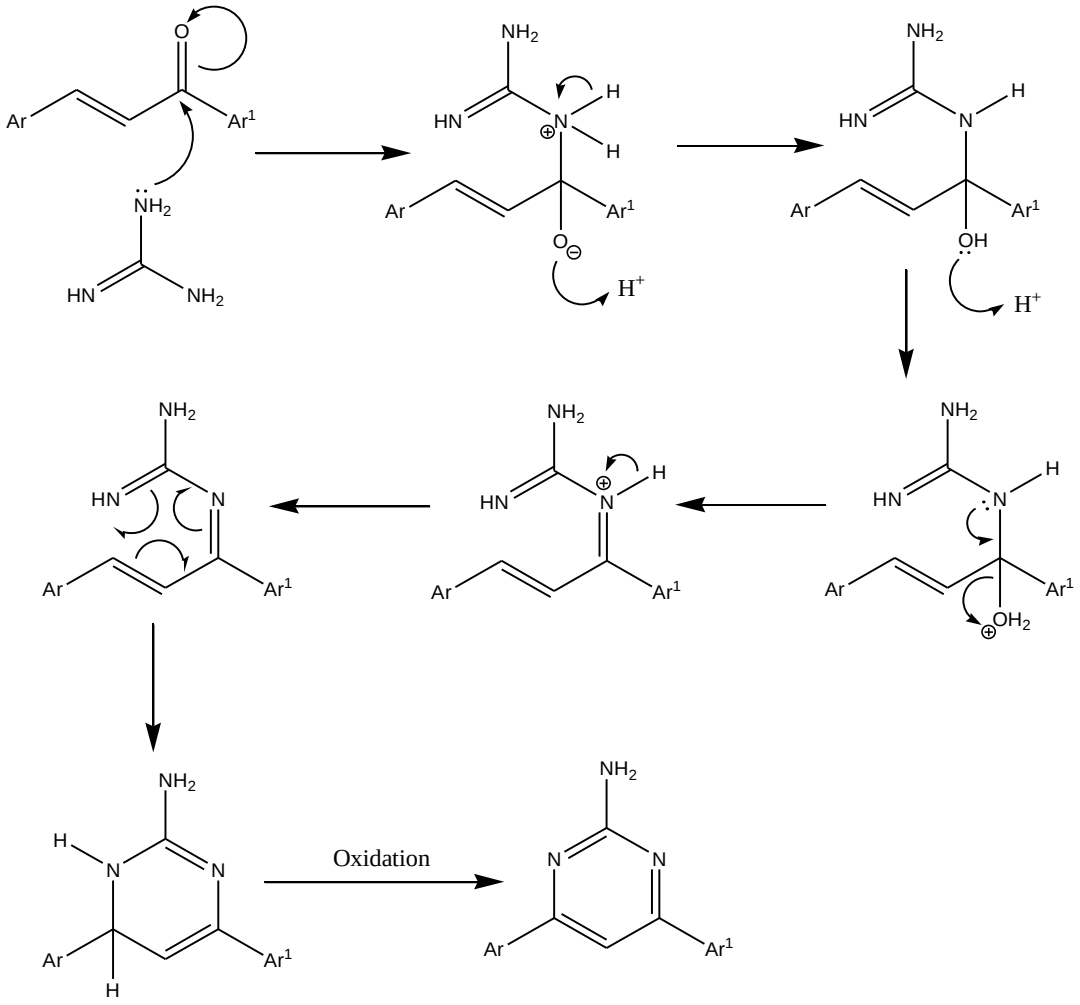

Scheme 6. Mechanism for the synthesis of pyrimidines via chalcones

The mechanism of hydrogen peroxide oxidation is considered complex, as this proceeds through the formation of free radicals via three stages.[212] The first stage of initiation requires the dissociation of the hydrogen peroxide molecule forming two hydroxy radicals (Figure 50).

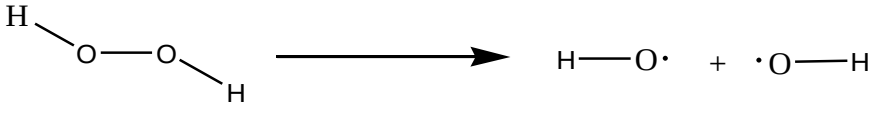

Figure 50. Initiation step of hydrogen peroxide

The second stage of propagation involves the formation of a new radical species through the first free radical formed through the initiation stage (Scheme 7). The last stage of termination sees the formation of a new bond through the joining of two radical species, ending the propagation reaction.

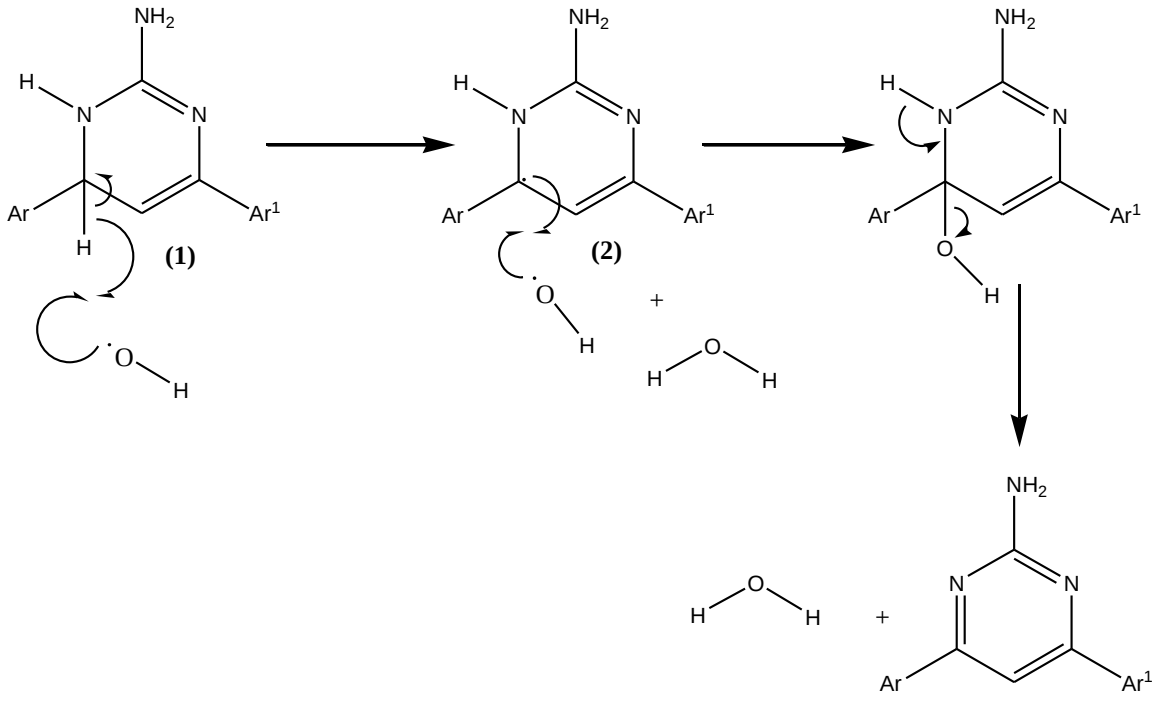

Scheme 7. Oxidation mechanism of dihydro-pyrimidines via the propagation (1) and termination (2) steps

All pyrimidines were synthesised by the method used by *Varga et al*. Guanidine hydrochloride (1.5 equivalents) was stirred with potassium hydroxide (4 equivalents, 50% w/v) in ethanol under reflux for thirty minutes to sufficiently yield the free guanidine. The chalcone (1 equivalent) was then added and the reaction was left to stir under reflux for six hours producing the dihydro-pyrimidine. Hydrogen peroxide (3 equivalents, 50% w/v) was added and the reaction continued to stir under reflux for one hour. TLC analysis was used to monitor the progress of the reaction and the pyrimidine product formed a single fluorescent blue spot when viewed under UV light. Water was added to quench the reaction and the resulting mixture was extracted with dichloromethane. The organic extract was dried over $MgSO_4$ and the solvent removed *in vacuo*. The pyrimidine was purified by either recrystalisation from methanol or ethanol, or by flash chromatography on silica gel using ethyl acetate − hexane (6:4) as eluent.

Table 12. Library of pyrimidines synthesised

Entry	DMU No.	Structure	% Yield	M.P °C	Appearance
1	10200	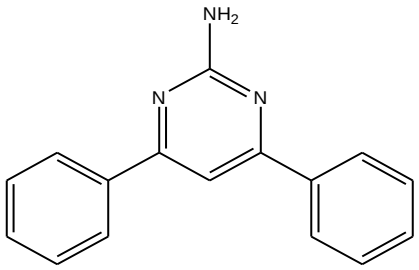	30	119-121	Beige Crystals
2	10201	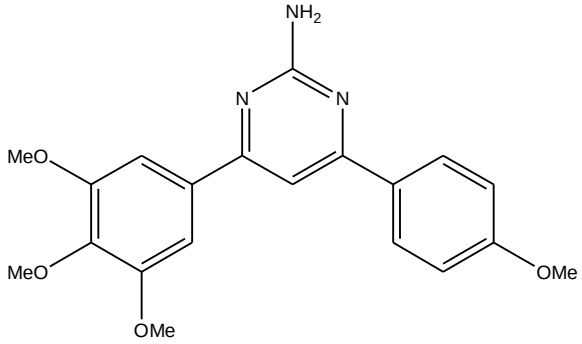	31	142-144	Beige Crystals
3	10202	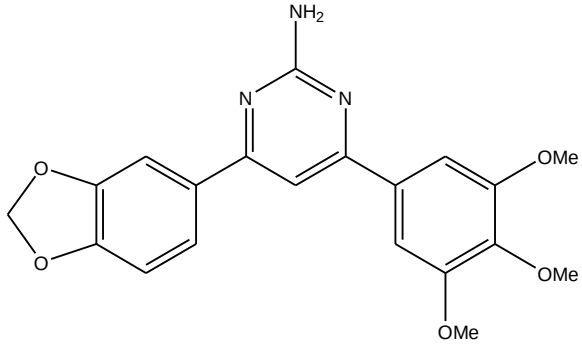	9	192-193	Light Brown Crystals
4	10203	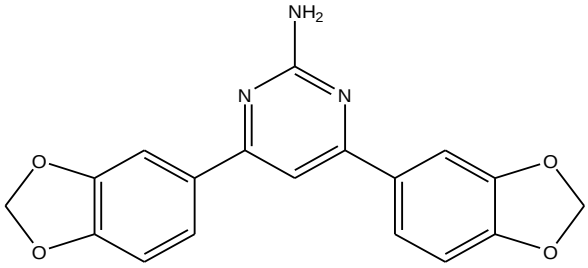	33	222-224	Off white Crystals

5	10214	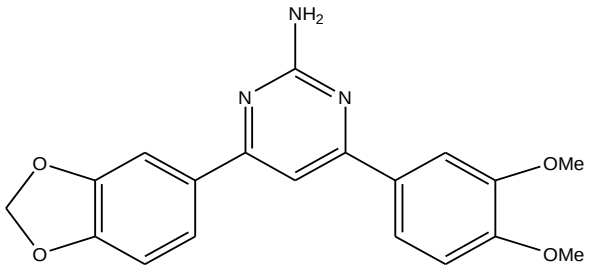	25	180-182	Beige Crystals
6	10204	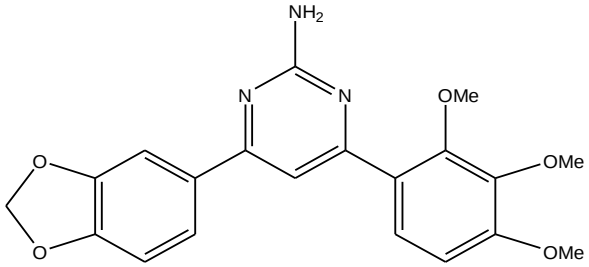	17	181-183	Light Brown Crystals
7	10212	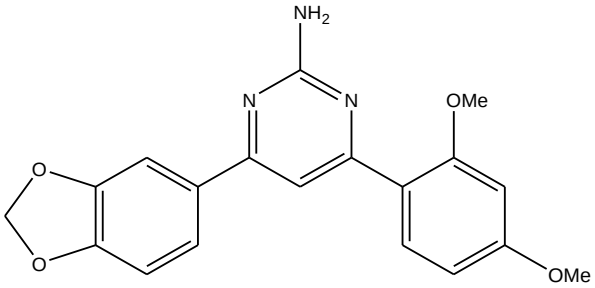	31	133-135	Beige Crystals
8	10205	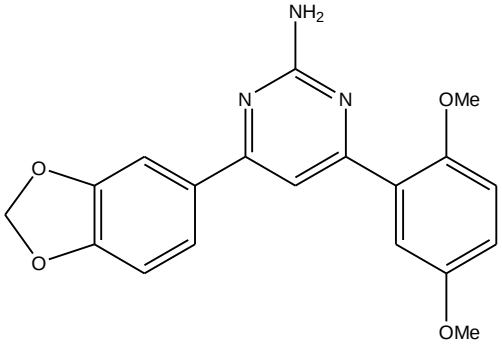	11	133-135	Beige Crystals
9	10206	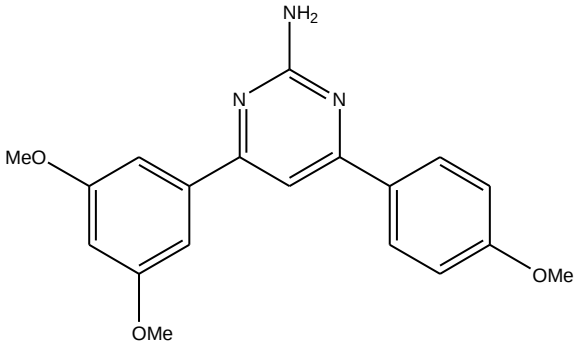	20	172-174	Pale Yellow Crystals

10	10213	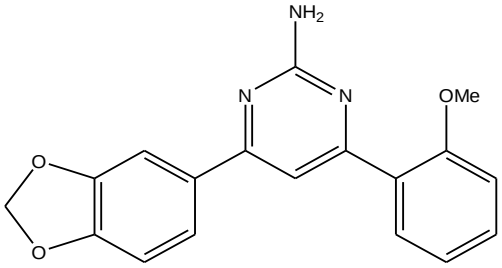	32	142-144	Light Yellow Crystals
11	10207	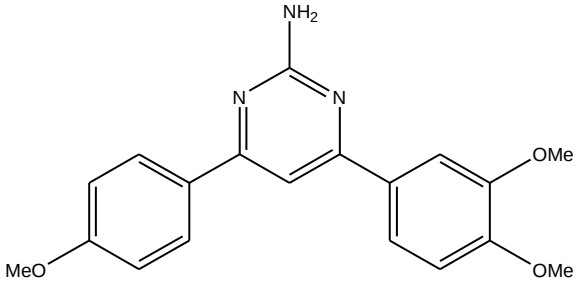	22	145-147	Off White Crystals
12	10208	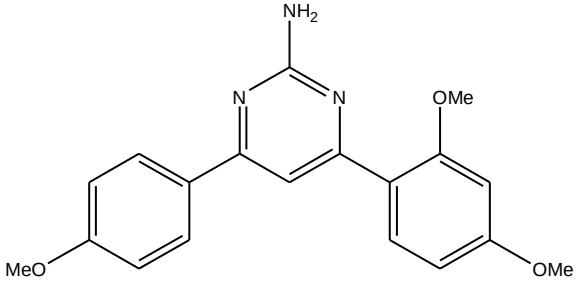	15	119-121	Light Yellow Crystals
13	10209	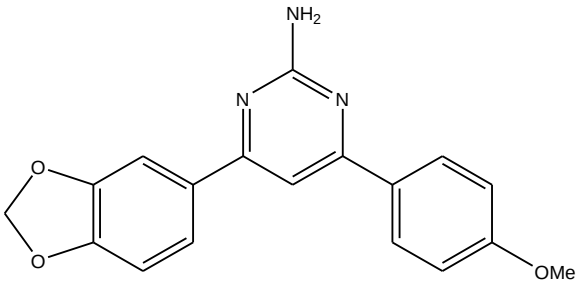	29	132-134	Beige Crystals
14	10210	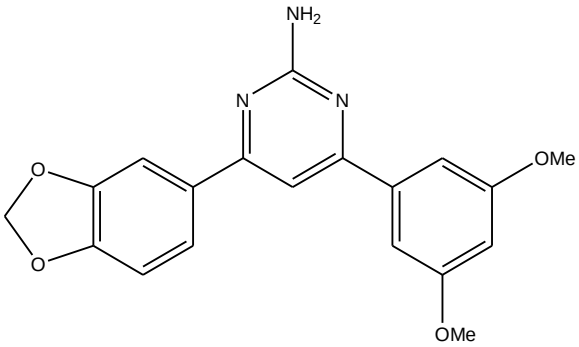	32	125-127	Beige Crystals

15	10211	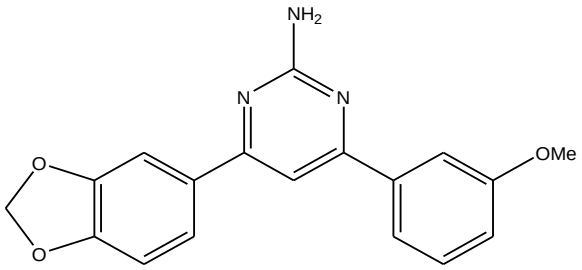	32	134-136	Yellow Crystals

A library of fifteen pyrimidines were synthesised in yields ranging from 9-33% (Table 12), with melting points recorded between 119-183ºC. The ^{1}H NMR spectra showed characteristic broad signals between 5.00-6.02ppm corresponding to the NH_2 protons at the 2-position of the pyrimidine heterocycle. The heterocyclic ring proton at C5 was observed between 7.30-7.86ppm. MS data was correct upon interpretation with an $(M+1)^+$ peak being observed and IR spectroscopy showed absorptions in the region of 3250-3400cm^{-1} as expected for the presence of NH_2 bonds.

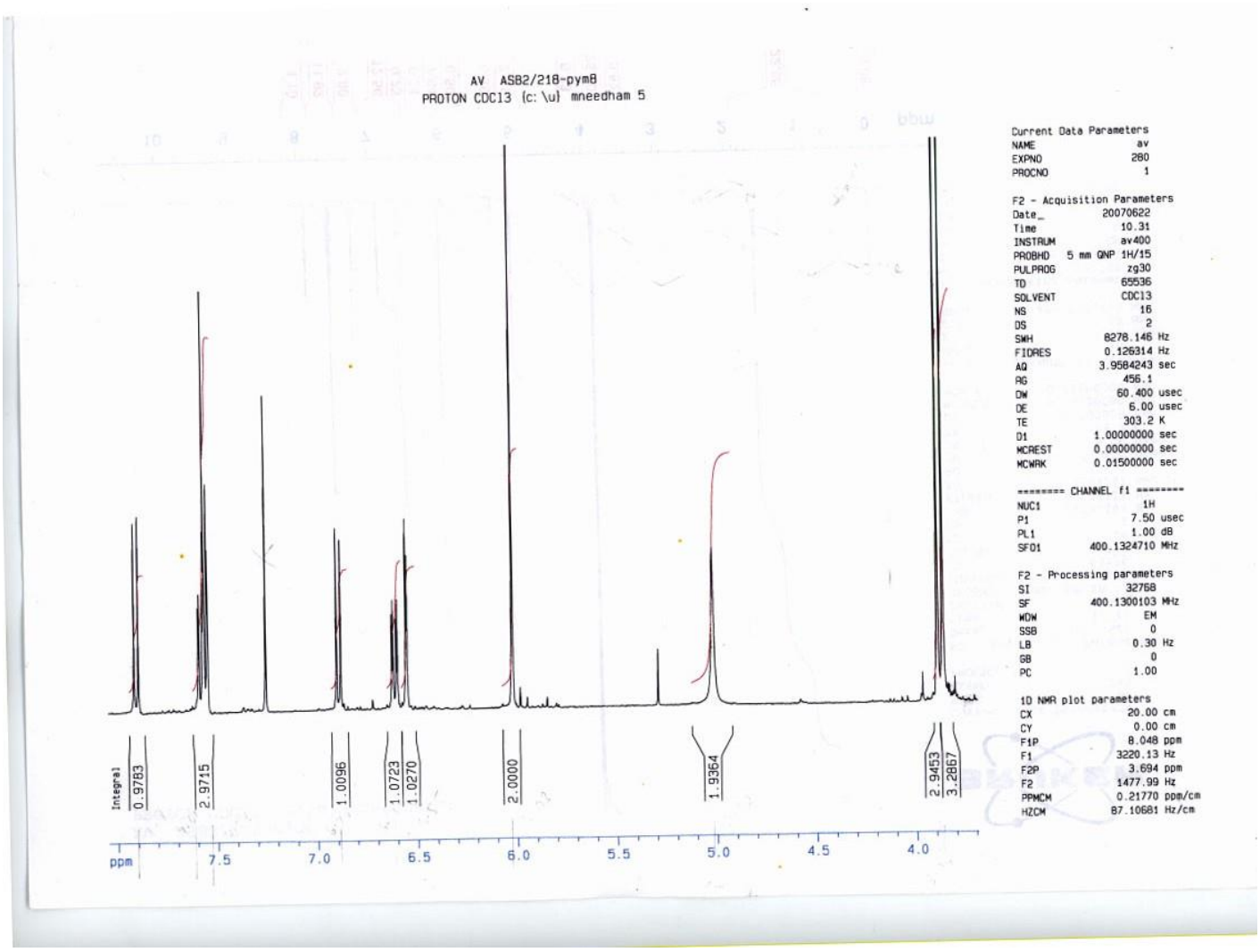

Figure 51. ^{1}H NMR spectrum of DMU 10212

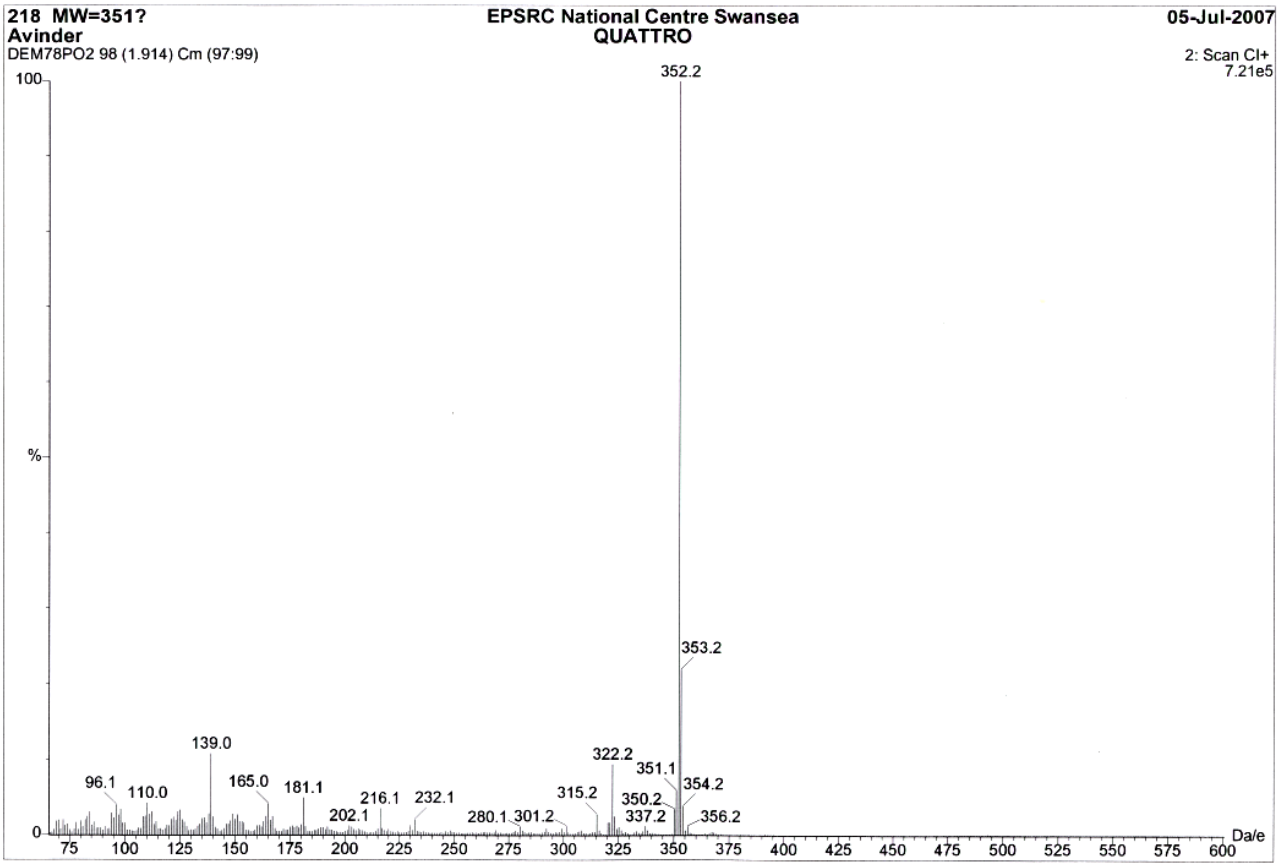

Figure 52. MS spectrum of DMU 10212

Figure 51 illustrates the ^{1}H NMR spectrum and Figure 52 shows the MS spectrum of DMU 10212.

Yields obtained for the synthesis of pyrimidines ranged from 9% achieved for DMU 10202 to 33% gained for DMU 10203, which in general was not significantly high. This may be explicable by the way in which the initial nucleophilic addition step between the guanidine and chalcone occurs. The kinetically favoured 1,2-nucleophilic addition is required (Figure 53) to enable the imine intermediate to form, and for the reaction to proceed to produce the pyrimidine heterocycle. [225] However, there is also the possibility that 1,4-nucleophilic addition can occur which is thermodynamically favoured. This would form an undesired cyclised product, hence lowering the yield of the overall reaction.

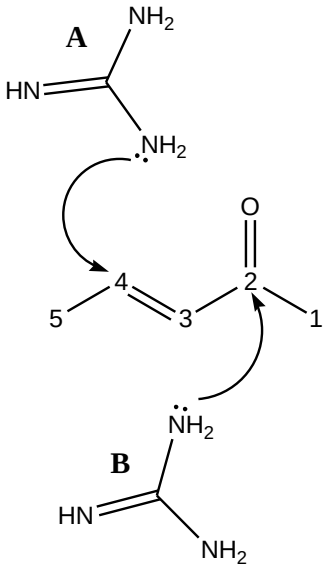

Figure 53. Guanidine A shows the possibility of 1,4-nucleophilic addition and guanidine B shows the required 1,2-nucleophilic addition required to achieve the pyrimidine

It has also been reported that the addition of hydrogen peroxide too early into the reaction resulted in the formation of a 5-membered heterocyclic by-product, which may also be formed if sufficient chalcone remains un-reacted with the free guanidine. Therefore it is vital for the chalcone and guanidine to be stirred without the presence of hydrogen peroxide in order to achieve the maximum amount of dihydro-pyrimidine possible to prevent further side-products forming.

The uses of several bases have been reported in the synthesis of pyrimidines from chalcones, including potassium hydroxide, sodium hydroxide, potassium carbonate and sodium isopropoxide.[226, 227]

Agarwal et al have also reported the synthesis of similar substituted pyrimidines for the treatment of malaria, achieving yields between 59-77% for their compound library. This method employed the use of sodium isopropoxide as the base under anhydrous conditions, which is a stronger base than potassium hydroxide used in the synthesis of the pyrimidines in Table 12. The addition of an oxidising agent in order to achieve an aromatised heterocycle was not used in the reactions carried out. A more recent publication has shown the synthesis of pyrimidines from chalcones using potassium carbonate as the base stirred in DMF as the solvent.[228] The reaction was carried out at room temperature with yields of up to 96% being recorded.

Therefore, it could be possible that in order to achieve a higher yield of pyrimidine, the reaction may require the use of different reaction conditions which could be investigated for

future work. Also, an exploration can be made to see if the addition of hydrogen peroxide is required or not to achieve the final pyrimidine product, or whether stirring the reactions in air could suffice as there appears to be conflicting literature data.

Another approach used to synthesise pyrimidine heterocycles from α,β-unsaturated compounds has been shown by *Lin et al* (Figure 54).[229] *S*-methylisothiourea was reacted with α,β-unsaturated compounds using NaOMe in MeOH producing pyrimidines in yields ranging from 7-55%. The 2-positioned SMe on the pyrimidine heterocycle was then substituted with various amines to yield 2-amino substituted pyrimidines. This was achieved either using 1,4-dioxane or THF as the solvent, with yields ranging from 25-55%. However, as this method uses a two step synthesis, the overall yield obtained may be lower than that achieved from the one-step approach used to synthesise the 2-amino-4,6-diaryl pyrimidines in this project.

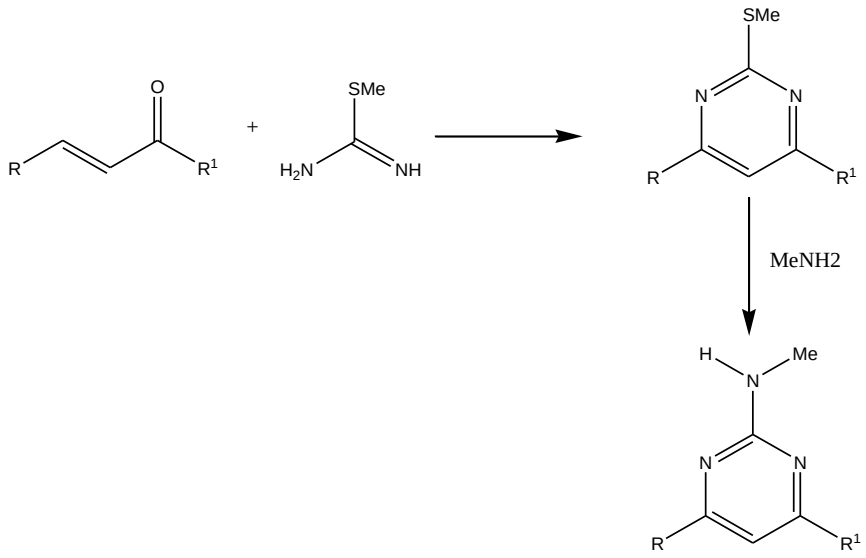

Figure 54. Substituted pyrimidine synthesised by *Lin et al*

3.1 Biological Evaluation of the 2-Amino-4,6-Diarylpyrimidines

Fifteen 2-amino-4,6-diarylpyrimidines were synthesised and evaluated for their cytotoxic properties against the MDA 468, MCF7 and MDA 231 breast cancer cell lines. This was achieved using the MTT assay described in Chapter 2, Section 2.4, with experimentations conducted by Dr. D. Ankrett of the CDDG. The cytotoxicity data recorded for the

pyrimidines will be discussed in accordance to the substitutions on the A and B-rings (Figure 55) and grouping together compounds with the same constant substitutions.

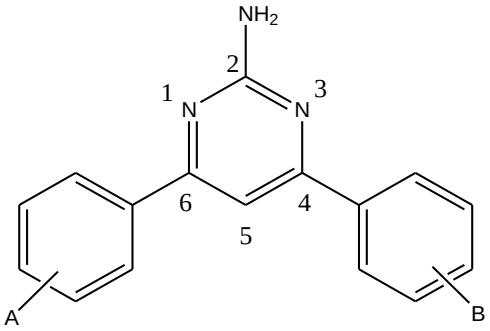

Figure 55. A and B-rings of the pyrimidine

3.1.1 Methylenedioxy Substituted A-Ring

Ten pyrimidines with constant 3,4-methylenedioxy substituted A-rings were synthesised with either single, double or triple methoxy groups on the B-rings, and one with a methylenedioxy substituted B-ring. These compounds will be further divided in respect to the B-ring substitutions in order to facilitate discussion of the cytotoxicity data achieved.

3.1.1.1 Biological Evaluation of DMU 10213, DMU 10211 and DMU 10209

Three amino-pyrimidines were synthesised with methylenedioxy substituted A-rings and mono methoxy substituted B-rings (Figure 56).

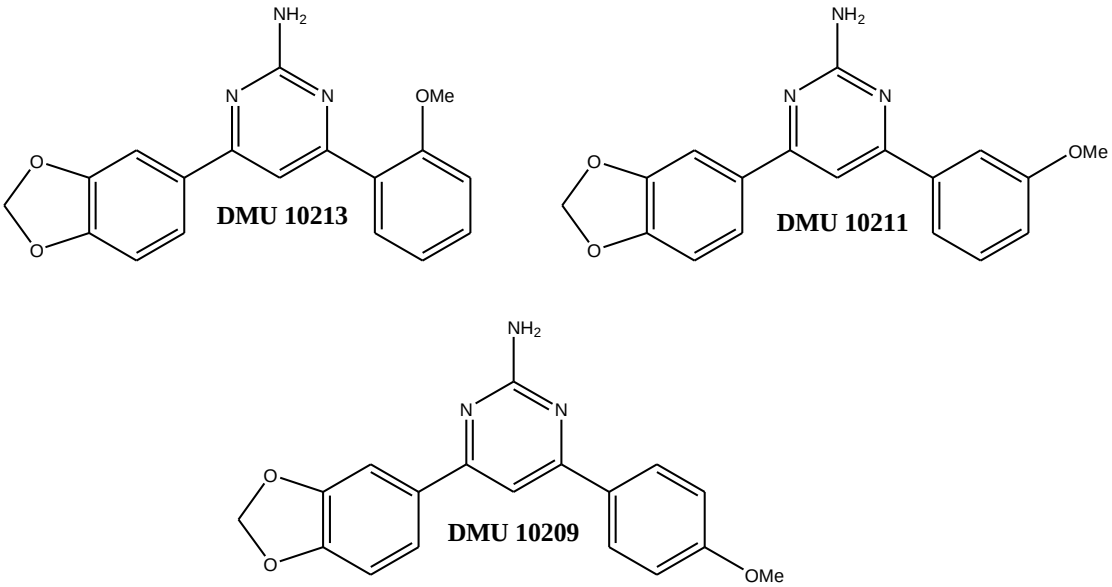

Figure 56. Structures of DMU 10213, DMU 10211 and DMU 10209

Table 13. Cytotoxicity data for the mono-methoxy substituted B-ring pyrimidines

		Substitution		IC_{50} (µM)		IC_{50} (µM)		IC_{50} (µM)	
Entry	**DMU No.**	**A-Ring**	**B-Ring**	**MCF10A**	**MDA 468**	**MCF7**	**MCF7 + TCDD**	**MDA 231**	**MDA 231 + TCDD**
1	10209	3,4-OCH_2O-C_6H_3	4-$MeOC_6H_4$	50	0.6	>100	>100	95	55
2	10211	3,4-OCH_2O-C_6H_3	3-$MeOC_6H_4$	100	18	60	60	70	70
3	10213	3,4-OCH_2O-C_6H_3	2-$MeOC_6H_4$	50	0.2	0.06	0.05	1	1

n=1

With a 2-methoxy substituted B-ring, DMU 10213 (Table 13, entry 3) displayed the greatest toxicity towards the tumour cell lines out of the mono methoxy substituted B-ring compounds. In the MDA468 cancer cell line which constitutively expresses both CYP1A1 and CYP1B1 an IC_{50} value of 0.2µM was obtained, which was 250 times more toxic in comparison to the toxicity observed against the MCF10A cells (Figure 57). In comparison to its chalcone derivative of DMU 2265, DMU 10213 was 250 more potent towards the MDA 468 cell line.

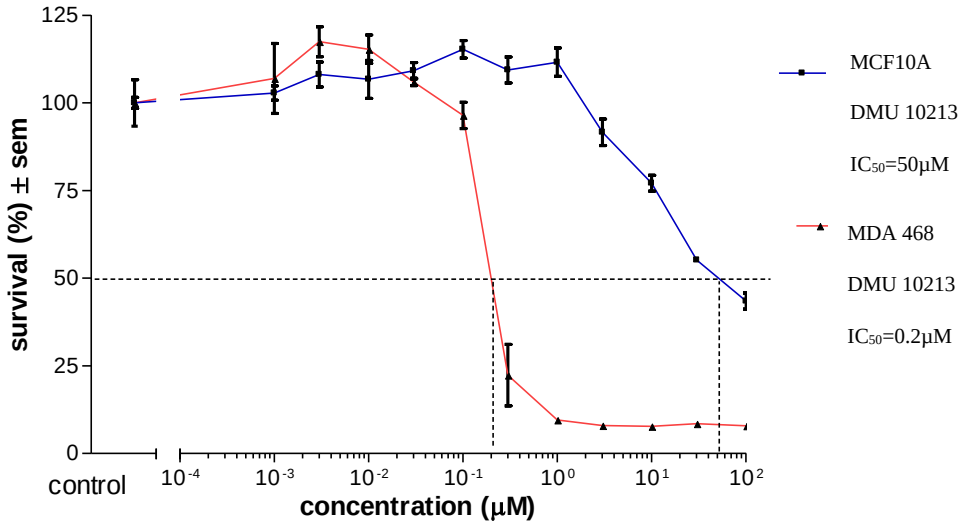

Figure 57. Cytotoxicity plot of MDA 468 and MCF10A treated with DMU 10212

IC_{50} values of 1µM were observed when DMU 10213 was screened against the TCDD induced and non-induced MDA 231 cells, the lowest IC_{50} results obtained from the methylenedioxy substituted A-ring pyrimidines. In the MCF7 cell line which constitutively expresses very low levels of CYP1 enzymes, IC_{50} values of 0.05µM and 0.06µM were recorded against the TCDD induced and non-induced MCF7 cells (Figure 58). This result was considerably lower than that observed from DMU 2265, as IC_{50} values of 50µM and 100µM were recorded against the TCDD induced and non-induced MCF7 cells.

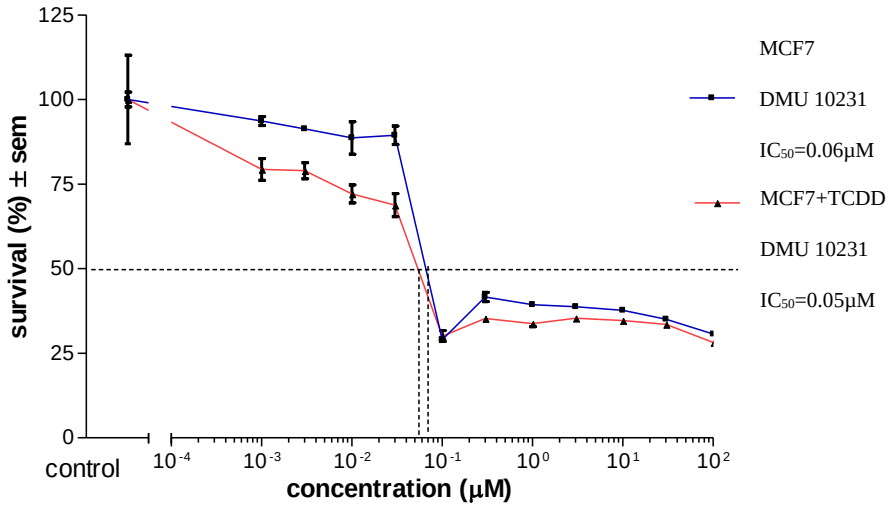

Figure 58. Cytotoxicity plot of MCF7 and MCF7 + TCDD treated with DMU 2285

DMU 10211 (Table 13, entry 2) was synthesised bearing a 3-methoxy substituted B-ring. Unlike DMU 10213, DMU 10211 did not show toxicities of a considerable degree, as IC_{50} values were 18µM and over towards the tumour cell lines. DMU 10209 (Table 13, entry 2) was synthesised with a 4-methoxy substituted B-ring. An IC_{50} value of 0.6µM was observed towards the MDA 468 cells, 83 times more toxic in contrast to the non-tumour MCF10A cells. However, results from the MCF7 and MDA 231 cells were not low enough to warrant further investigation as IC_{50} values were 55µM and above.

3.1.1.2 Biological Evaluation of DMU 10212, DMU 10214, DMU 10210 and DMU 10205

Four pyrimidines were synthesised with dimethoxy substituted B-rings and methylenedioxy substituted A-rings (Figure 59).

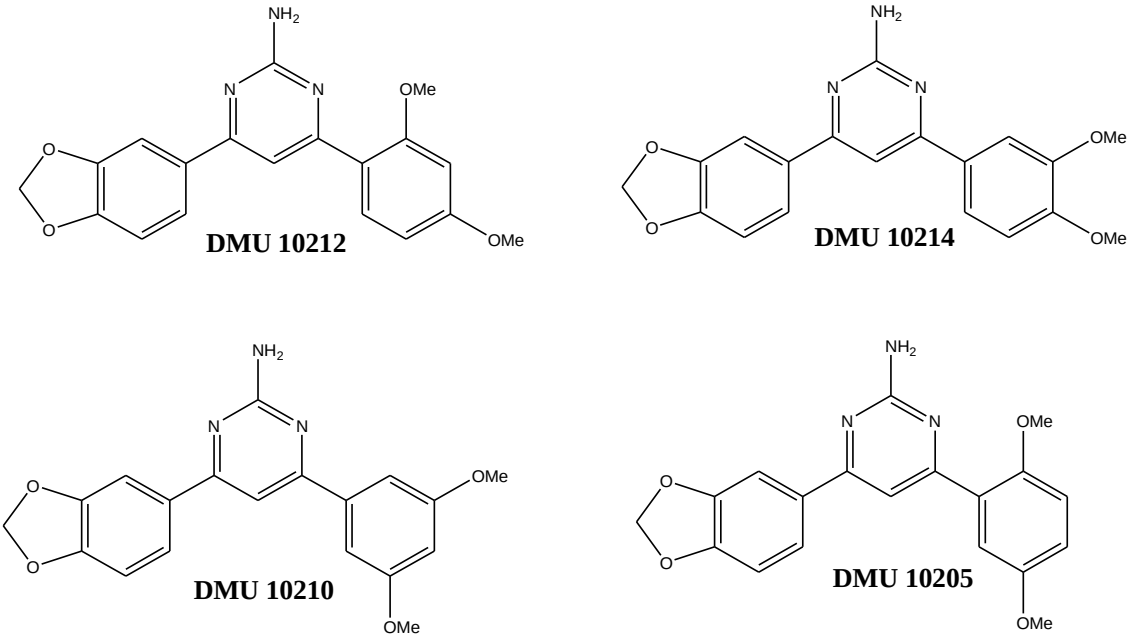

Figure 59. Structures of DMU 10212, DMU 10214, DMU 10210 and DMU 10205

Table 14. Cytotoxicity data for the dimethoxy substituted B-ring pyrimidines

		Substitution		**IC_{50} (μM)**		**IC_{50} (μM)**		**IC_{50} (μM)**	
Entry	**DMU No.**	**A-Ring**	**B-Ring**	**MCF10A**	**MDA 468**	**MCF7**	**MCF7 + TCDD**	**MDA 231**	**MDA 231 + TCDD**
1	10205	3,4-OCH_2O-C_6H_3	2,5-$(MeO)_2C_6H_3$	>100	1.5	3	3	10	10
2	10210	3,4-OCH_2O-C_6H_3	3,5-$(MeO)_2C_6H_3$	>100	3	3	7	40	3
3	10212	3,4-OCH_2O-C_6H_3	2,4-$(MeO)_2C_6H_3$	>100	0.01	0.07	0.3	30	20

4	10214	3,4-OCH_2O-C_6H_3	3,4-$(MeO)_2C_6H_3$	>100	60	>100	>100	30	18

n=1

DMU 10212 (Table 14, entry 3), synthesised with a 2,4-dimethoxy substituted B-ring showed exciting toxicity towards the MDA 468 cell line giving an IC_{50} value of 0.01µM whilst remaining non-toxic against the non-tumour MCF10A cell line (Figure 60).

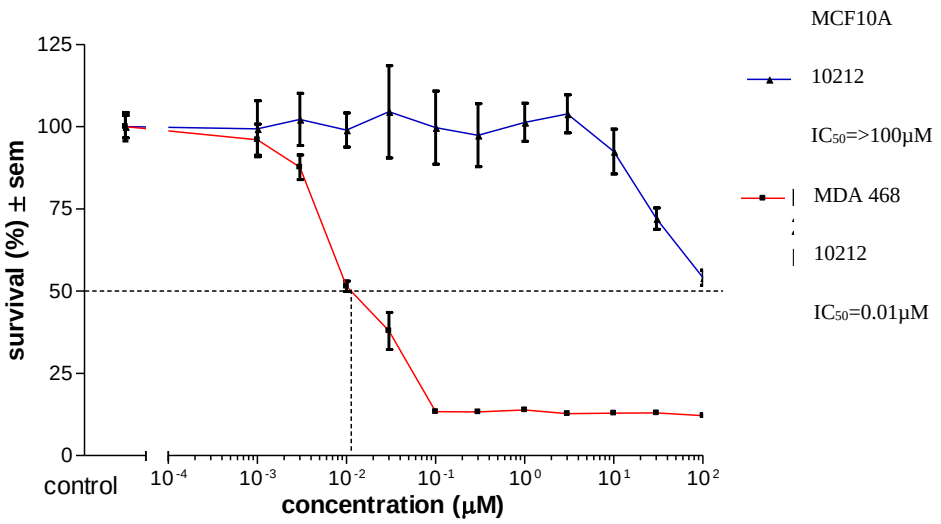

Figure 60. Cytotoxicity plot of MDA 468 and MCF10A treated with DMU 10212

The MCF7 cells, both induced and non-induced with TCDD also gave significant cytotoxic activity when screened with DMU 10212. The TCDD induced cells gave an IC_{50} value of 0.3µM and the non-TCDD induced cells gave an IC_{50} value of 0.07µM (Figure 61).

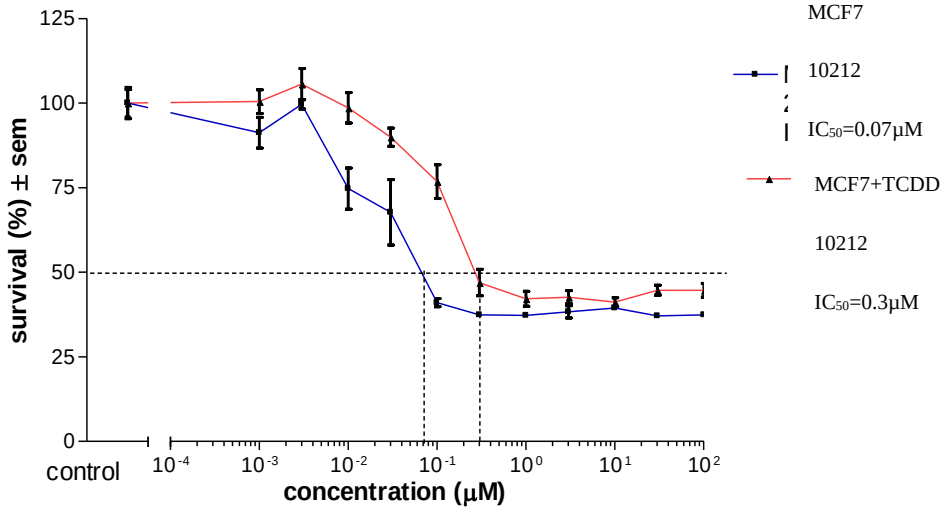

Figure 61. Cytotoxicity plot of MCF7 and MCF7 + TCDD treated with DMU 10212

DMU 10212 was not as potent towards the MDA 231 cells in contrast to the results obtained from the MDA 468 and MCF7 cells. IC_{50} values of 20µM and above were observed which are not considered significantly toxic. In comparison to its pyrazole analogue of DMU 10108, DMU 10212 was 5500 times more toxic towards the MDA 468 cell line (Table 15, entry 2). It can also be seen that the toxicity of DMU 10212 against the MCF7 and MDA 231 cells was significantly greater than that of DMU 10108. DMU 10212 also proved to be more cytotoxic in comparison to its chalcone analogue of DMU 407 (Table 15, entry 3), showing 125 times more toxicity towards the MDA 468 cell line and increased toxicity towards the MCF7 cells.

Table 15. Cytotoxicities of DMU 10212, DMU 10108, DMU 407 and DMU 981

			IC_{50} (µM)					
Entry	**DMU No.**	**Structure**	**MCF 10A**	**MDA 468**	**MCF7**	**MCF7 + TCDD**	**MDA 231**	**MDA 231 + TCDD**
1	10212	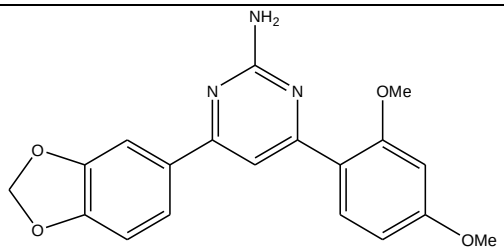	>100	0.01	0.07	0.3	30	20
2	10108	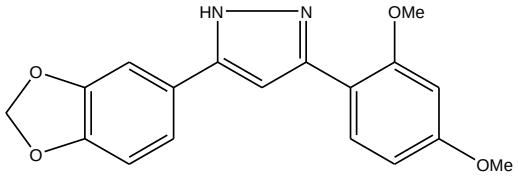	>100	55	>100	>100	>100	>100
3	407	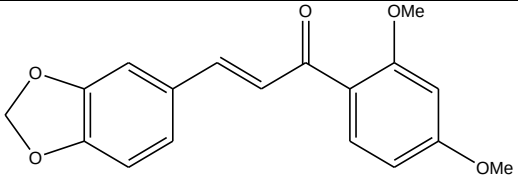	>100	10	45	11	11	8

DMU 10214 (Table 14, entry 4) was designed with a 3,4-dimethoxy substitution on the B-ring, however, IC_{50} results observed from screening this compound were not toxic enough for

this compound to warrant further investigation. DMU 10210 (Table 14, entry 2) was synthesised with a 3,5-dimethoxy substitution on the B-ring. A noticeable toxicity of 3µM was observed towards the MDA 468 cell line whilst no toxicity was seen against the MCF10A cells (Figure 62). The chalcone analogue DMU 160 was 4 times less toxic towards the MDA 468 cells and also showed toxicity towards the non-tumour MCF10A cells. A lower toxicity towards the MCF7 cells was also observed from the amino-pyrimidine in contrast to the chalcone derivative. DMU 10210 and DMU 160 also showed similar toxicity towards the TCDD induced MDA 231 cells, but results from the non-induced MDA 231 cells showed greater toxicity from DMU 160.

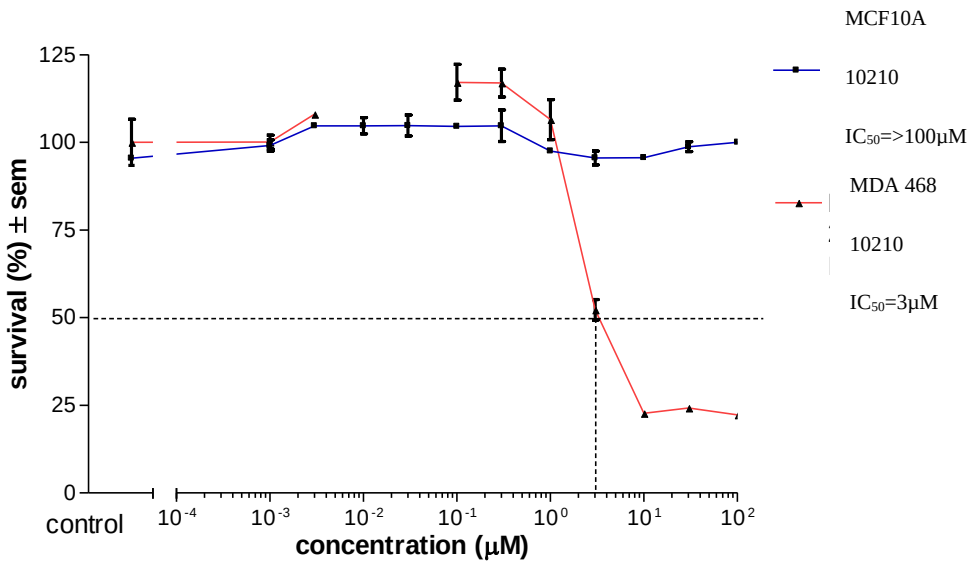

Figure 62. Cytotoxicity plot of MDA 468 and MCF10A treated with DMU 10210

DMU 10205 (Table 14, entry 1) was synthesised with a 2,5-dimethoxy substitution on the B-ring. The result from the MDA 468 cell line gave an IC_{50} value of 1.5µM whilst no toxicity was seen towards the MCF10A cell line. An IC_{50} value of 3µM was recorded for both the TCDD induced and non-induced MCF7 cells, and the MDA 231 TCDD induced and non-induced cells also gave an identical result of 10µM. DMU 423, the chalcone analogue of DMU 10205 gave a considerably toxic IC_{50} value of 0.7µM when screened against the non-tumour MCF10A cells compared to the non-toxic data observed from DMU 10205. The incorporation of the amino-pyrimidine heterocycle in this case has lowered the toxicity towards the non-tumour MCF10A cells significantly, while maintaining an encouraging toxicity towards the MDA 468 cell line.

3.1.1.3 Biological Evaluation of DMU 10204 and DMU 10202

Two amino-pyrimidines were synthesised with tri-methoxy substitutions on the B-rings and methylenedioxy substitutions on the A-rings (Figure 63).

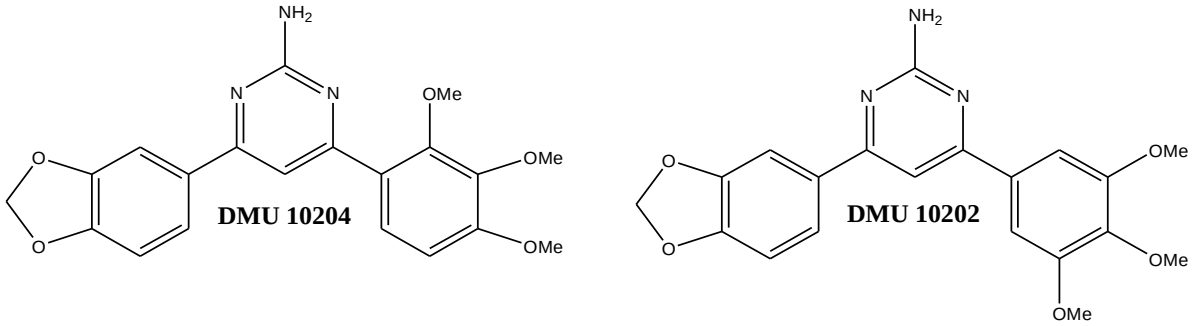

Figure 63. Structures of DMU 10204 and DMU 10202

Table 16. Cytotoxicity data for the trimethoxy substituted B-ring pyrimidines

		Substitution		**IC_{50} (µM)**		**IC_{50} (µM)**		**IC_{50} (µM)**	
Entry	**DMU No.**	**A-Ring**	**B-Ring**	**MCF10A**	**MDA 468**	**MCF7**	**MCF7 + TCDD**	**MDA 231**	**MDA 231 + TCDD**
1	10202	3,4-OCH_2O-C_6H_3	3,4,5-$(MeO)_3C_6H_2$	80	80	70	>100	15	20
2	10204	3,4-OCH_2O-C_6H_3	2,3,4-$(MeO)_3C_6H_2$	>100	1	10	2	9	0.6

n=1

DMU 10204 (Table 16, entry 2) showed interesting cytotoxicity when screened against the MDA 468 cell line, giving an IC_{50} value of 1µM whilst showing no toxicity towards the non-tumour MCF10A cell line. This was encouraging as DMU 419, the chalcone analogue of DMU 10204 gave an IC_{50} value of 14µM when screened against the MCF10A cell line, showing the incorporation of the amino-pyrimidine heterocycle advantageous in this case. An significant IC_{50} value of 0.6µM was obtained for the cytotoxicity of DMU 10204 against the

TCDD induced MDA 231 cells, whilst the non-induced cells showed a less potent effect with an IC_{50} value of 9µM being recorded. Toxicity was also observed in the MCF7 cell lines with an IC_{50} value of 10µM being achieved for the non-induced cells, whereas the TCDD treated MCF7 cells showed a five-fold increase in toxicity. This could be explained by the increased expression of CYP1 enzymes by TCDD metabolising DMU 10204 to its cytotoxic metabolites. DMU 10107, the pyrazole analogue was shown to be the most effective prodrug synthesised in chapter two. But DMU 10204 clearly exhibited enhanced toxicities towards the tumour cell lines in contrast to DMU 10107 (Table 17, entry 1), showing 8 times more cytotoxicity towards the MDA 468 cells, but more noticeably towards the MDA 231 cells induced with TCDD as an IC_{50} value of 0.6µM was recorded.

Table 17. Cytotoxicities of DMU 10107 and DMU 10204

			IC_{50} (µM)					
Entry	**DMU No.**	**Structure**	**MCF 10A**	**MDA 468**	**MCF7**	**MCF7 + TCDD**	**MDA 231**	**MDA 231 + TCDD**
1	10107	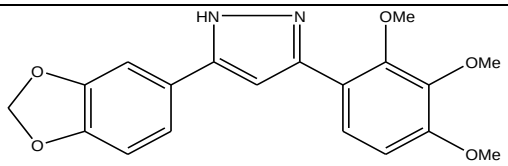	>100	8	10	10	>100	>100
2	10204	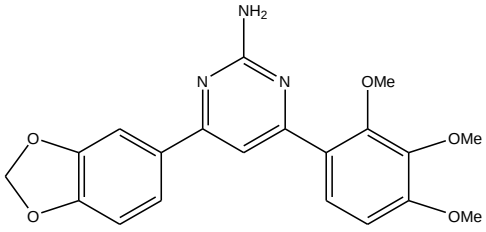	>100	1	10	2	9	0.6

DMU 10202, substituted with a tri-methoxy B-ring (Table 16, entry 1) did not show toxicities comparable to DMU 10204 as all IC_{50} values were 15µM and greater. This was a disappointing result as DMU 135, the chalcone precursor of DMU 10102 showed significant anti-tumour toxicities, especially towards the MDA 468 cell line with an IC_{50} value of 0.006µM.

3.1.1.4 Biological Evaluation of DMU 10203

The amino-pyrimidine DMU 10203 was synthesised with methylenedioxy substituted A and B-rings (Figure 64).

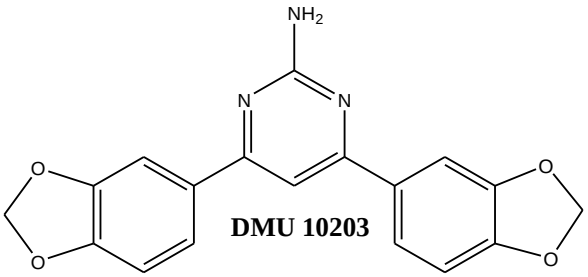

Figure 64. Structure of DMU 10203

However, the results obtained from the MTT assays only appeared to show relative toxicity towards the MDA 231 cells, where IC_{50} values of 6µM for both the TCDD induced and non induced cells were observed. Undesirable toxicity was also seen towards the MCF10A cells hence this compound will not warrant further investigation.

3.1.2 4-Methoxy Substituted A-Ring

Four pyrimidines were synthesised with consistent 4-methoxy substituted A-rings (Figure 65).

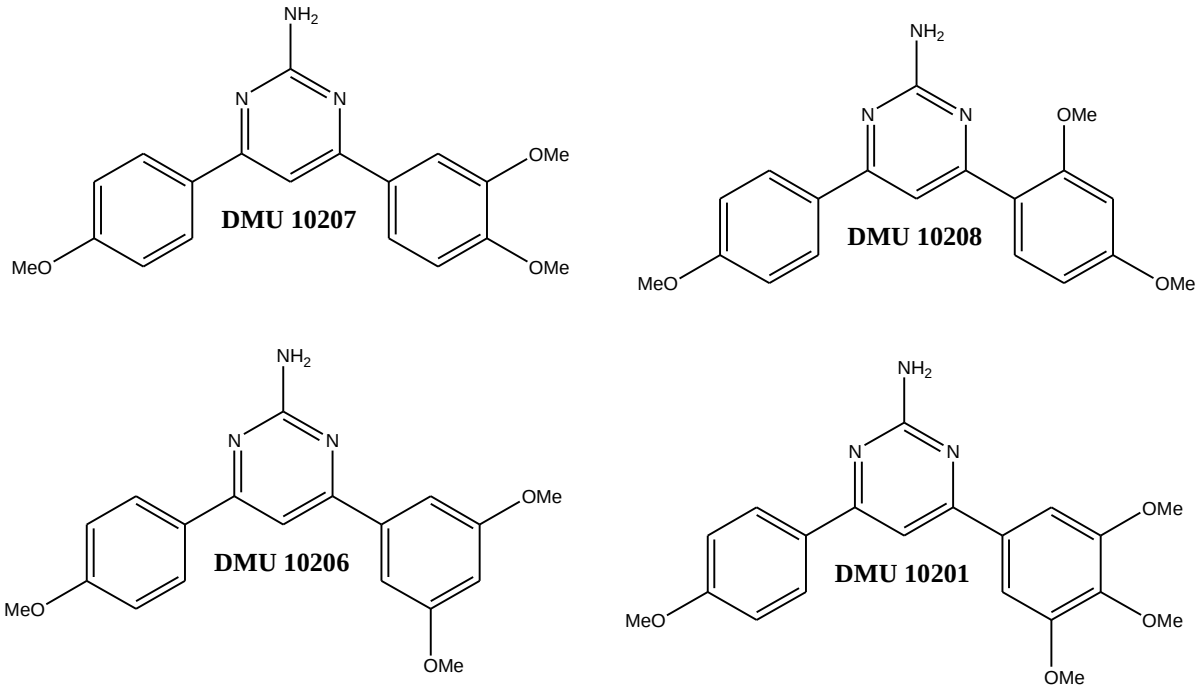

Figure 65. Structures of DMU 10207, DMU 10208, DMU 10201 and DMU 10206

Table 18. Cytotoxicity data for the A-ring 4-methoxy substituted pyrimidines

		Substitution		IC_{50} (µM)		IC_{50} (µM)		IC_{50} (µM)	
Entry	**DMU No.**	**A-Ring**	**B-Ring**	**MCF10A**	**MDA 468**	**MCF7**	**MCF7 + TCDD**	**MDA 231**	**MDA 231 + TCDD**
1	10207	4-$MeOC_6H_4$	3,4-$(MeO)_2C_6H_2$	30	0.6	42	42	55	55
2	10208	4-$MeOC_6H_4$	2,4-$(MeO)_2C_6H_2$	>100	0.2	0.2	0.05	3	3
3	10201	4-$MeOC_6H_4$	3,4,5-$(MeO)_3C_6H_2$	>100	13	45	70	30	30
4	10206	4-$MeOC_6H_4$	3,5-$(MeO)_2C_6H_2$	>100	6	30	60	>100	>100

n=1

DMU 10207 (Table 18, entry 1) synthesised with a 3,4-dimethoxy substituted B-ring showed interesting toxicity towards the MDA 468 cells giving an IC_{50} value of 0.6µM. The non-tumour MCF10A cells gave an IC_{50} value of 30µM, showing DMU 10207 was 50 times more toxic towards the CYP1 expressing MDA 468 cell line. However, this compound was not particularly toxic to the MCF7 and MDA 231 cells, with IC_{50} values of 42µM and above being recorded. DMU 10208 (Table 18, entry 2) was synthesised with a 2,4-dimethoxy substituted B-ring. As observed with previous compounds, a methoxy group in the 2-position has shown to be important for cytotoxic activity of the compound. As expected, DMU 10208 exhibited significant toxicity towards the MDA 468 cell line with an IC_{50} value of 0.2µM, and showed little toxicity towards the MCF10A cells (Figure 66). DMU 10208 was more toxic compared to its chalcone derivative of DMU 133 against the MDA 468 cell line but importantly was shown to be significantly less toxicity towards the non-tumour MCF10A cells.

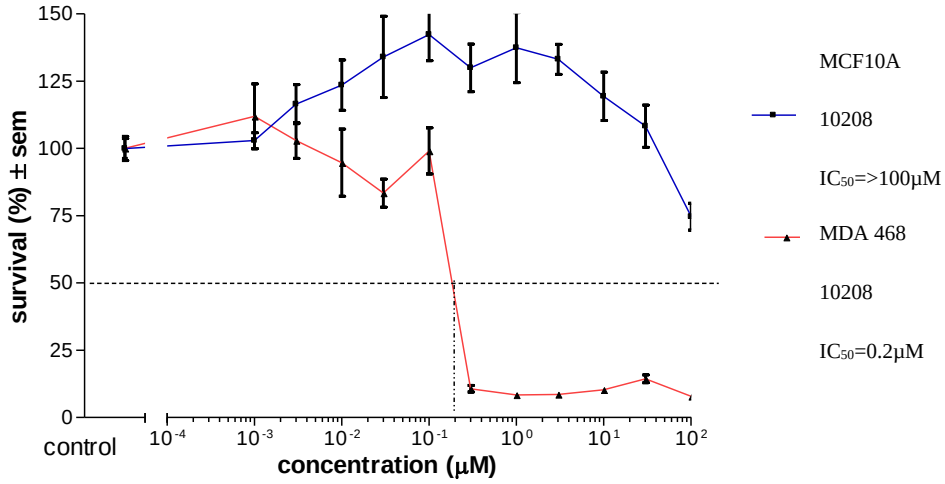

Figure 66. Cytotoxicity plot of MDA 468 and MCF10A treated with DMU 10208

Significant toxicity was recorded from screening DMU 10208 against the MCF7 cells, with IC_{50} values of 0.05µM and 0.2µM being observed for the TCDD induced and non-induced cells (Figure 67). Again, this result was an increase in cytotoxicity than that observed from DMU 133.

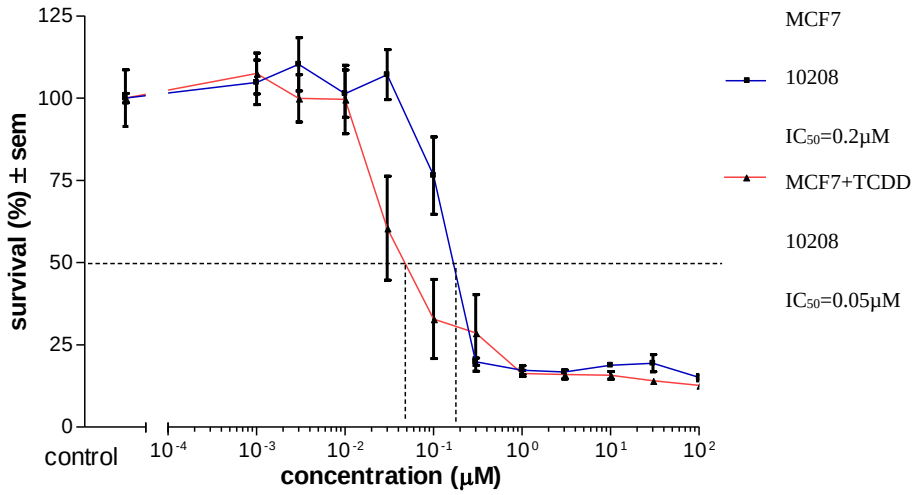

Figure 67. Cytotoxicity plot of MCF7 and MCF7 induced with TCDD treated with DMU 10208

An IC_{50} value of 3µM was recorded when DMU 10208 was screened against the MDA 231 cells with and without TCDD induction. It can been seen that DMU 10208 was more toxic in comparison to DMU 10207, especially against the MCF7 and MDA 231 cells which indicates

further that a methoxy group in the 2-position of the B-ring is important for activity against the tumour cells. DMU 10201 (Table 18, entry 3) appeared to show its most effective cytotoxicity against the MDA 468 cell line achieving an IC_{50} value of 13µM. However, the chalcone analogue of DMU 10201, DMU 102 appeared to be more toxic towards the MDA 468 cell line as an IC_{50} value of 0.5µM was recorded. IC_{50} values from screening DMU 10201 against the MCF7 and MDA 231 were also not to a noteworthy degree, as values of 30µM and above were seen.

Modification of DMU 10201 by the addition of a methoxy group in the 4-position of the B-ring gave DMU 10206 (Table 18, entry 4). Results from screening DMU 10206 against the MDA 468 cell line showed a 2-fold increase in cytotoxicty compared to DMU 10201, but no significant toxicities were observed from the MCF7 and MDA 231 cells as IC_{50} values were 15µM and above.

3.1.3 Non-Substituted A and B-Ring

DMU 10200 was synthesised without bearing any substitutions on the A and B-rings (Figure 68).

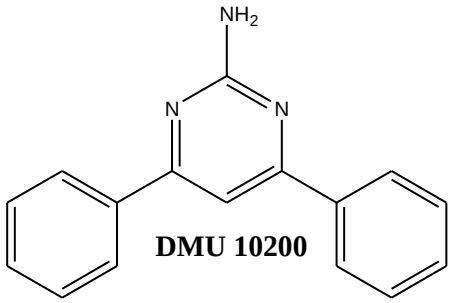

DMU 10200

Figure 68. Structure of DMU 10200

DMU 10200 showed considerable activity towards the MDA 468 cell line, with an IC_{50} of 0.2µM whereas no toxicity was observed against the MCF10A cell line (Figure 69). The MCF7 cell line showed sufficient cytotoxicity as the TCDD induced cells gave an IC_{50} value of 7µM and the non-induced cells showed an IC_{50} value of 3µM. However, the MDA 231 cell line did not show toxicities to a noteworthy degree as IC_{50} values of 50µM were observed for the TCDD induced and non-induced cells.

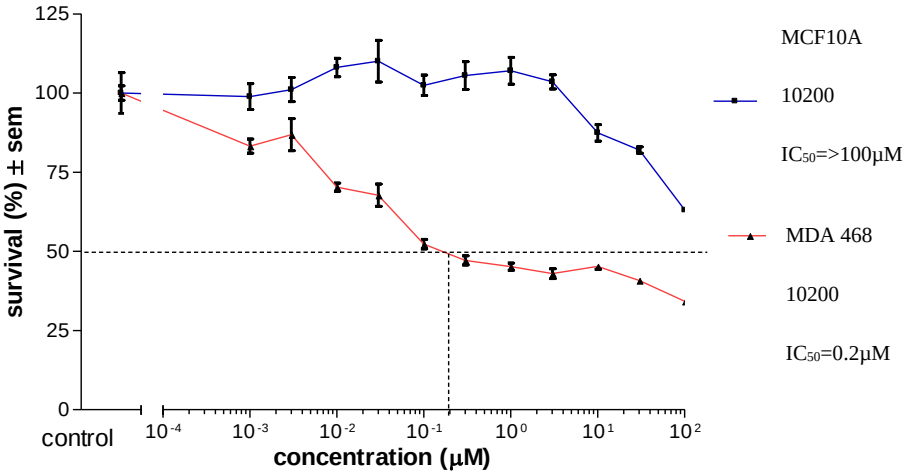

Figure 69. Cytotoxicity plot of MDA 468 and MCF10A treated with DMU 10200

DMU 10200 showed comparative toxicity towards the MDA 468 cells with the results observed from DMU 10212 and DMU 10213 (Figure 70), but showed significantly less toxicity towards the MCF7 and MDA 231 cells. It can be seen from DMU 10200 that without substituted phenyl groups present the amino-pyrimidine is an effective anti-cancer prodrug against the MDA 468 cell line. But it appears that 3,4-methylenedioxy or methoxy substituted phenyl groups must be present in order for cytotoxicity to be seen towards the MCF7 and MDA 231 cell lines too.

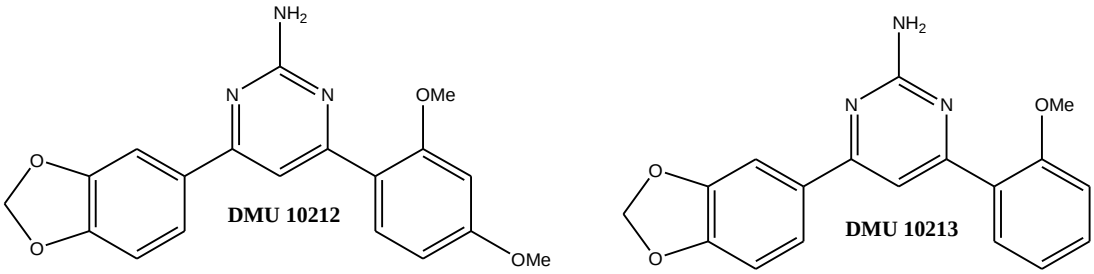

Figure 70. Structures of DMU 10212 and DMU 10213

3.2 Summary and Conclusions

In chapter two, pyrazole heterocycles were integrated into the α,β-unsaturated moiety of chalcones to yield 3,5-diarylpyrazoles. The pyrazoles were synthesised to lock chalcones in their biologically active *trans* isomers as these are liable to the problematic reaction of

photoisomerisation, producing the less potent *cis* isomer. However, the pyrazoles were not as cytotoxic towards the tumour cell lines as their chalcone derivatives. Therefore, the α,β-unsaturated moiety required further exploration in an attempt to produce compounds which solved the problem of photoisomerisation occurring and were comparatively similar or greater than the chalcones in cytotoxicity against the tumour cell.

Therefore, fifteen 2-amino-4,6-diarylpyrimidines were synthesised from a method taken by *Varga et al* with yields ranging from 9-33%. The amino-pyrimidines were evaluated for their prodrug activity against a panel of tumour cell lines, which included the MDA 468, MCF7 and MDA 231 cells. Exciting anti-tumour activity was observed from the amino-pyrimidines, especially with DMU 10212, DMU 10213 and DMU 10200 (Table 19). Out of these three compounds, DMU 10212 appeared to be the most effective anti-cancer prodrug as it provided the most effective IC_{50} values across the tumour panel of cell lines screened against. An IC_{50} value of 0.01μM was recorded against the MDA 468 cell line, which constitutively expresses CYP1 enzymes. IC_{50} values of 0.07μM and 0.3μM were observed against the non-induced and TCDD induced MCF7 cells, which expresses CYP1A1 after exposure to TCDD. Importantly, no toxicity was observed towards the non-tumour MCF10A cells.

Table 19. Cytotoxicities of DMU 10212, DMU 10213 and DMU 10200

			IC_{50} (μM)					
Entry	**DMU No.**	**Structure**	**MCF 10A**	**MDA 468**	**MCF7**	**MCF7 + TCDD**	**MDA 231**	**MDA 231 + TCDD**
1	10212	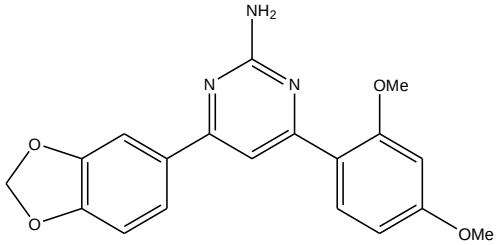	>100	0.01	0.07	0.3	30	20

2	10213	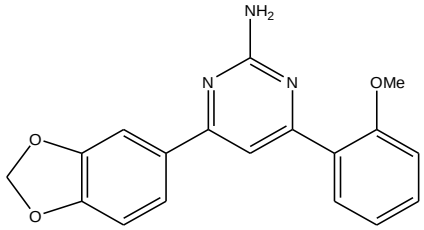	50	0.2	0.06	0.05	1	1
3	10200	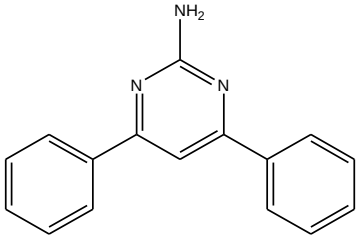	>100	0.2	7	3	50	50

Overall, improved cytotoxicities were observed from the amino-pyrimidines in comparison to their pyrazole derivatives synthesised in chapter two. DMU 10212 and DMU 10213 also showed greater toxicities in contrast to their chalcone analogues, whilst forming the rigid structures required to prevent photoisomerisation occurring. It can be stated that the incorporation of the pyrimidine heterocycle across the α,β-unsaturated chalcones have proved advantageous providing exciting anti-cancer prodrug activity.

Chapter 4

Synthesis and Biological Evaluation of 4,6-Diarylpyrimidones

4.0 Synthesis of 4,6-Diarylpyrimidones

The 2-amino-4,6-diarylpyrimidines synthesised in chapter three gave very exciting cytotoxicity results from screening against the MDA 468, MCF7 and MDA 231 cancer cell lines. Significant results were obtained from DMU 10212 (Figure 71) which showed an IC_{50} value of 0.01µM when screened against the MDA 468 cells and IC_{50} values of 0.07µM and 0.3µM when screened against the MCF7 and MCF7 cells induced with TCDD.

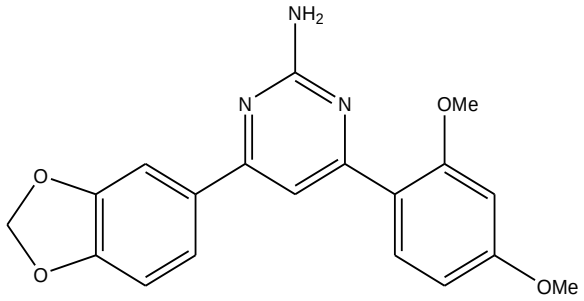

Figure 71. DMU 10212

DMU 10204 (Figure 72) showed significant toxicity towards the MDA 231 cells induced with TCDD, giving an IC_{50} value of 0.6µM. To summarise, the amino-pyrimidine heterocycle has been shown to be important for better cytotoxicities to be observed across the tumour cell lines in contrast to their pyrazole and chalcone derivatives.

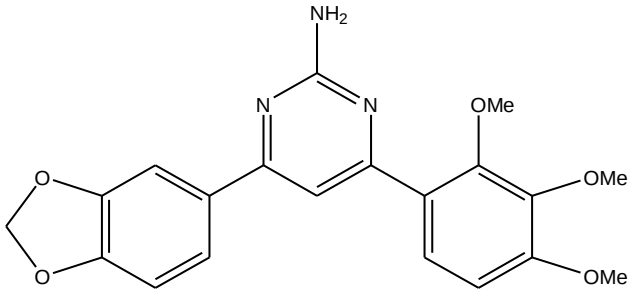

Figure 72. DMU 10204

The next stage of the project was to investigate whether the amino group at the 2-position of the heterocycle was important for the pyrimidines synthesised in chapter three to exhibit their cytotoxic activity, and to explore if other functional groups at the 2-position would alter the toxicity observed. Therefore, pyrimidones were designed which have a carbonyl group at the

2-position of the heterocycle. The lone pair of electrons on the amino group may be involved in electron interactions with CYP1 binding sites, by acting as a hydrogen bond acceptor, or on the other hand the amino protons may act as hydrogen donators. Carbonyl groups have two lone pairs of electrons available on the oxygen atom, which may also partake in electronic interactions between the CYP1 enzymes and the pyrimidones, consequently increasing selectivity and prodrug toxicity.

Pyrimidones have been synthesised by the reaction of urea and chalcones under acidic conditions by *Fathalla et al* (Figure 73).[230]

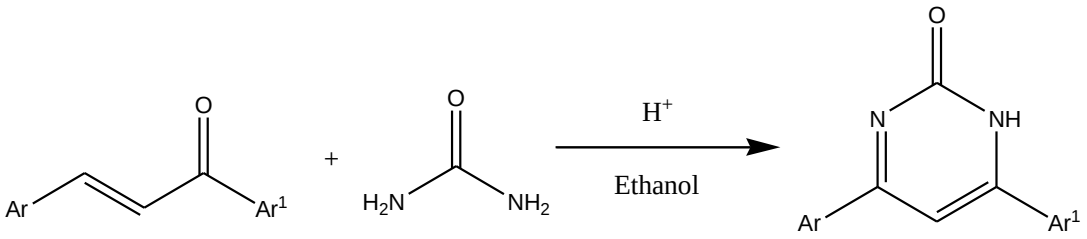

Figure 73. Synthesis of the pyrimidone from the reaction of chalcone and urea

The method involved stirring a mixture of chalcones, urea and hydrochloric acid in ethanol under reflux for 12h. Half of the solvent was removed *in vacuo* followed by the addition of ammonium hydroxide solution to neutralise the reaction. This formed a precipitate which was recrystallised from a mixture of DMF and water, producing the purified pyrimidones in a yield of 67%. However, an approach carried out by *Borovik et al* who converted 2-aminopyrimidoindoles to 2-oxopyrimidoindoles (Figure 74) via diazotisation in a one step reaction using sodium nitrate was found.[231] This reaction reportedly produced the 2-oxopyrimidoindoles in greater than 90% yields, whereas the synthesis of pyrimidones by *Fathalla et al* gave yields of up to 67%. *Borovic et al* stirred 2-aminopyrimidoindoles with aqueous sodium nitrate in acetic acid under reflux, which resulted in the precipitation of the desired 2-oxopyrimidoindoles.

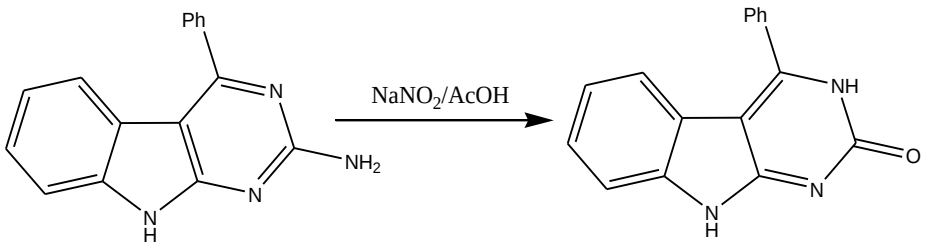

Figure 74. Conversion of aminopyrimidoindoles to 2-oxopyrimidoindoles using sodium nitrate

This method of *Borovic et al* was used as the previously synthesised amino-pyrimidines could be directly converted to the pyrimidones through the diazotisation reaction without the need to re-synthesise chalcones as required for the method used by *Fathalla et al*. Also, direct comparisons in cytotoxicities of the amino-pyrimidines and pyrimidones could be made, indicating the more favourable functional group required for greater cytotoxicty to occur.

The mechanism for the diazotisation of the amino-pyrimidines begins with the dissociation of sodium nitrate in water to give a nitrite ion, which then protonates to form nitrous acid (Scheme 8).[210] The nitrous acid protonates again, resulting in dehydration and the creation of a reactive NO^+ cation. The lone pair of electrons on the amine at the 2-position of the pyrimidine ring attack the nitrogen of the NO^+ cation, followed by dehydration and formation of a diazonium salt. Nitrogen is lost forming a pyrimidine carbocation which undergoes nucleophilic attack by water. The initially formed 2-hydroxypyrimidine tautomerises to give the pyrimidone.

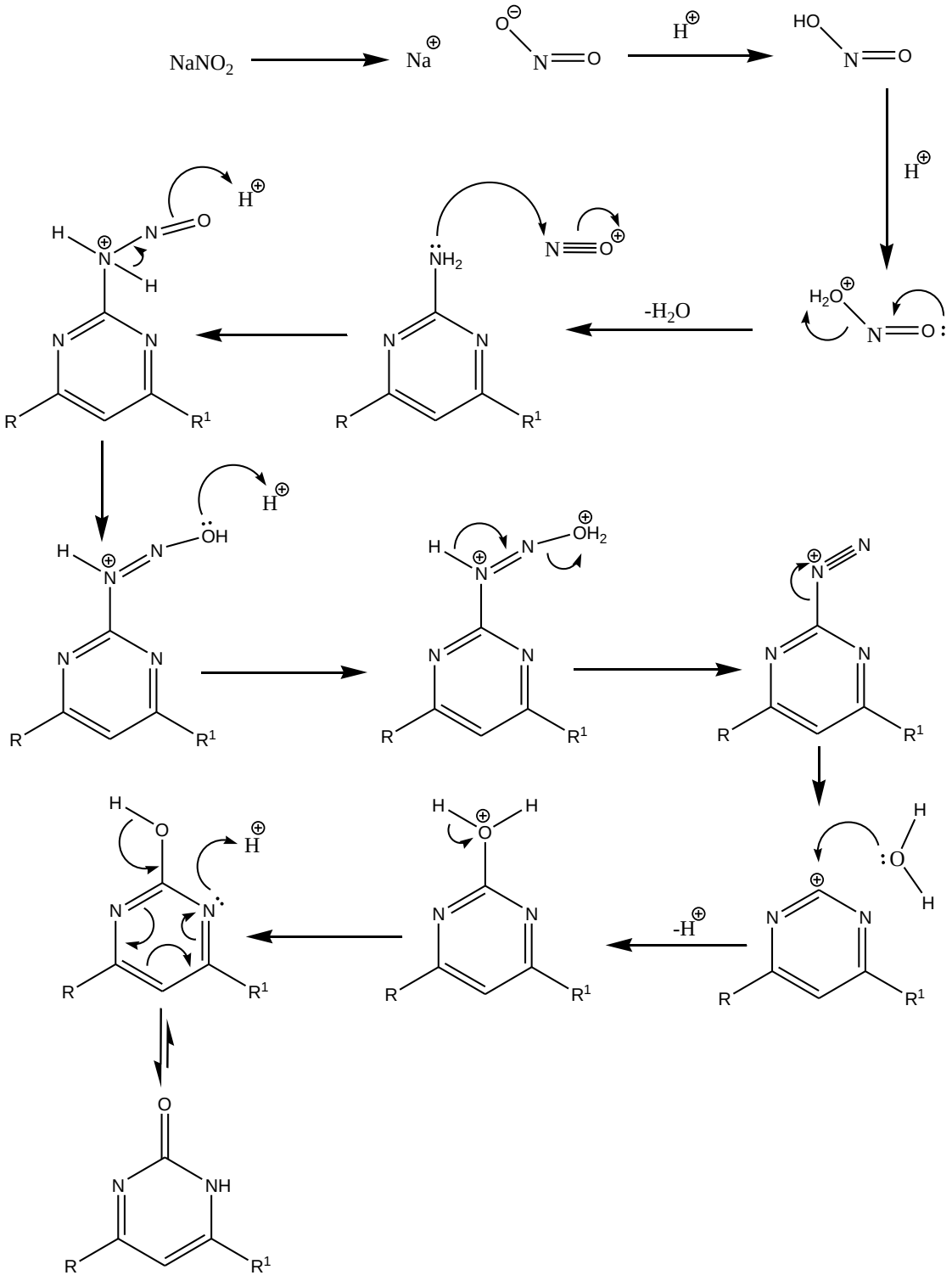

Scheme 8. Mechanism for the conversion of the pyrimidines to the pyrimidones

The pyrimidine conversion reaction was achieved by stirring the pyrimidines (1.31 mmol) in glacial acetic acid (50 ml) under reflux for one hour. Aqueous sodium nitrite (1.08 cm^3, 50%

w/v, 7.8 mmol) was then added and the reaction was stirred under reflux for a further three hours. Once the reaction cooled the glacial acetic acid was removed *in vacuo* resulting in the solid crude pyrimidone, recrystallised from ethanol to yield the pure pyrimidone.

Table 20. Library of the synthesised pyrimidones

Entry	DMU No.	Structure	% Yield	M.P	Appearance
1	10300	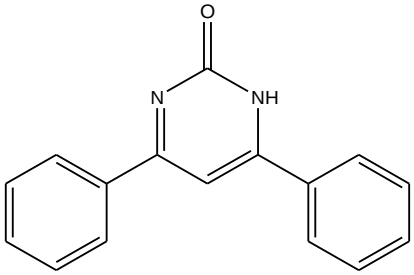	75	221-223	Orange Crystals
2	10301	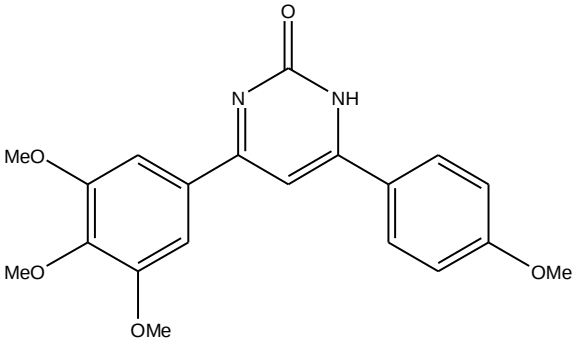	85	275-277	Orange Crystals
3	10302	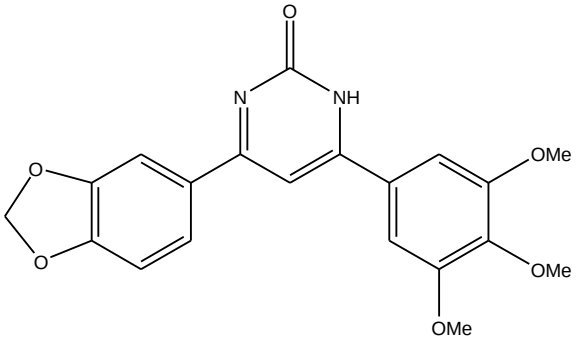	3	271-273	Orange Crystals

4	10303	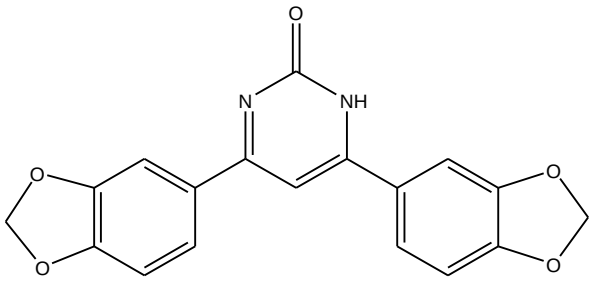	65	296-298	Orange Crystals
5	10314	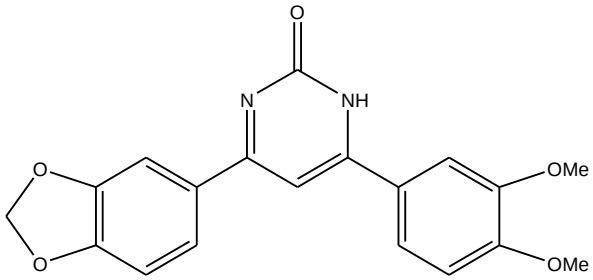	72	290-292	Orange Crystals
6	10304	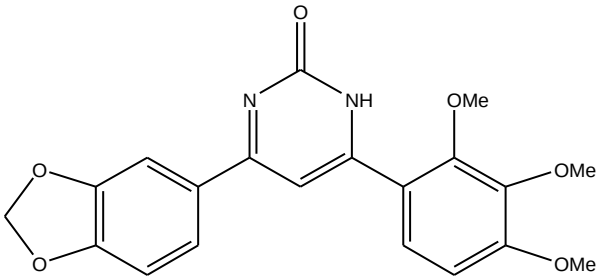	84	261-263	Orange Crystals
7	10312	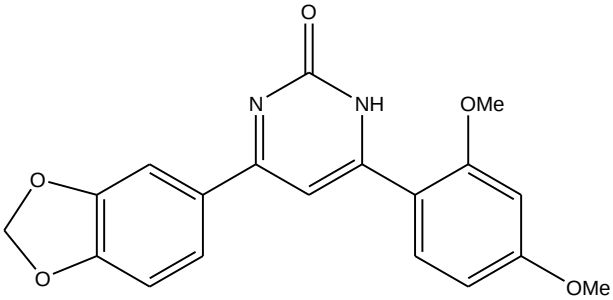	84	198-200	Orange Crystals
8	10305	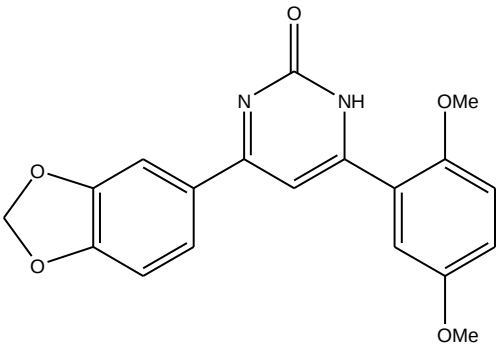	72	244-246	Orange Crystals

9	10306	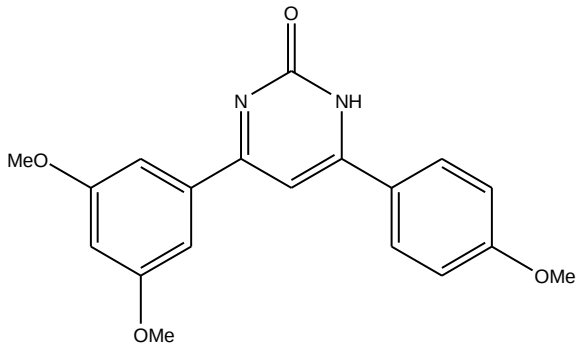	56	231-233	Orange Crystals
10	10313	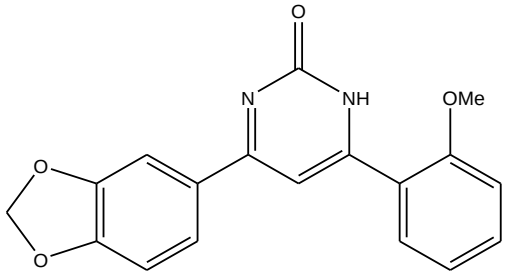	85	165-167	Orange Crystals
11	10307	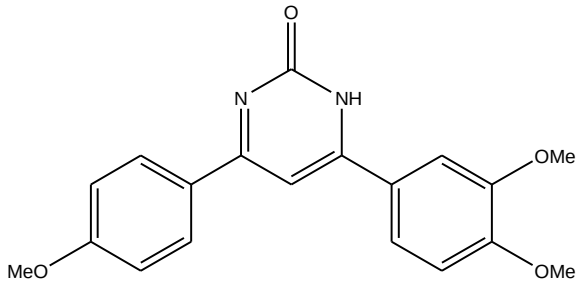	78	253-255	Orange Crystals
12	10309	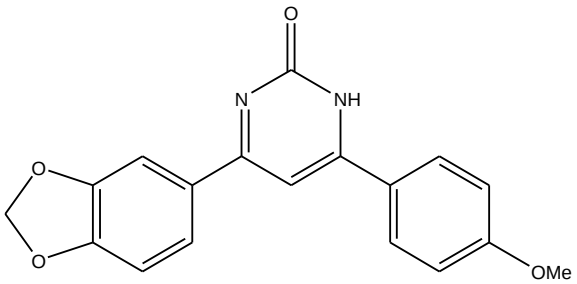	47	300-302	Orange Crystals
13	10310	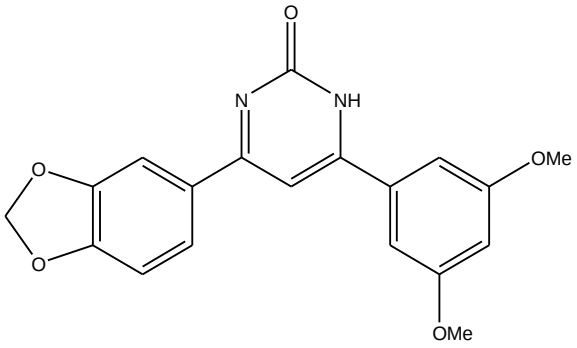	73	272-274	Orange Crystals

14	10311	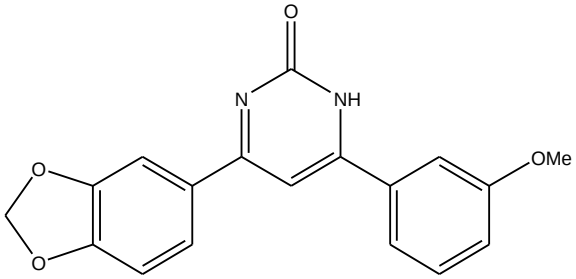	76	269-271	Orange Crystals

A library of fourteen pyrimidones were synthesised (Table 20) with yields ranging from 47-85%. An exception was DMU 10302 which gave an overall yield of 3%. Melting points ranged between 142-308ºC. The ^{1}H NMR spectra of the amino-pyrimidines characteristically showed peaks for the NH_2 group between 5.00-6.02ppm, but this was no longer present in the spectra of the pyrimidones. MS spectra were correct with either an M^+ or $(M+1)^+$ ion peak being observed. IR spectroscopy showed absorptions in the region of 1690-1750 cm^{-1} as would be expected for the presence of the carbonyl group. For example, the ^{1}H NMR spectrum for DMU 10314 showed the C5 heterocyclic proton as a singlet at 7.42ppm. The MS spectrum showed an ion mass of 353 representing the $[M+H]^+$ ion. An IR absorption at 1630cm^{-1} was observed for the carbonyl group and a melting point range between 290-292ºC was recorded. Figure 75 shows the ^{1}H NMR and Figure 76 shows the MS spectrum for DMU 10312.

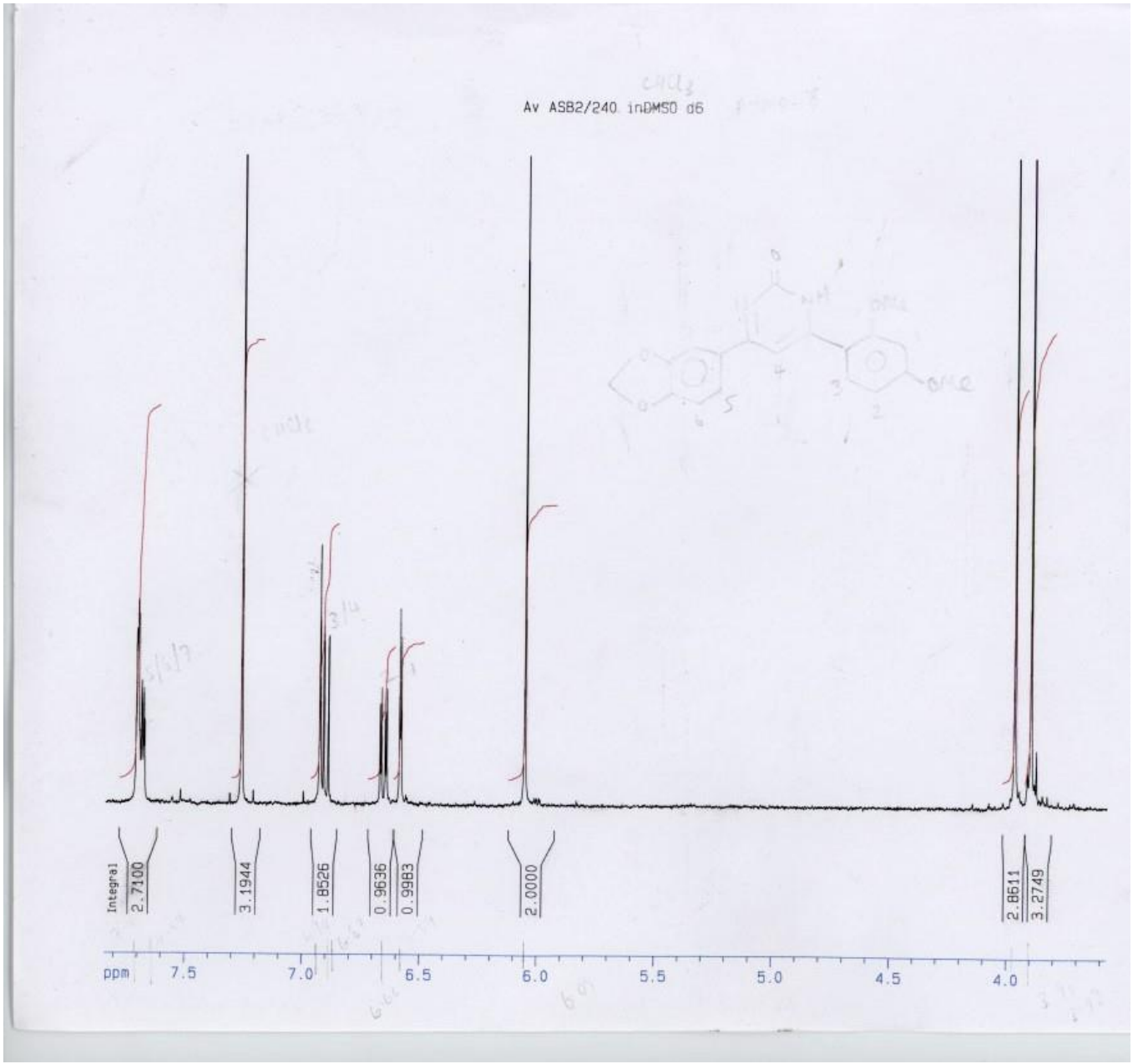

Figure 75. ^{1}H NMR spectrum of DMU 10312

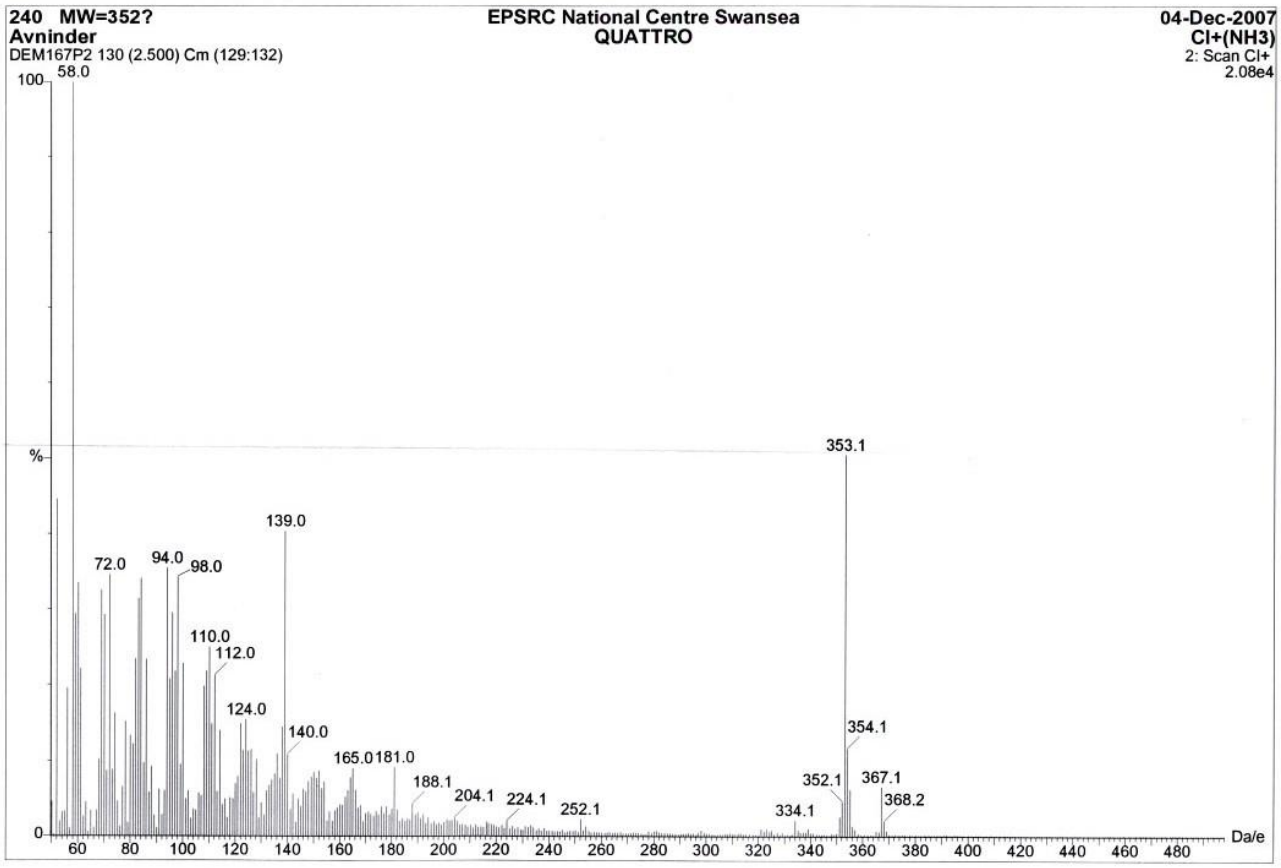

Figure 76. MS spectrum of DMU 10312

4.1 Pyrimidone Synthesis via Thio-Pyrimidines

Another method to synthesise the pyrimidones was discovered through the attempted synthesis of thio-pyrimidines (Figure 77). These were designed to investigate the 2-position of the heterocycle by the incorporation of a sulfur atom, to which comparisons in cytotoxicities could be made with the pyrimidines and pyrimidones.

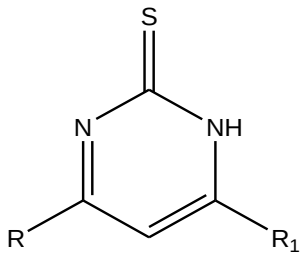

Figure 77. Structure of thio-pyrimidine

It was anticipated that thio-pyrimidines could have been synthesised by reacting thiourea with chalcones under the same conditions used to synthesise the amino-pyrimidines in chapter 3. DMU S16 was designed with a 4-methoxy substituted A-ring and 3,4-dimethoxy substituted B-ring. The synthesis required the corresponding chalcone to be stirred under reflux with 1.5 equivalents of thiourea and 4 equivalents of aqueous NaOH in ethanol for 6h. Three equivalents of hydrogen peroxide were added and the reaction continued to stir under reflux for 1h. Water was used to quench the reaction and the organic phase was extracted with DCM and dried over $MgSO_4$. The solvent was removed *in vacuo* producing the crude solid which was purified by flash chromatography using ethyl acetate and hexane (5:5) as eluent. A yield of 15% was obtained and a melting point range between 258-260^{o}C was observed.

However, after analysing the major product of this reaction the thio-pyrimidine was not present. MS results showed that the synthesised compound was 16 atomic mass units below what was expected and also signified the absence of the sulfur atom. DMU S16 was synthesised with a 4-methoxy substituted A-ring and 3,4-dimethoxy substituted B-ring. This compound should have given a mass of 354 but an actual mass of 338 was observed, the same as that observed for DMU 10307 (Table 20, entry 11). The ^{1}H NMR produced peaks as expected giving a total of 8 protons, but this would be expected for both the thio-pyrimidine and pyrimidone.

As hydrogen peroxide was used in the reaction to aid aromatisation of the heterocycle, it can be suggested that the thio-pyrimidine was generated but then underwent an oxidation reaction

to form pyrimidones (Figure 78). Subsequently, it was found that desulfurisation of thio-pyrimidines has been shown to occur with hydrogen peroxide of pyrimidines by *Samour et al*, which supports the desulfurisation predicted.[232]

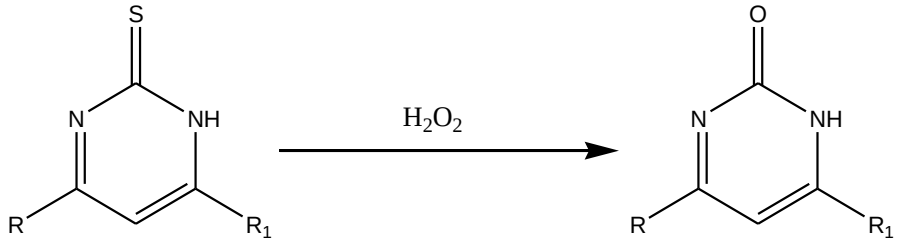

Figure 78. Desulfurisation of thio-pyrimidine with H_2O_2

The synthesis of thio-pyrimidines warrants further investigation. Literature methods have been found which use the same method as used above but do not utilise hydrogen peroxide to aid the aromatisation of the compound.[76]

4.2 Biological Evaluation of the 4,6-Diarylpyrimidones

Pyrimidones were synthesised from the direct conversion of amino-pyrimidines via a one step diazotisation reaction. The rationale for the conversion was to investigate the importance of the amino group for the cytotoxicities observed in chapter two, and to determine cytotoxicities with the incorporation of the carbonyl function group in comparison.

The synthesised pyrimidones were evaluated for their cytotoxicity against MDA 468, MCF7 and MDA 231 breast cancer cell lines using the MTT assay as described in chapter two. The cytotoxicity data will be grouped and discussed in accordance to the substitutions on the A and B-rings of the pyrimidones synthesised (Figure 79).

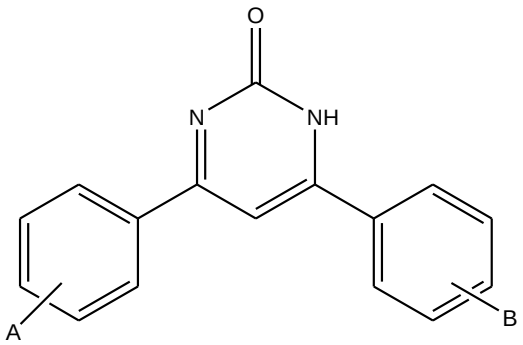

Figure 79. A and B-rings of the pyrimidone

4.2.1 Methylenedioxy Substituted A-Ring

Ten pyrimidones with 3,4-methylenedioxy substituted A-rings were synthesised. These compounds will be further divided according to the B-ring substitutions present to facilitate discussion of the cytotoxicity data observed.

4.2.1.1 Mono-Methoxy Substituted B-Rings

DMU 10311, DMU 10309 and DMU 10313 were synthesised with mono-methoxy substituted B-rings (Figure 80).

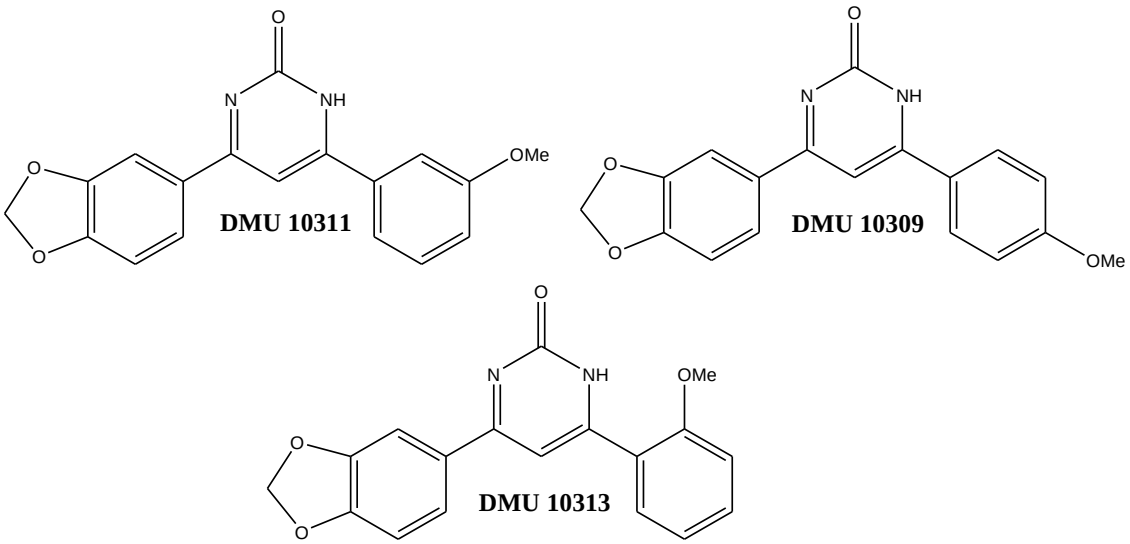

Figure 80. Structures of DMU 10311, DMU 10309 and DMU 10313

Table 21. Cytotoxicity data for the mono-methoxy substituted B-ring pyrimidones

		Substitution		**IC_{50} (μM)**		**IC_{50} (μM)**		**IC_{50} (μM)**	
Entry	**DMU No.**	**A-Ring**	**B-Ring**	**MCF10A**	**MDA 468**	**MCF7**	**MCF7 + TCDD**	**MDA 231**	**MDA 231 + TCDD**
1	10309	3,4-OCH_2O-C_6H_3	4-$MeOC_6H_4$	>100	18	>100	>100	40	40
2	10311	3,4-OCH_2O-C_6H_3	3-$MeOC_6H_4$	>100	1.7	8	8	5	2

3	10313	3,4-OCH_2O-C_6H_3	2-$MeOC_6H_4$	>100	0.07	1.8	0.5	ND	ND

n=1, ND=No data

DMU 10313 (Table 21, entry 3) was synthesised with a 2-methoxy substituted B-ring. The cytotoxicity of DMU 10313 towards the CYP1 expressing MDA 468 cell line was notable, with an IC_{50} value of 0.07µM (Figure 81). This was 700 times more toxic in comparison to its chalcone analogue of DMU 2265 (Table 21, entry 3), and 3 times more toxic than its amino-pyrimidine analogue of DMU 10213 (Table 21, entry 2). Importantly, DMU 10313 did not appear to show cytotoxicity towards the non-tumour MCF10A cell line.

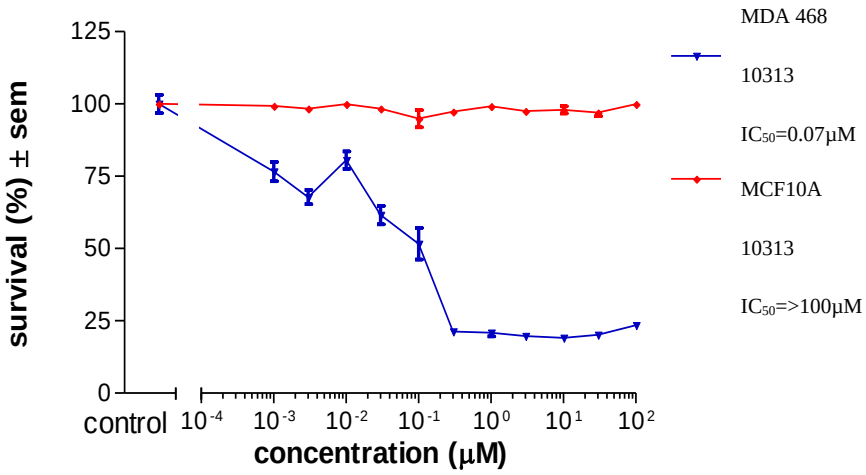

Figure 81. Cytotoxicity plot of MDA 468 and MCF10A treated with DMU 10313

IC_{50} values observed from DMU 10313 when screened against the MCF7 TCDD induced and non-induced cells were 0.5µM and 1.8µM. These values were significantly lower than that observed from DMU 2265 but slightly higher than that achieved for DMU 10213.

Table 22. Comparison of cytotoxicities of DMU 10313 with its pyrimidine and chalcone analogues

			IC_{50} (μM)					
Entry	**DMU No.**	**Structure**	**MCF 10A**	**MDA 468**	**MCF7**	**MCF7 + TCDD**	**MDA 231**	**MDA 231 + TCDD**
1	10313	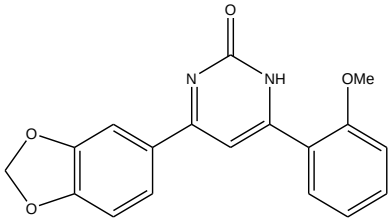	>100	0.07	1.8	0.5	ND	ND
2	10213	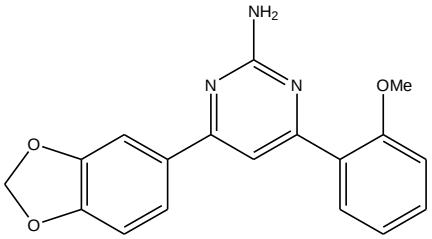	50	0.2	0.08	0.08	3	3
3	2265	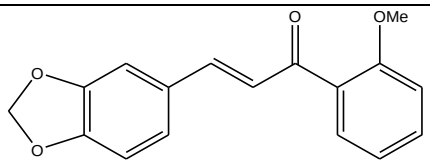	>100	50	100	50	ND	ND

With a 3-methoxy substituted B-ring DMU 10311 (Table 21, entry 2) showed encouraging toxicity towards the MDA 468 cells giving an IC_{50} value of 1.7μM, whilst showing no toxicity against the MCF10A cell line (Figure 82). Toxicity was also observed against the MDA 231 cells, where the TCDD induced cells gave an IC_{50} value of 2μM. This was over two times more toxic than the result obtained from the non-TCDD induced MDA 231 cells. Cytotoxicity was also observed towards the MCF7 cells, where the TCDD induced and non-induced cells gave identical IC_{50} values of 8μM. In general, DMU 10311 showed higher toxicity in contrast to its amino-pyrimidine analogue of DMU 10211, with a ten-fold increase in activity against the MDA 468 cell line and up to a thirty five-fold increase in activity against the MDA 231 cells.

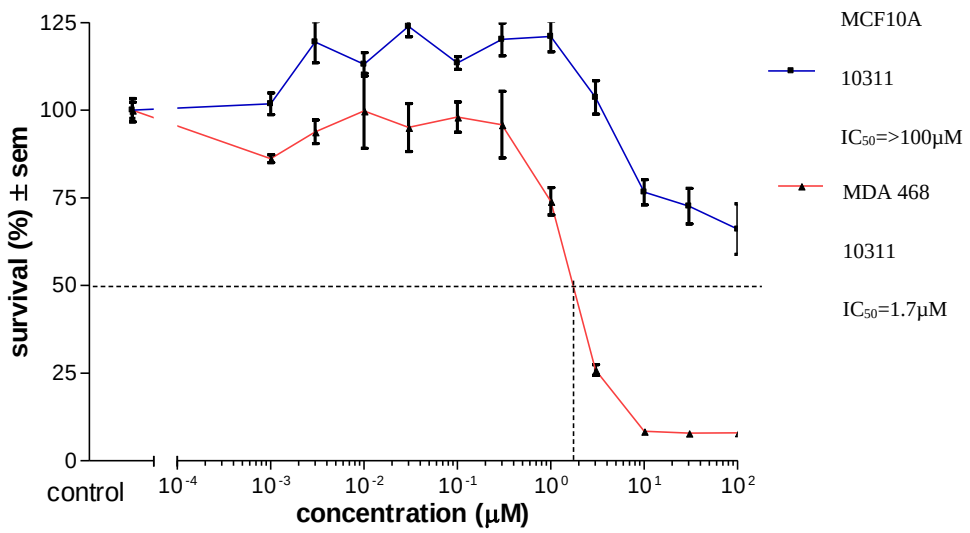

Figure 82. Cytotoxicity plot of MDA 468 and MCF10A treated with DMU 10311

DMU 10309 (Table 21, entry 1) did not show cytotoxic effects of any interest as all IC_{50} values were greater than 18µM, too high to be further evaluated.

4.2.1.2 Di-Methoxy Substituted B-Rings

Four pyrimidones were synthesised with di-methoxy substituted B-rings (Figure 83).

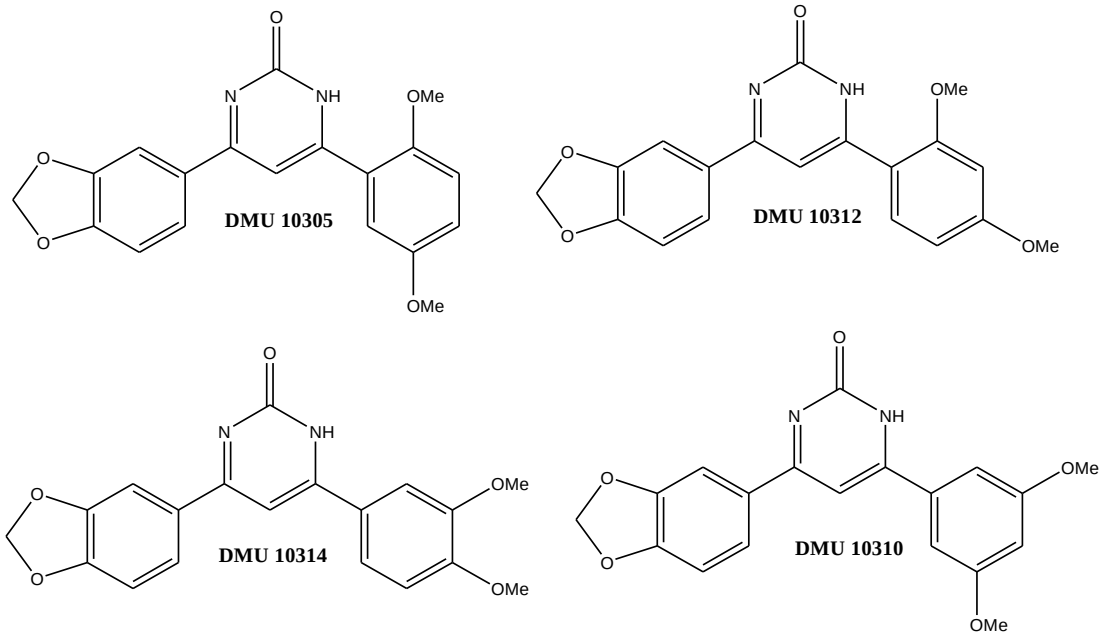

Figure 83. Structures of DMU 10312, DMU 10314, DMU 10310 and DMU 10305

Table 23. Cytotoxicities for the di-methoxy substituted B-ring pyrimidones

		Substitution		IC_{50} (µM)		IC_{50} (µM)		IC_{50} (µM)	
Entry	**DMU No.**	**A-Ring**	**B-Ring**	**MCF10A**	**MDA 468**	**MCF7**	**MCF7 + TCDD**	**MDA 231**	**MDA 231 + TCDD**
1	10312	3,4-OCH_2O-C_6H_3	2,4-$(MeO)_2C_6H_3$	>100	1.5	8	8	10	10
2	10314	3,4-OCH_2O-C_6H_3	3,4-$(MeO)_2C_6H_3$	>100	100	>100	>100	35	15
3	10310	3,4-OCH_2O-C_6H_3	3,5-$(MeO)_2C_6H_3$	>100	8	9	9	>100	60
4	10305	3,4-OCH_2O-C_6H_3	2,5-$(MeO)_2C_6H_3$	60	10	9	15	60	30

n=1, ND=No data

DMU 10312 (Table 23, entry 1) was synthesised with a 2,4-dimethoxy substituted B-ring. An IC_{50} value of 1.5µM was observed against the MDA 468 cell line whilst no toxicity was seen towards the non-tumour MCF10A cell line (Figure 84).

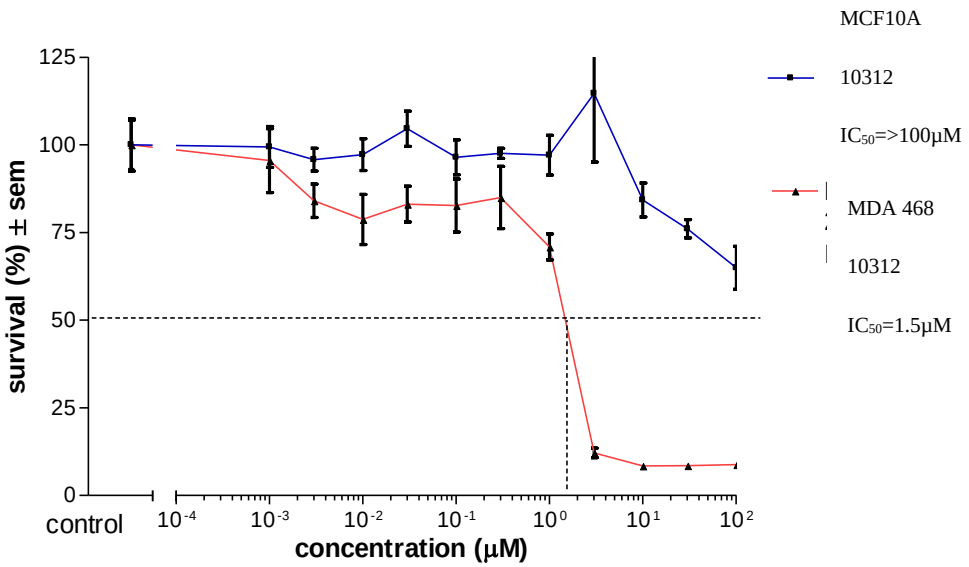

Figure 84. Cytotoxicity plot of MDA 468 and MCF10A treated with DMU 10312

An IC_{50} value of 8µM was obtained for both the TCDD induced and non-induced MCF7 cells. Also, identical IC_{50} values of 10µM were recorded for DMU 10312 when screened against both the TCDD induced and non-induced MDA 231 cells.

Table 24. Comparison of cytotoxicities of DMU 10212 and DMU 10312

Entry	DMU No.	Structure	MCF 10A	MDA 468	MCF7	MCF7 + TCDD	MDA 231	MDA 231 + TCDD
1	10212	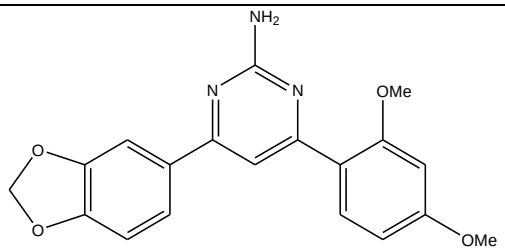	>100	0.01	0.07	0.3	30	20
2	10312	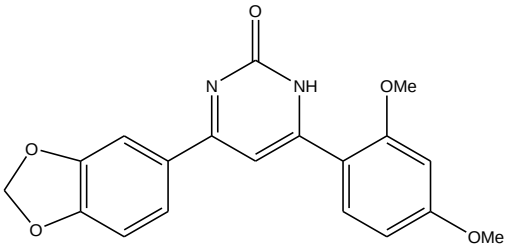	>100	1.5	8	8	10	10

DMU 10212, the pyrimidine analogue of DMU 10312 was shown to be the most cytotoxic prodrug synthesised in chapter two. It can be seen from Table 24 that the conversion of DMU 10212 to its pyrimidone analogue did not improve its cytotoxicity towards the MDA 468 and MCF7 cell lines. An increase in cytotoxicity was observed in the MDA 231 cell line, but not to a substantial degree. DMU 10314 (Table 23, entry 2) was synthesised with a 3,4-dimethoxy substitution on the B-ring. However, similarly to its amino-pyrimidine analogue of DMU 10214 little cytotoxicity was observed towards the tumour cell lines. With a 3,5-dimethoxy substituted B-ring, DMU 10310 (Table 23, entry 3) gave an IC_{50} value of 8µM from screening against the MDA 468 cell line whilst no toxicity was observed towards the MCF10A cell line. The toxicity of DMU 10310 in the MDA 468 cell line was significantly lower than that observed with DMU 10314. This suggests that the presence of a 3,4-dimethoxy substituted B-ring is more favourable for cytotoxicity to occur in contrast to a 3,5-

dimethoxy substituted B-ring, as this is was the only difference between DMU 10310 and DMU 10314. DMU 10305 (Table 23, entry 4) was synthesised with a 2,5-dimethoxy substitution on the B-ring, but showed to be less potent than its amino-pyrimidine analogue of DMU 10205.

4.2.1.3 Biological Evaluation of DMU 10304 and DMU 10302

Two pyrimidones were synthesised with tri-methoxy substitutions on the B-rings (Figure 85).

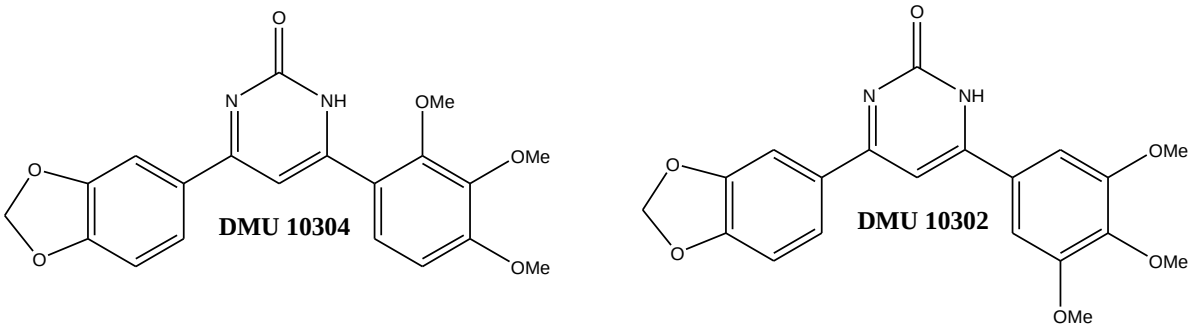

Figure 85. Structures of DMU 10304 and DMU 10302

Table 25. Cytotoxicities of DMU 10304 and DMU 10302

		Substitution		**IC_{50} (µM)**		**IC_{50} (µM)**		**IC_{50} (µM)**	
Entry	**DMU No.**	**A-Ring**	**B-Ring**	**MCF10A**	**MDA 468**	**MCF7**	**MCF7 + TCDD**	**MDA 231**	**MDA 231 + TCDD**
1	10304	3,4-OCH_2O-C_6H_3	2,3,4-$(MeO)_3C_6H_4$	>100	6	7	7	18	9
2	10302	3,4-OCH_2O-C_6H_3	3,4,5-$(MeO)_3C_6H_4$	>100	30	70	70	50	60

n=1

DMU 10304 (Table 25, entry1), with a 2,3,4-trimethoxy substitution on the B-ring demonstrated an IC_{50} value of 6µM towards the MDA 468 cells, whilst no toxicity towards the non-tumour MCF10A cells. An identical IC_{50} value of 7µM was observed for the TCDD induced and non-induced MCF7 cells. The MDA 231 cells gave IC_{50} values of 9µM and 18µM for the TCDD induced and non-induced cells. DMU 10302 (Table 25, entry 2), with a

3,4,5-trimethoxy substituted B-ring showed to be less cytotoxic than DMU 10304 towards the tumour cell lines. There was a 5-fold decrease in toxicity towards the CYP1 expressing MDA 468 cell line and 10-fold decrease in toxicity towards the MCF7 cell lines in contrast. It appears that a 2,3,4-trimethoxy substitution on the B-ring has a more potent cytotoxic effect than a 3,4,5-trimethoxy substitution on the B-ring towards the tumour cell lines. The amino-pyrimidine analogues of DMU 10302 and DMU 10304 were more cytotoxic across the tumour cell lines in comparison.

4.2.1.4 Biological Evaluation of DMU 10303

DMU 10303 was synthesised with 3,4-methylenedioxy substitutions on both of the A and B-rings (Figure 86).

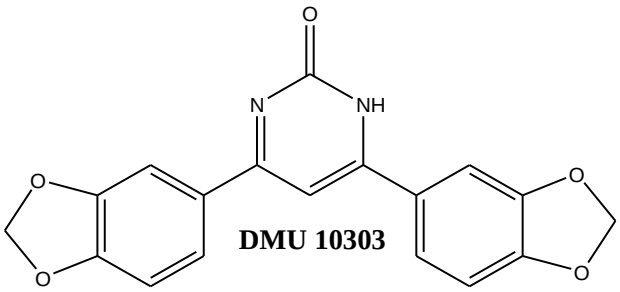

Figure 86. Structure of DMU 10303

Screening DMU 10303 against the MDA 468 cell line gave an IC_{50} value of 10µM, comparable to that observed from its amino-pyrimidine derivative of DMU 10203. However, unlike DMU 10203, the pyrimidone did not show toxicity towards the non-tumour MCF10A cells. results from the MCF7 and MDA 231 cells were not substantially toxic, as IC_{50} values of 25µM and above were recorded.

4.2.2 4-Methoxy Substituted A-Ring

DMU 10307 (Figure 87) was prepared with a 4-methoxy substitution on the A-ring and a 3,4-dimethoxy substitution on the B-ring. However, there appeared to be no cytotoxic effect from this compound against the MDA 468 and MCF7 cells as IC_{50} values were greater than 100µM. Slight cytotoxicity was observed on the MDA 231 cells but not to a great degree as IC_{50} values of 60µM and 30µM were obtained for the TCDD induced and non-induced cells.

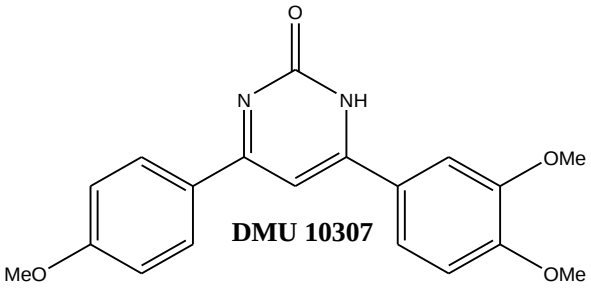

Figure 87. Structure of DMU 10307

In contrast to its amino-pyrimidine analogue of DMU 10207, DMU 10307 showed a substantial decrease in activity towards the MDA 468 cells as toxicity towards this cell line from DMU 10207 was recorded at 0.8µM.

4.2.3 4-Methoxy Substituted B-Ring

DMU 10301 and DMU 10306 (Figure 88) were synthesised with 4-methoxy substitutions on the B-rings.

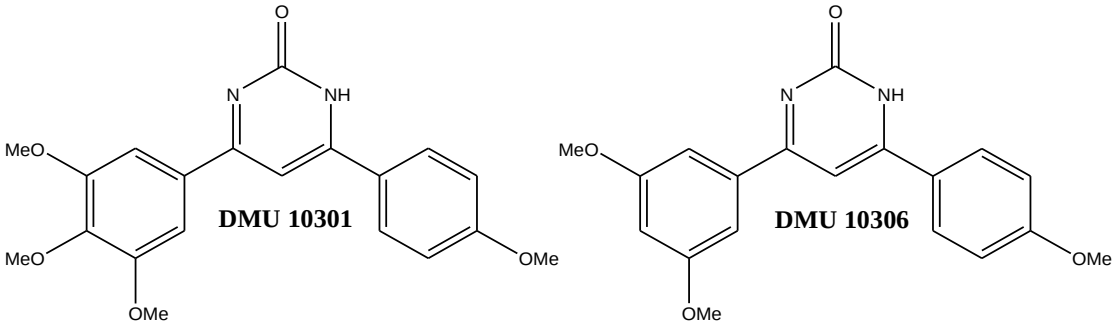

Figure 88. Structures of DMU 10301 and DMU 10306

Table 26. Cytotoxicities of DMU 10301 and DMU 10306

		Substitution		IC_{50} (µM)		IC_{50} (µM)		IC_{50} (µM)	
Entry	**DMU No.**	**A-Ring**	**B-Ring**	**MCF10A**	**MDA 468**	**MCF7**	**MCF7 + TCDD**	**MDA 231**	**MDA 231 + TCDD**
1	10301	3,4,5-$(MeO)_3C_6H_2$	4-$MeOC_6H_4$	>100	>100	>100	>100	80	70
2	10306	3,5-$(MeO)_2C_6H_2$	4-$MeOC_6H_4$	>100	30	20	30	90	30

n=1

With a 3,4,5-trimethoxy substituted A-ring, DMU 10301 (Table 26, entry 1) did not show toxicity towards the tumour cell lines, with IC_{50} values of 70µM and above being recorded. DMU 10306 (Table 26, entry 2), synthesised with a 3,4,5-trimethoxy substituted A-ring showed slightly increased toxicities towards the cancer cell lines in contrast to DMU 10301, but not to a significant degree. However, it can be noted that the increase in toxicity appears to occur due to the incorporation of the extra methoxy group in the 4-position of the A-ring. Also, the toxicities of DMU 10301 and DMU 10306 were not as potent as their corresponding amino-pyrimidine derivatives of DMU 10201 and DMU 10206 respectively.

4.2.4 Non-Substituted A and B-Rings

DMU 10300 (Figure 89), was synthesised with non-substituted phenyl A and B-rings.

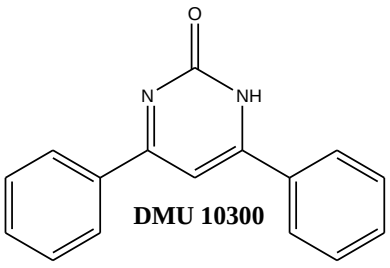

DMU 10300

Figure 89. Structure of DMU 10300

Cytotoxicity results from the MDA 468 cells gave an IC_{50} value of 2µM whilst no toxicity was observed towards the non-tumour MCF10A cell line. The screening of DMU 10300 against the MCF7 cells gave IC_{50} values of 3µM and 7µM for the TCDD induced and non-induced cells. The IC_{50} results from the MDA 231 cells were recorded at 50µM each for the TCDD induced and non-induced cells. This result was not as potent as that observed towards the MDA 468 and MCF7 cells.

Table 27. Cytotoxicity comparison of DMU 10200 and DMU 10300

			IC_{50} (µM)					
Entry	**DMU No.**	**Structure**	**MCF 10A**	**MDA 468**	**MCF7**	**MCF7 + TCDD**	**MDA 231**	**MDA 231 + TCDD**
1	10300	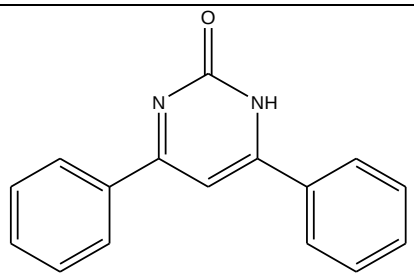	>100	2	7	3	50	50
2	10200	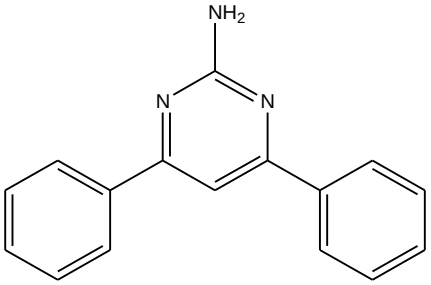	>100	0.2	8	10	50	50

DMU 10200, the pyrimidine analogue of DMU 10300 (Table 27, entry 2) also gave exciting results when screened against the MDA 468 cells with an IC_{50} value of 0.2µM being recorded. Similarly to DMU 10200, DMU 10300 (Table 27, entry 1) showed no toxicity towards the non-tumour MCF10A cells but a ten-fold decrease in toxicity towards the MDA 468 cells was seen. A three-fold increase towards the MCF7 cells induced with TCDD was observed also. The MDA 231 toxicities of both compounds appeared to be identical at 50µM for both the TCDD induced and non-induced cells. it is thought that the compounds designed

in this project undergo CYP1 metabolism to produce their cytotoxic analogues via dealkylation or hydroxylation reactions. As there are no substitutions on the phenyl groups present on the A or B-rings of either DMU 10200 or DMU 10300, hydroxylation by CYP1 enzymes would most likely occur. This would produce hydroxy substituted metabolites of these two compounds which may be explicable for the anti-tumour activity seen. An example of this mode of hydroxylation can be seen with tamoxifen, which undergoes metabolism by CYP enzymes to produce 4-hydroxytamoxifen. The metabolite is 100 times more potent than its parent compound.

4.3 Summary and Conclusions

Fourteen pyrimidones were synthesised in good yields from a one-step diazotisation conversion reaction using the amino-pyrimidines synthesised in chapter three. The pyrimidones were synthesised to determine and evaluate the importance of the amino group at the 2-position of the pyrimidine ring for the cytotoxicities observed with the amino-pyrimidines, and to observe the cytotoxic effect of the carbonyl group in comparison. Exciting results were observed from the pyrimidones when screened against the MDA 468, MCF7 and MDA 231 tumour cell lines, especially with DMU 10300, DMU 10311, DMU 10313 and DMU 10312.

Table 28. Comparison of toxicities of DMU 10300, DMU 10311, DMU 1013 and DMU 10312 with their amino-pyrimidine derivatives

			IC_{50} (μM)					
Entry	**DMU No.**	**Structure**	**MCF 10A**	**MDA 468**	**MCF7**	**MCF7 + TCDD**	**MDA 231**	**MDA 231 + TCDD**
1	10300	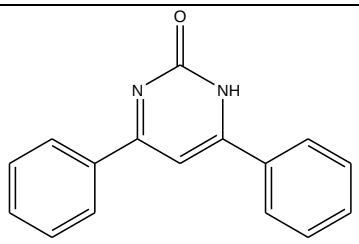	>100	2	7	3	50	50

2	10200	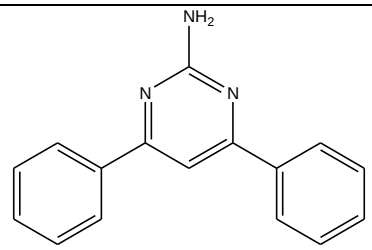	>100	0.2	8	10	50	50
3	10311	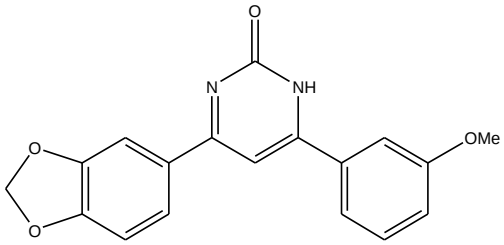	>100	1.7	8	8	5	2
4	10211	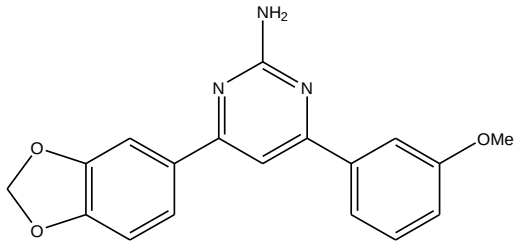	100	18	60	60	70	70
5	10313	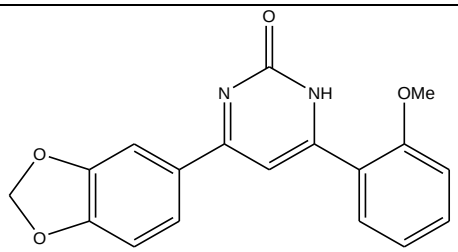	>100	0.07	1.8	0.5	ND	ND
6	10213	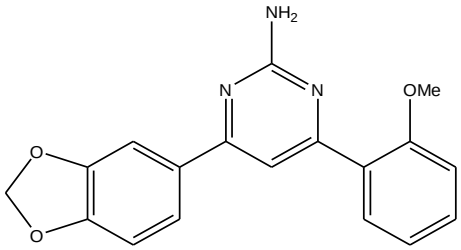	50	0.2	0.06	0.05	1	1
7	10312	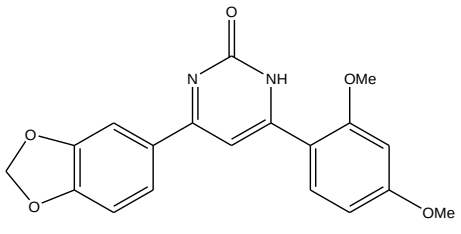	100	1.5	8	8	10	10

8	10212	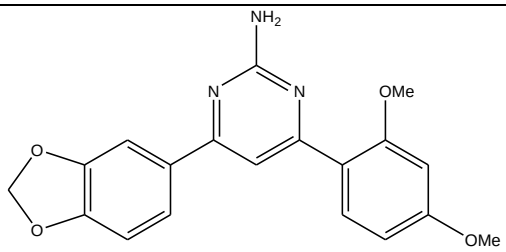	>100	0.08	0.07	0.3	30	20

DMU 10300 (Table 28, entry 1) gave an IC_{50} value of 2µM against the MDA 468 cell line whilst showing no toxicity towards the non-tumour MCF10A cells. An IC_{50} of 3µM was recorded when screened against the TCDD induced MCF7 cells. DMU 10311 (Table 28, entry 3) did not show toxicity towards the non- tumour MCF10A cells but a potent IC_{50} value of 1.7µM was seen towards the MDA 468 cells. DMU 10313 (Table 28, entry 5) showed significant toxicity towards the MDA 468 cells giving an IC_{50} value of 0.07µM whilst no toxicity was observed towards the MCF10A cells. IC_{50} values of 1.8µM and 0.5µM were recorded when DMU 10313 was screened against the MCF7 and MCF7 cells induced with TCDD. DMU 10312 did not show toxicity towards the MCF10A cells but an IC_{50} value of 1.5µM was observed against the MDA 468 cells.

However, in general, the conversion of the amino-pyrimidines to pyrimidones did not enhance the cytotoxicity of the compounds comparatively even though notable results were seen from the pyrimidones. The pyrimidine DMU 10212 (Table 28, entry 8) was the most effective prodrug synthesised in chapter three. The pyrimidone analogue, DMU 10312 (Table 28, entry 7) showed approximately a 20-fold decrease in cytotoxicity towards the MDA 468 cell line compared to DMU 10212. The toxicity seen towards the MCF7 cells was 115 times less with DMU 10312 than that observed from DMU 10212, and approximately 30 times less towards the MCF7 cells induced with TCDD.

On the contrary, DMU 10311 showed lower IC_{50} values across the tumour cell lines in contrast to DMU 10211, including a ten-fold increase in toxicity towards the MDA 468 cell line. More noticeable was the increased toxicity observed from DMU 10311 towards the MDA 231 cells, with 35 times more cytotoxicity recorded towards the TCDD induced cells than DMU 10211.

Solubility of the pyrimidones in DMSO, a crucial solvent used in the MTT assay was poor. This was not apparent with the amino-pyrimidines, indicating the amino group is more important for solubility.

Chapter 5

Synthesis and Biological Evaluation of 2-Morpholino-4,6-Diarylpyrimidines

5.0 Synthesis of 2-Morpholino-4,6-Diarylpyrimidines

The library of amino-pyrimidines synthesised in chapter three was valuable in providing compounds with exciting anti-cancer activity against tumour cell lines selected for their ability to constitutively or inductively express CYP1 enzymes. DMU 10212 (Figure 90) was shown to be the most cytotoxic prodrug synthesised, with significant IC_{50} values including 0.01µM observed towards the MDA 468 cell line.

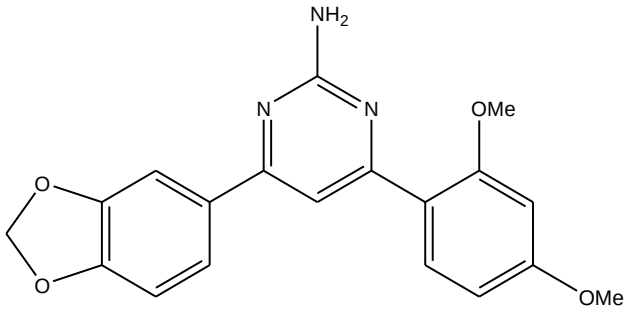

Figure 90. Structure of DMU 10212

The amino group at the 2-position of the pyrimidine ring was investigated for its importance in the cytotoxicity observed in chapter three. The amino-pyrimidines were converted by diazotisation to yield pyrimidones, allowing a contrast in cytotoxic properties of the amino-pyrimidines and pyrimidones to be made. The pyrimidone ring was also selected as the lone pairs of electrons on the oxygen atom could possibly interact with CYP1 binding sites in the aim to increase binding towards CYP1 enzymes and in turn improving cytotoxicity. Significant toxicities were seen from the pyrimidones towards the tumour cell lines, with IC_{50} values including 0.07µM observed towards the MDA 468 cell line from DMU 10313 (Figure 91).

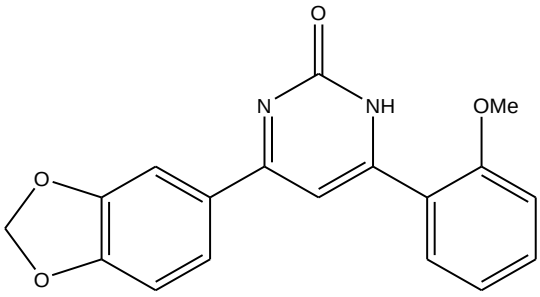

Figure 91. Structure of DMU 10313

The amino group has been shown to be important for pyrimidines to show toxicity towards the CYP1 expressing tumour cell lines. In an attempt to improve cytotoxicities already

observed, the 2-position of the pyrimidine ring was further explored. On this occasion, a morpholine group was selected. Morpholine is a 6-membered heterocycle which consists of four carbon atoms, a nitrogen atom and oxygen atom (Figure 92). The heteroatoms are in the 1 and 4-positions of the ring. Incorporation of morpholine maintained the presence of a nitrogen atom at the 2-position of the pyrimidine ring whilst introducing the bulkiness of the morpholine ring to explore the binding site of the CYP1 enzymes. The oxygen atom also present in the morpholine ring may participate in binding with the active site of the enzymes by lone pair electronic interactions or possible hydrogen bonding.

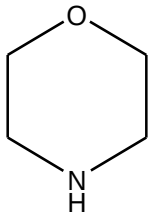

Figure 92. Structure of morpholine

In order to form the morpholino-pyrimidine heterocycle, 4-morpholinylformamidine hydrobromide was reacted with chalcones. The reaction conditions and equivalents of parallel reagents were the same as that used to synthesise the pyrimidines in chapter three. Therefore, the synthesis of the 2-morpholino-4,6-diarylpyrimidines required the dissolution of 4-morpholinylformamidine hydrobromide (1.5 equivalents) in ethanol using sodium hydroxide (4 equivalents). This mixture was stirred at reflux for thirty minutes producing the free 4-morpholinylformamidine. The required chalcone (1 equivalent) was added to the mixture and the reaction continued to stir under reflux for 6h. This was followed by the addition of hydrogen peroxide (3 equivalents, 50% w/v) to aromatise the heterocyclic ring and the reaction was stirred under reflux for a further 1h.

TLC analysis showed the formation of the morpholino-pyrimidine as a fluorescent blue spot when viewed under UV light. The solvent was removed *in vacuo* and the product purified by recrystallisation from ethanol. Flash chromatography was used to isolate the morpholinopyrimidines if recrystallisation was unsuccessful using dichloromethane and methanol (9:1) as eluent.

The first part of the mechanism for the formation of the morpholino-pyrimidines requires the conversion of the 4-morpholinylformamidine hydrobromide to the free amidine using sodium

hydroxide (Figure 93). Next, the free amidine forms an imine with the carbonyl group on the chalcone via 1,2-nucleophilic addition (Scheme 9). Intramolecular cyclisation then occurs forming the 6-membered dihydro-pyrimidine ring. The addition of hydrogen peroxide oxidises the pyrimidine ring forming the aromatised pyrimidine heterocycle.

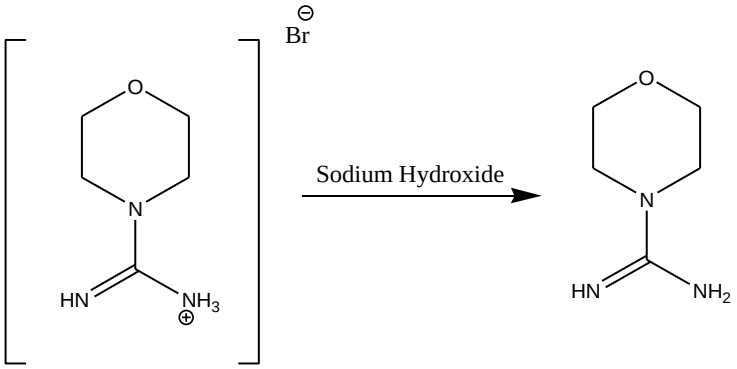

Figure 93. Dissociation of the 4-morpholinylformamidine hydrobromide

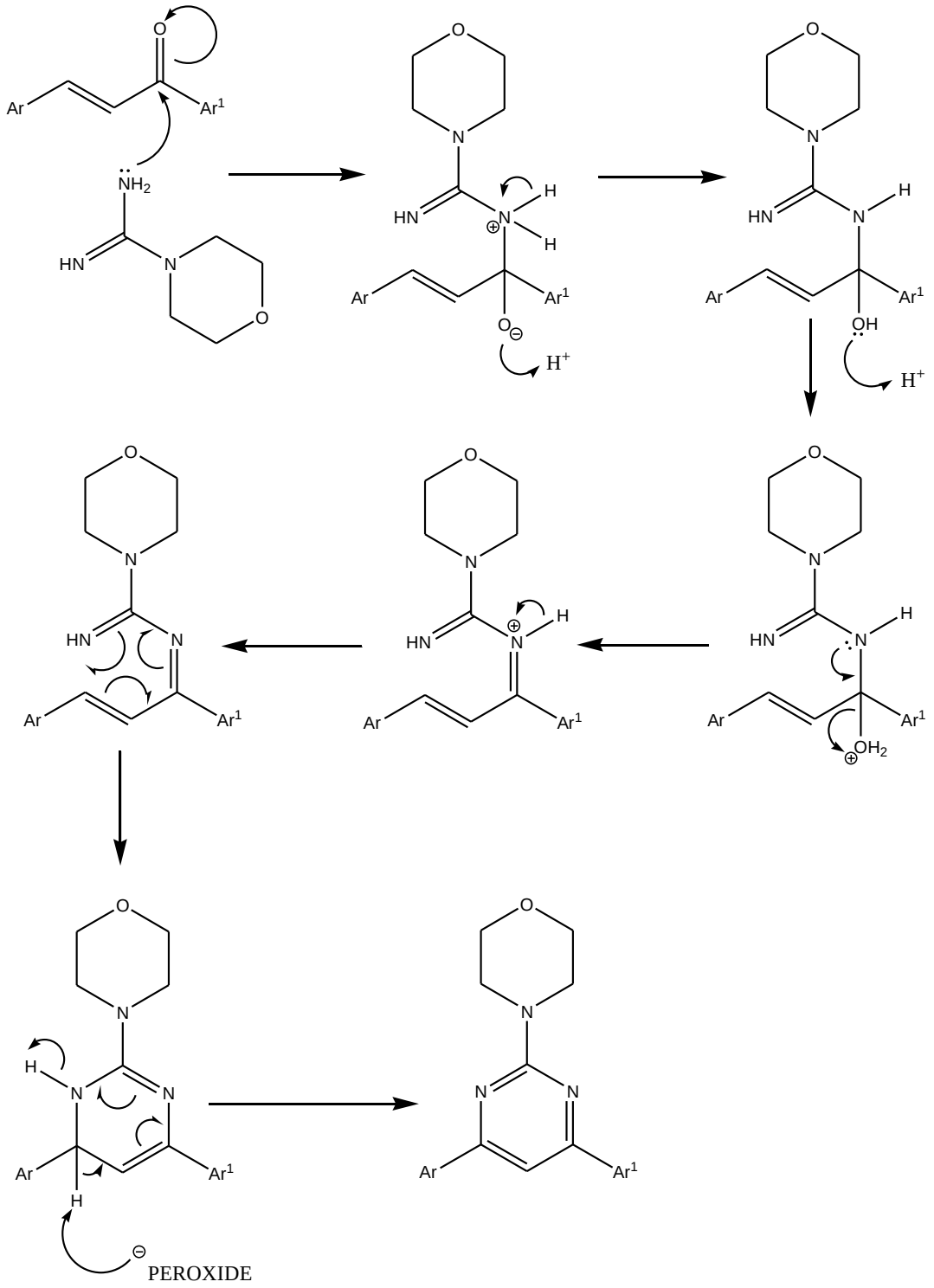

Scheme 9. Mechanism for the formation of the morpholino-pyrimidines

Table 29. Synthesised library of morpholino-pyrimidines

Entry	DMU No.	Structure	% Yield	m.p °C	Appearance
1	10400	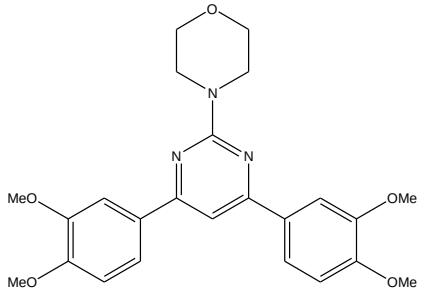	20	194-196	Yellow Crystals
2	10401	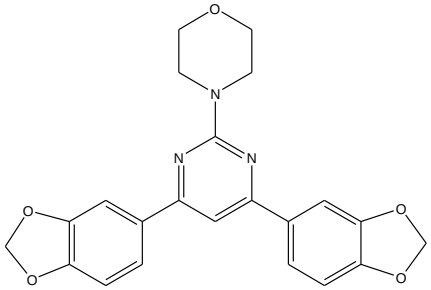	20	213-215	Yellow Crystals
3	10402	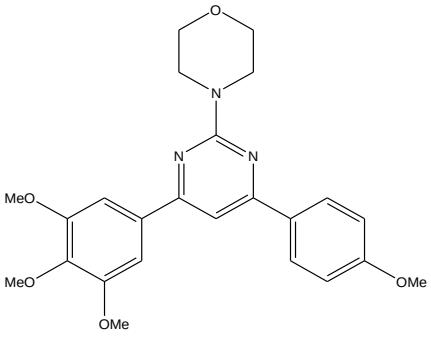	31	135-137	Beige Crystals
4	10403	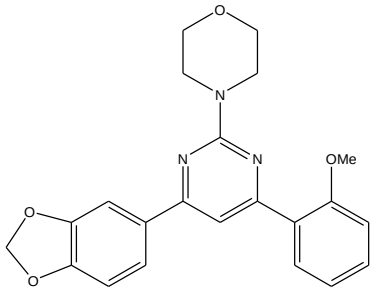	17	-	Oily Residue

5	10404	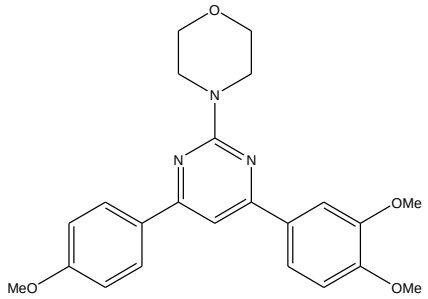	29	146-148	Yellow Crystals
6	10405	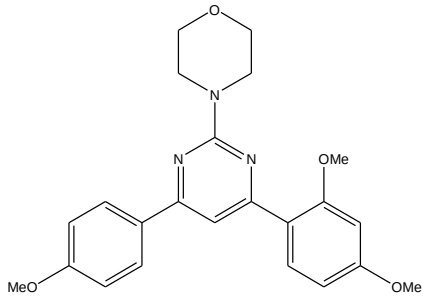	26	145-147	Light Yellow Crystals
7	10406	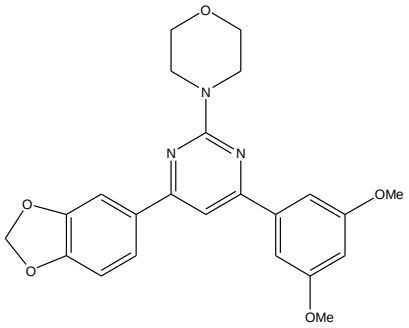	22	181-183	Light Yellow Crystals
8	10408	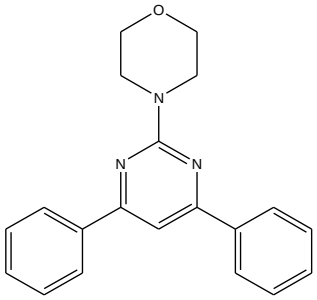	36	121-123	Light Yellow Crystals
9	10409	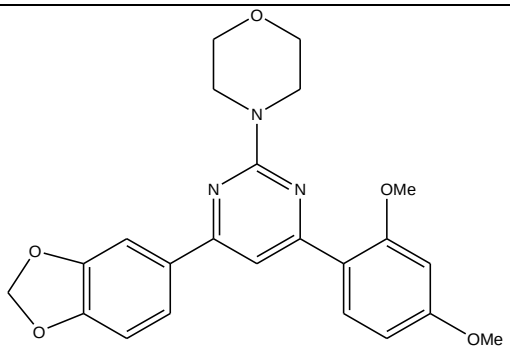	12	156-158	Light Yellow Crystals

A library of nine 2-morpholino-4,6-diarylpyrimidines was synthesised with yields in the range of 12 to 36% and melting points between 121-215^{o}C. The substitutions on the A and B-rings were selected from the most effect amino-pyrimidines synthesised in chapter three.

The ^{1}H NMR spectra of the morpholino-pyrimidines were consistent with the expected structures. The pyrimidine ring proton at C5 appeared between 7.22-7.63ppm (Figure 94). The 8 protons bonded to the C19, C20, C21 and C22 carbons of the morpholine appeared as two separate triplets, each representative of four carbons between 3.75-4.20ppm. MS spectra were correct with either an M^{+} or $(M+1)^{+}$ ion peak being observed. Figure 95 shows the ^{1}H NMR and Figure 96 shows the MS spectrum of DMU 10408.

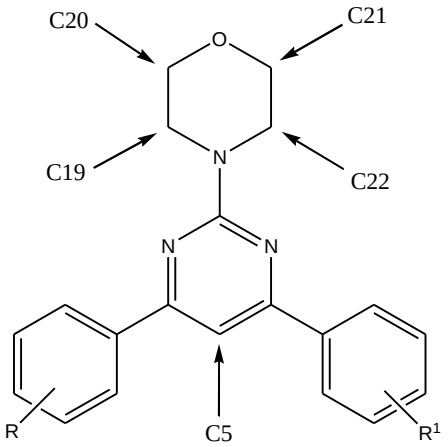

Figure 94. Position of the C5, C19, C20, C21 and C22 carbons of the morpholino-pyrimidine heterocycle

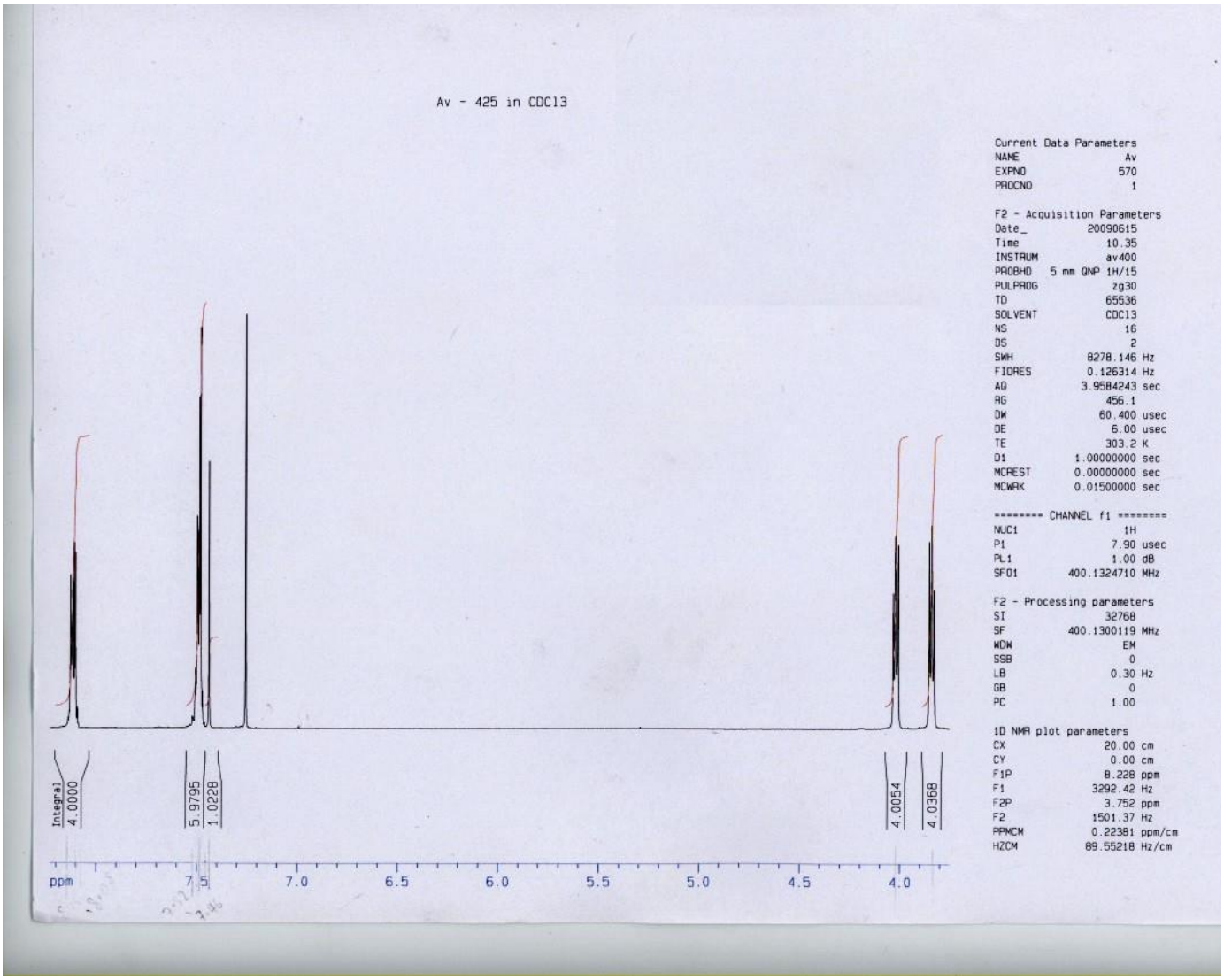

Figure 95. 1H NMR spectrum of DMU 10408

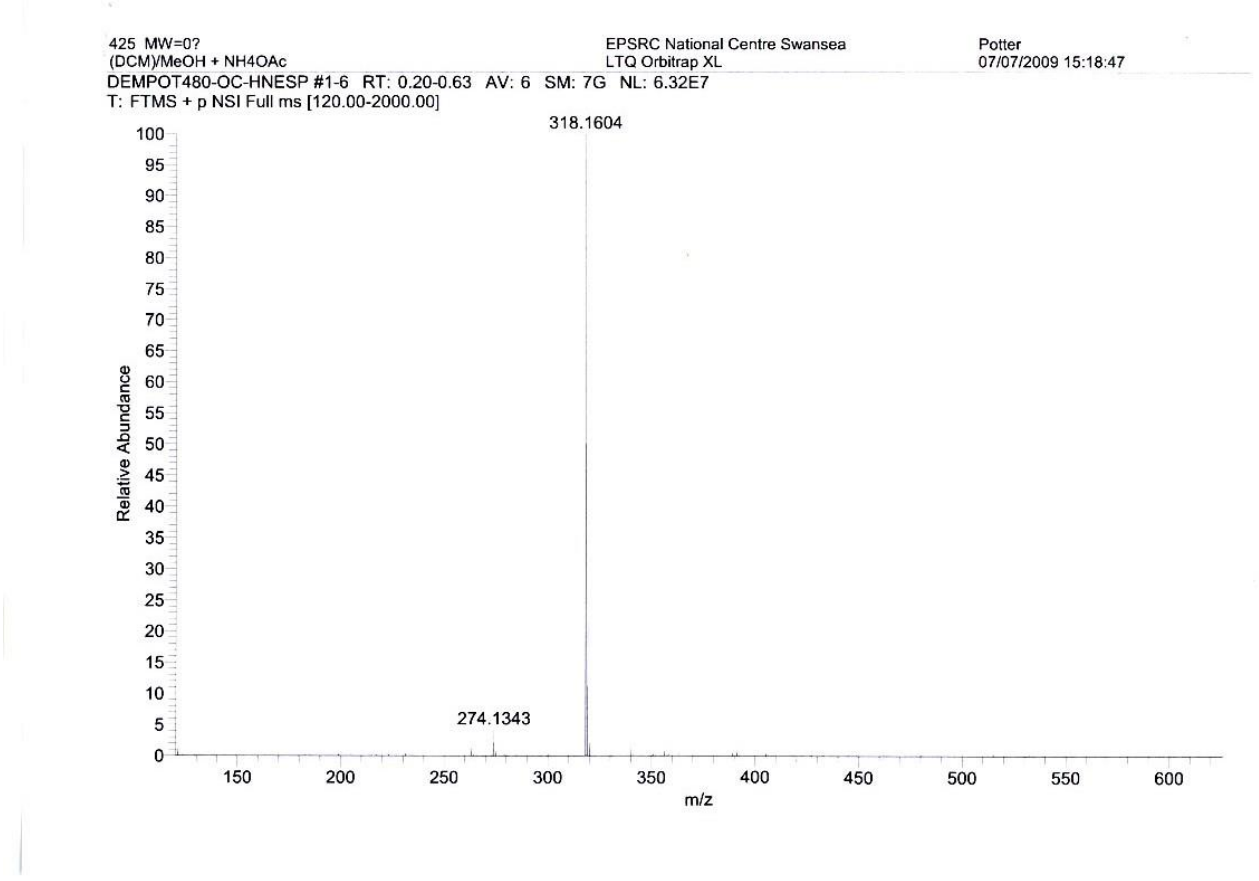

Figure 96. MS spectrum of DMU 10408

The yields obtained for the library of compounds in Table 29 were relatively low, with the highest yield of 36% being obtained with DMU 10408. An optimisation of the synthetic route for the synthesis of DMU 10409 was carried out prior to the synthesis of the library synthesised. Variables investigated were the reaction time, equivalents of sodium hydroxide and 4-morpholinylformamidine hydrobromide (MBr) used. DMU 407 (Figure 97) was the constant chalcone used (one equivalent) in the optimisation reactions as the substitution on the A and B-rings was the same as DMU 10212, the lead amino-pyrimidine synthesised in chapter three.

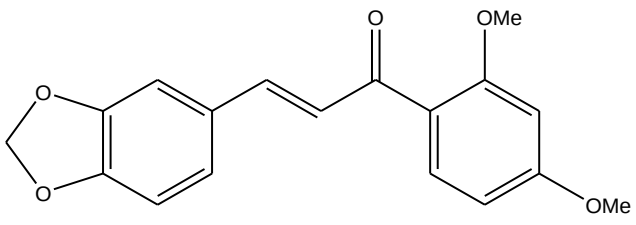

Figure 97. Structure of DMU 407

It was concluded that a reaction time of 6 h, 4 equivalents of NaOH and 1.5 equivalents of MBr produced the highest yield of 12%. This was achieved with a reaction time of 6h, 4 equivalents of NaOH and 1.5 equivalents of 4-morpholinylformamidine hydrobromide. However, DMU 10409 (Table 29, entry 9) the morpholino-pyrimidine analogue of DMU 407 produced the lowest yield out of the substituted morpholino-pyrimidines synthesised, whilst DMU 10408 (Table 29, entry 8) non-substituted on either the A or B-rings produced the greatest yield. This could signify that the substitutions on the A and B-rings can affect the yield of the reaction, as it has already been shown that the substitutions on the A and B-rings can influence the yields of epoxides (Chapter 2, 2.2). Therefore, the substituted A and B-rings could either hinder the 1,2-nucleophilic addition process or increase the rate of 1,4-nucleophilic addition occurring as discussed in chapter three (Figure 98). This is important as the reaction product required proceeds through 1,2-nucleophilic addition which is kinetically favoured, but there is also the possibility that 1,4-nucleophilic addition can occur which is thermodynamically favoured. The latter would form a heterocyclic product but would not provide the cyclised compound of interest, hence producing an undesired by-product lowering the yield. As this reaction also favours basic conditions, further investigations could be made experimenting with bases of varying strength including sodium isopropoxide, a stronger base than sodium hydroxide. However, if the pH of the reaction is too high, the protonation steps involved in the reaction mechanism may not occur hence inhibiting completion of the reaction product required.

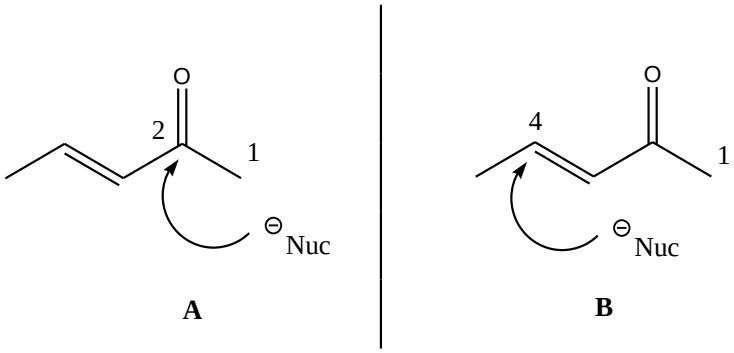

Figure 98. 1,2-nucleophilic addition (A) and 1,4-nucleophilic addition (B)

5.1 Biological Evaluation of the 2-Morpholino-4,6-Diarylpyrimidines

The 2-position of the pyrimidine ring was investigated with the aim to achieve comparable or greater prodrug toxicities than those observed with the amino-pyrimidines in chapter two. Morpholine was incorporated into the pyrimidines yielding 2-morpholinopyrimidines (Table 29) which were screened for their ability to inhibit cell growth against the MDA 468, MCF7 and MDA 231 tumour cell lines as previously discussed in chapter two. To assist discussion, the aryl groups at the 4 and 6 positions have been assigned as A and B-rings (Figure 99). Also, the cytotoxicity results obtained have been grouped together according to the substitution patterns on the A and B-rings.

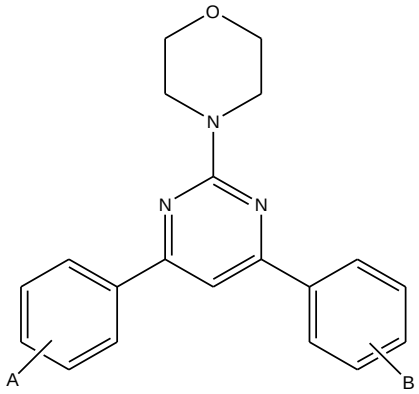

Figure 99. A and B-rings of the morpholino-pyrimidines

5.1.1 3,4-Methylenedioxy Substitution

5.1.1.1 Biological Evaluation of DMU 10401, 10403 and DMU 10406

Three morpholino-pyrimidine derivatives were synthesised with 3,4-methylenedioxy substituted A-rings (Figure 100).

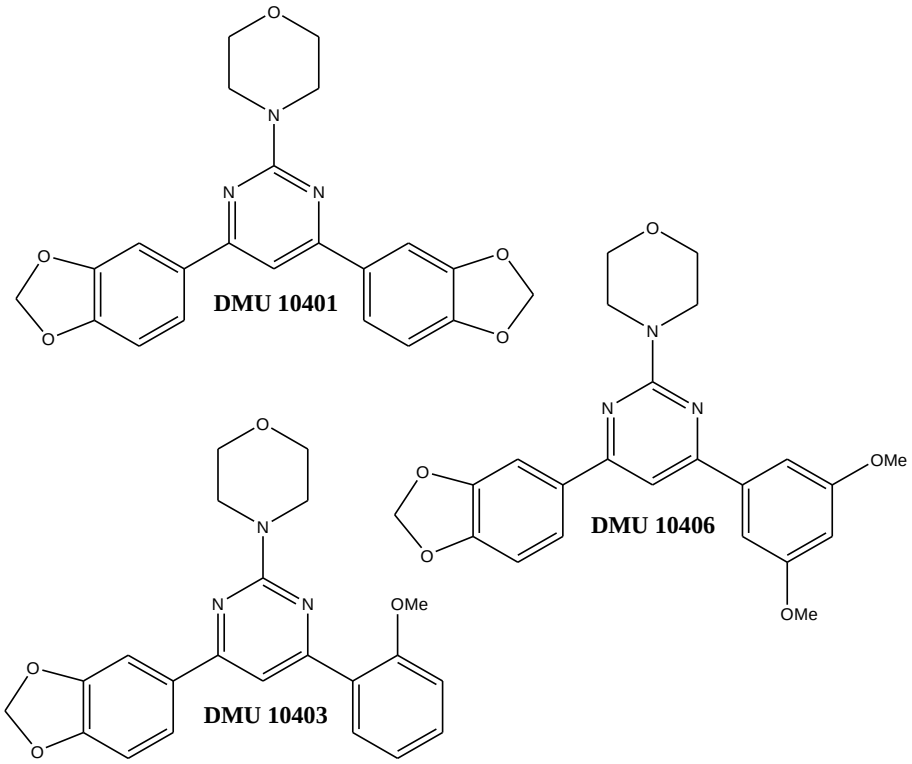

Figure 100. Structures of DMU 10401, DMU 10403 and DMU 10406

Table 30. Cytotoxicity data for DMU 10401, DMU 10403 and DMU 10406

Entry	DMU No.	IC_{50} (μM)		IC_{50} (μM)		IC_{50} (μM)	
		MCF10A	MDA468	MCF7	MCF7 + TCDD	MDA231	MDA231 + TCDD
1	10401	>100	>100	>100	>100	25	25
2	10403	>100	22	10	7	>100	100
3	10406	>100	70	>100	>100	ND	ND

n=1, ND=No data

With a 3,4-methylenedioxy substitution on the B-ring, DMU 10401 showed no toxicity towards the MCF10A, MDA468 and MCF7 cell lines as IC_{50} values of greater than 100µM were recorded in each case. Slight toxicity towards the MDA231 cells was observed with identical IC_{50} values of 25µM recorded for both the TCDD induced and non induced cells. Substituted with a 2-methoxy B-ring, DMU 10403 showed the greatest toxicity towards the MCF7 cells out of the methylenedioxy substituted A-ring compounds. IC_{50} values of 7µM for the TCDD induced cells and 10µM for the non TCDD induced cells were observed. No toxicity towards the non-tumour MCF10A cell line was seen but an IC_{50} value of 22µM was obtained when DMU 10403 was screened against the CYP1 expressing MDA468 cell line. No toxicity was observed from screening DMU 10403 against the MDA231 cells as IC_{50} values of 100µM and greater were seen in the TCDD induced and non-TCDD induced cells. DMU 10213, the amino-pyrimidine analogue of DMU 10403 showed exciting anti-tumour activity with an IC_{50} values significantly more potent than that of DMU 10403. The toxicity of DMU 10403 was 110 times less than that observed from DMU 10213 against the MDA 468 cell line and over a 100 times less toxic towards the MCF7 cells. DMU 10403 did not show toxicity towards the MDA 231 cells whereas DMU 10213 gave IC_{50} values of 3µM each towards the TCDD induced and non-induced cells. DMU 10406, with a 3,5-dimethoxy substitution on the B-ring did not show to exhibit interesting toxicities against the tumour cel lines as IC_{50} values of 70µM and above were recorded.

5.1.1.2 4-Methoxy A-Ring Substitution

Three morpholino-pyrimidines were synthesised with 4-methoxy substituted A-rings (Figure 101).

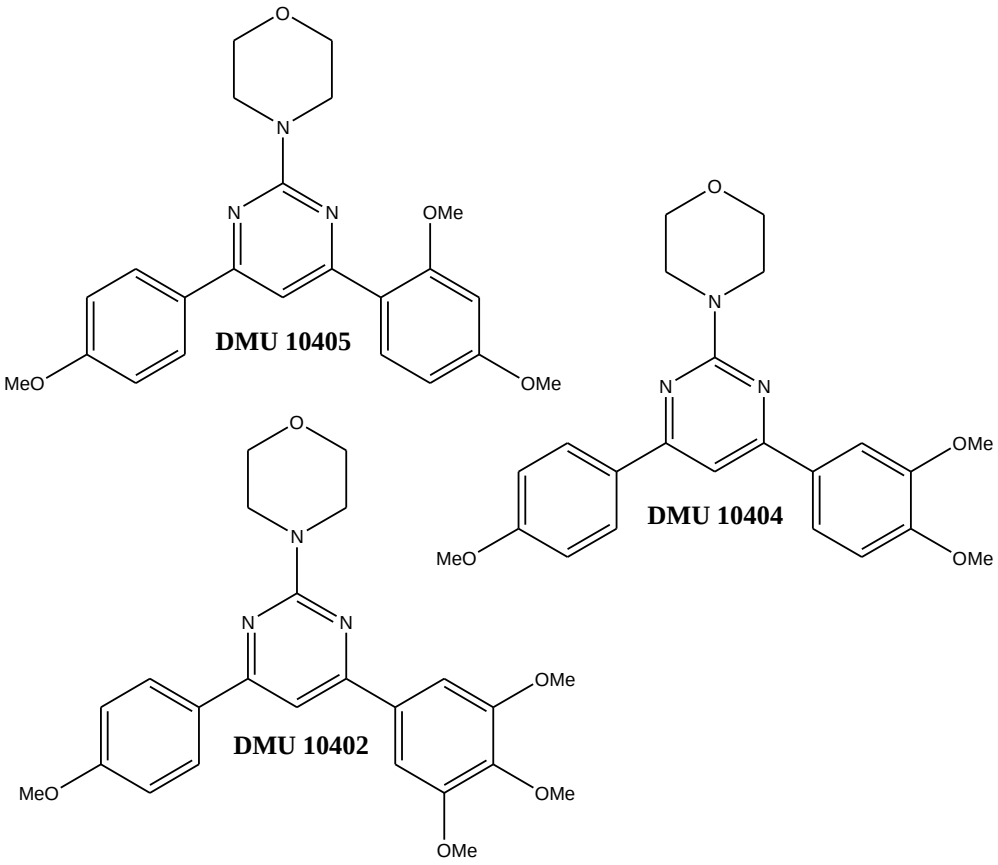

Figure 101. Structures of DMU 10405, DMU 10404 and DMU 10402

Table 31. Cytotoxicity data of DMU 10404, DMU 10405 and DMU 10402

Entry	DMU No.	IC_{50} (μM)		IC_{50} (μM)		IC_{50} (μM)	
		MCF10A	MDA468	MCF7	MCF7 + TCDD	MDA231	MDA231 + TCDD
1	10404	>100	>100	>100	>100	30	30

2	10405	>100	10	60	60	>100	>100
3	10402	>100	25	55	28	>100	>100

n=1

DMU 10404 (Table 32, entry 1) was synthesised with a 3,4-dimethoxy B-ring but this compound did not show any activity of interest towards the MCF10A, MDA 468 and MCF7 cells as all IC_{50} values observed were above 100µM. Activity was observed towards the MDA 231 cell lines which primarily express CYP1B1 to a greater extent than CYP1A1. IC_{50} values of 30µM were recorded for both the TCDD induced and non-induced cells, but this result was not toxic enough to warrant further investigation. DMU 10405 (Table 32, entry 2) was synthesised with a 2,4-dimethoxy substituted B-ring. This compound showed toxicity towards the MDA 468 cell line giving an IC_{50} value of 10µM whereas no toxicity was observed towards the MCF10A cells. IC_{50} values of 60µM were recorded for the TCDD induced and non-induced MCF7 cells, and no toxicity was observed towards the MDA 231 cell lines. DMU 10208, the amino-pyrimidine derivative of DMU 10405 showed greater toxicities across the tumour cell lines in comparison to DMU 10405. DMU 10402, substituted with a 3,4,5-trimethoxy A-ring gave an IC_{50} value of 25µM towards the MDA 468 cell line whilst not showing toxicity towards the MCF10A cell line. The non TCDD induced MCF7 cells gave an IC_{50} value of 55µM, but the TCDD induced MCF7 cells showed a two-fold increase in activity. Results from the MDA 231 cells did not show anything of interest as no toxicity was observed.

5.1.1.3 DMU 10400

DMU 10400 (Figure 102) was designed with 3,4-dimethoxy substituted A and B. However, this compound did not prove to exhibit any type of prodrug or anti-cancer activity as all IC_{50} values were greater than 100µM.

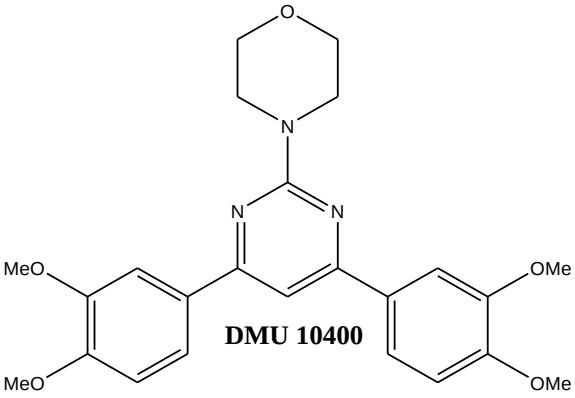

Figure 102. Structure of DMU 10400

5.2 Summary and Conclusions

A library of nine morpholino-pyrimidines were synthesised from the same method used to yield the amino-pyrimidines in chapter three. The morpholino-pyrimidines were screened against a panel of selected tumour cell lines to assess their prodrug properties. DMU 10405 (Figure 103) showed the most effective toxicity out of the synthesised morpholino-pyrimidines towards the MDA 468 cell line where an IC_{50} value of 10µM was observed.

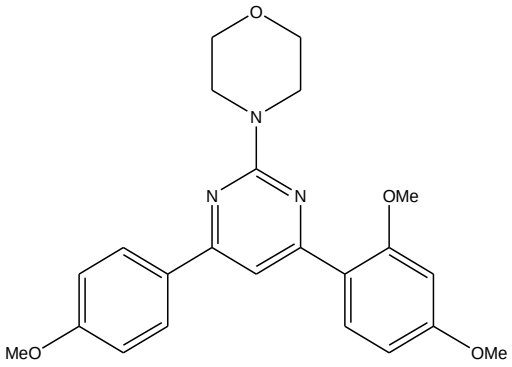

Figure 103. Structure of DMU 10405

DMU 10403 (Figure 104) showed the most effective toxicity towards the MCF7 cell lines with IC_{50} values of 7µM and 10µM being obtained from the TCDD induced and non-induced

cells. However, no significant toxicity was observed towards the MDA 231 cells from the morpholino-pyrimidines.

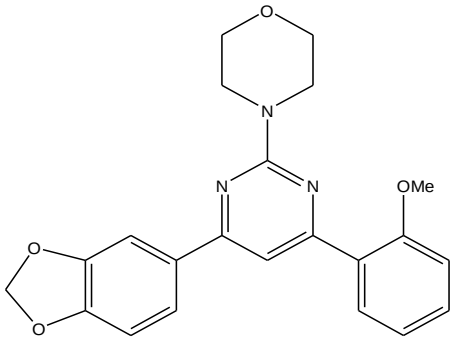

Figure 104. Structure of DMU 10403

Overall, the incorporation of the morpholine group at the 2-position of the pyrimidine heterocycle did not show toxicities comparable to that obtained from the amino-pyrimidines synthesised in chapter three. Therefore it can be said that the morpholine group proves unfavourable compared with an amine group at the 2-position of the pyrimidine heterocycle.

The amino group changes from a primary amine to a secondary amine when comparing the amino-pyrimidines and morpholino-pyrimidines. It may be a possibility that the two hydrogen atoms of the primary amine participate in hydrogen bonding when present in the active site of the CYP1 enzymes, increasing the metabolism and cytotoxicity towards the tumour cells. On the other hand, the bulk of the morpholine of the morpholino-pyrimidines may be problematic and prevent the compound from fitting correctly into the active site of the CYP1 enzymes, preventing metabolism and for any cytotoxicity to occur.

Chapter 6

Synthesis and Biological Evaluation of Further Heterocyclic Pyrimidines

6.0 Synthesis of Dimethylethylenediamino-4,6-Diarylpyrimidines

The amino-pyrimidines synthesised in chapter two produced compounds with exciting anti-tumour prodrug activity. In particular DMU 10212 (Figure 105), with a 3,4-methylenedioxy substitution on the A-ring and 2,4-dimethoxy substitution on the B-ring showed significant cytotoxicity towards the tumour cells. An IC_{50} value of 0.01µM was observed towards the MDA 468 cell line which constitutively expresses CYP1A1 and CYP1B1. Also, IC_{50} values of 0.07µM and 0.3µM were observed towards the MCF7 and MCF7 cells induced with TCDD.

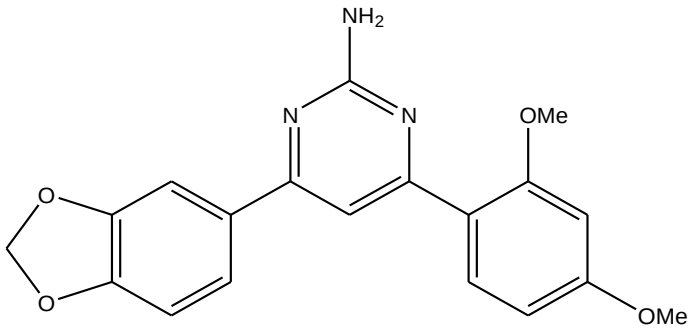

Figure 105. Structure of DMU 10212

With the aim to improve cytotoxicities of the pyrimidines and to explore the importance of the amino group at the 2-position, pyrimidones were synthesised. Significant toxicities were also obtained from screening the pyrimidones against the tumour cell lines but the amino derivatives proved more favourable with greater tumour toxicities. The 2-position of the pyrimidine ring was further investigated by incorporating a morpholine group. However, the toxicities towards the CYP1 expressing tumour cell lines of the morpholino-pyrimidines were not as potent as that observed from the amino-pyrimidines. The 2-position of the pyrimidine was subject to further investigation by the incorporation of dimethylethylenediamine. The notion of using the dimethylethylenediamine group was based on the fact that it is not rigid and is able to rotate and move whilst attached to the 2-position of the pyrimidine heterocycle. This may allow for the dimethylethylenediamine group to explore the CYP1 binding sites and orientate itself spatially in order for the dimethylethylenediamino-pyrimidines to gain optimum binding within the enzymes. This could occur via electronic interactions of lone pairs of electrons of the nitrogen atoms, and through hydrogen interactions with the secondary amine present in the dimethylethylenediamine group.

The route used to synthesise the 2-dimethylethylenediamino-4,6-diarylpyrimidines was taken from *Agarwal et al* who prepared various substituted guanidines (Figure 106), by reacting their corresponding amines with S-methylisothiourea sulphate to produce guanidinium salts.[233] The salts were then reacted with chalcones to produce the substituted pyrimidines.

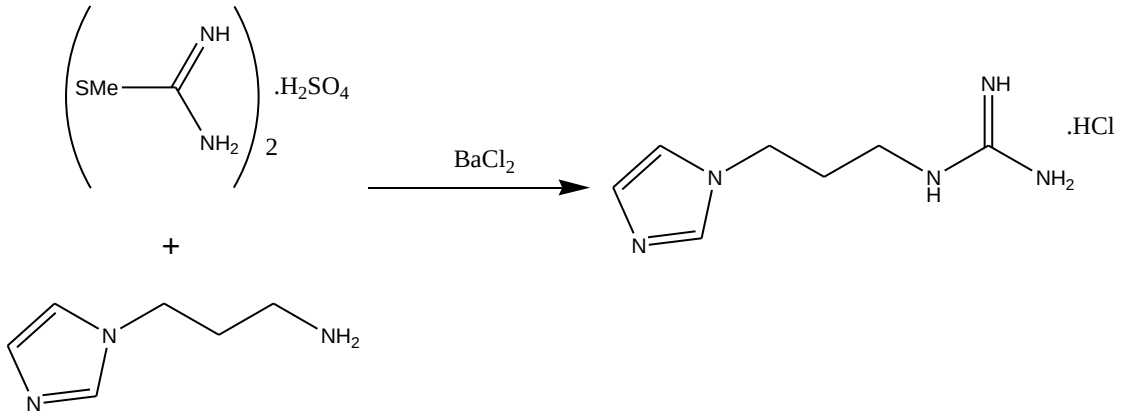

Figure 106. Preparation of guanidinium salts using S-methylisothiourea sulphate and amines

The first stage of this process required the synthesis of the dimethylethylenediamino-guanidine. The procedure was taken from *Andrews et al* who synthesised 4-amidinomorpholine hydrochloride by stirring S-methylisothiourea sulphate and morpholine in water under reflux for 5 minutes.[234] This was followed by the addition of aqueous barium chloride and the reaction was stirred under reflux for a further 30 minutes. The mixture was then filtered through kieselguhr giving a colourless solution. The water was removed *in vacuo* leaving a white gum, which was recrystallised from ethanol with the addition of acetone, allowing the hydrochloride salt to separate out as solid white crystals. The solid was subject to further recrystallisation from a mixture of 2-ethoxyethanol and ethyl acetate.

The above reaction was repeated in order to verify the successful synthesis of the morpholine salt, as the commercially available product used in chapter five was also available which could be used to compare analysis with the synthesised compound. The synthesis was successful but yields were very low of 5%, therefore an investigation into the length of time the reaction was allowed to proceed was made. Results showed that the highest yield of 7%

was obtained when the reaction was allowed to reflux for one hour prior to the addition of the aqueous barium chloride solution.

A problematic factor associated with the low yields can be accounted for by the recrystallisation process. The literature method requires dissolving the crude product in ethanol followed by the addition of acetone to precipitate out the guanidine hydrochloride. The separated guanidine hydrochloride solid is then collected by filtration and subject to a second recrystallisation with a mixture of 2-ethoxyethanol and ethyl acetate to yield the final purified product. However, it was found that the second recrystallisation process used by *Andrews et al* was not required as the compound was pure after undergoing recrystallisation with ethanol and acetone. It was also observed that recrystallising the solid with the 2-ethoxyethanol and ethyl acetate reduced the yields as the compound did not solidify out completely.

Dimethylethylenediamino-guanidine was then synthesised by a modified literature method of *Andrews et al* by removing the second recrystallisation step using 2-ethoxyethanol and ethyl acetate in preparation for the synthesis of the dimethylethylenediamino-4,6-diarylpyrimidines. Therefore, *N,N*-dimethylethylenediamine (2 equivalents) was reacted with S-methylisothiourea sulphate *(*1 equivalent) in boiling water for 5 minutes. This was followed by the addition of aqueous barium chloride solution (1.5 equivalents, 50% w/v), producing $BaSO_4$ precipitate as the side product almost instantaneously. The reaction continued to stir under reflux for 1h and was then filtered through kieselguhr giving a colourless filtrate solution. The solvent was removed *in vacuo* leaving a white gum. This was dissolved in ethanol with the addition of acetone of the same volume. The mixture was allowed to cool and the dimethylethylenediamino-guanidine hydrochloride separated out as white crystals, collected by filtration. However yields were still poor with 7% of the salt being obtained.

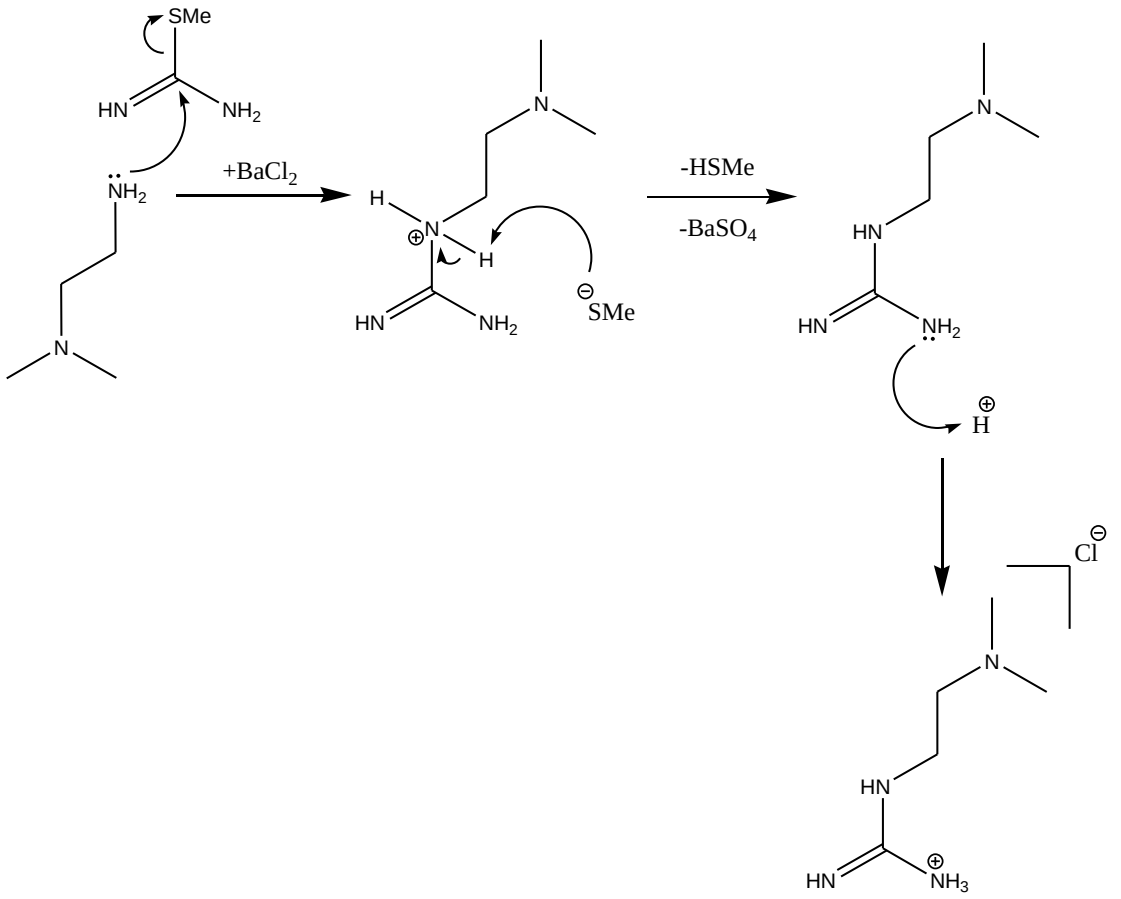

Scheme 10. Mechanism for the synthesis of Dimethylethylenediamino-guanidine

The mechanism for the synthesis of the dimethylethylenediamino-guanidine proceeds as the nucleophilic amine attacks the central carbon of the S-methylisothiourea sulphate, leading to the loss of methanethiol (Scheme 10). The positively charged nitrogen becomes neutral as an extra proton is abstracted by the negatively charged SMe ion, forming methyl-mercaptan. $BaSO_4$ was also produced as a white precipitate by-product, which also aids in the driving force for the reaction to proceed.

The ^1H NMR spectra of the dimethylethylenediamino-guanidine synthesised was consistent with the expected structure. The two CH_2 groups of the dimethylethylenediamino chain were observed as triplets between 2.78-3.39 ppm. A singlet corresponding to the 6 methyl protons was seen at 2.39 ppm. MS data was consistent with the M^+ ion peak observed at 166 m/z.

The next phase of the synthesis was the reaction between the chalcone and the synthesised novel dimethylethylenediamino-guanidine to produce the dimethylethylenediamino-4,6-diarylpyrimidines. Three chalcones were selected based on the best pyrimidine prodrugs

synthesised in previous chapters. Dimethylethylenediamino-guanidine (1.5 equivalents) was stirred with of sodium hydroxide (4 equivalents) under reflux in ethanol for 0.5h. Chalcone (1 equivalent) was then added and the reaction continued to stir under reflux for 6h. The product was observed by TLC analysis appearing as a fluorescent blue spot when observed under UV-light. The solvent was removed *in vacuo* and the compound purified by flash chromatography using DCM and methanol (8.5:1.5) as eluent. The three dimethylethylenediamino-4,6-diarylpyrimidines synthesised produced light brown oils.

The mechanism for the above reaction begins with the formation of the free guanidine by stirring dimethylethylenediamino-guanidine with sodium hydroxide. The free nucleophilic guanidine then attacks the carbonyl of the chalcone forming an imine (Scheme 11). Intramolecular cyclisation then occurs forming the dihydropyrimidine heterocycle. Aromatisation of the heterocycle then occurs via oxidation with air forming the dimethylethylenediamino-4,6-diarylpyrimidine.

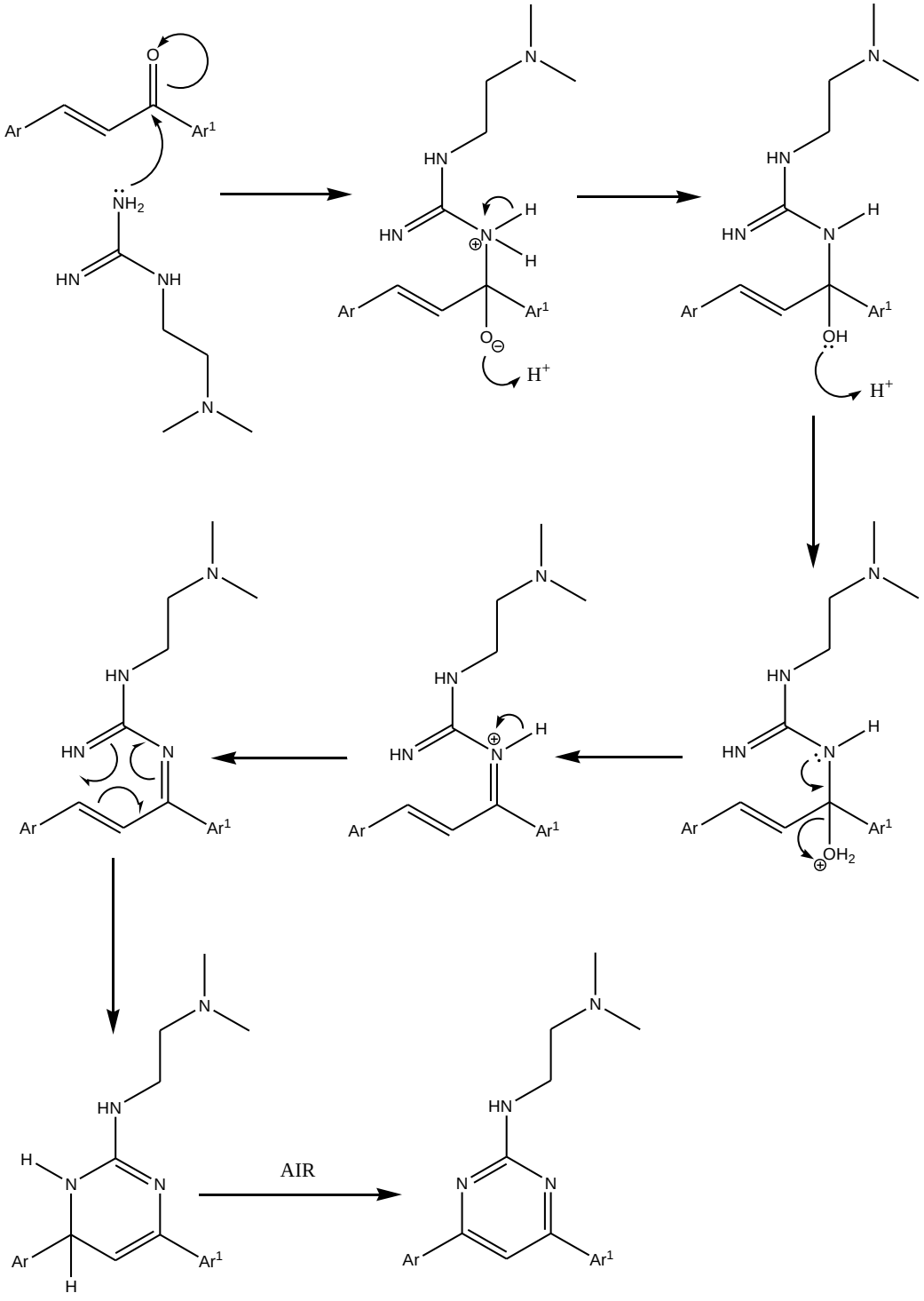

Scheme 11. Mechanism for the synthesis of the dimethylethylenediamino-4,6-diarylpyrimidine

Three dimethylethylenediamino-4,6-diarylpyrimidines were synthesised with yields ranging from 29-42%. The ^{1}H NMR spectra of the compounds synthesised were consistent with the

expected structures, with the heterocyclic ring proton at C5 appearing between 7.43-7.60ppm. The four methylene protons appeared as two separate triplet peaks between 2.70-3.92ppm, each representative of two hydrogens. Figure 109 shows the ^{1}H NMR spectrum and Figure 110 shows the MS spectrum for DMU 10602. The six methoxy group protons appeared between 2.38-2.66ppm. MS data gave $(M+H)^{+}$ ion peaks of correct masses. Due to the small scale of reagents used in the synthesis, hydrogen peroxide was not used in aiding the aromatisation of the pyrimidine heterocycle, as air was sufficient to achieve this. To support this, a parallel reaction with the synthesis of DMU 10600 was carried out which included the addition of hydrogen peroxide resulting in DMU 10600P (Figure 108). However, the addition of hydrogen peroxide unexpectedly did not produce the aromatised dimethylethylenediamino-4,6-diarylpyrimidine. MS data revealed that DMU 10600P had an additional mass of 16 in comparison to DMU 10600. As the only difference between the two reactions was the addition of the peroxide, an unwanted possible oxidation could have occurred and the extra mass of 16 would account for the incorporation of an oxygen atom in the compound at some point. NMR interpretation of DMU 10600P showed only 6 aromatic protons present when compared to the 7 aromatic protons present in DMU 10600. It was also observed that the heterocyclic proton at C5 was absent in the spectra, indicating that the C5 position may have undergone oxidation and was bonded to an OH group (Figure 108).

Table 32. Synthesised dimethylethylenediamino-4,6-diarylpyrimidines

Entry	DMU No.	Structure	% Yield	m.p °C	Appearance
1	10600	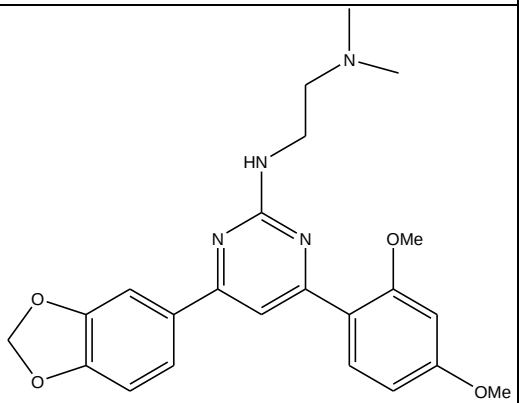	39	-	Light Brown Oil

2	10601	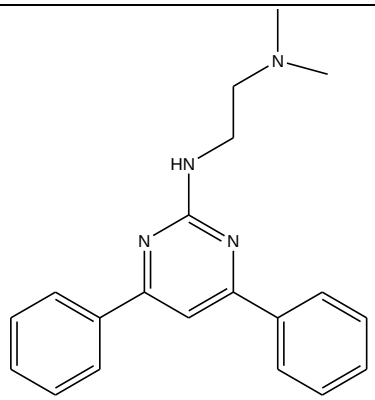	42	-	Light Brown Oil
3	10602	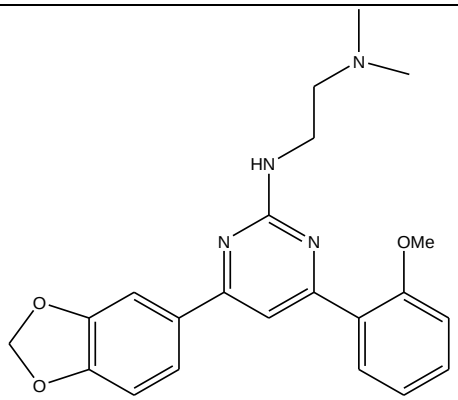	29	-	Light Brown Oil

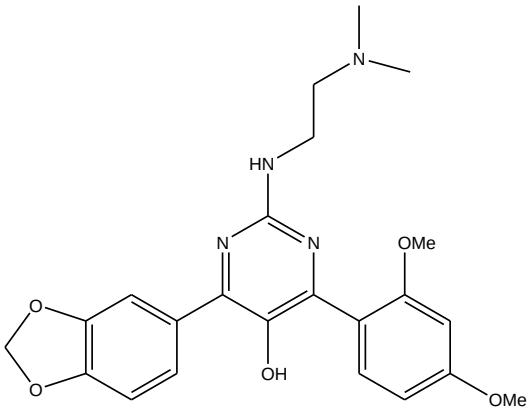

Figure 108. Suggested structure of DMU 10600P

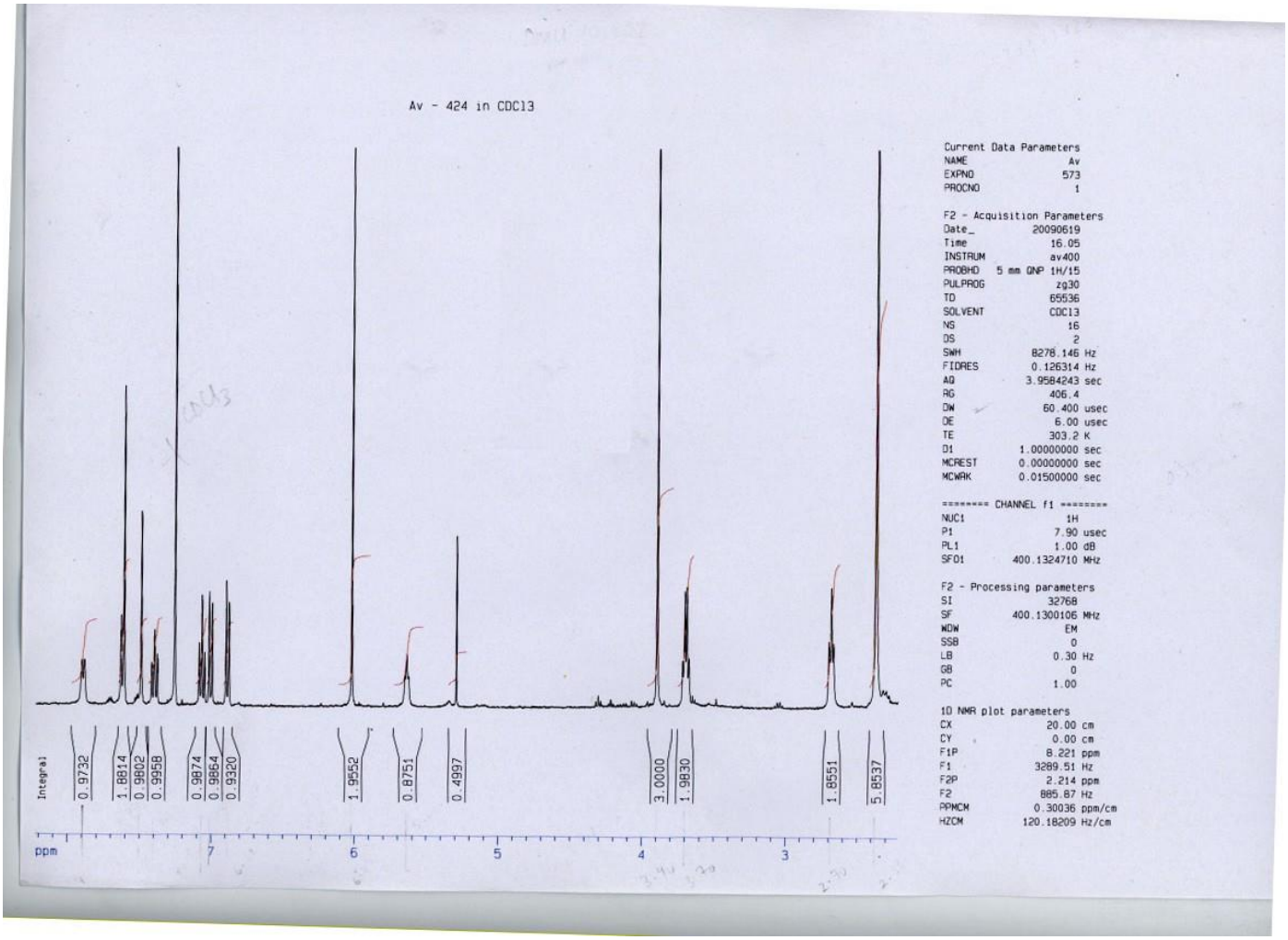

Figure 109. ^{1}H NMR spectrum of DMU 10602

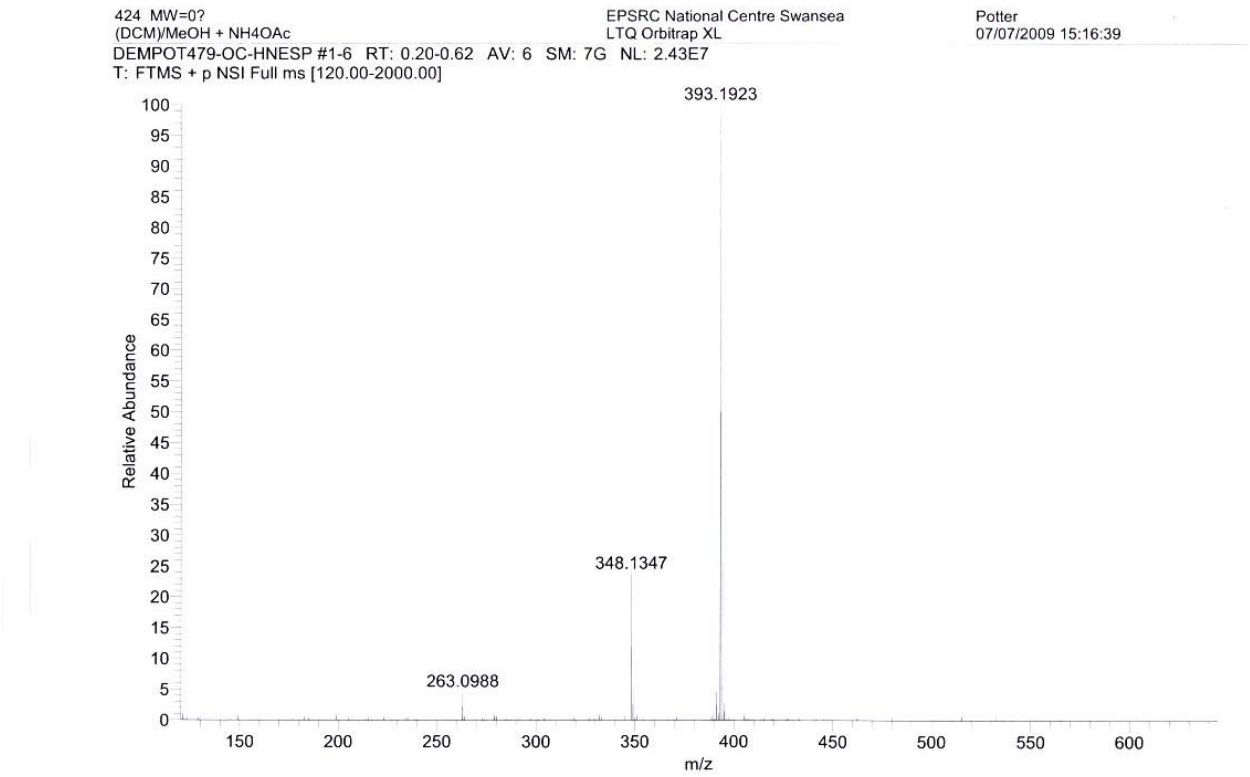

Figure 110. MS spectrum of DMU 10602

6.1 Biological Evaluation of the 2-dimethylethylenediamino-4,6-diarylpyrimidines

The three substituted 2-dimethylethylenediamino-4,6-diarylpyrimidines (Figure 111) were synthesised and screened for their cytotoxicities against the MDA 468, MCF7 and MCF10A cell lines as described in chapter 2. The substitutions on the A and B-rings were selected from the amino-pyrimidines DMU 10212, DMU 10313 and DMU 10200 as these exhibited the best overall anti-cancer activity when screened against the tumour cell lines in chapter three.

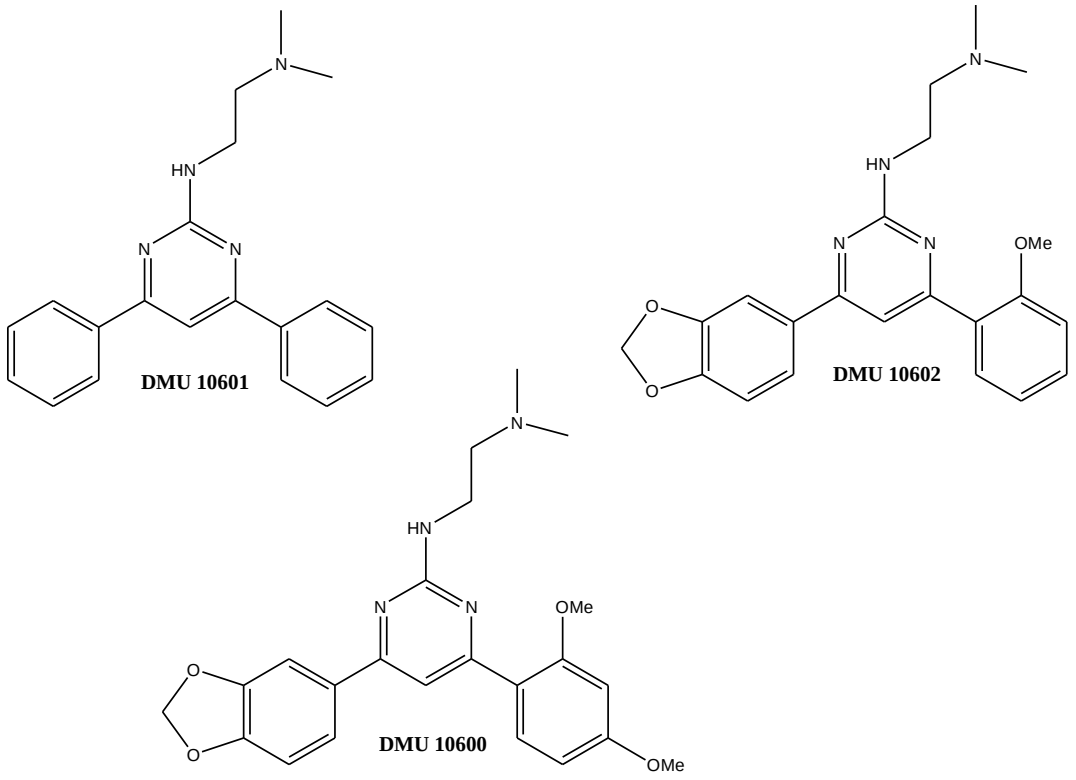

Figure 111. Structures of DMU 10601, DMU 10602 and DMU 10600

Table 33. Cytotoxicities of DMU 10600, DMU 10601 and DMU 10602

Entry	DMU No.	IC_{50} (µM)		IC_{50} (µM)	
		MCF10A	**MDA468**	**MCF7**	**MCF7 + TCDD**
1	10600	60	7	10	10
2	10601	35	15	21	19
3	10602	>100	>100	20	20

n=1

6.1.1 DMU 10601

DMU 10601 (Figure 113) was synthesised without any functional groups on the A and B-rings. The design was based on the amino-pyrimidine DMU 10200 (Figure 112) which showed exciting anti-tumour activity, especially against the MDA 468 cell line giving an IC_{50} value of 0.2µM.

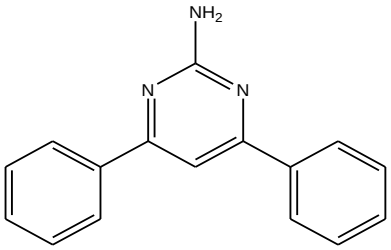

Figure 112. Structure of DMU 10200

Screening DMU 10601 against the MDA 468 cell line gave an IC_{50} value of 15µM (Table 34, entry 2), 75 times less toxic than DMU 10200. Toxicity was also observed towards the MCF10A cells. The IC_{50} values recorded against the MCF7 and MCF7 cells induced with TCDD were 15µM and 21µM respectively. Again, the toxicities of the amino-pyrimidine DMU 10200 were more potent towards the MCF7 cells.

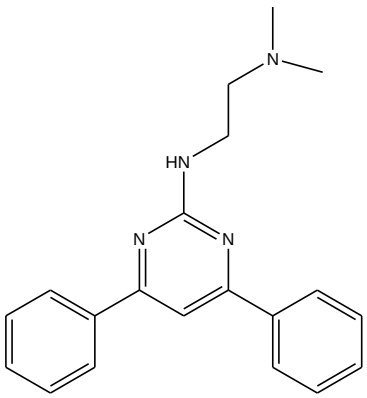

Figure 113. Structure of DMU 10601

6.1.2 DMU 10602

DMU 10213 (Figure 114), synthesised with a 3,4-methylenedioxy substitution on the A-ring and 2-methoxy substitution on the B-ring provided the basis for the synthesis of DMU 10602.

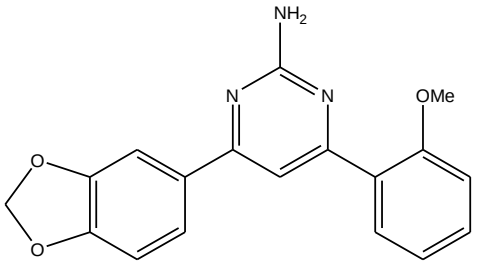

Figure 114. Structure of DMU 10213

DMU 10602 (Figure 115) showed no cytotoxic activity towards the MDA 468 cell line which constitutively expresses the CYP1A1 and CYP1B1 enzymes. This was a disappointing result as DMU 10213 provided an IC_{50} value of 0.5µM when screened against the MDA 468 cells whilst remaining non-toxic towards the non-tumour MCF10A cells.

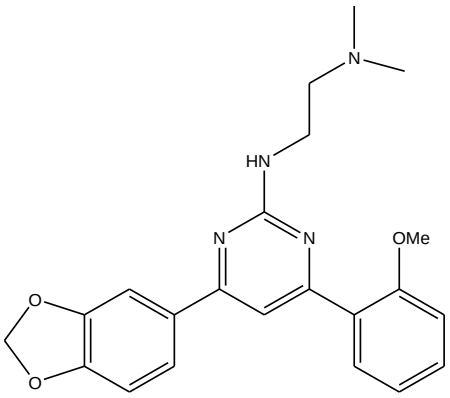

Figure 115. Structure of DMU 10602

Screening of DMU 10602 against the MCF7 cell lines gave an IC_{50} value of 20µM for both the TCDD induced and non-induced cells, proving to be 250 times less toxic than DMU 10213.

6.1.3 DMU 10600

DMU 10600 was designed based on the amino-pyrimidine DMU 10212 (Figure 116), with a 3,4-methylenedioxy substitution on the A-ring and a 2,4-dimethoxy substitution on the B-ring.

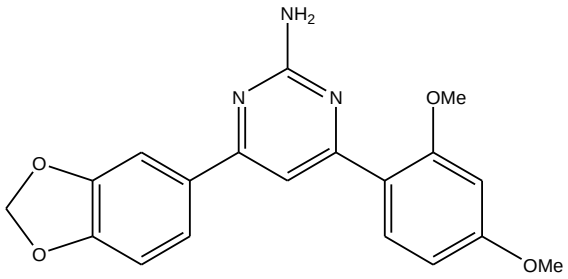

Figure 116. Structure of DMU 10212

When screened against the MDA 468 cell line, DMU 10600 gave an IC_{50} value of 7µM. Slight toxicity was also observed towards the non-tumour MCF10A cells. However, DMU 10600 was approximately 700 times less toxic towards the MDA 468 cells in comparison to DMU 10212 which was also non toxic towards the MCF10A cells. Identical IC_{50} values of 10µM were observed when DMU 10600 was screened against the MCF7 cells, for both the TCDD induced and non-induced cells. This result was also less toxic than the cytotoxicity of DMU 10212 observed against the MCF7 cells.

6.2 Synthesis of 2-methyl-4-(2,4-dimethoxyphenyl)-6-(3,4-methylenedioxyphenyl)pyrimidine, DMU 10700

The synthesised 2-dimethylethylenediamino-4,6-diarylpyrimidines were synthesised to explore the 2-position of the pyrimidine ring. This was carried out in the aim to develop compounds with improved toxicities than those recorded with the amino-pyrimidines. DMU 10600 showed the most effective anti-cancer activity from the 2-dimethylethylenediamino-4,6-diarylpyrimidines synthesised, with an IC_{50} value of 7µM observed towards the MDA 468 cell line. However, this result was not as significant as the cytotoxicity observed from the amino-pyrimidine DMU 10212, for which an IC_{50} value of 0.01µM was seen against the

MDA 468 cell line and IC_{50} values of 0.07µM and 0.3µM recorded against the MCF7 and MCF7 cells induced with TCDD.

Subsequently, DMU 10700 (Figure 117) was synthesised with a methyl group on the 2-position of the pyrimidine ring. This was synthesised to observe the effect of a non-conjugating electron donating group at the 2-position of the pyrimidine ring towards the cytotoxicity of this compound. The methyl group does not have lone pairs of electrons like the amino group of DMU 10212 which can possibly participate in binding to CYP1 enzymes.

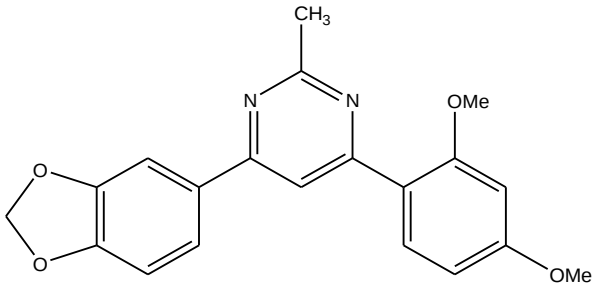

Figure 117. Structure of DMU 10700

The method used to synthesise DMU 10700 was the same as that used to synthesise the pyrimidines in chapter three, replacing guanidine hydrochloride with acetamidine hydrochloride (Figure 118).

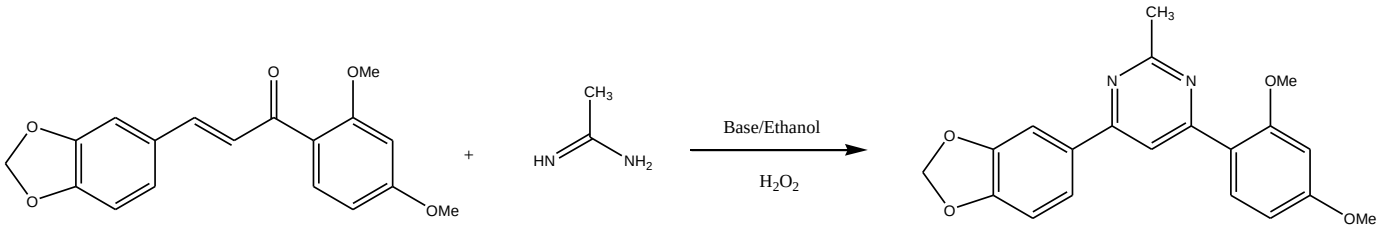

Figure 118. General reaction of the synthesis of DMU 10700

Therefore, acetamidine hydrochloride (1.5 equivalents) was stirred with sodium hydroxide (4 equivalents) in ethanol. The reaction was stirred at reflux for thirty minutes producing the free acetamide. DMU 407 (1 equivalent) was added to the mixture and the reaction continued to proceed for 6h. This was followed by the addition of hydrogen peroxide (3 equivalents, 50% w/v) and the reaction was stirred under reflux for a further 1h to aromatise the pyrimidine ring. TLC analysis showed the formation of the 2-methylpyrimidine as a fluorescent blue spot when viewed under UV light. The solvent was removed *in vacuo* and the product purified by recrystallisation from ethanol affording yellow crystals.

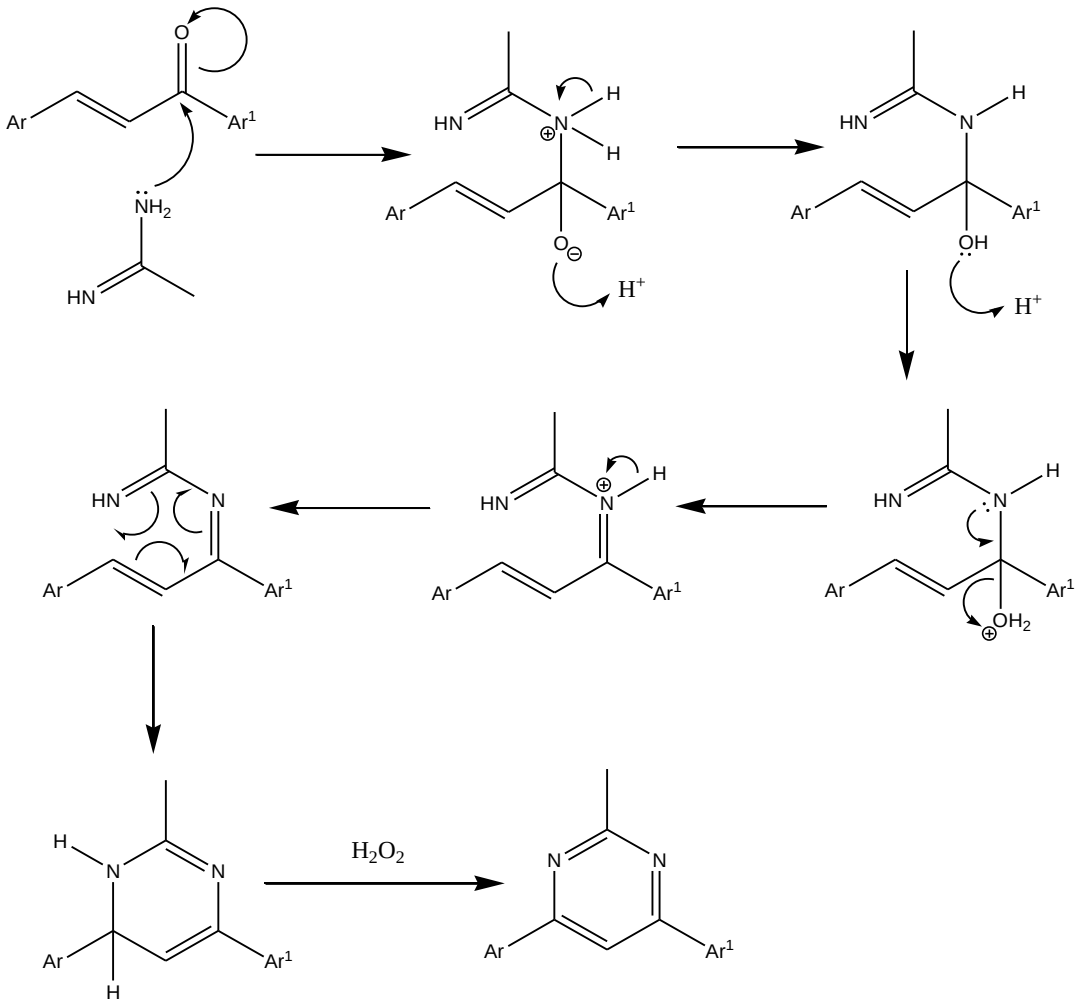

Scheme 12. Mechanism for the synthesis of DMU 10700

The mechanism for the synthesis of DMU 10700 is shown in Scheme 12. Under basic conditions the free acetamide reacts with DMU 407 via nucleophilic addition forming an imine. Intramolecular cyclisation then follows forming the dihydro-pyrimidine. The peroxide oxidises the pyrimidine ring forming the aromatised pyrimidine heterocycle.

The reaction produced a yield of 10% with the melting point of DMU 10700 being recorded between 127-129^{o}C. The ^{1}H NMR spectrum gave a singlet at 2.80ppm for the three methyl protons at the 2-position of the pyrimidine ring. Seven aromatic protons, alongside the two methylenedioxy protons were also observed. The MS spectrum was correct upon interpretation with the $(M+1)^{+}$ peak being observed.

6.2.1 Biological Evaluation of DMU 10700

DMU 10700 (Figure 119), was screened against the MDA 468, MCF7 and MDA 231 tumour cell lines to evaluate its prodrug activity.

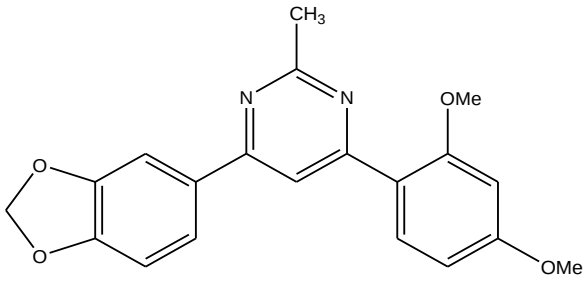

Figure 119. DMU 10700

Results from the MDA 468 cell line gave an IC_{50} value of 2.5µM (Figure 120), whilst no toxicity was observed towards the non-tumour MCF10A cell line. Unfortunately, no cytotoxicity was recorded from the MCF7 and MDA 231 cells as IC_{50} values were above 100µM.

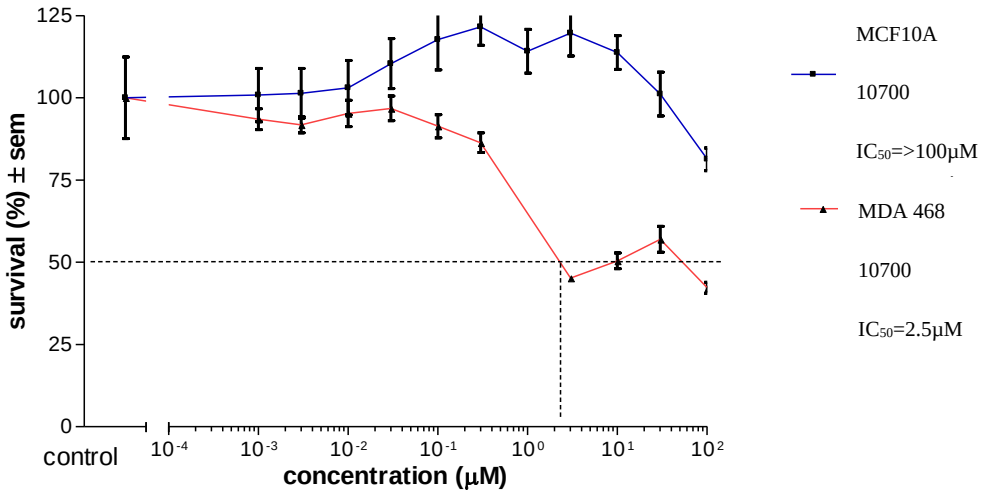

Figure 120. Cytotoxicity plot of MDA 468 and MCF10A treated with DMU 10700

The cytotoxicity of DMU 10700 was 250 times less potent than that observed from DMU 10212, the amino-pyrimidine analogue of DMU 10700 towards the MDA 468 cell line. However, the pyrimidone analogue DMU 10312 like DMU 10212 also showed greater toxicity across the panel of cell lines tested against in comparison to DMU 10700.

6.3 Synthesis of 4-(2,4-dimethoxyphenyl)-6-(3,4-methylenedioxyphenyl)pyrimidine, DMU 10800

The synthesis of substituted pyrimidines has produced compounds showing valuable toxicity against the tumour cell lines screened against, particularly towards the MDA 468 cell line. A further compound, DMU 10800 was designed without a functional group at the 2-position of the pyrimidine ring to show that the amino substitution at this position is important for the cytotoxicities observed from the pyrimidines in this project. The substitutions on the A and B-rings were identical to that of DMU 10212.The synthesis of DMU 10800 was parallel to that of DMU 10700 (6.2), with the replacement of acetamidine hydrochloride with formamidine hydrochloride (Figure 121).

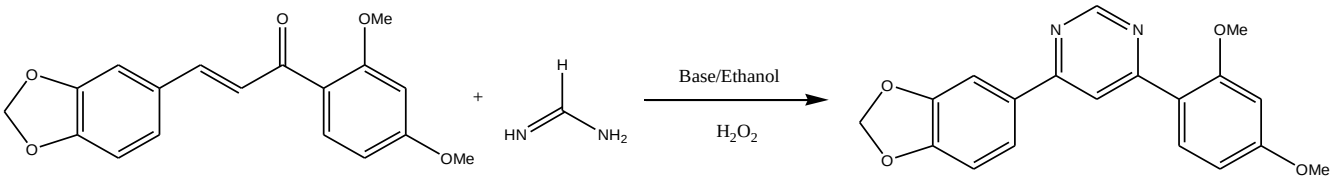

Figure 121. General reaction for the synthesis of DMU 10800

Pale brown crystals with a yield of 10% were obtained for DMU 10800, with a melting point recorded between 132-134^{o}C. The ^{1}H NMR spectrum showed eight aromatic protons as expected with the structure. The MS spectrum was correct with a 337 $(M+1)^{+}$ ion peak being observed.

6.3.1 Biological Evaluation of DMU 10800

DMU 10800 (Figure 122) was synthesised to display the importance of the 2-position of the pyrimidine ring and its effect on cytotoxicity when substituted with different functional groups. The amino group has proved to be the most favourable functional group providing significant cytotoxicities when substituted in the 2-position of the pyrimidine ring as shown in chapter three.

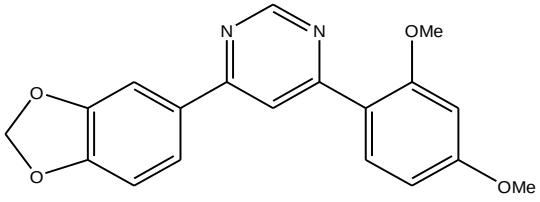

Figure 122. Structure of DMU 10800

The result from DMU 10800 when screened against the MDA 468 cell line was notably cytotoxic, showing an IC_{50} value of 0.08µM whilst remaining non-toxic towards the non-tumour MCF10A cells (Figure 123).

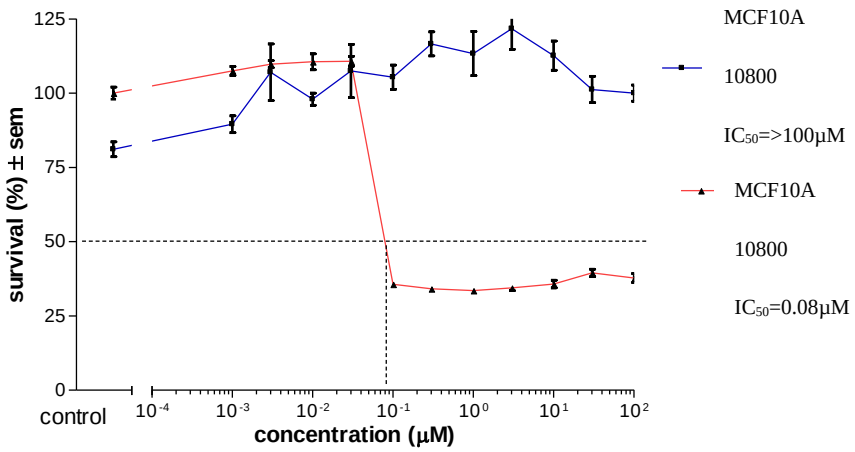

Figure 123. Cytotoxicity plot of MDA 468 and MCF10A treated with DMU 10800

The MCF7 cells, induced and non-induced with TCDD gave identical IC_{50} values of 0.2µM respectively (Figure 124). However, toxicity was not observed towards the MDA 231 cell line, as IC_{50} values recorded were greater than 100µM.

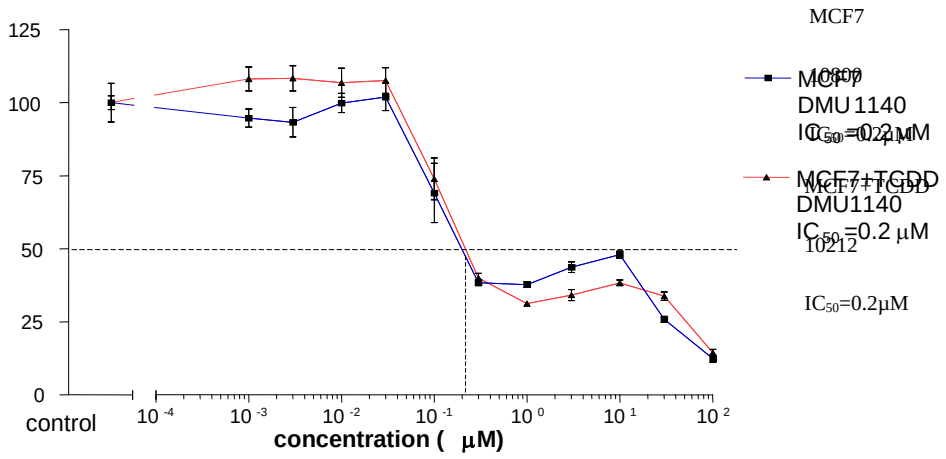

Figure 124. Cytotoxicity plot of MCF7 and MCF7 cells induced with TCDD treated with DMU 10800

6.4 Summary and Conclusions

Three dimethylethylenediamino-4,6-diarylpyrimidines were synthesised by methods used by *Andrews et al* and *Agarwal et al*. These compounds were screened for their prodrug activities against a panel of cell lines made up of the non-tumour MCF10A cell line, and the tumour MDA 468 and MCF7 cell lines. From the data obtained, it appeared that DMU 10600 (Table 35, entry 4) was the most effective anti-cancer dimethylethylenediamino-4,6-diarylpyrimidine synthesised. IC_{50} values of DMU 10600 included a value of 7µM towards the MDA 468 cell line. However, it was concluded that the incorporation of the dimethylethylenediamino group did not enhance the cytotoxicity of the pyrimidine compounds in comparison to the previously synthesised 2-aminopyrimidines in chapter three.

DMU 10700 (Table 35, entry 2), an analogue of DMU 10212 was synthesised with a methyl group at the 2-position of the pyrimidine heterocycle to investigate the effect of a non-conjugating electron donating group in contrast to the amino substituted pyrimidine DMU 10212. Valuable toxicity was observed from this compound against the MDA 468 cell line, giving an IC_{50} value of 2.5µM, greater than that seen from the previously synthesised dimethylethylenediamino-4,6-diarylpyrimidineanalogue derivative of DMU 10600. No toxicity was recorded towards the non-tumour MCF10A cell line by DMU 10700. However, the amino-pyrimidine DMU 10212 (Table 35, entry 3) has shown to still be the most effective prodrug synthesised in comparison to its heterocyclic analogues.

DMU 10800 (Table 35, entry 1), another analogue of DMU 10212 was synthesised without any functional group incorporated at the 2-position of the pyrimidine ring. Significant cytotoxicity was observed towards the MDA 468 cell line, with an IC_{50} of 0.08µM being observed. The MCF7 and MCF7 cells induced with TCDD gave IC_{50} values of 0.2µM each. These results were more potent than the pyrimidone analogue of DMU 10312 (Table 35, entry 5) and are comparable with DMU 10212, but the amino-pyrimidine showed to be more favourable as an anti-cancer prodrug with overall toxicities lower than those of DMU 10800.

Table 34. Cytotoxicity of DMU 10212 and its synthesised derivatives

Entry	DMU No.	Structure	MCF 10A	MDA 468	MCF7	MCF7 + TCDD	MDA 231	MDA 231 + TCDD
1	10800	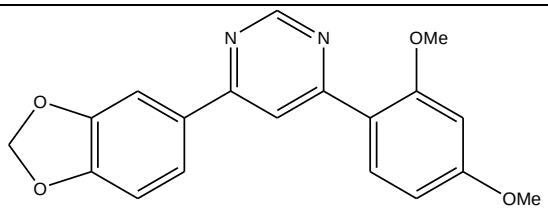	>100	0.08	0.2	0.2	>100	>100
2	10700	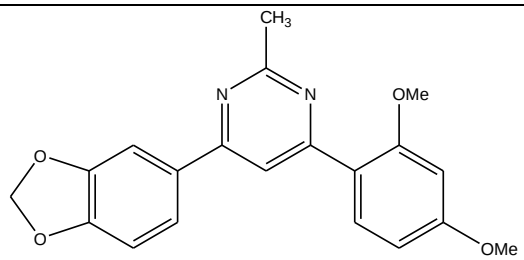	>100	2.5	>100	>100	>100	>100
3	10212	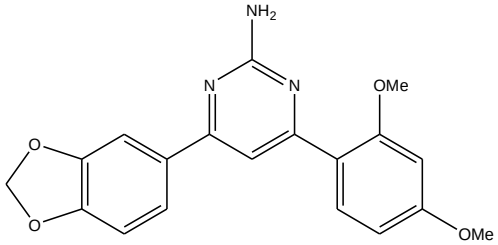	>100	0.01	0.07	0.3	30	20
4	10600	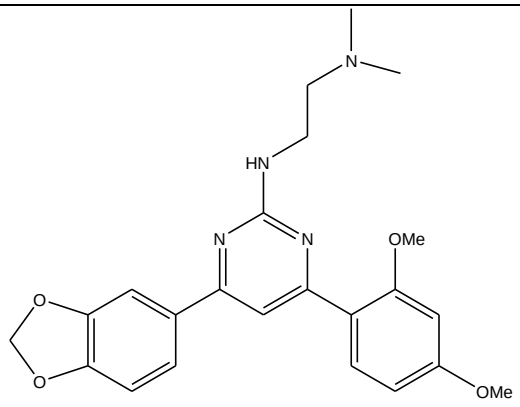	60	7	>100	>100	>100	>100
5	10312	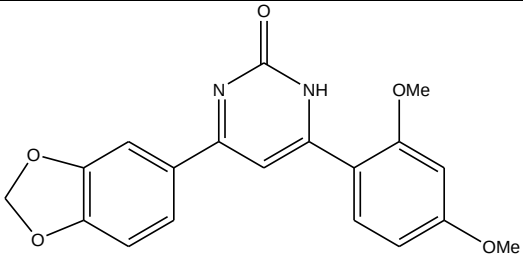	>100	1.5	8	8	10	10

Therefore, the functional group at the 2-position of the pyrimidine ring is important for cytotoxicity to occur towards the tumour cell lines whilst remaining non-toxic to non-tumour cells. It has been experimentally shown that the primary NH_2 functional group integrated into the 2-position of the pyrimidine heterocycle is the most favourable for anti-cancer prodrug activity to be observed out of the pyrimidines synthesised in this project.

Further work would entail an investigation to determine and synthesise the metabolites of DMU 10212 formed via CYP1 metabolism.

Chapter 7

Metabolism Studies on DMU 10212 with CYP1 Isoforms

7.0 Metabolism Studies on DMU 10212

The 2-amino-4,6-diarylpyrimidine DMU 10212 (Figure 125) was found to be the most effective anti-cancer prodrug from the libraries of compounds synthesised in this project.

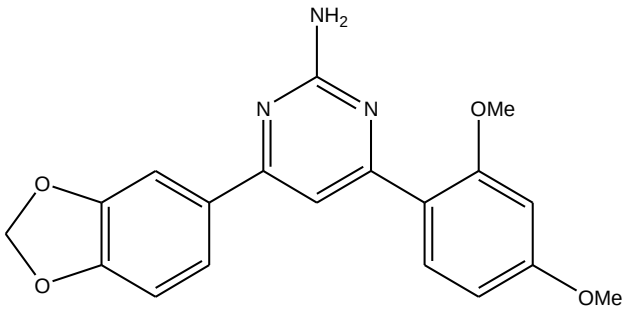

Figure 125. Structure of DMU 10212

An IC_{50} value of 0.01µM was obtained from screening DMU 10212 against the MDA 468 cell line whilst no toxicity was seen towards the non-tumour MCF10A cells, suggesting that a prodrug anti-cancer mechanism of action occurs. The MCF7 cells induced with TCDD gave an IC_{50} value of 0.3µM and the non-TCDD induced cells gave an IC_{50} value of 0.07µM. The significant cytotoxicity demonstrated by DMU 10212 motivated the further investigation of this compound in order to verify that the CYP1 enzymes were actually involved in the metabolism of DMU 10212, and to make an identification of the metabolites generated. The metabolism experimentations were conducted by Dr. D. Ankrett of the CDDG.

7.1 Inhibition Studies of DMU 10212

α-naphthoflavone (α-NF) is a well known CYP1A1 and CYP1B1 inhibitor due to its high binding affinity towards these enzymes (Figure 126).[235, 236] It has been reported that the inhibition of the CYP1 enzymes occurs as the α-NF competitively binds to the active site or ferric haem of the CYP1 enzymes, preventing other substrates from binding to the CYP1 enzymes. Inhibition studies were conducted to demonstrate that DMU 10212 was a genuine substrate for the CYP1 enzymes. DMU 10212 was screened against the tumour cell lines using the standard MTT assay with the addition of α-NF.

.

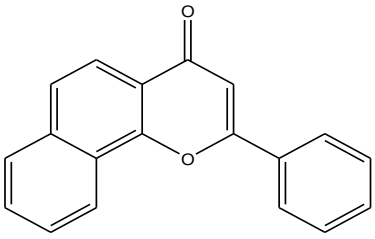

Figure 126. Structure of α-naphthoflavone (α-NF)

The MDA 468 cell line constitutively expresses both the CYP1A1 and CYP1B1 enzymes.[216] Screening of DMU 10212 against the MDA 468 cell line gave a notable IC_{50} value of 0.01µM (Figure 127), which was the most cytotoxic result seen towards this cell line in comparison to the toxicities observed from the compounds in this project. Importantly, no toxicity towards the non-tumour MCF10A control cell line was recorded.

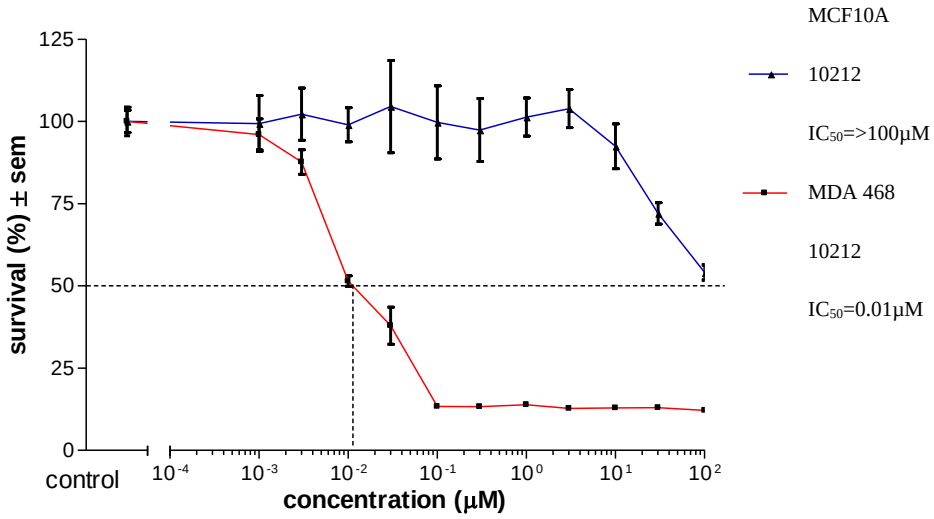

Figure 127. Cytotoxicity plot of MDA 468 and MCF10A treated with DMU 10212 without α-NF

When DMU 10212 was screened against the MDA 468 cells with the addition of the CYP1 inhibitor α-NF, the previously observed toxicity of 0.01µM was completely eliminated (Figure 128). The control MCF10A cells were also screened against DMU 10212 with the addition of α-NF, and as expected, no toxicity was observed at all.

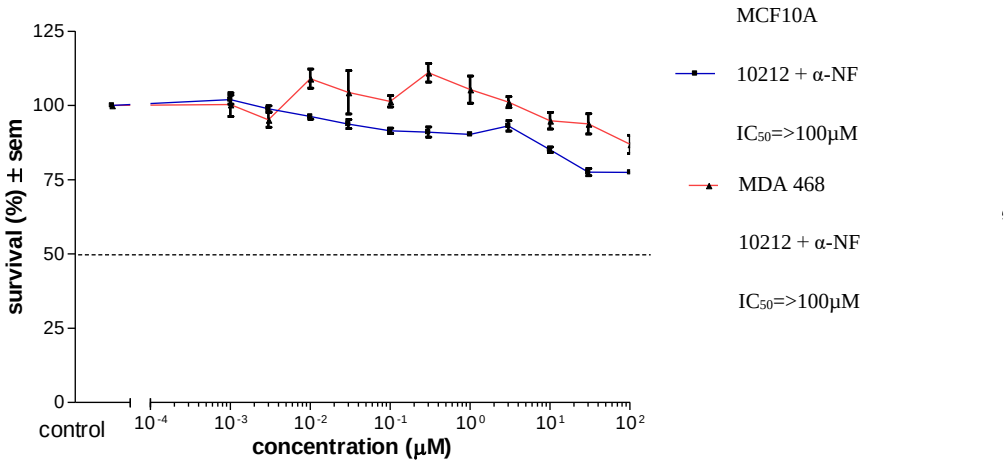

Figure 128. Cytotoxicity plot of MCF10A and MDA 468 cells treated with DMU 10212 and α-NF

The MCF7 cell line does not constitutively expresses CYP1 enzymes, but within five minutes of exposure to TCDD the expression of CYP1A1 is amplified.[237] Screening of DMU 10212 against the MCF7 cells and MCF7 cells induced with TCDD gave encouraging results, with IC_{50} values of 0.07µM and 0.3µM being observed (Figure 129).

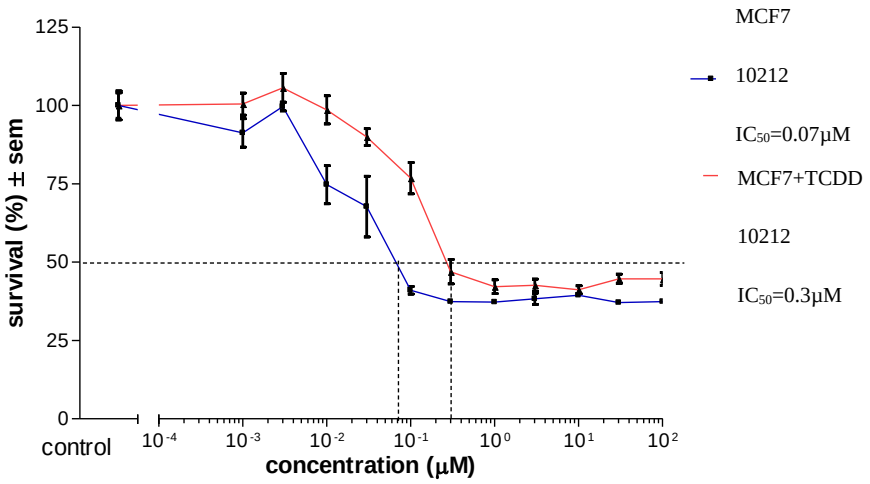

Figure 129. Cytotoxicity plot of MCF7 and MCF7 + TCDD treated with DMU 10212

DMU 10212 was screened against the MCF7 cells incubated with the CYP1 inhibitor α-NF. The results showed that the toxicity observed in Figure 129 was entirely eliminated as illustrated in Figure 130.

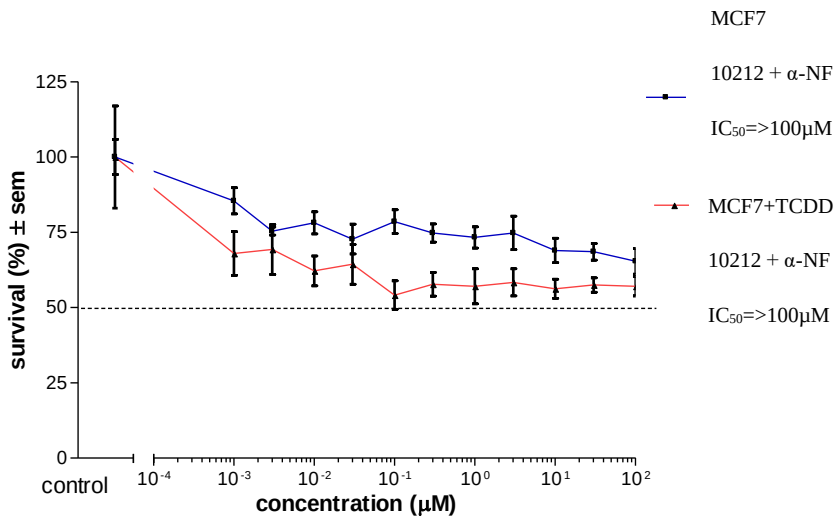

Figure 130. Cytotoxicity plot of MCF7 and MCF7 cells induced with TCDD treated with DMU 10212 and α-NF

The MDA231 cell line expresses very low levels of CYP1 enzymes. Treatment with TCDD primarily induces CYP1B1 expression but CYP1A1 is also expressed to a lesser extent. The screening of DMU 10212 against the MDA 231 and MDA 231 cells induced with TCDD showed reasonable toxicity with IC_{50} values of 20µM and 30µM being recorded correspondingly. The results observed from screening DMU 10212 with the incubation of α-NF against the MDA 231 cells (Figure 131) did not show any cell death towards this cell line. This result is in line with the observed data from the MDA 468 and MCF7 cell lines incubated with α-NF.

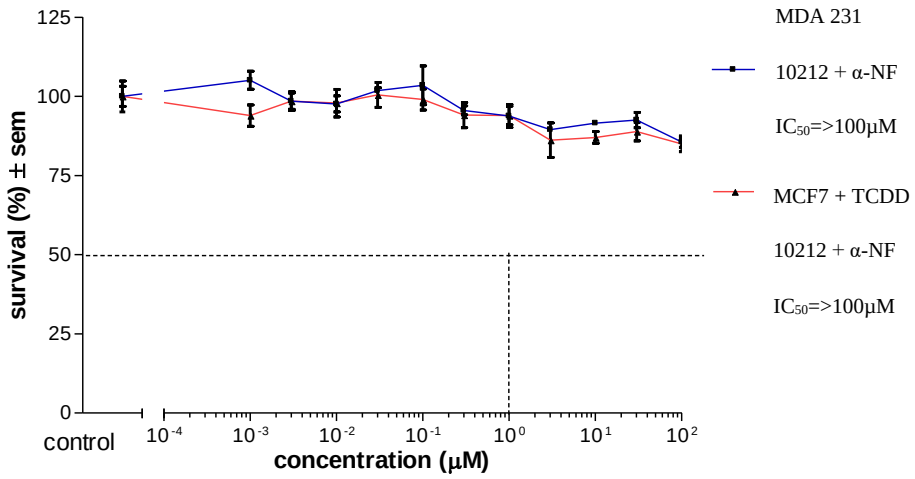

Figure 131. Cytotoxicity plot of MDA 231 and MDA 231 cells induced with TCDD treated with DMU 10212 and α-NF

7.2 Metabolism Study of DMU 10212

DMU 10212 was investigated in inhibition studies using the CYP1 inhibitor α-NF, which indicated that DMU 10212 was a substrate of the CYP1 enzymes. It was concluded that the CYP1 enzymes are responsible for the metabolism of DMU 10212, in turn producing its cytotoxic metabolite or metabolites important for the anti-cancer effect of DMU 10212 observed against the CYP1 expressing tumour cell lines.

The next stage of this study was to deduce the CYP1 metabolites of DMU 10212 formed. The affinity of DMU 10212 towards CYP1A1, CYP1A2 and CYP1B1 was also investigated alongside the rate of the metabolism of DMU 10212 by each enzyme. CYP3A4 was also explored in this study, as this enzyme is the most abundant in the liver. This would provide an insight if possible hepatic toxicity of this drug would occur if administered orally, as the liver would be the location of first pass metabolism which is undesired.

To achieve the above, DMU 10212 was incubated with human recombinant CYP family enzymes; CYP1A1 CYP1A2, CYP1B1, CYP3A4 and the non-CYP expressing control Supersomes™. The LCMS mobile phase consisted of 33% acetonitrile acidified to pH5 with formic acid, 65% aqueous ammonium formate also acidified to pH5 with formic acid and 2% propan-2-ol. A gradient was initiated at time zero. The run time was 12.5 minutes with an additional 3 minute re-equilibration time. The column compartment temperature was maintained at 50ºC. The flow rate was 0.6mL.min^{-1}. LCMS analysis was carried out using positive mode electrospray ionization, (ESI) Standard-enhanced scan mode was employed (scan speed 8100 m/z /sec and scan range 50-450 m/z) and with drying gas 350ºC, flow rate of 9L/min-1, nebuliser pressure 40psi, MS/MS and MS^3 fragmentation amplitude 3.5V. Incubations were carried out at 37ºC using the following final concentrations; PO4 buffer (20mM), MgCl2 (0.5mM), NADPH (0.5mM), DMU 10212 (10μM), enzyme 20pmol.mL^{-1} and an appropriate volume of water to give a final incubate volume of 250μL. Control incubations were carried out using either non-CYP-expressing insect Supersomes™ or with the omission of either DMU 10212, NADPH or the active enzyme. At zero and 30 minutes, 100μL of the incubate were removed and added to an equal volume of ice-cold acetonitrile to terminate the reaction. Samples were then centrifuged at 3500rpm for 15 minutes at 4ºC, and aliquots (25μL) of the supernatant were analysed by LCMS.

The results showed that four metabolites (M1, M2, $M3^1$/$M3^2$ and M4) were produced by each of the CYP1A1, CYP1A2 and CYP1B1 enzymes which can be seen from the total ion chromatograms (TIC) in Figures 132, 133 and 134. Encouragingly, no metabolites were detected in the CYP3A4 enzyme assay which is a strong indication that liver toxicity from DMU 10212 would not be observed if DMU 10212 was administered orally (Figure 135). Importantly, the metabolites from the CYP1 assays were not detected in the control assays (Figures 136 and 137) as these did not contain CYP1 enzymes, showing no other entity could be responsible for the metabolism of DMU 10212.

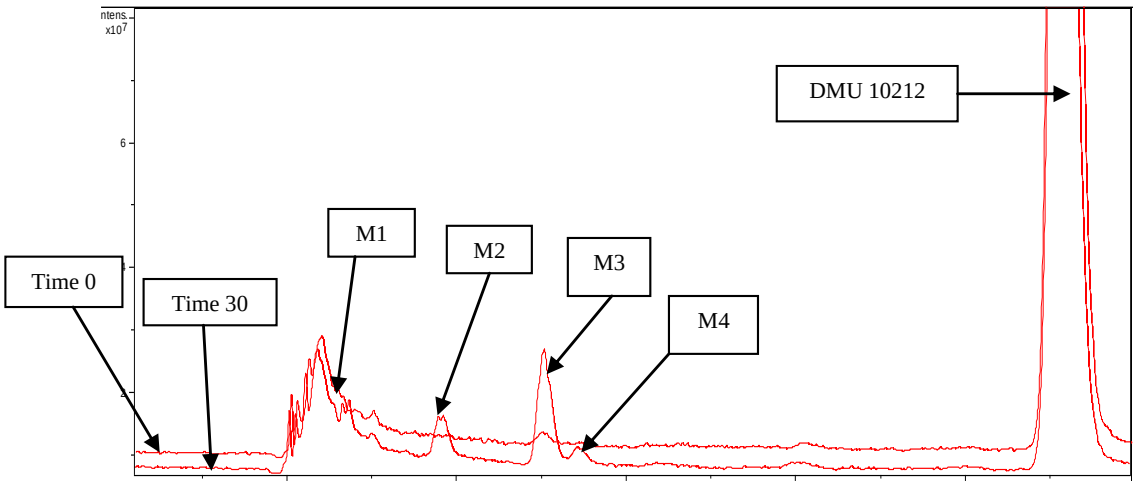

Figure 132. TIC of DMU 10212 incubated with CYP1A1 and extracted at time 0 and 30 mins

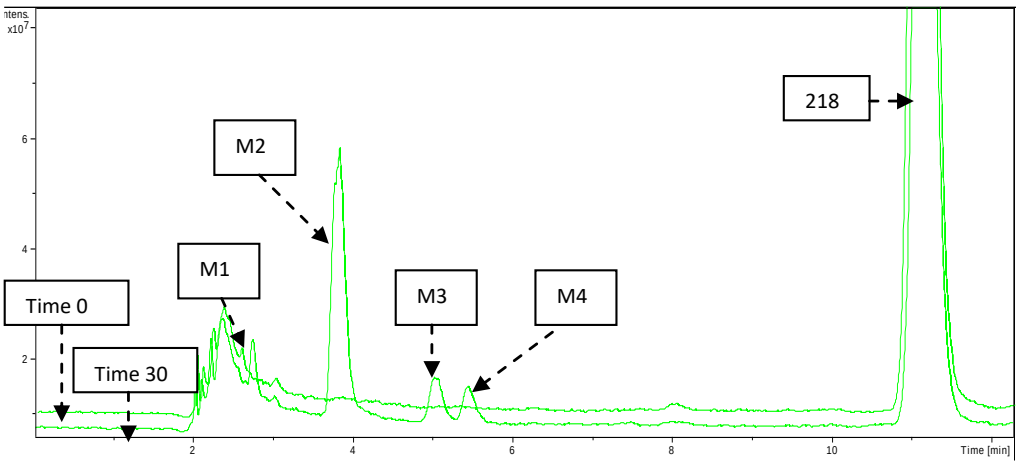

Figure 133. TIC of DMU 10212 incubated with CYP1A2 and extracted at time 0 and 30 mins

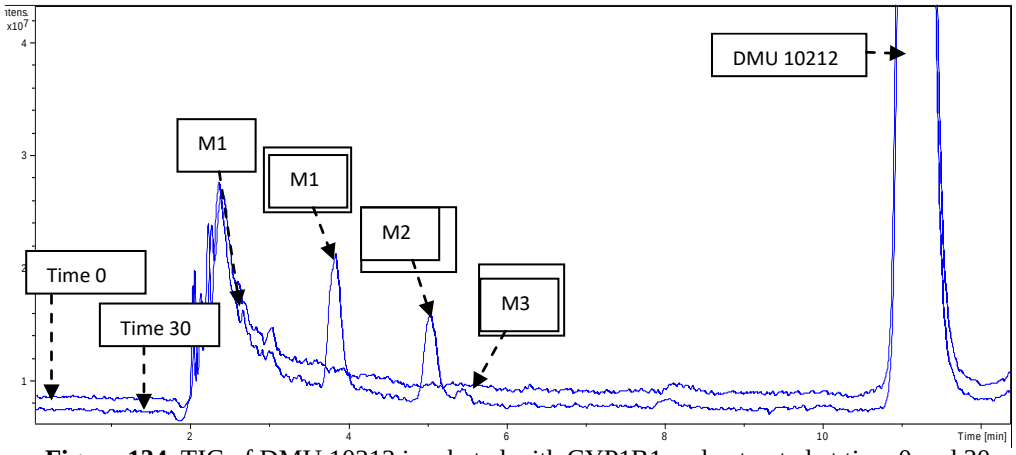

Figure 134. TIC of DMU 10212 incubated with CYP1B1 and extracted at time 0 and 30 mins

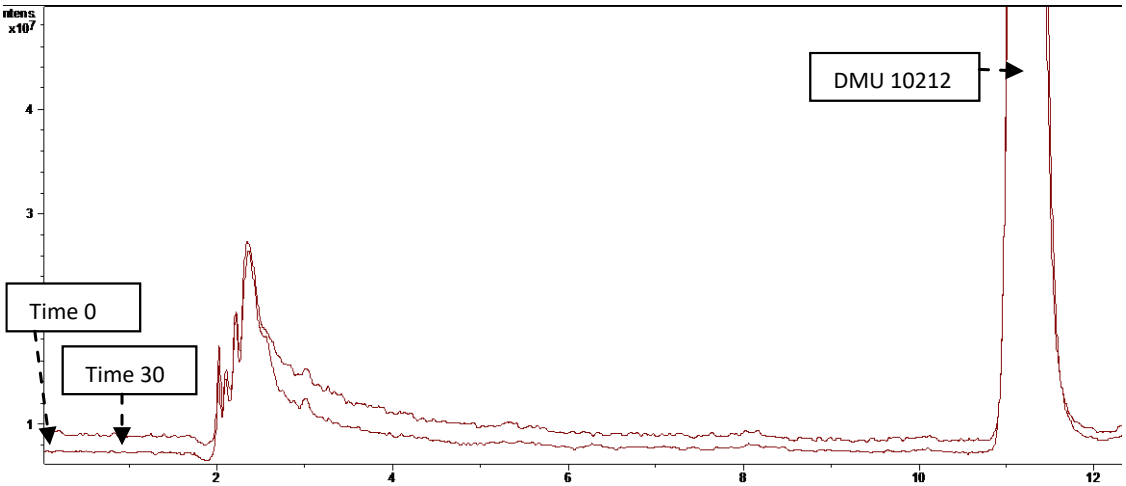

Figure 135. TICs of DMU 10212 incubated with CYP3A4 and extracted at time 0 and 30 mins

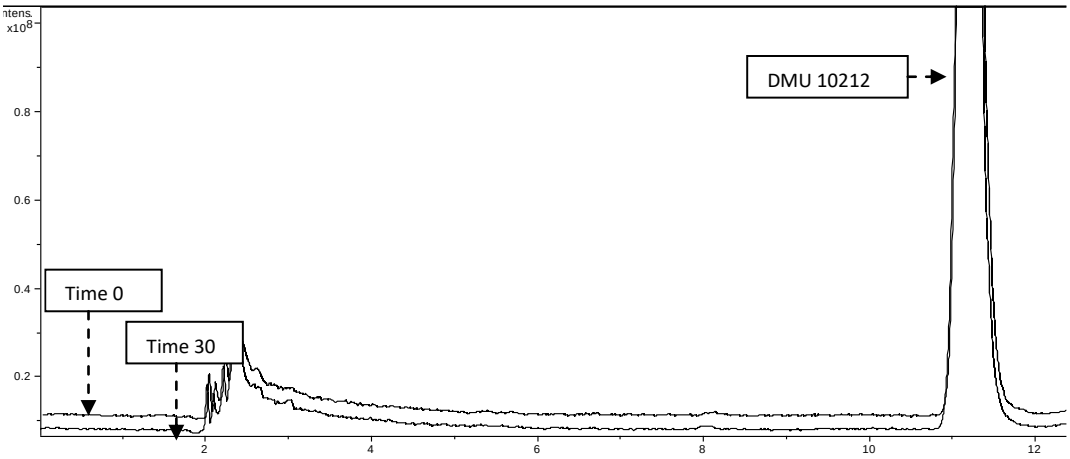

Figure 136. TICs of DMU 10212 incubated with Control Supersomes™ and extracted at time 0 and 30 mins

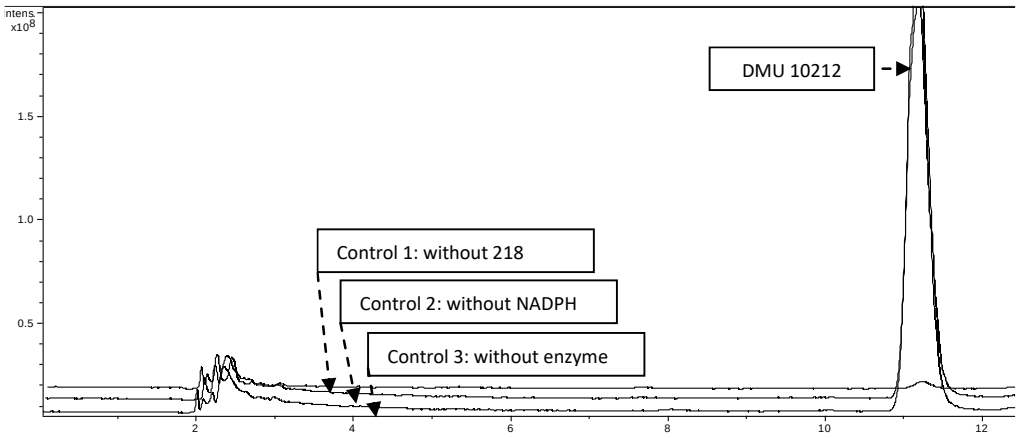

Figure 137. TICs of DMU 10212 incubated with Control 1, 2 and 3 and extracted at time 0 and 30 mins

ble 35. RT's and MW's observed for the metabolites of DMU 10212

Compound	**RT (mins)**	**$[M+H]^+$**	**Metabolic Alteration**	**CYP Involved in Production**
DMU 10212	11.2	352	N/A	N/A
M1 or M1[2]	2.8	326	Dealkylation	CYP1A1 CYP1A2 CYP1B1
M2	3.8	340	Dealkylation	CYP1A1 CYP1A2 CYP1B1
M3[1] or M3[2]	5.0	338	2´O- Dealkylation	CYP1A1 CYP1A2 CYP1B1

M4	5.4	368	3´-Hydroxylation	CYP1A1 CYP1A2 CYP1B1

The rate of metabolism of DMU 10212 by the CYP1A1, CYP1B1 and CYP1A2 enzymes was also measured. The rate of disappearance of DMU 10212 was measured over 15 minutes at 3 minute intervals. The calculated rates show that DMU 10212 was preferentially metabolised by CYP1A1, followed by CYP1A2 and then CYP1B1.

The functions of the CYP family of enzymes are well known (Introduction, section 1.8). Reactions catalysed by CYP enzymes include carbon hydroxylation, heteroatom oxygenation and dealkylation. With the molecular weights known for each metabolite (Table 36), proposed structures were determined (Scheme 13). Each metabolite also produced its own specific retention time. This can be used as the proposed metabolites can be synthesised and co-eluted with the enzymatically produced metabolites which would give the same RT if they are the same compound.

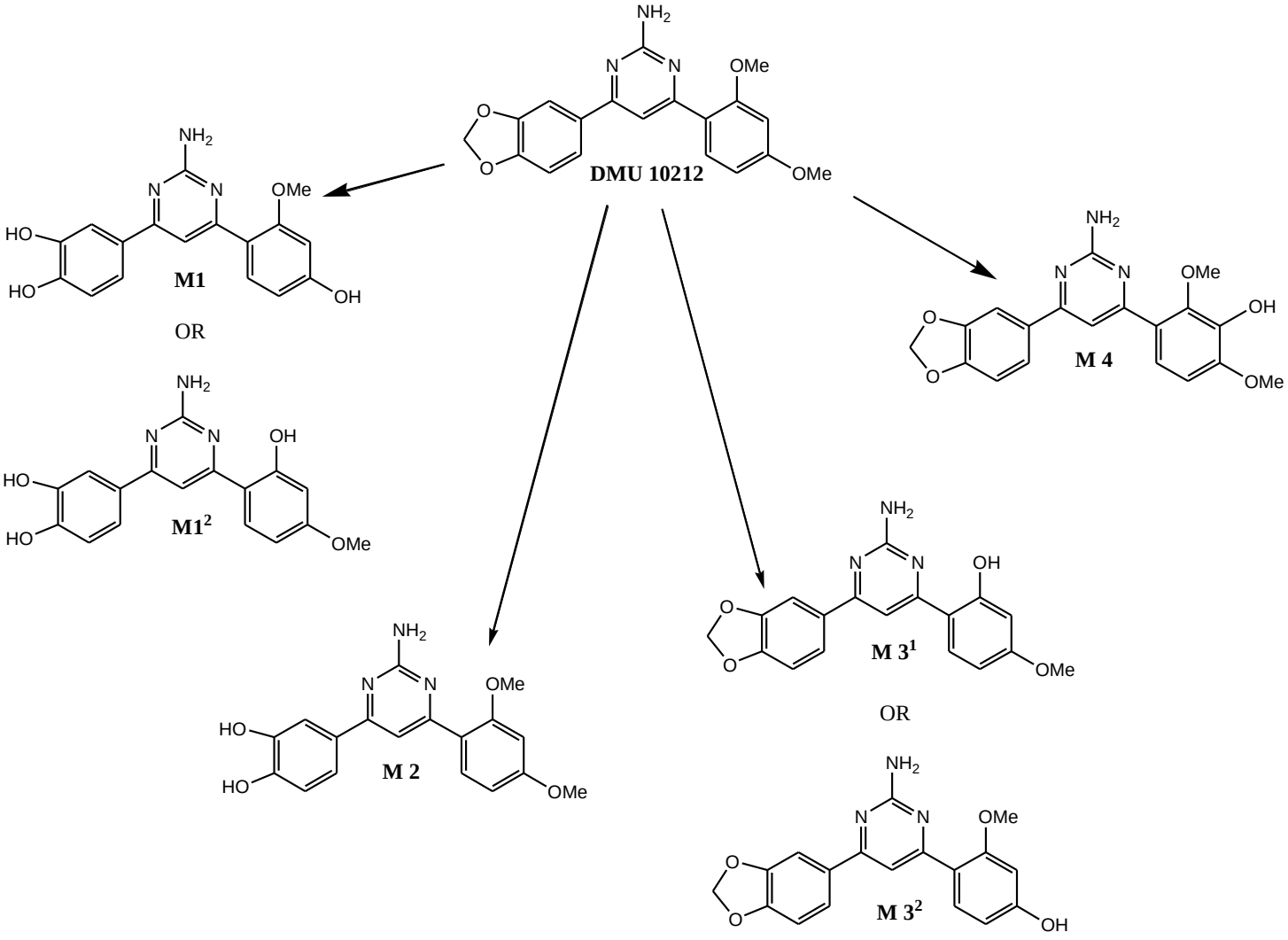

Scheme 13. Proposed metabolites of DMU 10212 via CYP1 metabolism

7.2.1 Synthesis of Metabolites M2 and M3^2

Proposed metabolite structures were synthesised to act as authentic standards for co-elution studies, which would allow for the confirmation of metabolite identity. The metabolites chosen for synthesis were M2 and M3^2, as these were the first structures identified as possible metabolites.

The M2 metabolite, with a 3,4-dihydroxy substitution on the A-ring and 2,4-dimethoxy substitution on the B-ring was first to be synthesised (Figure 138).

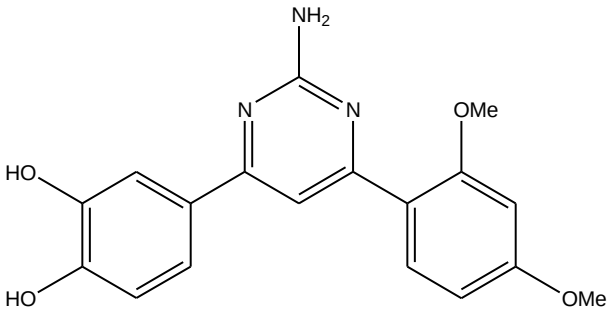

Figure 138. Structure of M2

The method used to synthesise M2 was taken from *Castro et al*, who modified podophyllotoxin by demethylating the methylenedioxy group substituted on the A-ring using boron-trichloride.[238] This resulted in the formation of a dihydroxy analogue of podophyllotoxin (Figure 139), with yields of up to 80% reported.

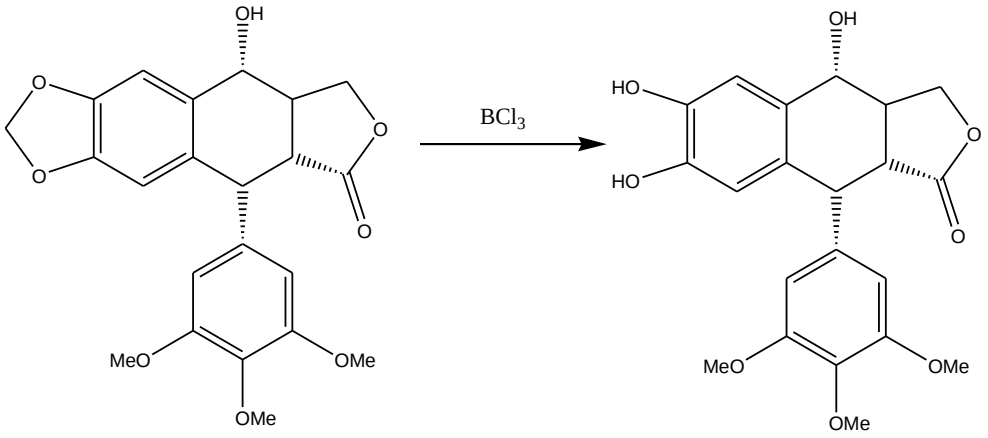

Figure 139. Demethylation of the methylenedioxy group on podophyllotoxin using boron-trichloride

For the synthesis of M2, a solution of DMU 10212 and boron trichloride in dichloromethane was stirred at -5^{o}C under nitrogen for 24 h. The reaction was quenched with water and extracted with ethyl acetate. The combined organic extracts were dried over $MgSO_4$ and the solvent was removed *in vacuo*. The catechol was purified by flash chromatography using dichloromethane and methanol (9:1) as eluent.

The purified catechol was collected as a brown oil with a yield of 17%. The ^{1}H NMR spectrum of the compound synthesised was consistent with the expected structure, with the pyrimidine ring proton at C5 appearing as a singlet at 7.46ppm. The singlet observed at

6.03ppm for the methylenedioxy protons seen for DMU 10212 was no longer present, confirming the successful dealkylation of the methylenedioxy group. The MS spectrum gave an $[M+H]^+$ ion peak of 340 which was correct for the catechol structure.

The second metabolite to be synthesised was M3[2], which required a four step process (Figure 140).

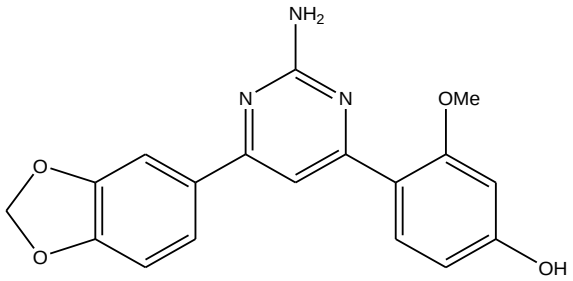

Figure 140. Structure of M3[2]

The first step required the synthesis of the chalcone analogue, but due to the presence of the 4-hydroxy group this could not be achieved immediately using the same Claisen-Schmidt reaction used to afford the previously synthesised chalcones in chapter two. It has been shown that hydroxy substituted chalcones require their hydroxy substituted precursors to be treated with protecting groups, or reactions rates are very slow producing low yields. This is due to the fact that the base involved in the Claisen-Schmidt reaction reacts with the hydroxy precursor delocalising the anion, slowing down the reactive steps required for the formation of the chalcone (Figure 141).[239]

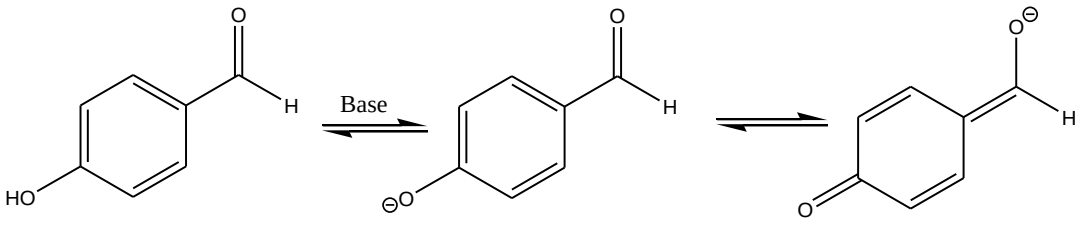

Figure 141. Delocalisation of the benzaldehyde anion

Therefore, the 4-hydroxy-2-methoxybenzaldehyde chalcone precursor was treated with 3, 4-dihydro-2*H*-pyran as the OH protecting agent (Scheme 14).[240, 197] The resulting 2-(methoxy-4-tetrahydropyran-2-yloxy)-benzaldehyde was then reacted with 3,4-methylenedioxyacetophenone to yield the protected chalcone via the Claisen-Schmidt reaction. The protected chalcone was reacted with guanidine hydrochloride to yield the

protected amino-pyrimidine. In order to gain the dihydroxy-pyrimidine, the tetrahydropyran protecting group was removed by treatment with acid.

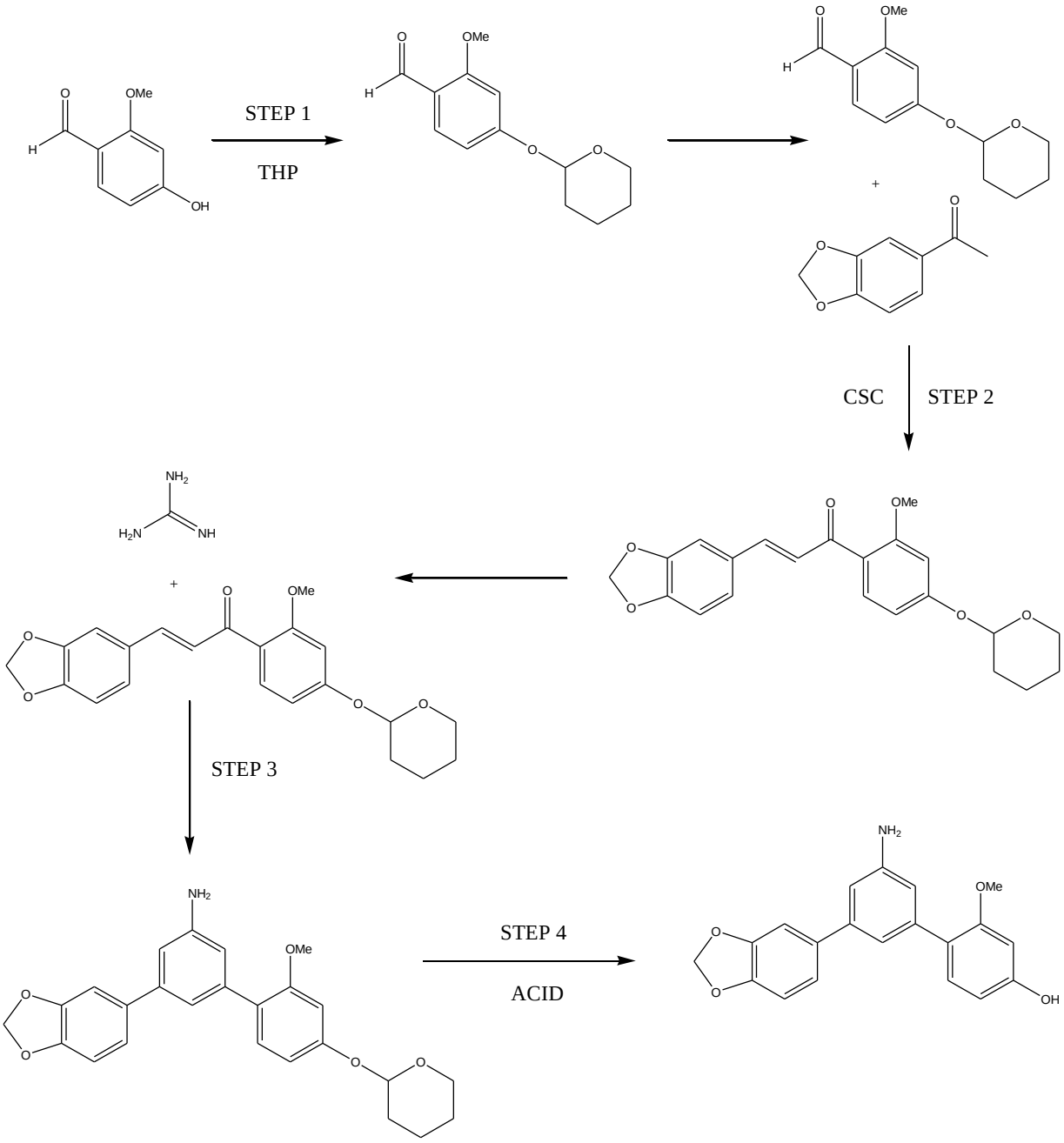

Scheme 14. Reaction scheme for the synthesis of the 4-hydroxy amino-pyrimidine

7.2.1.1 Synthesis of 2-(methoxy-4-tetrahydropyran-2-yloxy)-benzaldehyde, DMU 10500

A mixture of 4-hydroxy-2-methoxybenzaldehyde (1 equivalent) and pyridinium ρ-toluene sulfonate (0.024 equivalents, catalytic quantity) in dichloromethane was stirred at room temperature for 0.5 h. This was followed by the drop-wise addition of 3,4-dihydro-2*H*-pyran (3 equivalents) in dichloromethane and the reaction was stirred for a further 24 h. The reaction was quenched with water and the organic mixture extracted with dichloromethane. The organic extracts were dried over $MgSO_4$ and the solvent was removed *in vacuo*. The protected benzaldehyde was purified by flash chromatography using dichloromethane – methanol (9:1) as eluent.

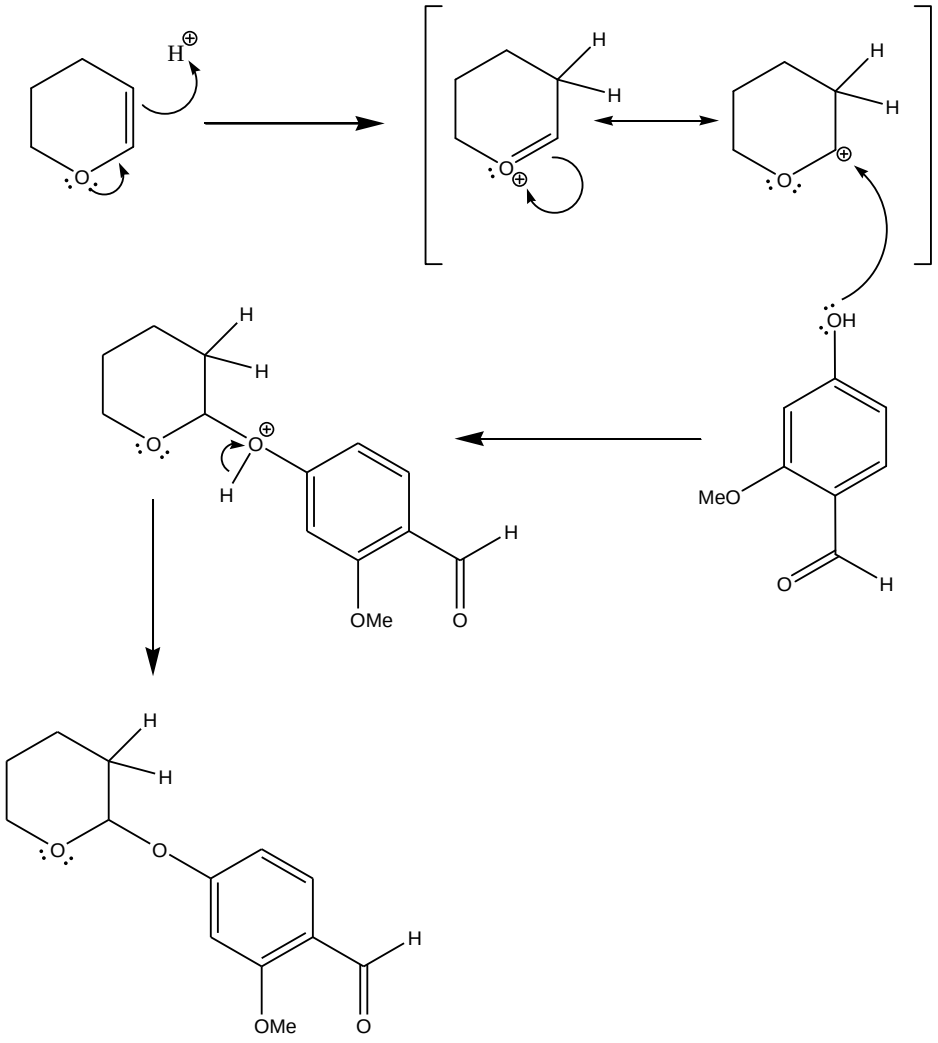

Scheme 15. Mechanism for the THP protection of 4-hydroxy-2-methoxybenzaldehyde

The mechanism for the protection of the benzaldehyde is shown in (Scheme 15). The pyran protecting group requires activating which is achieved by the presence of the pyridinium ρ-toluene sulfonate. This protonates the protecting tetrahydropyran group, forming a resonance stabilised carbocation intermediate. The nucleophilic alcohol of the benzaldehyde attacks the carbocation, which undergoes deprotonation to form the 2-(methoxy-4-tetrahydropyran-2-yloxy)benzaldehyde. This produced a yellow oil with a yield of 49%. The ^{1}H NMR spectrum showed the correct amount of protons required and MS analysis gave an $(M+1)^{+}$ ion peak of 237.

7.2.1.2 Synthesis of (E)-1-(3,4-methylenedioxyphenyl)-3-(2-methoxy-4-tetrahydropyran-2-yloxyphenyl)-2-propen-1-one, DMU 10501

The 2-methoxy-4-tetrahydropyran-2-yloxybenzaldehyde was stirred with 3,4-methylenedioxyacetophenone and sodium hydroxide (4 equivalents) in methanol and stirred at room temperature 24h. The reaction was then quenched with water and the organic mixture was extracted with dichloromethane. The combined organic extracts were dried over $MgSO_4$ and the solvent was removed *in vacuo*. Flash chromatography was used to purify the protected chalcone, using ethyl acetate – hexane as eluent (5:5). The mechanism for this reaction is the same as that described for the chalcones in chapter two.

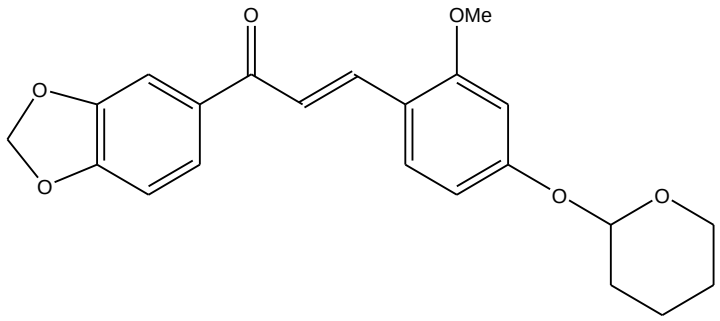

Figure 142. Structure of 2-(methoxy-4-tetrahydropyran-2-yloxy)benzaldehyde

The protected chalcone (Figure 142) produced a yellow oil with a yield of 77%. The ^{1}H NMR spectrum showed the correct number of protons required and MS analysis gave an ion mass of 383, corresponding to the $(M+1)^{+}$ ion.

7.2.1.3 Synthesis of 2-amino-4-(3,4-methylenedioxyphenyl)-6-(2-methoxy-4-tetrahydropyran-2-yloxyphenyl)pyrimidine, DMU 10502

The protected chalcone was stirred under reflux with guanidine hydrochloride (1.5 equivalents) and sodium hydroxide (4 equivalents, 50% w/v) in ethanol for 24h. TLC analysis showed the formation of a new product spot, blue when viewed under UV light representing the 2-amino-4-(3,4-methylenedioxyphenyl)-6-(2-methoxy-4-tetrahydropyran-2-yloxyphenyl)pyrimidine. The reaction was quenched with water and the organic mixture extracted with dichloromethane. The organic extracts were combined and dried over $MgSO_4$. The solvent was removed *in vacuo* and the crude mixture was purified by flash chromatography using ethyl acetate − hexane (4:6) as eluent. A yield of 3% was obtained with the compound produced as a yellow oil. The appropriate protons were observed in the ^1H NMR spectrum and MS analysis gave the $(M+1)^+$ ion mass of 422.

The reaction followed the same mechanism as the synthesis to yield the amino-pyrimidines in chapter three, however, a yield of 3% was achieved for the protected pyrimidine (Figure 143). This was surprisingly low as a yield of 31% was achieved for DMU 10212. The cause for the low yield could be accredited to the additional protecting group involved in the synthesis.

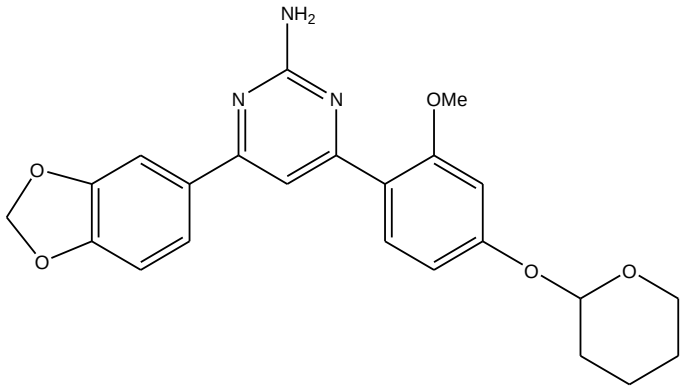

Figure 143. 2-amino-4-(3,4-methylenedioxyphenyl)-6-(2-methoxy-4-tetrahydropyran-2-yloxyphenyl)pyrimidine

7.2.1.4 Synthesis of 2-amino-4-(3,4-methylenedioxyphenyl)-6-(2-methoxy-4-hydroxyphenyl)pyrimidine, DMU 10503

The 2-amino-4-(3,4-methylenedioxyphenyl)-6-(2-methoxy-4-tetrahydropyran-2-yloxyphenyl)pyrimidine and *p*-toluenesulfonic acid (0.042 equivalents, catalytic quantity)

were stirred in methanol with at room temperature for 24h (Scheme 16). The solvent was removed *in vacuo* and the crude product was recrystallised from ethanol. The reaction gave a yield of 36% (5mg) which gave only enough compound to obtain a MS spectrum. The molecular weight observed from the MS spectrum gave an ion mass of 338 which corresponded to the $[M+H]^+$ ion. However, this reaction was not repeated due to time restraints but warrants further investigation.

The cyclisation step to form the pyrimidine heterocycle appeared to produce the lowest yield from the steps involved in the synthesis of DMU 10503. The addition of the protecting group may have decreased the reactivity of the carbonyl group of the chalcone, reducing the ability of the nucleophilic guanidine to form the imine. On the other hand, the intramolecular cyclisation step may have been hindered preventing the heterocycle from forming. These are concepts that can be investigated, alongside other protecting groups available which would be suitable for the reaction conditions used.

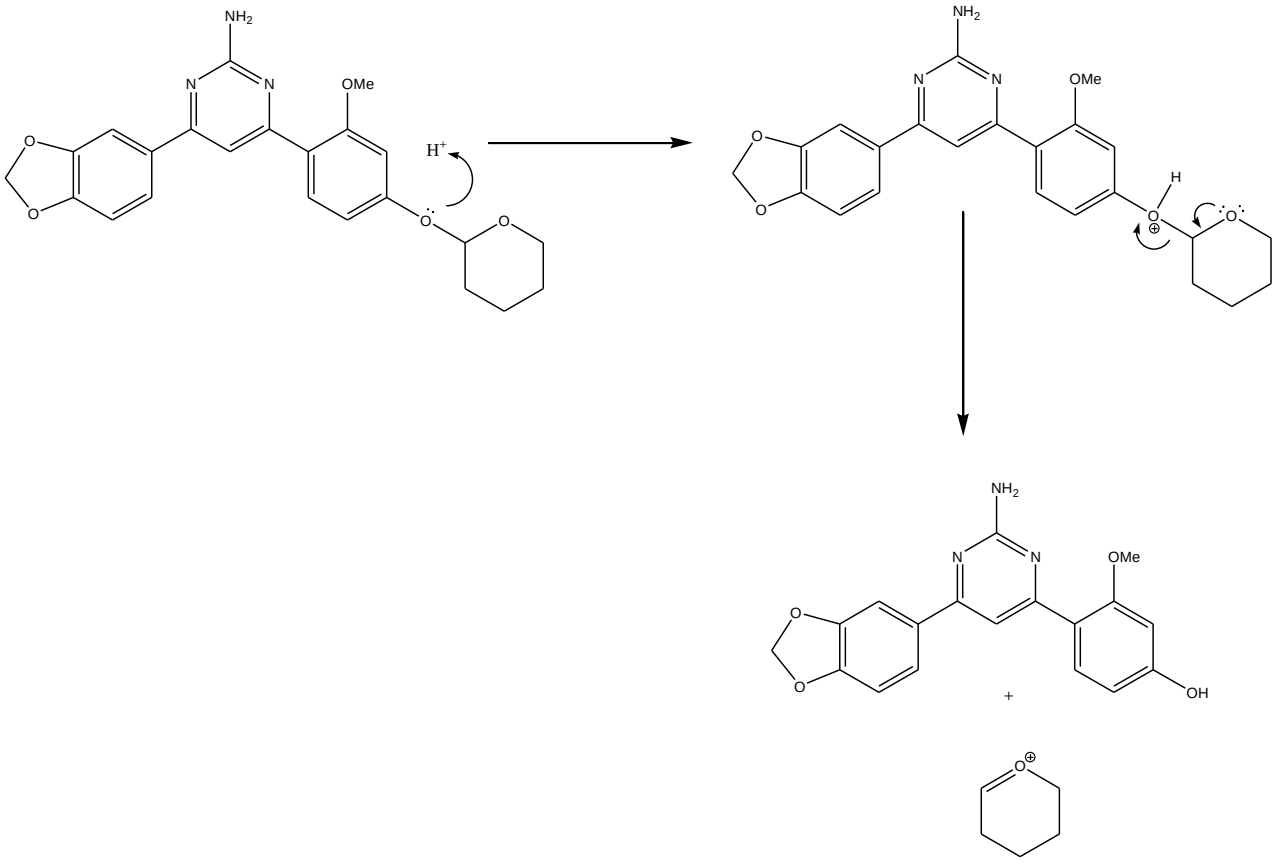

Scheme 16. Mechanism for the synthesis of DMU 10503

7.2.2 LCMS Analysis of M2

The proposed metabolites, M2 and $M3^2$ were synthesised to verify that they were authentic metabolites of DMU 10212. The synthetic M2 metabolite was analysed by LCMS and the results were compared to the data obtained from the enzymatically produced M2 metabolite. $M3^2$ could not be verified as the synthesis did not produce enough product for LCMS analysis to be conducted.

The retention times (RT) and mass spectrum of the enzymatically produced and synthetically produced M2 were identical. The TIC showed that the RT for the synthetically produced M2 was 3.8 mins (Figure 144), identical with that of the enzymatically produced M2.

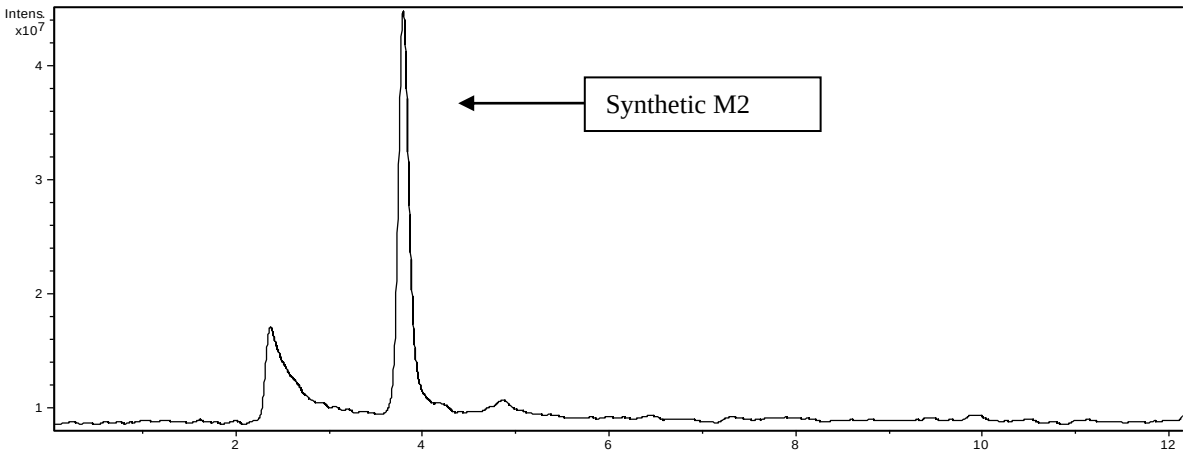

Figure 144. RT of the synthetic M2 of 3.8 mins

MS/MS analysis was conducted on the synthetically and enzymatically produced M2. This process further ionises the 340 M2 ion found which fragments to give distinctive molecules of M2. Identical fragmentation patterns were observed which verifies that both the enzymatically and synthetically produced M2 molecules were identical (Figures 145 and 146). Fragments included masses of 135.1, 282.1 and 296.0.

MS^3 experimentation were conducted on the MS/MS analyte, which further ionises the fragments producing characteristic splitting patterns of the MS/MS ions. The data of the enzymatically produced and synthetic M2 compounds both showed the presence of fragment *m/z* 308 (Figures 147 and 148).

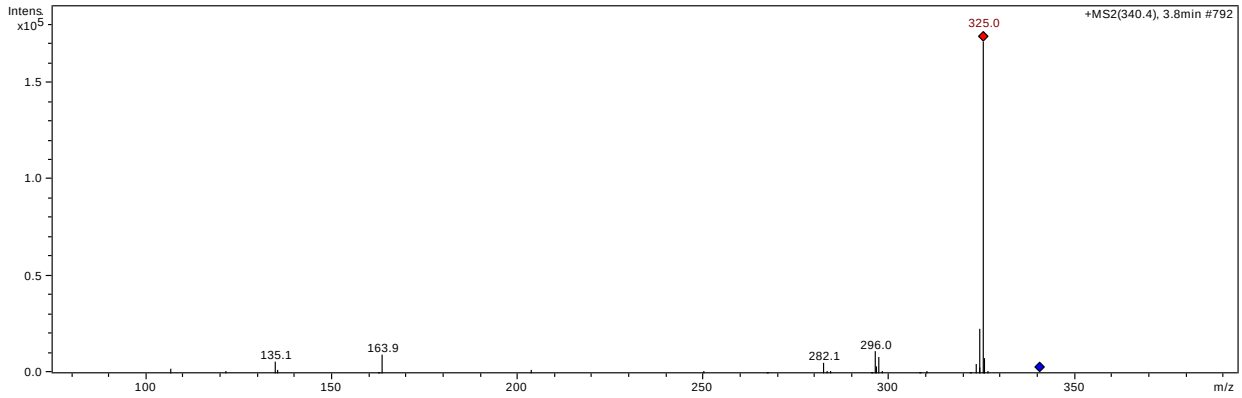

Figure 145. MS/MS of enzymatically produced M2

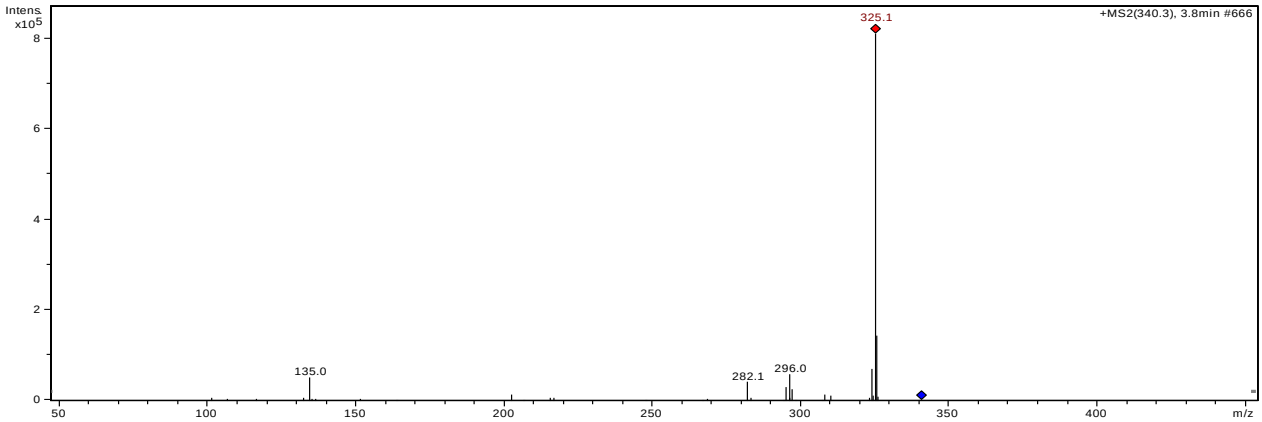

Figure 146. MS/MS of synthetic M2

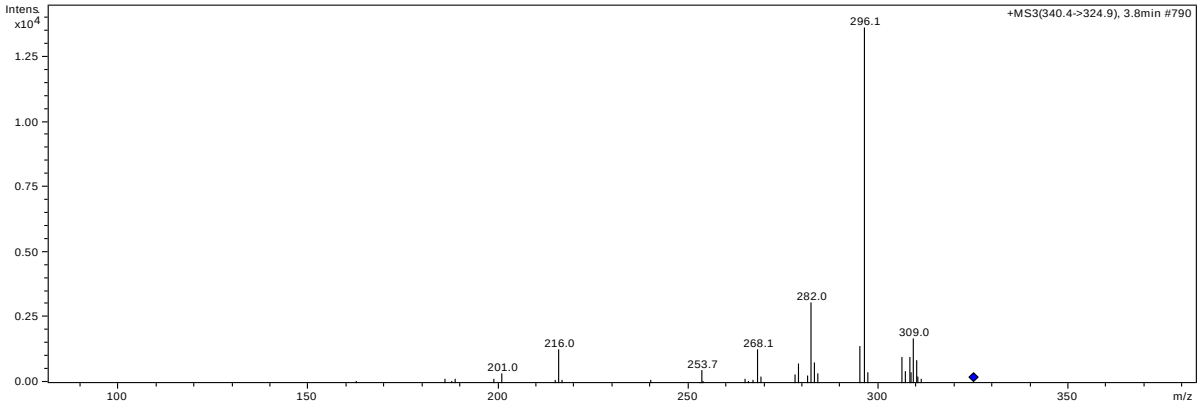

Figure 147. MS3 spectrum of the enzymatically produced M2

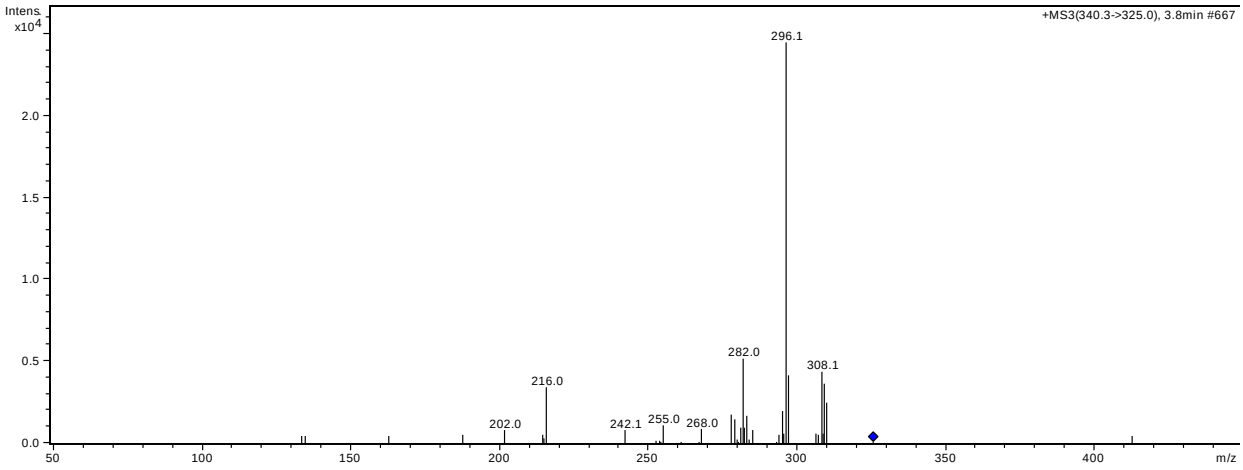

Figure 148. MS3 spectrum of the synthetic M2

The next step was to confirm the synthetic M2 metabolite was indeed identical to the enzymatically produced M2 by co-elution. The sample produced from incubating DMU 10212 with CYP1A1 was spiked with a sample of the synthetically produced M2. The LCMS analysis showed that the M2 peaks were identical, which can be seen from Figure 149. The red peaks show the CYP1A1 sample without the co-elution study. The grey peaks show the CYP1A1 enzyme sample co-eluted with the synthetically produced M2 metabolite, and it can be clearly seen that the M2 peak is amplified.

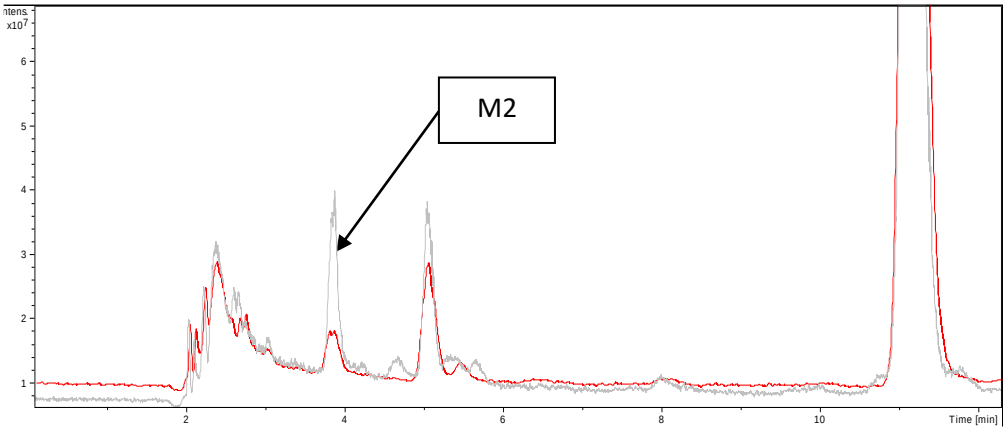

Figure 149. Spiking of the CYP1A1 enzymes sample with the synthetic M2 compound

The above result, alongside the data from the MS analysis, confirms that M2 is a genuine metabolite of DMU 10212 produced via CYP1A1, CYP1B1 and CYP1A2 metabolism.

7.2.3 Cytotoxicity of M2

The confirmation of M2 as a CYP1 metabolite of DMU 10212 prompted the cytotoxicity of this compound to be determined. This was conducted to corroborate that M2 is in fact toxic and contributes towards the cytotoxicity observed from DMU 10212 towards the tumour cell lines.

The results observed from screening M2 against the MDA 468 cell line gave an IC_{50} value of 0.6µM (Figure 150). The IC_{50} values recorded from the MCF7 and MCF7 cells induced with TCDD were 0.6µM and 1µM respectively.

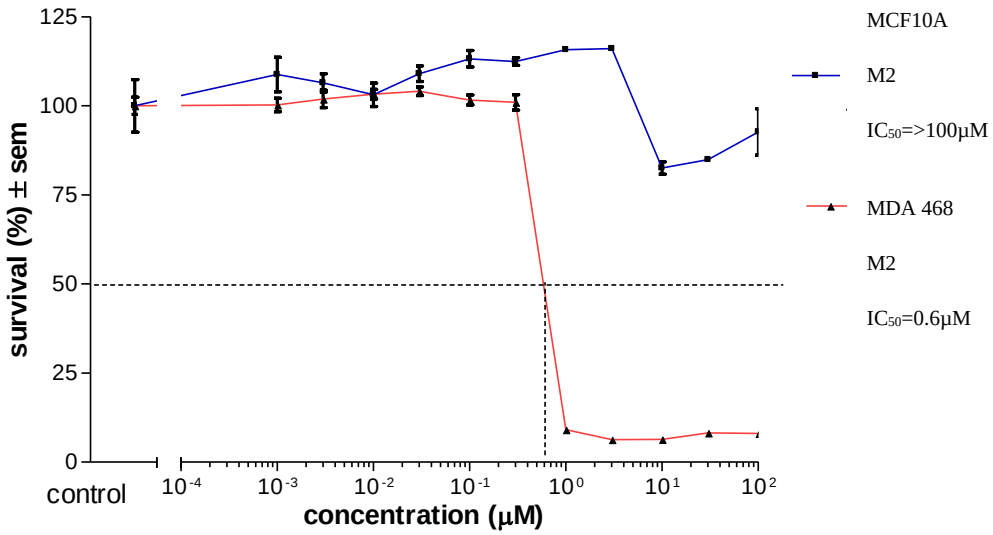

Figure 150. Toxicity plot of M2 against the MDA 468 and MCF10A cells

As can be seen from Figure 138, no toxicity was observed towards the non-tumour MCF10A cells. A primary toxic metabolite would be expected to show toxicity towards the MCF10A cells as well as the tumour cells, but M2 only shows toxicity against the tumour cells. This may be explicable due to the fact that the primary metabolite M2 is non-toxic, but then undergoes further CYP1 metabolism forming a secondary toxic metabolite which exhibits the cytotoxicity observed towards the MDA 468 and MCF7 cells. M1 or $M1^2$ (Scheme 11) may be possible structures for the secondary metabolites formed. However, M1 and $M1^2$ would require synthesis to verify which metabolite is formed by CYP1 DMU 10212 metabolism. This would be established through LCMS and co-elution studies as conducted for M2. Also,

the predicted metabolite M1 or $M1^2$ would require screening against the tumour and non-tumour cell lines to establish whether it possesses cytotoxic capabilities.

7.3 Summary and Conclusions

DMU 10212 was investigated to determine whether the CYP1 family of enzymes were actually involved in the metabolism and cytotoxic effect of this compound, and to establish that DMU 10212 exhibits its anti-cancer ability via a prodrug mechanism.

DMU 10212 was screened against the MDA 468, MCF7, MDA 231 and MCF10A cell lines with the included incubation of α-NF, a known CYP1 inhibitor. The results from the assays showed that α-NF completely eliminated the cytotoxic effect of DMU 10212. This strongly indicated that DMU 10212 is a substrate of the CYP1 family of enzymes.

Metabolism studies to determine and identify the metabolites of DMU 10212 produced by CYP1A1, CYP1B1 and CYP1A2 were conducted using LCMS techniques. Six metabolites were detected and it was shown that CYP1A1, CYP1A2 AND CYP1B1 produced the same six metabolites. The structures of the metabolites were proposed from the molecular masses and retention times observed. It was also observed that the affinity of DMU was preferential towards the CYP1A1 enzyme, followed by CYP1A2 and CYP1B1.

The proposed metabolites M2 and $M3^2$ were synthesised to verify their authenticity as DMU 10212 metabolites through LCMS experimentations. It was successfully concluded that M2 was a genuine metabolite of DMU 10212 produced through CYP1 metabolism, with a retention time of 3.8 mins. Co-elution of the synthetic M2 with the enzymatically produced M2 showed an identical match of the metabolite peak, confirming that they are equal. Screening of M2 against the MDA 468 and MCF7 tumour cells showed toxicities comparable to that observed from DMU 10212. However, as no toxicity was observed towards the non-tumour MCF10A cells. It has been suggested that M2 is metabolised further by CYP1 enzymes to produce a toxic secondary metabolite which exhibits the toxicity observed from screening M2 against the tumour cell lines. In order to confirm this theory, the suggested secondary toxic M1 and $M1^2$ metabolites would require investigation in the same techniques as that used to determine M2 as an authentic metabolite of DMU 10212.

Chapter 8

Conclusion and Future Direction

8.0 Conclusion and Future Direction

Several groups of chemotherapeutic agents are currently used to treat cancer. Examples include alkylating agents, platinum containing compounds and antimetabolites. However, undesirable side effects are a major problem associated with chemotherapy due to the inability of the drugs to differentiate between tumour cells and normal cells. This narrow therapeutic index leads to patients experiencing debilitating problems such as nausea, alopecia, heart failure and the formation of secondary tumours to name a few.

The cytochrome P450 is a superfamily of enzymes which are vital in the metabolism of endogenous and exogenous compounds. Importantly, the over-expression of CYP's, including CYP1A1 and CYP1B1 have been detected in tumour cells whilst undetected or present at very low levels in their corresponding normal tissue. The over-expressed CYP1 enzymes presented a legitimate target for anti-cancer prodrugs, which could be designed to undergo specific metabolism by over-expressed CYP1 enzymes to their cytotoxic entity whilst remaining non-toxic to normal cells.

Chalcones have been shown to function as anti-tumour prodrugs which are selectively activated by CYP1 enzymes over-expressed in breast tumour cell lines. DMU 135 synthesised by the CDDG was identified as a lead chalcone which gave an IC_{50} value of 0.09μM when screened against the MDA 468 cell line and IC_{50} values of 0.2μM and 0.03μM against the MCF7 and MCF7 cells induced with TCDD.

However, a problematic factor of the chalcones is their susceptibility to undergo photoisomerisation reactions, converting the more potent *trans* isomer to the less effective *cis* isomer. To overcome this problem, heterocyclic ring systems were incorporated across the α,β-unsaturated moiety of the chalcones locking the *trans* isomer in a rigid structure, preventing photoisomerisation occurring.

The synthesised compounds were screened *in vitro* using the standard MTT assay against a panel of breast tumour cell lines characterised for their CYP1 expression. The panel consisted of the MDA 468 cell line which constitutively expresses CYP1A1 and CYP1B1, the MCF7 cell line which expresses low levels of CYP1 enzymes, the MCF7 cells treated with TCDD which induces increased CYP1A1 expression, the MDA 231 breast tumour cell line which expresses low levels of CYP1 enzymes and TCDD treated MDA 231 cells which induces

increased CYP1 expression. The non-tumour MCF10A cell line which has no basal CYP1 expression was included as the control cell line.

A library of eighteen 3,5-diarylpyrazoles were synthesised starting from chalcones in good yields. Epoxychalcone intermediates were treated with hydrazine to form the pyrazole heterocycles. DMU 10107 (Figure 151), substituted with a 3,4-methylenedioxy A-ring and a 2,3,4-trimethoxy substitution on the B-ring showed the greatest toxicity towards the MDA 468 cell line with an IC_{50} value of 8µM, whilst proving non-toxic to the non-tumour MCF10A cells.

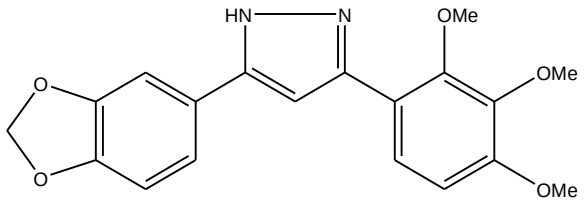

Figure 151. DMU 10107

DMU 10104 (Figure 152), with a 3,4-methylenedioxy substitution on the A-ring and a 3,4,5-trimethoxy substitution on the B-ring gave IC_{50} values of 8µM and 5µM towards the MCF7 and MCF7 cells induced with TCDD. This was the most potent result observed towards the MCF7 cell line from the pyrazoles synthesised.

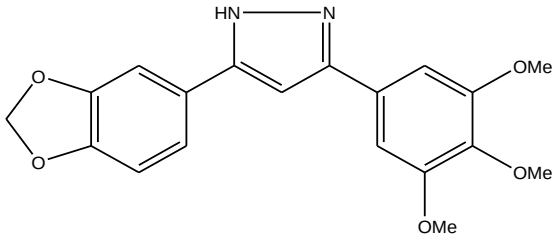

Figure 152. DMU 10104

The toxicities observed from the pyrazoles were not as potent as those recorded from their corresponding chalcone derivatives. Therefore, six membered heterocycles were investigated by incorporating a pyrimidine ring across the α,β-unsaturated moiety of the chalcones. A library of fifteen 2-amino-4,6-diarylpyrimidines were synthesised from the reaction of chalcones with guanidine hydrochloride. The cytotoxicity data from screening the aminopyrimidines showed significant cytotoxicities across the tumour cell lines. DMU 10212 (Figure 142, 1), with a 3,4-methylendioxy substitution on the A-ring and 2,4-dimethoxy substitution on the B-ring showed an IC_{50} value of 0.01µM against the MDA 468 cells

(Figure 153). IC_{50} values of 0.07µM and 0.3µM were recorded against the MCF7 and MCF7 cells induced with TCDD.

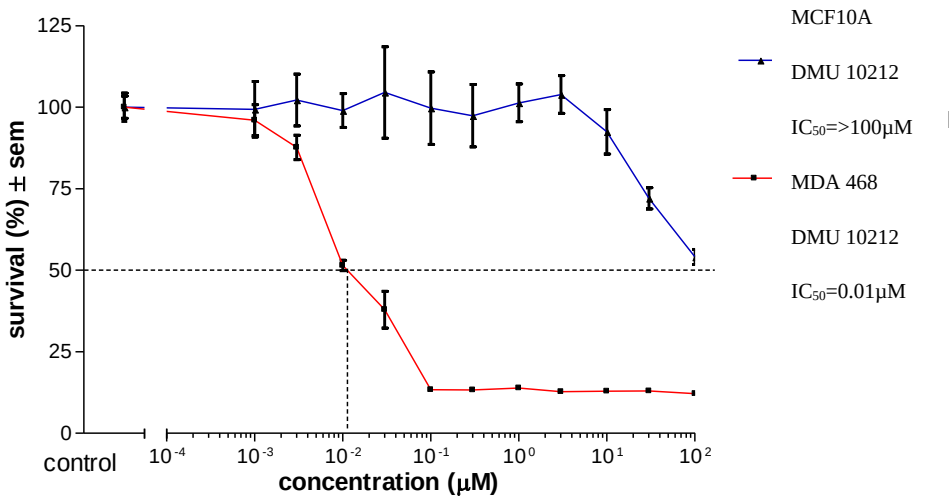

Figure 153. Cytotoxicity plot of MDA 468 and MCF10A treated with DMU 10212

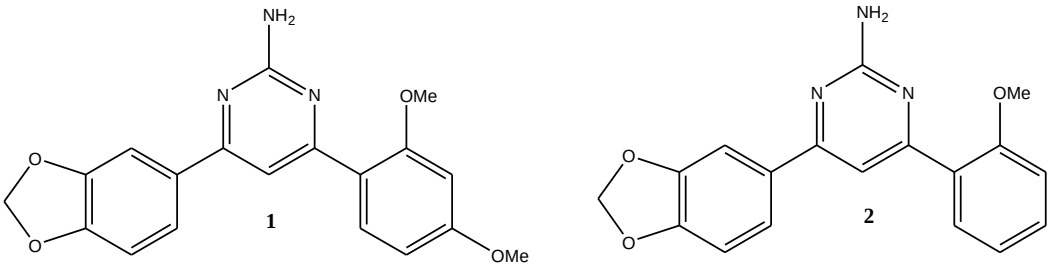

Figure 154. Structures of DMU 10212 (1) and DMU 10213 (2)

DMU 10213 (Figure 154, 2), with a 3,4-methylenedioxy substitution on the A-ring and 2-methoxy substitution on the B-ring gave an IC_{50} value of 0.2µM towards the MDA 468 cell line and IC_{50} values of 0.06µM and 0.05µM against the MCF7 and MCF7 cells induced with TCDD. Equal IC_{50} values of 1µM were also observed towards the MDA 231 and MDA 231 cells induced with TCDD. With a 4-methoxy substitution on the A-ring and 2,4-dimethoxy substitution on the B-ring, DMU 10208 (Figure 155, 1) gave an IC_{50} value of 0.2µM against the MDA 468 cells and IC_{50} values of 0.2µM and 0.05µM towards the MCF7 and MCF7 cells induced with TCDD.

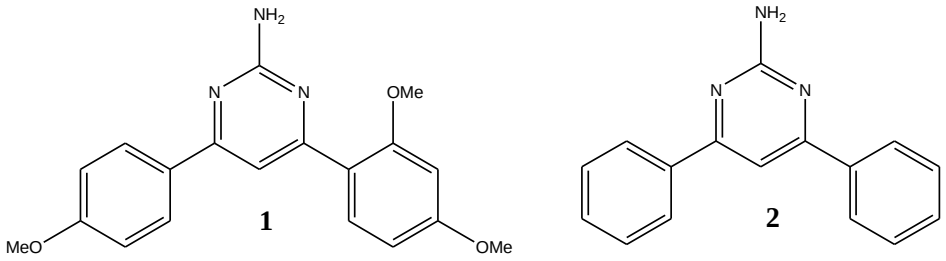

Figure 155. Structures of DMU 10208 (1) and DMU 10200 (2)

DMU 10200 (Figure 155, 2), with no substitutions on either the A or B-rings gave an IC_{50} value of 0.2µM towards the MDA 468 cell line and IC_{50} values of 7µM and 3µM against the MCF7 and MCF7 cells induced with TCDD. It was concluded that the incorporation of the pyrimidine ring into the chalcones showed greater toxicities towards the tumour cell lines in contrast to the chalcones. It was also observed that increasing the heterocycle from a 5-membered pyrazole to a 6-membered amino-pyrimidine ring significantly improved the tumour toxicities of the compounds.

The 2-amino-4,6-diarylpyrimidines were converted to 4,6-diarylpyrimidones via a one step diazotisation reaction. The rationale for the conversion was to investigate the importance of the amino group in the 2-position of the pyrimidine ring for the cytotoxicity observed from the aminopyrimidines. Also, the carbonyl functional group was evaluated for its tumour toxicity when incorporated in the 2-position of the pyrimidine ring. A library of fifteen 4,6-diarylpyrimidones were synthesised in yields of up to 85%. In general, significant cytotoxicity from the pyrimidones was recorded when screened against the tumour cell lines. DMU 10313 (Figure 156, 1), with a 3,4-methylenedioxy substitution on the A-ring and 2-methoxy substitution on the B-ring gave an IC_{50} value of 0.07µM towards the MDA 468 cells. IC_{50} values of 1.8µM and 0.5µM were recorded against the MCF7 and MCF7 cells induced with TCDD. DMU 10312 (Figure 156, 2) was synthesised with a 3,4-methylenedioxy substitution on the A-ring and 2,4-dimethoxy substitution on the B-ring. This compound showed an IC_{50} value of 1.5µM towards the MDA 468 cells. Tumour toxicities were also observed towards the MDA 468 cell line from DMU 10311 (Figure 156, 3) and 10300 (Figure 156, 4), with IC_{50} values of 1.7µM and 2µM being recorded respectively.

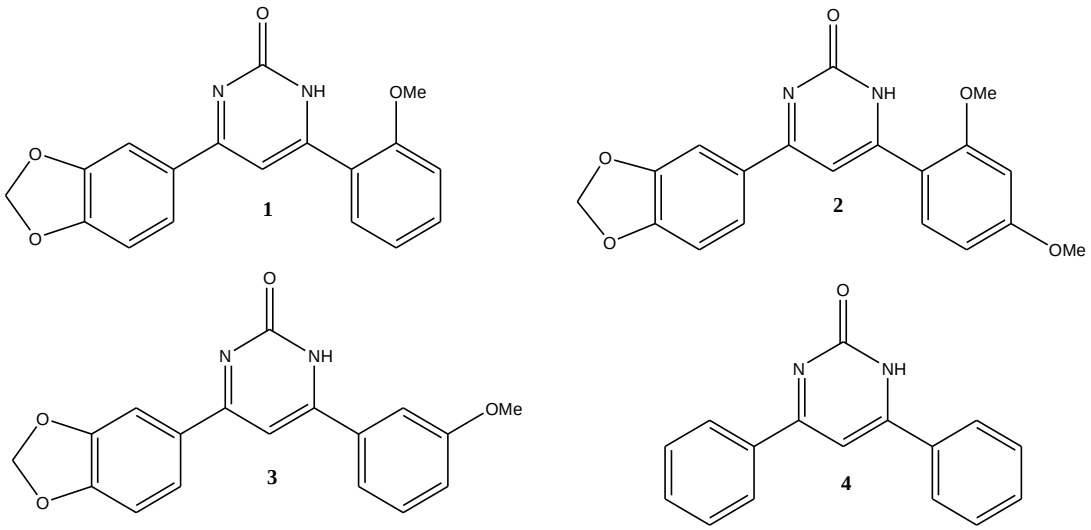

Figure 156. Structures of DMU 10313 (1), DMU 10312 (2), DMU 10311 (3) and DMU 10300 (4)

From the promising cytotoxicity results observed from the 2-aminopyrimidines and pyrimidones, the 2-position of the pyrimidine ring was explored by synthesising 2-morpholinopyrimidines. Chalcones were reacted with morpholinoformamidine hydrobromide producing the 2-morpholinopyrimidines, from which DMU 10403 and DMU 10405 (Figure 157) showed to be the most potent anti-cancer compounds. DMU 10403 showed an IC_{50} value of 7µM towards the MCF7 cells induced with TCDD and 10µM towards the non-induced MCF7 cells. DMU 10405 showed an IC_{50} value of 10µM towards the MDA 468 cell line.

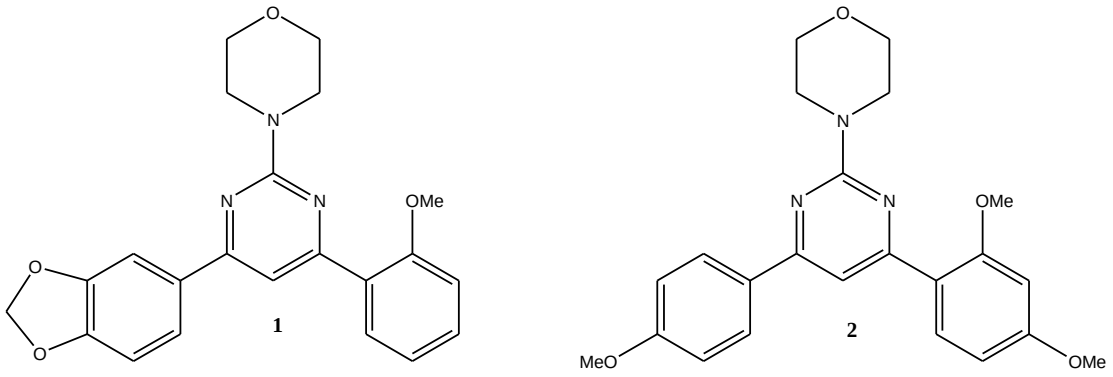

Figure 157. Structures of DMU 10403 (1) and DMU 10405 (2)

However, the morpholine group did show greater tumour activity in contrast to the 2-aminopyrimidines and pyrimidones. This may be attributed to the bulkiness of the

morpholine group preventing the compound from fitting correctly into the active site of CYP1 enzymes.

The investigation of the 2-position was continued with the synthesis of 2-dimethylaminoethylamino-4,6-diarylpyrimidines. *N*,*N*-dimethylaminoethylguanidine hydrochloride was synthesised by reacting S-methylisothiourea with *N*,*N*-dimethylethylenediamine. The guanidinium salt was reacted with the chalcone derivatives of the 2-aminopyrimidines DMU 10200, DMU 10212 and DMU 10213, as these compounds showed the most effective anti-tumour activity from the compounds synthesised. DMU 10600, DMU 10601 and DMU 10602 were synthesised, from which DMU 10600 (Figure 158) based on DMU 10212 showed the most cytotoxicity. Included was an IC_{50} value of 7µM against the MDA 468 cell line.

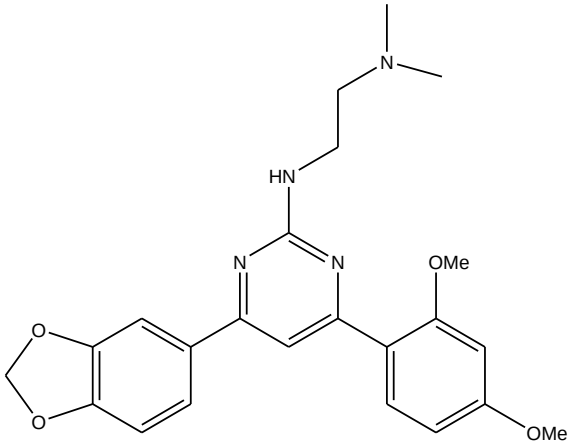

Figure 158. DMU 10600

Two final pyrimidines, DMU 10700 (Figure 159) and DMU 10800 (Figure 148) were synthesised based on the A and B-ring substitutions of the 2-aminopyrimidine DMU 10212. The 2-position of the pyrimidine ring of DMU 10700 was substituted with a methyl group, and this compound showed effective toxicity towards the MDA 468 cell line with an IC_{50} value of 2.5µM.

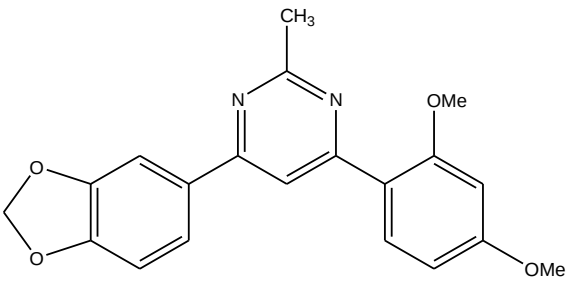

Figure 159. DMU 10700

DMU 10800 (Figure 160) was synthesised with a proton at the 2-position of the pyrimidine ring. Significant tumour toxicities were recorded for this compound, with an IC_{50} value of 0.08µM seen against the MDA 468 cells, and identical IC_{50} values of 0.2µM were observed towards the MCF7 and MCF7 cells induced with TCDD.

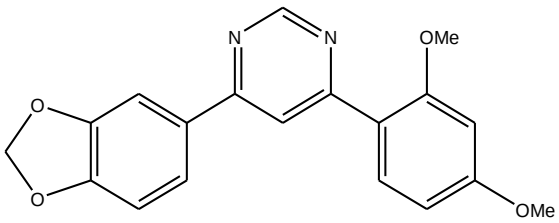

Figure 160. DMU 10800

Significant cytotoxicity data was observed from screening pyrimidine compounds synthesised in this project. The amino-pyrimidine DMU 10212 was selected as the lead compound due to its overall cytotoxicity towards the tumour cell lines. DMU 10212 was investigated further to prove it was a CYP1 enzyme substrate by conducting inhibition studies. DMU 10212 was screened using the MTT assay against the MDA 468, MCF7 and MDA 231 cells with the inclusion of the known CYP1 inhibitor, α-naphthoflavone (α-NF). The results obtained showed the complete elimination of the toxicity of DMU 10212 in contrast to screening DMU 10212 without α-NF (Figure 162), supporting the fact that DMU 10212 is a genuine CYP1 enzyme substrate. This can be seen from Figure 161 which illustrates DMU 10212 screened against the MDA 468 cell line with the inclusion of α-NF, showing no cell death, whereas Figure 150 shows DMU 10212 without the addition of α-NF.

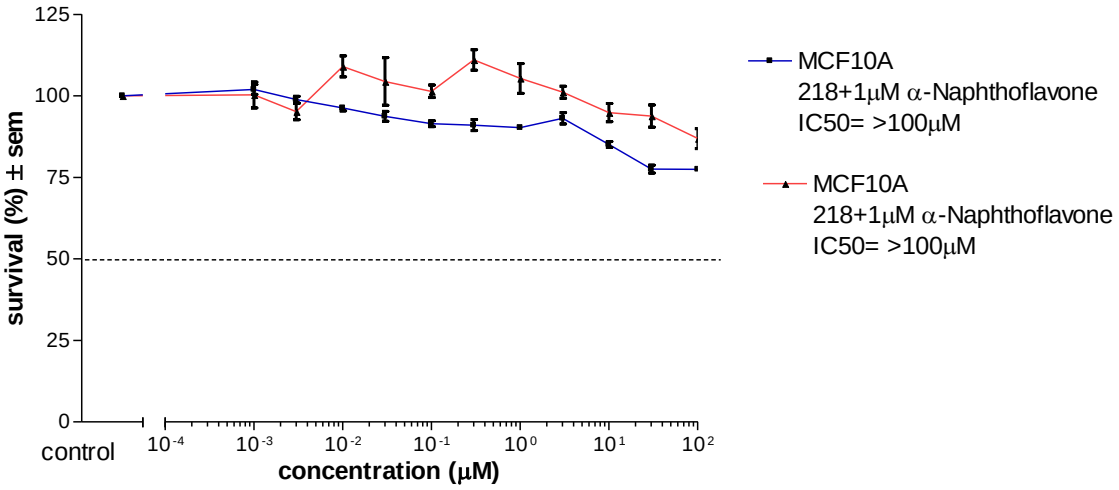

Figure 161. Inhibition study of DMU 10212 including α-NF

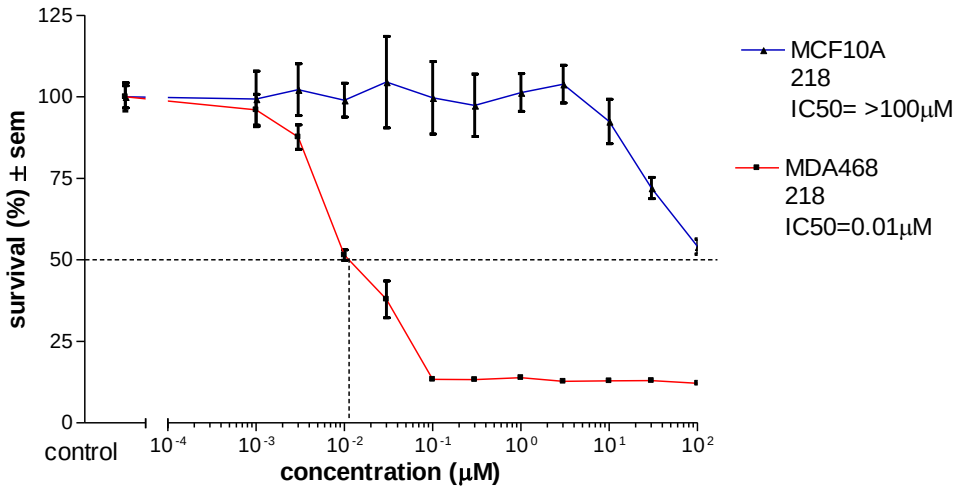

Figure 162. DMU 10212 screened against the MDA 468 cell line

The inhibition studies prompted the investigation of identifying and determining the metabolites formed once DMU 10212 underwent metabolism by the CYP1 enzymes. DMU 10212 was incubated with isolated CYP1 isoforms including CYP1A1, CYP1B1 and CYP1A2. Four metabolites were formed by each isoforms, which were identified by their unique retention times (RT) and molecular masses (MW) observed via LCMS analysis. It was also concluded that the metabolism of DMU 10212 by the CYP1 enzymes occurred at different rates, with CYP1A1>CYP1A2>CYP1B1. The functions of CYP1 enzymes, including oxidative and dealkylation reactions are known, therefore the structures of the metabolites were proposed from the LCMS data gained (Scheme 17).

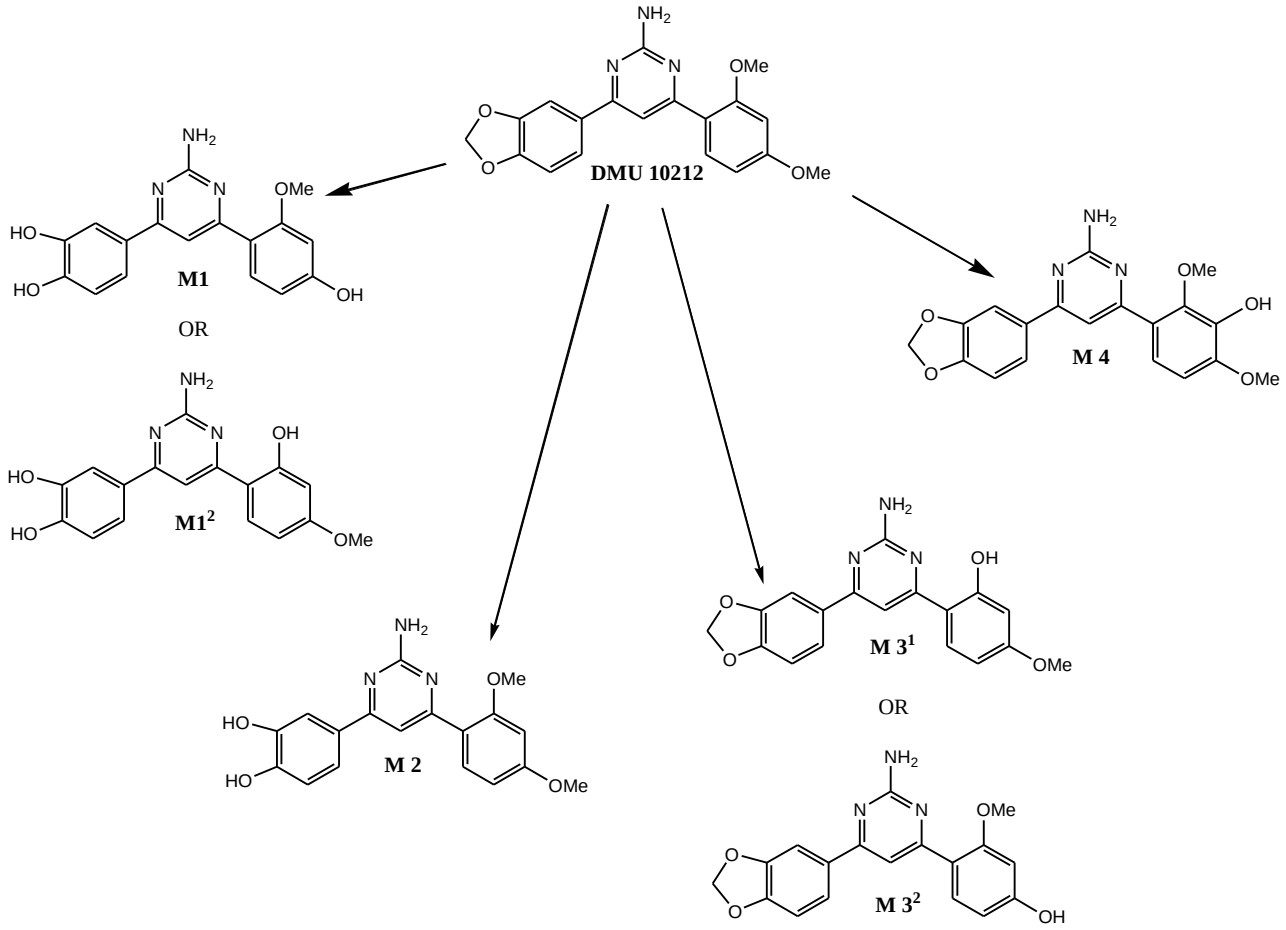

Scheme 17. Predicted CYP1 metabolites of DMU 10212

From the metabolites predicted in Scheme 17, M2 was selected for synthesis to determine that the proposed structure was a genuine metabolite produced from the metabolism of DMU 10212 by CYP1 enzymes.

Therefore, M2 was synthesised by treating DMU 10212 with boron trichloride. M2 was analysed via LCMS which showed that the synthetically produced M2 showed an identical RT and MW to the enzymatically produced M2 metabolite. The next stage involved co-eluting the synthesised M2 compound with a sample of DMU 10212 metabolised by CYP1A1. As expected, the compounds were identical as the M2 peak of the CYP1A1 sample co-eluted with the synthesised M2 was amplified shown by the grey plot of the total ion chromatogram (TIC) in Figure 163. This study confirmed that the predicted M2 metabolite structure was correct and that M2 was a genuine metabolite of DMU 10212 CYP1 metabolism.

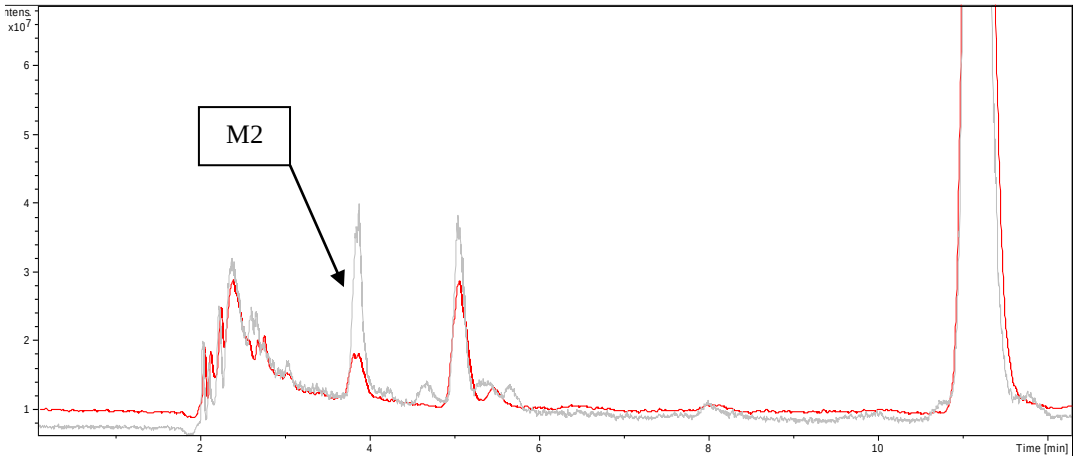

Figure 163. TIC of the CYP1A1 produced metabolites of DMU 10212 (red plot) and the co-elution of the synthesised M2 with the CYP1A1 metabolite sample (grey plot)

M2 was screened using the MTT assay to determine its cytotoxicity. An IC_{50} value of 0.6µM was observed towards the MDA 468 cells whilst no toxicity was observed towards the non-tumour MCF10A cells (Figure 164). IC_{50} values of 0.6µM and 1µM were observed towards the MCF7 and MCF7 cells induced with TCDD. As no toxicity was observed towards the MCF10A cells, it can be suggested that M2 undergoes further metabolism to exhibit its toxic effect seen towards the tumour cell lines.

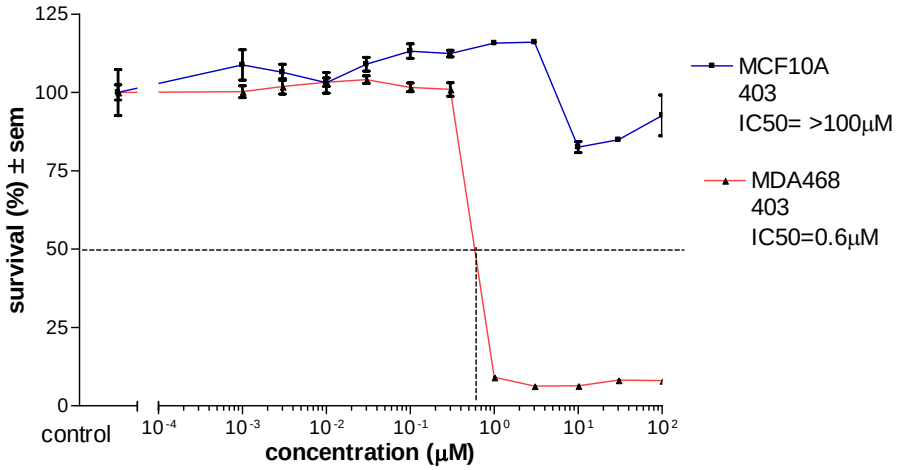

Figure 164. Cytotoxicity plot of M2 screened against MDA 468 and MCF10A cells

Therefore, through the inhibition and LCMS studies conducted, DMU 10212 was confirmed as a CYP1 activated anti-cancer prodrug. The 2-position of the pyrimidine ring proved pivotal in the cytotoxicity observed from the synthesised pyrimidine analogues. The primary

amine derivatives showed the greatest toxicities than that observed from the other pyrimidine compounds.

The future direction of work would require the synthesis of the remaining predicted metabolites in Scheme 15, which would also be evaluated through LCMS to conclude if they are CYP1 metabolites of DMU 10212. Once the metabolites were identified, they would require screening to assess their cytotoxicities. Another parameter to investigate would be the mechanism in which DMU 10212 and its metabolites exert their cytotoxic effect towards the tumour cells.

This thesis has demonstrated that the over-expressed CYP1 enzymes in tumour cells are legitimate targets for chemotherapeutic prodrugs that selectively kill tumour cells.

Chapter 9

Experimental

9.1 Materials and Apparatus

Chemicals were used as received from Sigma-Aldrich Chemical Company (Dorset, UK), Alfa Aesar (Lancashire, UK) or Fisher Scientific (Loughborough, UK).

The ^{1}H and ^{13}C-NMR spectra were recorded on a 400MHz super-conducting Bruker Spectrometer at 30°C. TMS was used as an internal standard.

Infra-red spectra were recorded on a Perkin-Elmer 298 Spectrophotometer as potassium bromide disks for solid samples and liquids as thin films using NaCl plates.

Mass spectra were recorded on a Micromass Quattro II Low Resolution Triple Quadruple Mass Spectrometer (EPSRC National Mass Spectrometry Service Centre, Swansea UK).

Melting points (uncorrected) were determined on a Gallenkamp melting point apparatus.

Thin layer chromatography was performed on Merck Aluminium Sheet- Silica Gel $60f_{254}$ coated plates. The TLC plates were visualised under Multiband UVGL-58 UV-254/366nm UV light and stained with either 2,4-dinitrophenylhydrazine, iodine absorbed on sand or phosphomolybdic acid. Flash Column Chromatography was conducted using silica gel (Fluka Silica 60; standard 30-45µ fine grade 20-45µ).

9.2 General Procedure for the Synthesis of Chalcones

To a stirring mixture of the acetophenone (33mmol) and benzaldehyde (33mmol) in methanol (80 ml), aqueous sodium hydroxide solution (50 % w/v, 26 cm^3, 0.33 mol) was added. The reaction was monitored by TLC and upon reaching completion was quenched with water (80 ml) and the crude product extracted with dichloromethane (3 x 60 ml). The combined organic extracts were dried ($MgSO_4$) and the solvent removed *in vacuo*. The crude product was recrystallised from methanol producing yellow crystals.

(E)-1-(3,4-dimethoxyphenyl)-3-(3,4-dimethoxyphenyl)-2-propen-1-one, DMU 2210

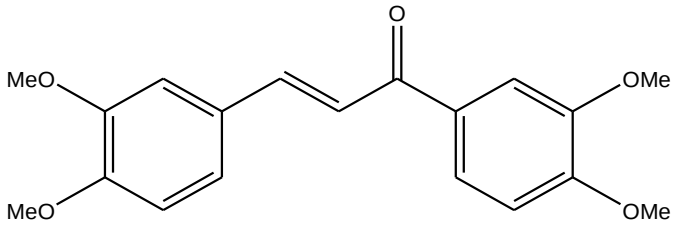

Yellow crystals (8.00g, 74%), mp 111-113ºC; δ_H ($CDCl_3$) 3.90 (12H, s, 4 x OCH_3), 6.8-6.9 (2H, m, Ar-H), 7.1 (1H, s, Ar-H), 7.18 (1H, d, Ar-H), 7.35 (1H, d, J=15.0Hz, C=C-H), 7.57 (1H, s, Ar-H), 7.63 (1H, d, Ar-H), 7.71 (1H, d, J=15.0Hz, C=C-H); δ_C ($CDCl_3$) 56.0, 56.1, 76.7, 77.0, 77.2, 77.3, 110.0, 110.4, 111.0, 111.2, 120.0, 123.0, 128.1, 131.6, 144.1, 149.3, 151.3, 153.2, 188.7; m/z [MALDI]$^+$ 329 ([M+H]$^+$, 100%); υ_{max} (KBr) /cm^{-1} 1650 (C=O).

(E)-1-(4-methoxyphenyl)-3-(3,4,5-trimethoxyphenyl)-2-propen-1-one, DMU 1113

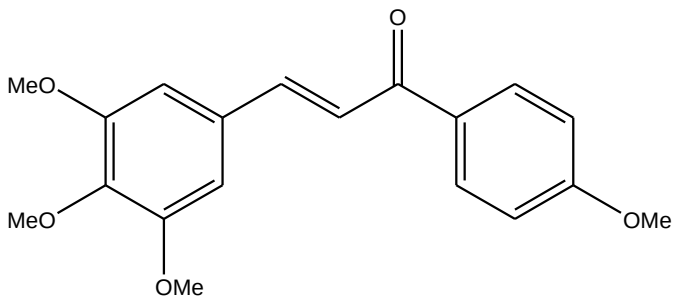

Yellow crystals (8.20g, 75%), mp 133-135ºC; δ_H ($CDCl_3$) 3.90 (3H, s, OCH_3), 3.95 (3H, s, OCH_3), 3.98 (6H, s, 2 x OCH_3), 6.88 (2H, s, Ar-H), 7.04 (2H, d, Ar-H), 7.45 (1H, d, J=15.0Hz, C=C-H), 7.74 (1H, d, J=15.0Hz, C=C-H), 8.05 (2H, d, Ar-H); δ_C ($CDCl_3$) 55.5, 56.2, 61.0, 105.5, 113.8, 121.1, 130.6, 130.8, 131.1, 140.2, 144.1, 153.5, 163.4, 188.7; m/z $[FAB]^+$ 313 ($[M+H]^+$, 100%); υ_{max} (KBr) /cm^{-1} 1654 (C=O).

(E)-1-(4-methoxyphenyl)-3-(4-methoxyphenyl)-2-propen-1-one, DMU 2300

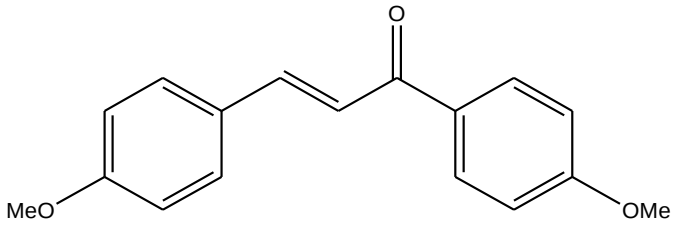

Yellow crystals (5.94g, 68%), mp 107-109ºC; δ_H ($CDCl_3$) 3.85 (3H, s, OCH_3), 3.95 (3H, s, OCH_3), 6.92-7.03 (4H, m, Ar-H), 7.44 (1H, d, J=15.0Hz, C=C-H), 7.61 (2H, Ar-H), 7.80 (1H, d, J=15.0Hz, C=C-H), 8.05 (2H, d, Ar-H); δ_C ($CDCl_3$) 55.4, 55.5, 113.8, 114.4, 119.5, 127.8, 130.1, 130.7, 131.3, 143.8, 161.5, 163.3, 188.8; m/z $[MALDI]^+$ 269 ($[M+H]^+$, 100%); υ_{max} (KBr) /cm^{-1} 1674 (C=O).

(E)-1-(3,4,5-trimethoxyphenyl)-3-(3,4-methylenedioxyphenyl)-2-propen-1-one, DMU 135

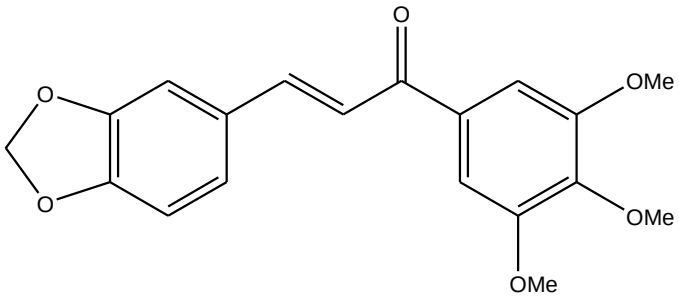

Yellow crystals (7.34g, 65%), mp 133-135ºC; δ_H ($CDCl_3$) 3.95 (9H, s, 3 x OCH_3), 6.04 (2H, s, OCH_2O), 6.86 (1H, d, Ar-H), 7.13 (1H, d, Ar-H), 7.20 (1H, s, Ar-H), 7.28 (2H, s, Ar-H), 7.34 (1H, d, J=15.0Hz, C=C-H), 7.76 (1H, d, J=15.0Hz, C=C-H); δ_C ($CDCl_3$) 56.4, 61.0,

101.7, 105.9, 106.6, 108.7, 119.7, 125.3, 129.3, 133.7, 142.3, 144.6, 148.4, 149.9, 153.1, 189.0; m/z $[FAB]^+$ 343 ($[M+H]^+$, 100%); υ_{max} (KBr) /cm^{-1} 1656 (C=O).

(E)-1-(3,4-methylenedioxyphenyl)-3-(3,4-methylenedioxyphenyl)-2-propen-1-one, DMU 2301

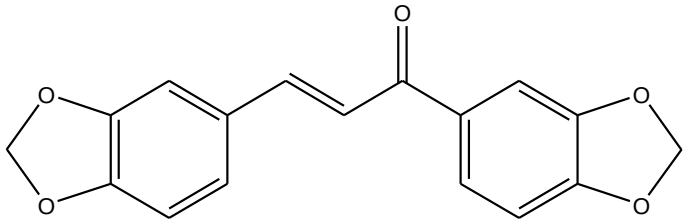

Yellow crystals (7.13g, 69%), mp 132-134ºC; δ_H ($CDCl_3$) 6.05 (2H, s, CH_2O_2), 6.10 (2H, s, OCH_2O), 6.87 (1H, d, Ar-H), 6.91 (1H, d, Ar-H), 7.14 (1H, d, Ar-H), 7.18 (1H, s, Ar-H), 7.35 (1H, d, J=15.0Hz, C=C-H), 7.54 (1H, s, Ar-H), 7.65 (1H, d, Ar-H), 7.75 (1H, d, J=15.0Hz, C=C-H); m/z $[MALDI]^+$ 297 ($[M+H]^+$, 100%); υ_{max} (KBr) /cm^{-1} 1647 (C=O).

(E)-1-(3,4-dimethoxyphenyl)-3-(3,4-methylenedioxyphenyl)-2-propen-1-one, DMU 160

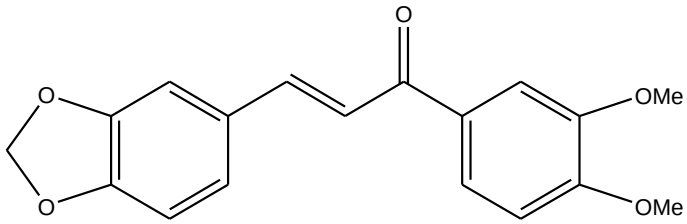

Yellow crystals (6.73g, 68%), mp 137-139ºC; δ_H ($CDCl_3$) 4.00 (6H, s, 2 x OCH_3), 6.05 (2H, s, OCH_2O), 6.86 (1H, d, Ar-H), 6.94 (1H, d, Ar-H), 7.15 (1H, d, Ar-H), 7.19 (1H, s, Ar-H), 7.41 (1H, d, J=15.0Hz, C=C-H), 7.62 (1H, s, Ar-H), 7.67 (1H, dd, Ar-H), 7.76 (1H, d, J=15.0Hz, C=C-H); δ_C ($CDCl_3$) 56.0, 56.1, 101.6, 106.6, 108.6, 110.0, 110.7, 119.6, 122.9, 125.1, 129.5, 131.4, 143.8, 148.3, 149.2, 149.7, 153.1, 188.3; m/z $[MALDI]^+$ 313 ($[M+H]^+$, 100%); υ_{max} (KBr) /cm^{-1} 1651 (C=O).

(E)-1-(2,3,4-trimethoxyphenyl)-3-(3,4-methylenedioxyphenyl)-2-propen-1-one, DMU 419

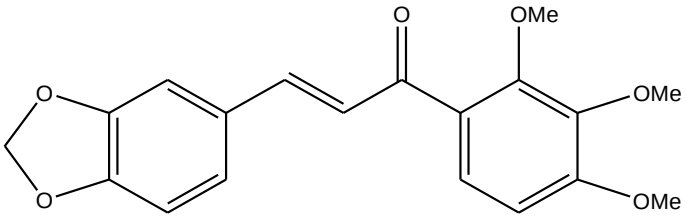

Yellow crystals (6.11g, 65%), mp 101-103°C; δ_H ($CDCl_3$) 3.90-3.98 (9H, m, 3 x OCH_3), 6.02 (2H, s, OCH_2O), 6.76 (1H, d, Ar-H), 6.83 (1H, d, Ar-H), 7.1 (1H, d, Ar-H), 7.16 (1H, s, Ar-H), 7.35 (1H, d, J=15.8Hz, C=C-H), 7.48 (1H, d, Ar-H), 7.62 (1H, d, J=15.8Hz, C=C-H); δ_C ($CDCl_3$) 56.1, 61.1, 62.1, 101.6, 106.7, 107.3, 108.6, 124.7, 125.0, 125.8, 126.9, 129.6, 142.1, 143.0, 148.4, 149.7, 153.7, 156.9, 190.8; m/z $[MALDI]^+$ 343 ($[M+H]^+$, 100%); υ_{max} (KBr) /cm^{-1} 1657 (C=O).

(E)-1-(2,4-dimethoxyphenyl)-3-(3,4-methylenedioxyphenyl)-2-propen-1-one, DMU 407

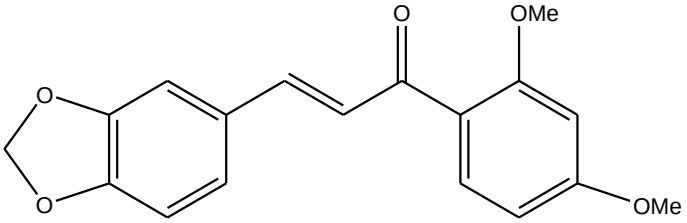

Yellow crystals (7.66g, 88%), mp 121-123°C; δ_H ($CDCl_3$) 3.86 (3H, s, 3 x OCH_3), 3.90 (3H, s, 3 x OCH_3), 6.00 (2H, s, OCH_2O), 6.49 (1H, s, Ar-H), 6.55 (1H, dd, Ar-H), 6.81 (1H, d, Ar-H), 7.07 (1H, dd, Ar-H), 7.11 (1H, s, Ar-H), 7.35 (1H, d, J=16.0Hz, C=C-H), 7.59 (1H, d, J=16.0Hz, C=C-H), 7.73 (1H, d, Ar-H); δ_C ($CDCl_3$) 55.6, 55.6, 98.7, 105.2, 106.6, 108.6, 121.2, 122.4, 124.9, 125.4, 129.9, 132.8, 142.0, 148.3, 149.4, 160.3, 164.1, 190.4; m/z $[MALDI]^+$ 313 ($[M+H]^+$, 100%); υ_{max} (KBr) /cm^{-1} 1747 (C=O).

(E)-1-(2,5-dimethoxyphenyl)-3-(3,4-methylenedioxyphenyl)-2-propen-1-one, DMU 423

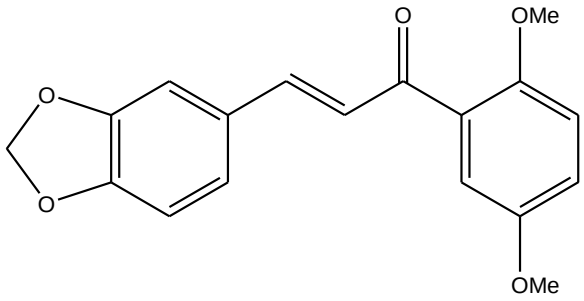

Yellow crystals (8.53g, 83%), mp 111-113ºC; δ_H ($CDCl_3$) 3.83 (3H, s, 3 x OCH_3), 3.88 (3H, s, 3 x OCH_3), 6.03 (2H, s, OCH_2O), 6.85 (1H, d, Ar-H), 6.97 (1H, d, Ar-H), 7.03 (1H, d, Ar-H), 7.08 (1H, d, Ar-H), 7.14 (1H, s, Ar-H), 7.19 (1H, s, Ar-H), 7.30 (1H, d, J=16.0Hz, C=C-H), 7.61 (1H, d, J=16.0Hz, C=C-H); δ_C ($CDCl_3$) 55.8, 56.5, 101.6, 106.6, 108.6, 113.8, 114.4, 119.0, 125.1, 128.1, 128.7, 129.6, 129.8, 143.3, 148.7, 152.5, 153.6, 192.4; m/z $[MALDI]^+$ 313 ($[M+H]^+$, 100%); υ_{max} (KBr) /cm^{-1} 1717 (C=O).

(E)-1-(2,5-dimethoxyphenyl)-3-(2,5-dimethoxyphenyl)-2-propen-1-one, DMU 2302

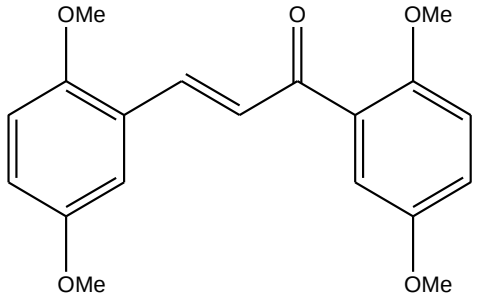

Yellow oil (8.99g, 92%), δ_H ($CDCl_3$) 3.77 (6H, s, 2 x OCH_3), 3.82 (3H, s, OCH_3), 3.84 (3H, s, OCH_3), 6.85 (1H, d, Ar-H), 6.85-6.94 (2H, m, Ar-H), 7.01 (1H, d, Ar-H), 7.14 (1H, d, Ar-H), 7.19 (1H, d, Ar-H), 7.46 (1H, d, J=17.6Hz, C=C-H), 7.99 (1H, d, J=17.6Hz, C=C-H); δ_C ($CDCl_3$) 55.7, 55.8, 56.0, 57.2, 112.4, 113.4, 114.5, 117.0, 118.9, 119.8, 124.7, 127.6, 129.9, 138.6, 152.5, 153.2, 153.5, 153.6, 199.8; m/z $[MALDI]^+$ 269 ($[M+H]^+$, 100%);υ_{max} (KBr) /cm^{-1} 1723 (C=O).

(E)-1-(4-methoxyphenyl)-3-(2,5-dimethoxyphenyl)-2-propen-1-one, DMU 2303

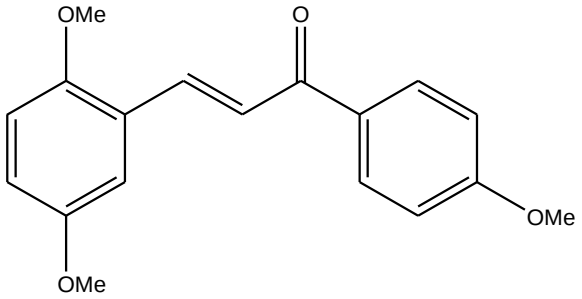

Yellow oil (8.01g, 94%), δ_H ($CDCl_3$) 3.80 (3H, s, OCH_3), 3.87 (3H, s, OCH_3), 3.88 (3H, s, OCH_3), 6.87 (1H, d, Ar-H), 6.90-6.94 (1H, m, Ar-H), 6.78 (2H, d, Ar-H), 7.16 (1H, d, Ar-H), 7.58 (1H, d, J=15.0Hz, C=C-H), 8.00-8.08 (3H, m, C=C-H, Ar-H); δ_C ($CDCl_3$) 55.5, 55.8, 56.1, 112.4, 113.8, 116.9, 123.0, 124.7, 130.8, 131.3, 139.3, 153.3, 153.5, 163.3, 189.3; m/z [MALDI]$^+$ 299 ([M+H]$^+$, 100%); υ_{max} (KBr) /cm^{-1} 1735 (C=O).

(E)-1-(4-methoxyphenyl)-3-(3,5-dimethoxyphenyl)-2-propen-1-one, DMU 2304

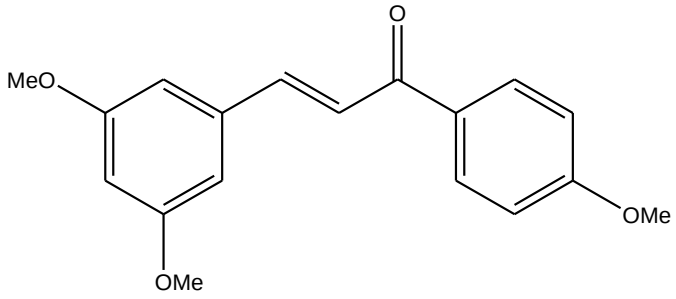

Yellow crystals (7.19g, 94%), mp 79-81^{o}C, δ_H ($CDCl_3$) 3.85 (6H, s, OCH_3), 3.89 (3H, s, OCH_3), 6.52 (1H, s, Ar-H), 6.78 (2H, s, Ar-H), 6.98 (2H, s, Ar-H), 7.48 (1H, d, J=15.6Hz, C=C-H), 7.70 (1H, d, J=15.6Hz, C=C-H), 8.03 (2H, d, Ar-H); δ_C ($CDCl_3$) 50.8, 55.5, 102.5, 106.3, 113.7, 122.4, 130.9, 137.0, 144.0, 160.4, 161.0, 163.5, 188.8; m/z [MALDI]$^+$ 299 ([M+H]$^+$, 100%); υ_{max} (KBr) /cm^{-1} 1740 (C=O).

(E)-1-(2-methoxyphenyl)-3-(3,4-methylenedioxyphenyl)-2-propen-1-one, DMU 2265

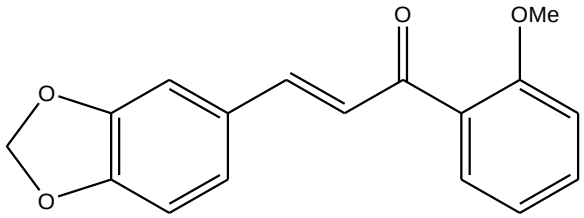

Yellow crystals (7.21g, 77%), mp 121-123ºC; δ_H ($CDCl_3$) 3.90 (3H, s, OCH_3), 6.00 (2H, S, OCH_2O), 6.83 (1H, d, Ar-H), 6.97-7.07 (3H, m, Ar-H), 7.10 (1H, s, Ar-H), 7.20 (1H, d, J=15.3Hz, C=C-H), 7.43-7.48 (1H, m, Ar-H), 7.53 (1H, d, J=15.3Hz, C=C-H), 7.59 (1H, dd, Ar-H); δ_C ($CDCl_3$) 55.8, 101.6, 106.6, 108.6, 111.7, 120.7, 125.0, 125.0, 125.3, 129.3, 129.5, 130.2, 142.9, 143.3, 148.3, 149.7, 193.0; m/z (MALDI)$^+$ Found 383.0962, $C_{17}H_{14}O_4$ requires 383.0965; m/z [MALDI]$^+$ 283 ([M+H]$^+$, 100%); υ_{max} (KBr) /cm^{-1} 1705 (C=O).

(E)-1-(3,4-dimethoxyphenyl)-3-(4-butoxyphenyl)-2-propen-1-one, DMU 2305

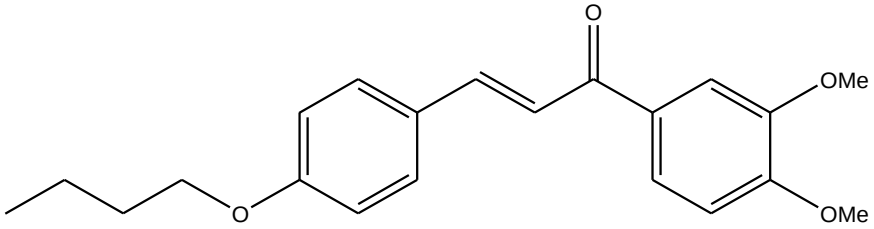

Yellow crystals (6.10g, 65%), mp 125-127ºC; δ_H ($CDCl_3$) 0.08 (3H, t, CH_3), 1.50 (2H, m, CH_2), 1.79 (2H, m, CH_2), 3.95 (6H, s, OCH_3), 4.00 (2H, t, CH_2), 6.86 (3H, d, Ar-H), 7.41 (1H, d, J=15.0Hz, C=C-H), 7.59 (2H, d, Ar-H), 7.61 (1H, s, Ar-H), 7.79 (1H, d, J=15.0Hz, C=C-H); δ_C ($CDCl_3$) 13.8, 19.2, 31.2, 56.1, 67.9, 110.1, 110.4, 114.9, 119.3, 122.8, 127.6, 130.1, 131.7, 143.9, 149.2, 153.1, 161.2, 188.6; m/z [MALDI]$^+$ 341 ([M+H]$^+$, 100%); υ_{max} (KBr) /cm^{-1} 1645 (C=O).

(E)-1-(3,4-dimethoxyphenyl)-3-(4-methoxyphenyl)-2-propen-1-one, DMU 2306

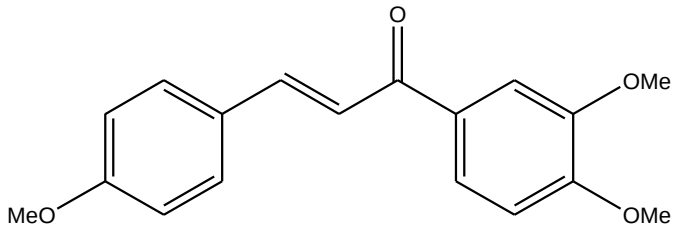

Yellow crystals (7.30g, 66%), mp 89-91ºC; δ_H ($CDCl_3$) 3.88 (3H, s, OCH_3), 3.99 (6H, s, OCH_3), 6.93-6.98 (3H, m, Ar-H), 7.45 (1H, d, J=14.3Hz, C=C-H), 7.60-7.66 (3H, m, Ar-H), 7.69 (1H, dd, Ar-H), 7.80 (1H, d, J=14.3Hz, C=C-H); δ_C ($CDCl_3$) 55.4, 56.0, 56.1, 110.0, 110.7, 114.4, 119.3, 122.9, 127.8, 130.1, 131.5, 143.8, 149.2, 153.1, 161.5, 188.6; m/z $[MALDI]^+$ 299 ($[M+H]^+$, 100%); υ_{max} (KBr) /cm^{-1} 1763 (C=O).

(E)-1-(2,4-dimethoxyphenyl)-3-(4-methoxyphenyl)-2-propen-1-one, DMU 2307

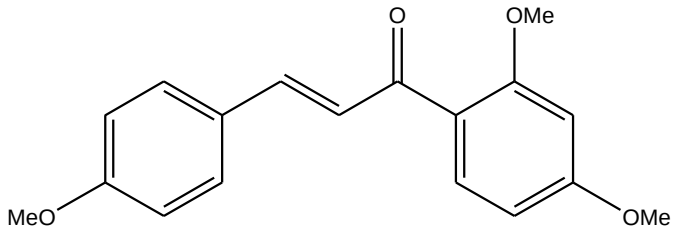

Yellow crystals (7.90g, 76%), mp 101-103ºC; δ_H ($CDCl_3$) 3.82 (3H, s, OCH_3), 3.85 (3H, s, OCH_3), 3.90 (3H, s, OCH_3), 6.49 (1H, s, Ar-H), 6.56 (1H, dd, Ar-H), 6.90 (2H, d, Ar-H), 7.38 (1H, d, J=16.0Hz, C=C-H), 7.54 (2H, d, Ar-H), 7.64 (1H, d, J=16.0Hz, C=C-H), 7.73 (1H, d, Ar-H); δ_C ($CDCl_3$) 55.50, 55.70, 98.70, 105.10, 114.30, 122.50, 125.00, 128.20, 129.90, 132.70, 142.10, 160.20, 161.20, 163.90, 190.70; m/z $[MALDI]^+$ 299 ($[M+H]^+$, 100%); υ_{max} (KBr) /cm^{-1} 1782 (C=O).

(E)-1-(3,4,5-trimethoxyphenyl)-3-(4-methoxyphenyl)-2-propen-1-one, DMU 102

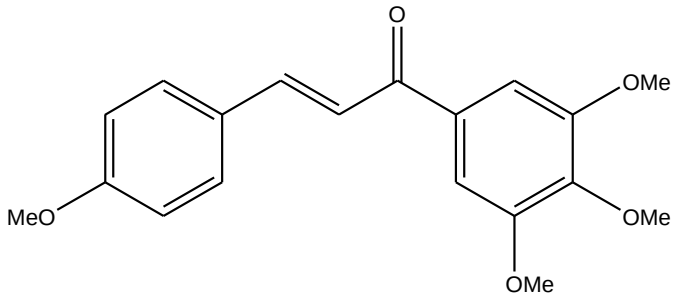

Yellow crystals (8.32g, 70%), mp 65-67^{o}C; δ_H ($CDCl_3$) 3.65 (3H, s, OCH_3), 3.72 (9H, s, OCH_3), 6.73 (2H, d, Ar-H), 7.06 (2H, s, Ar-H), 7.15 (1H, d, J=15.4Hz, C=C-H), 7.38 (2H, d, Ar-H), 7.57 (1H, d, J=15.4Hz, C=C-H); δ_C ($CDCl_3$) 55.1, 56.3, 60.9, 105.7, 114.0, 119.3, 127.6, 130.3, 133.8, 142.2, 144.6, 153.0, 161.7, 189.1; m/z [MALDI]$^+$ 329 ([M+H]$^+$, 100%); υ_{max} (KBr) /cm^{-1} 1679 (C=O).

(E)-1-(4-chlorophenyl)-3-(3,4-methylenedioxyphenyl)-2-propen-1-one, DMU 2222

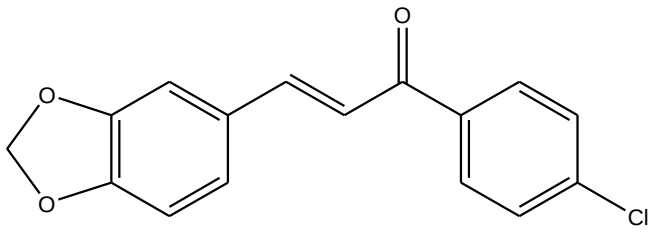

Yellow crystals (8.52g, 90%), mp 126-128^{o}C; δ_H ($CDCl_3$) 6.00 (2H, S, OCH_2O), 6.85 (1H, d, Ar-H), 7.13 (1H, d, Ar-H), 7.16 (1H, s, Ar-H), 7.32 (1H, d, J=16.25Hz, C=C-H), 7.47 (2H, d, Ar-H), 7.74 (1H, d, J=16.25Hz, C=C-H), 7.94 (2H, d, Ar-H); δ_C ($CDCl_3$) 101.7, 106.7, 108.7, 119.5, 125.5, 128.9, 129.2, 129.8, 136.7, 139.1, 145.3, 148.5, 150.1, 189.1; m/z [MALDI]$^+$ 287 ([M+H]$^+$, 100%); υ_{max} (KBr) /cm^{-1} 1660 (C=O).

(E)-1-(2-methoxyphenyl)-3-(2-methoxyphenyl)-2-propen-1-one, DMU 2308

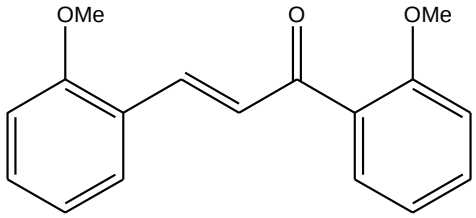

Yellow oil (8.72g, 88%); δ_H ($CDCl_3$) 3.85 (3H, s, OCH_3), 3.90 (3H, s, OCH_3), 6.88-7.05 (4H, m, Ar-H), 7.35 (1H, t, Ar-H), 7.38-7.47 (2H, d, J=16.0Hz, C=C-H), 7.59 (2H, t, Ar-H), 7.95 (1H, d, J=16.0Hz, C=C-H); δ_C ($CDCl_3$) 55.5, 55.6, 111.2, 111.6, 120.7, 124.2, 127.7, 128.8, 129.7, 130.3, 131.5, 132.5, 132.8, 138.8, 158.1, 158.7, 193.5; m/z $[MALDI]^+$ 269 ($[M+H]^+$, 100%); υ_{max} (KBr) /cm^{-1} 1750 (C=O).

(E)-1-(4-chlorophenyl)-3-(4-chlorophenyl)-2-propen-1-one, DMU 2309

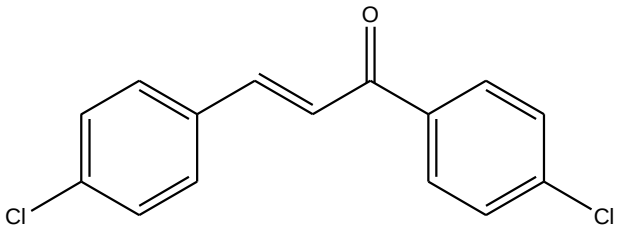

Yellow crystals (8.03g, 81%), mp 147-149^{o}C; δ_H ($CDCl_3$) 7.37-7.41 (2H, d, J=16.0Hz, C=C-H), 7.41-7.43 (1H, s, Ar-H), 7.46-7.50 (2H, d, Ar-H), 7.57 (2H, d, J=16.0Hz, C=C-H) 7.75 (1H, d, Ar-H), 7.95 (2H, d, Ar-H); δ_C ($CDCl_3$) 122.0, 129.0, 129.3, 129.6, 129.9, 133.2, 136.4, 136.7, 139.4, 143.6, 188.8; m/z $[MALDI]^+$ 277 ($[M+H]^+$, 100%); υ_{max} (KBr) /cm^{-1} 1656 (C=O).

(E)-1-(3, 4-dimethoxyphenyl)-3-(4-propoxyphenyl)-2-propen-1-one, DMU 2216

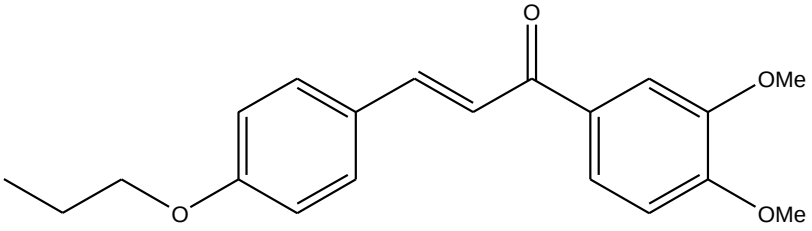

Yellow crystals (7.02g, 72%), mp 103-105°C; δ_H ($CDCl_3$) 1.05 (3H, t, CH_3), 1.72-1.85 (2H, m, CH_2), 3.70 (2H, s, CH_2), 3.95 (6H, s, OCH_3), 6.90 (3H, d, Ar-H), 7.40 (1H, d, Ar-H), 7.50-7.60 (3H, m, Ar-H), 7.65 (1H, dd, Ar-H), 7.75 (1H, d, Ar-H); δ_C ($CDCl_3$) 10.4, 18.3, 22.5, 56.0, 69.7, 110.1, 110.9, 114.9, 119.2, 122.8, 127.6, 130.1, 131.6, 144.0, 149.2, 153.1, 161.2, 188.8; m/z $[MALDI]^+$ 327 ($[M+H]^+$, 100%); υ_{max} (KBr) /cm^{-1} 1747 (C=O).

(E)-1-(4-methoxyphenyl)-3-(3,4-methylenedioxyphenyl)-2-propen-1-one, DMU 2267

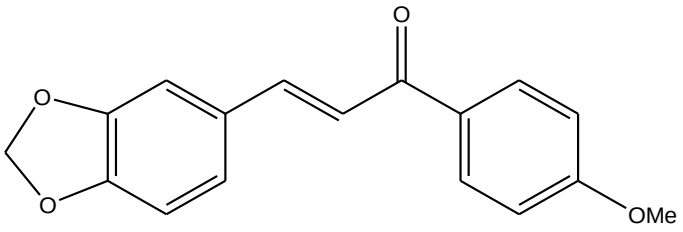

Yellow crystals (7.10g, 84%), m.p 126-128°C; δ_H ($CDCl_3$), 3.90 (3H, s, OCH_3), 6.00 (2H, s, OCH_2O), 6.85 (1H, d, Ar-H), 6.95 (2H, d, Ar-H), 7.10 (1H, d, Ar-H), 7.15 (1H, s, Ar-H), 7.45 (1H, d, J=15.0Hz, C=CH), 7.70 (1H, d, J=15.0Hz, C=CH), 8.00 (2H, d, Ar-H); δ_C ($CDCl_3$), 55.84, 101.9, 109.0, 114.2, 120.4, 125.3, 129.9, 131.1, 138.5, 144.4, 148.8, 150.1, 160.8, 163.7, 188.9; m/z (Electrospray)$^+$ Found 283.0965, $C_{17}H_{14}O_4$ requires 283.0965; m/z (Electrospray)$^+$ 283 ($[M+H]^+$, 100%); υ_{max} (KBr) /cm^{-1} 1651 (C=O).

(E)-1-(4-methoxyphenyl)-3-(3,4-methylenedioxyphenyl)-2-propen-1-one, DMU 403

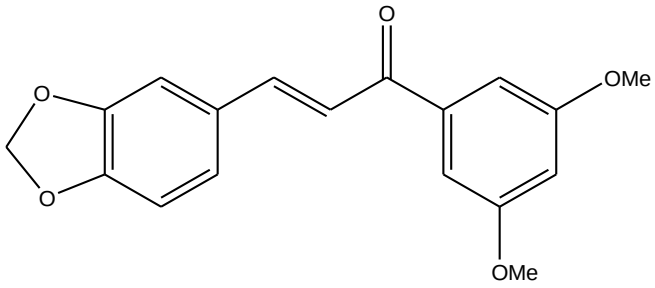

Yellow crystals (7.42g, 79%); m.p 104-106^{o}C;; δ_H ($CDCl_3$) 3.95 (6H, s, OMe), 6.00 (2H, s, OCH_2O), 6.75 (1H, s, Ar-H), 6.85 (1H, d, Ar-H), 7.05-7.15 (4H, m, Ar-H), 7.35 (1H, d, J=17.0Hz, C=CH), 7.85 (1H, d, J=17.0Hz, C=CH), δ_C ($CDCl_3$), 55.6, 101.6, 104.8, 106.3, 106.7, 108.6, 120.1, 125.2, 129.4, 140.4, 144.7, 148.4, 149.94, 160.9, 189.9; m/z (Electrospray)$^+$ Found 313.1070, $C_{18}H_{16}O_5$ requires 313.1071; m/z (Electrospray)$^+$ 313 ([M+H]$^+$, 100%); υ_{max} (KBr) /cm^{-1} 1668 (C=O).

(E)-1-(4-methoxyphenyl)-3-(3,4-methylenedioxyphenyl)-2-propen-1-one, DMU 416

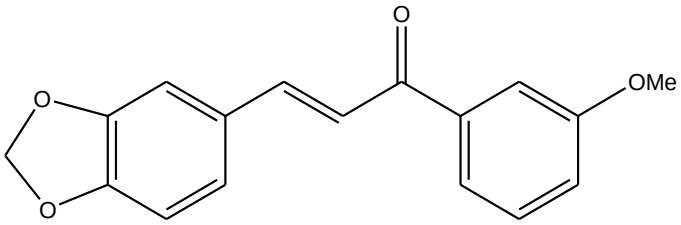

Yellow crystals (6.55g, 77%), m.p 81-83^{o}C, δ_H ($CDCl_3$) 3.79 (3H, s, OCH_3), 6.50(2H, s, OCH_2O), 6.85 (1H, d, Ar-H), 7.1 (3H, t, Ar-H), 7.31 (1H,d, J=15.6Hz, CH=CH), 7.41 (1H, d, Ar-H), 7.55 (2H, m, Ar-H), 7.75 (1H, d, J=15.6Hz, CH=CH); δ_C ($CDCl_3$), 56.18, 101.93, 107.08, 108.98, 112.09, 121.12, 125.35, 129.68, 130.64, 133.08, 138.52, 143.58, 148.73, 150.06, 158.43, 193.25; m/z (Electrospray)$^+$ Found 283.0966, $C_{17}H_{14}O_4$ requires 283.0965; m/z (Electrospray)$^+$ 283 ([M+H]$^+$, 100%); υ_{max} (KBr) /cm^{-1} 1659 (C=O).

9.3 General Procedure for the Synthesis of Epoxychalcones

To a stirring mixture of the chalcone (9.2 mmol) and potassium carbonate (27 mmol) in methanol (40 ml), hydrogen peroxide (50 % w/v, 12.4 cm^3, 368 mmol) was added. The reaction was monitored by TLC and upon reaching completion was quenched with water (80 ml) and the crude product extracted with dichloromethane (3 x 50 ml). The combined organic extracts were dried ($MgSO_4$) and the solvent removed *in vacuo*. The crude product was recrystallised from methanol producing white crystals.

1-(3, 4-dimethoxyphenyl)-2,3-epoxy-3-(3,4-dimethoxyphenyl)propan-1-one, DMU 10001

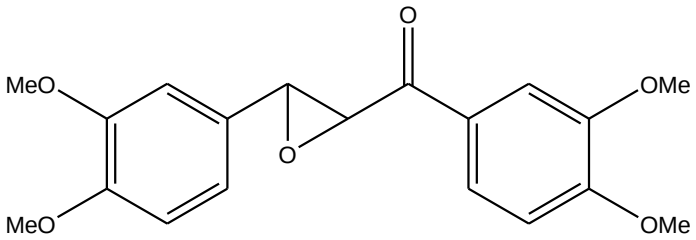

White crystals (2.49g, 79%), mp 119-121ºC; δ_H ($CDCl_3$) 3.85 (6H, s, 2 x OCH_3), 3.90 (6H, s, 2 x OCH_3), 3.98 (1H, d, CHO), 4.20 (1H, d, CHO), 6.77 (1H, s, Ar-H), 6.82 (1H, d, Ar-H), 6.84 (1H, d, Ar-H), 6.89 (1H, d, Ar-H), 7.52 (1H, d, Ar-H), 7.61 (1H, dd, Ar-H); δ_C ($CDCl_3$) 50.7, 56.1, 59.3, 60.9, 108.2, 110.2, 111.3, 118.8, 123.4, 128.1, 128.8, 149.4, 149.5, 154.2, 191.4; m/z (Electrospray)$^+$ Found 345.1336, $C_{19}H_{20}O_6$ requires 345.1333; m/z (Electrospray)$^+$ 345 ($[M+H]^+$, 100%); υ_{max} (KBr) /cm^{-1} 1800 (C=O).

1-(4-methoxyphenyl)-2,3-epoxy-3-(3,4, 5-trimethoxyphenyl)propan-1-one, DMU 10002

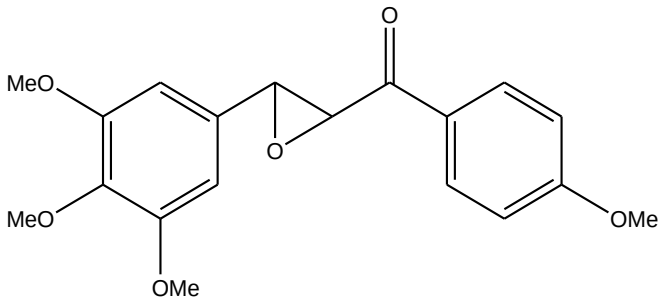

White crystals (2.40g, 76%), mp 118-120ºC; δ_H ($CDCl_3$) 3.80 (12H, s, 4 x OCH_3), 4.05 (1H, d, CHO), 4.21 (1H, d, CHO), 6.60 (2H, s, Ar-H), 7.00 (2H, d, Ar-H), 8.08 (2H, d, Ar-H); δ_C ($CDCl_3$); m/z (Electrospray)$^+$ Found 345.1336, $C_{19}H_{20}O_6$ requires 345.1333; m/z (Electrospray)$^+$ 345 ($[M+H]^+$, 100%); υ_{max} (KBr) /cm^{-1} 1700 (C=O).

1-(3-methoxyphenyl)-2,3-epoxy-3-(3-methoxyphenyl)propan-1-one, DMU 10003

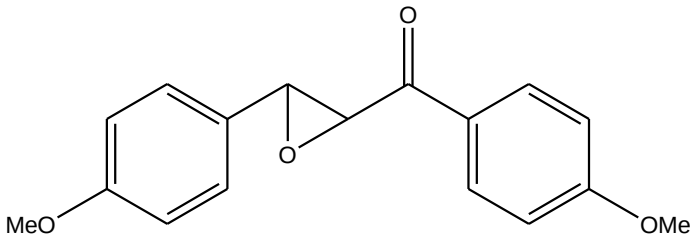

White crystals (2.49g, 79%), mp 119-121^{o}C; δ_H; δ_C ($CDCl_3$); m/z (Electrospray)$^+$ Found 285.1123, $C_{17}H_{19}O_4$ requires 285.1121; m/z (Electrospray)$^+$ 345 ([M+H]$^+$, 100%); υ_{max} (KBr) /cm^{-1} 1670 (C=O).

1-(3, 4, 5-trimethoxyphenyl)-2,3-epoxy-3-(3, 4-methylenedioxyphenyl)propan-1-one, DMU 10004

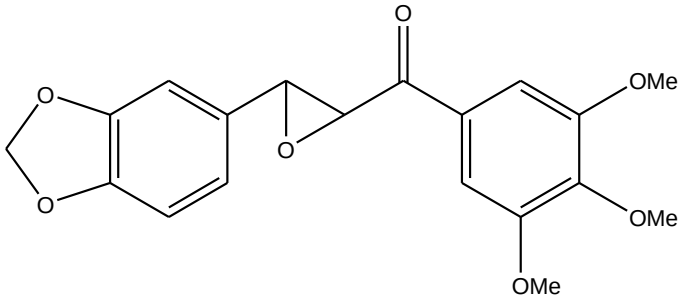

Oil (2.40g, 68%), mp 118-120^{o}C; δ_H ($CDCl_3$) 3.90 (6H, s, 2 x OCH_3), 3.95 (3H, s, OCH_3), 4.01 (1H, d, CHO), 4.18 (1H, d, CHO), 6.00 (2H, s, OCH_2O), 6.80 (1H, s, Ar-H), 6.88 (1H, d, Ar-H), 6.95 (1H, d, Ar-H), 7.35 (1H, s, Ar-H), 7.43 (1H, d, Ar-H); δ_C ($CDCl_3$); m/z (Electrospray)$^+$ 359 ([M+H]$^+$, 100%); υ_{max} (KBr) /cm^{-1} 1686 (C=O).

1-(3, 4-dimethoxyphenyl)-2,3-epoxy-3-(3,4-methylenedioxyphenyl)propan-1-one, DMU 10006

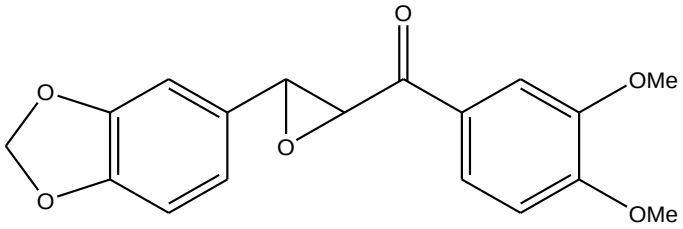

White crystals (2.04g, 68%), mp 161-163ºC; δ_H ($CDCl_3$) 3.98 (6H, s, 2 x OCH_3), 4.03 (1H, d, CHO), 4.25 (1H, d, CHO), 6.04 (2H, s, OCH_2O), 6.83 (2H, d, Ar-H), 6.91 (2H, d, Ar-H), 7.59 (1H, s, Ar-H), 7.68 (1H, d, Ar-H); δ_C ($CDCl_3$) 56.11, 59.3, 60.7, 101.4, 105.5, 108.7, 110.7, 120.2, 123.4, 128.8, 129.5, 143.9, 148.3, 149.2, 154.2, 188.5, 191.4; m/z (Electrospray)$^+$ Found 329.1024, $C_{18}H_{16}O_6$ requires 329.1020; m/z (Electrospray)$^+$ 329 ($[M+H]^+$, 67%); υ_{max} (KBr) /cm^{-1} 1680 (C=O).

1-(3, 4, 5-trimethoxyphenyl)-2,3-epoxy-3-(3,4-methylenedioxyphenyl)propan-1-one, DMU 10007

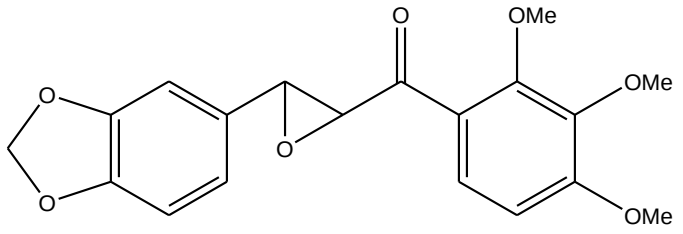

White crystals (2.85g, 87%), mp 123-125ºC; δ_H ($CDCl_3$) 3.75 (3H, s, OCH_3), 3.85 (3H, s, OCH_3), 3.95 (3H, s, OCH_3), 4.00 (1H, d, CHO), 4.35 (1H, d, CHO), 6.00 (2H, s, OCH_2O), 6.77 (1H, d, Ar-H), 6.82 (2H, d, Ar-H), 6.90 (1H, d, Ar-H), 7.65 (1H, d, Ar-H); δ_C ($CDCl_3$) 56.2, 59.8, 60.9, 61.8, 63.6, 95.0, 100.0, 101.3, 105.6, 107.5, 108.4, 120.4, 123.7, 126.0, 130.1, 141.7, 148.2, 154.7, 158.5, 193.2; m/z (Electrospray)$^+$ Found 359.1129, $C_{19}H_{18}O_7$ requires 359.1125; m/z (Electrospray)$^+$ 359 ($[M+H]^+$, 25%); υ_{max} (KBr) /cm^{-1} 1690 (C=O).

1-(2, 4-dimethoxyphenyl)-2,3-epoxy-3-(3,4-methylenedioxyphenyl)propan-1-one, DMU 10008

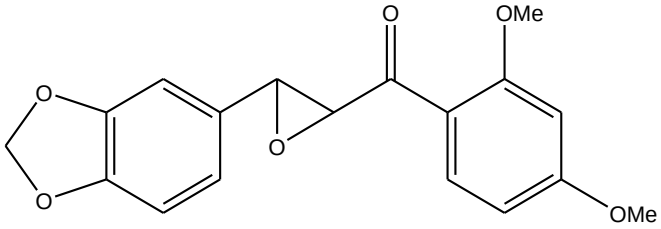

White crystals (2.85g, 86%), mp 123-125^{o}C; δ_H ($CDCl_3$) 3.65 (3H, s, OCH_3), 3.89 (3H, s, OCH_3), 3.90 (1H, d, CHO), 4.30 (1H, d, CHO), 6.01 (2H, s, OCH_2O), 6.43 (1H, d, Ar-H), 6.59 (1H, dd, Ar-H), 6.83 (2H, d, Ar-H), 7.90 (1H, d, Ar-H); δ_C ($CDCl_3$) 55.5, 59.3, 64.4, 98.2, 101.3, 105.0, 105.6, 108.3, 119.2, 120.1, 130.6, 132.9, 150.0, 161.6, 165.5, 192.7; m/z (Electrospray)$^+$ Found 329.1025, $C_{18}H_{16}O_6$ requires 329.1020; m/z (Electrospray)$^+$ 329 ($[M+H]^+$, 70%); υ_{max} (KBr) /cm^{-1} 1689 (C=O).

1-(2, 5-dimethoxyphenyl)-2,3-epoxy-3-(3,4-methylenedioxyphenyl)propan-1-one, DMU 10009

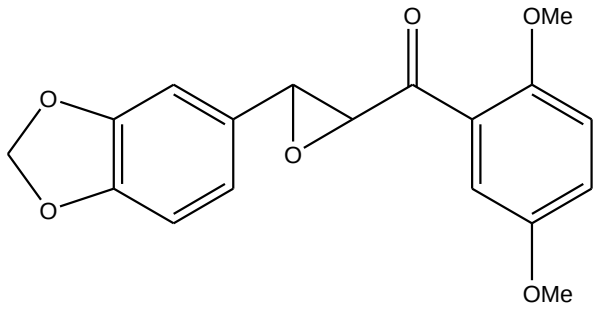

White crystals (2.75g, 82%), mp 124-126^{o}C; δ_H ($CDCl_3$) 3.55 (3H, s, OCH_3), 3.74 (3H, s, OCH_3), 3.86 (1H, d, CHO), 4.23 (1H, d, CHO), 5.92 (2H, s, OCH_2O), 6.76 (2H, d, Ar-H), 6.83 (2H, d, Ar-H), 7.01 (1H, dd, Ar-H), 7.27 (1H, d, Ar-H); δ_C ($CDCl_3$) 55.9, 56.2, 59.9, 64.3, 101.3, 105.6, 108.3, 113.2, 113.5, 120.2, 122.0, 126.0, 130.4, 148.1, 153.7, 154.2, 194.5; m/z (Electrospray)$^+$ Found 329.1023, $C_{18}H_{16}O_6$ requires 329.1020; m/z (Electrospray)$^+$ 329 ($[M+H]^+$, 83%); υ_{max} (KBr) /cm^{-1} 1697 (C=O).

1-(2, 5-dimethoxyphenyl)-2,3-epoxy-3-(2,5-dimethoxyphenyl)propan-1-one, DMU 10010

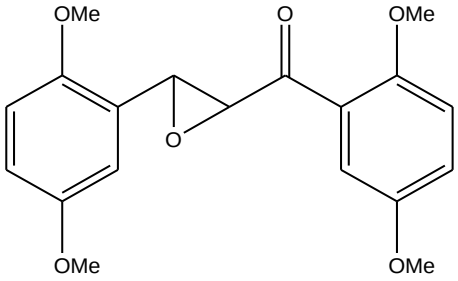

White crystals (2.88g, 86%), mp 113-115^{o}C; δ_H ($CDCl_3$) 3.64 (3H, s, OCH_3), 3.80 (3H, s, OCH_3), 3.81 (3H, s, OCH_3), 3.83 (3H, s, OCH_3), 4.27 (1H, d, CHO), 4.32 (1H, d, CHO), 6.86 (3H, s, Ar-H), 6.90 (1H, d, Ar-H), 7.10 (1H, dd, Ar-H), 7.38 (1H, d, Ar-H); δ_C ($CDCl_3$) 55.9, 64.1, 110.6, 111.7, 113.3, 113.5, 114.3, 121.8, 126.3, 152.7, 153.7, 153.9, 154.2, 194.8; m/z (Electrospray)$^+$ Found 345.1137, $C_{18}H_{16}O_6$ requires 345.1333; m/z (Electrospray)$^+$ 345 ($[M+H]^+$, 33%); υ_{max} (KBr) /cm^{-1} 1740 (C=O).

1-(4-methoxyphenyl)-2,3-epoxy-3-(2,5-dimethoxyphenyl)propan-1-one, DMU 10011

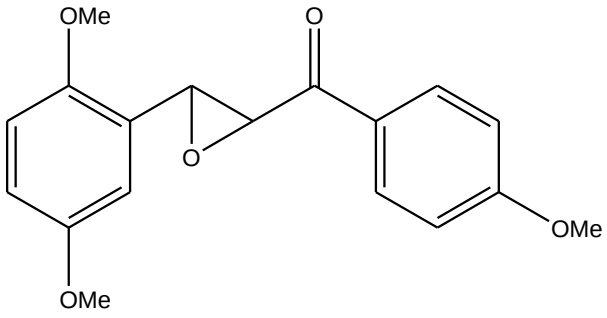

Oil (2.33g, 81%), δ_H ($CDCl_3$) 3.78 (6H, s, 2 x OCH_3), 3.88 (3H, s, OCH_3), 4.12 (1H, d, CHO) 4.37 (1H, d, CHO), 6.86 (3H, d, Ar-H), 6.95 (2H, d, Ar-H), 8.04 (2H, d, Ar-H); δ_C ($CDCl_3$) 55.4, 55.8, 56.0, 60.5, 111.1, 111.7, 113.6, 114.5, 123.5, 125.1, 125.5, 130.8, 152.5, 153.7, 164.1, 189.5, 191.6; m/z (Electrospray)$^+$ 315 ($[M+H]^+$, 88%); υ_{max} (neat) /cm^{-1} 1740 (C=O).

1-(4-methoxyphenyl)-2,3-epoxy-3-(3,5-dimethoxyphenyl)propan-1-one, DMU 10012

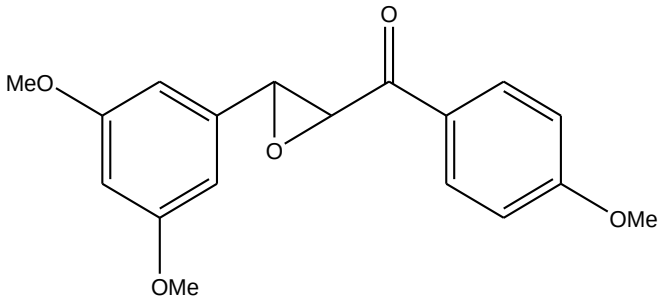

White crystals (1.98 g, 69%), mp 100-102°C; δ_H ($CDCl_3$) 3.83 (6H, s, 2 x OCH_3), 3.90 (3H, s, OCH_3), 4.03 (1H, d, CHO) 4.22 (1H, d, CHO), 6.48 (1H, t, Ar-H), 6.55 (2H, d, Ar-H), 6.99 (2H, d, Ar-H), 8.04 (2H, d, Ar-H); δ_C ($CDCl_3$) 55.4, 59.0, 60.0, 101.2, 103.6, 114.1, 128.5, 130.8, 139.4, 163.4, 164.0, 192.3; m/z (Electrospray)$^+$ 315 ([M+H]$^+$, 88%); υ_{max} (KBr) /cm^{-1} 1754 (C=O).

1-(2-methoxyphenyl)-2,3-epoxy-3-(3,4-methylenedioxyphenyl)propan-1-one, DMU 10013

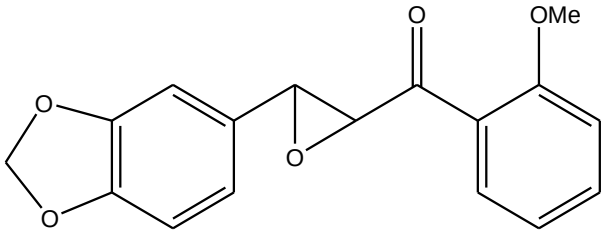

White crystals (1.98 g, 70%), mp 100-102°C; δ_H ($CDCl_3$) 3.68 (3H, s, OCH_3), 3.94 (1H, d, CHO) 4.27 (1H, d, CHO), 5.98 (2H, s, OCH_2O), 6.81-6.83 (2H, m, Ar-H), 6.90 (1H, d, Ar-H), 6.94 (1H, d, Ar-H), 7.05 (1H, t, Ar-H), 7.52 (1H, t, Ar-H), 7.81 (1H, d, Ar-H); δ_C ($CDCl_3$) 55.7, 59.9, 64.3, 94.9, 101.3, 105.6, 108.3, 111.6, 120.2, 121.0, 126.0, 130.4, 130.7, 134.9, 148.1, 148.1, 159.6, 194.9; m/z (Electrospray)$^+$ Found 299.0909, $C_{17}H_{14}O_5$ requires 299.0914; m/z (Electrospray)$^+$ 299 ([M+H]$^+$, 29%); υ_{max} (KBr) /cm^{-1} 1780 (C=O).

1-(3, 4-dimethoxyphenyl)-2,3-epoxy-3-(4-butoxyphenyl)propan-1-one, DMU 10014

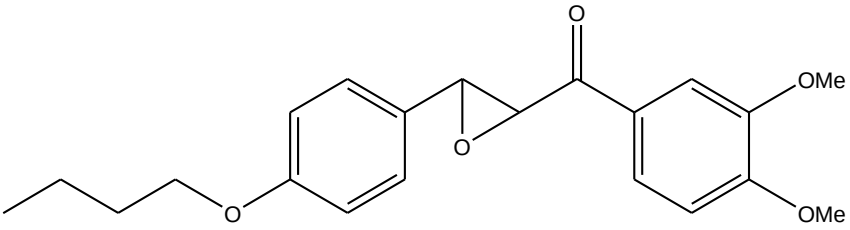

White crystals (2.14 g, 66%), mp 153-155ºC; δ_H ($CDCl_3$) 0.98 (3H, t, CH3), 1.45-1.57 (2H, m, CH_2), 1.74-1.81 (2H, m, CH_2), 3.89-3.95 (9H, m, CH_2, CHO, OCH_3), 4.24 (1H, d, CHO), 6.87-6.92 (3H, m, Ar-H), 7.27 (2H, d, Ar-H), 7.65 (1H, s, Ar-H), 7.68 (1H, d, Ar-H); δ_C ($CDCl_3$) 13.8, 19.2, 31.3, 56.1, 59.3, 60.9, 67.9, 110.2, 114.8, 123.3, 127.1, 128.9, 149.4, 154.2, 159.9, 191.6; m/z (Electrospray)$^+$ 356 ([M+H]$^+$, 100%); υ_{max} (KBr) /cm^{-1} 1779 (C=O).

1-(3,4-dimethoxyphenyl)-2,3-epoxy-3-(4-methoxyphenyl)propan-1-one, DMU 10016

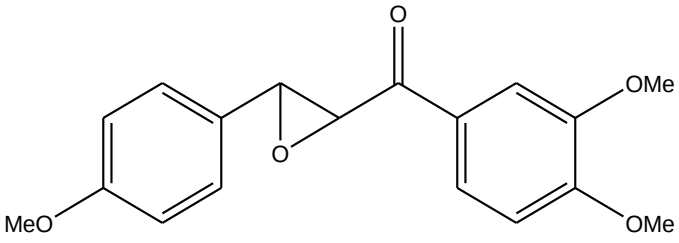

White crystals (2.20 g, 77%), mp 82-84ºC; δ_H ($CDCl_3$) 3.84 (3H, s, OCH_3), 3.95 (6H, s, 2 x OCH_3), 4.03 (1H, d, CHO) 4.26 (1H, d, CHO), 6.90 (1H, d, Ar-H), 6.95 (2H, d, Ar-H), 7.30 (2H, t, Ar-H), 7.59 (1H, d, Ar-H), 7.68 (1H, dd, Ar-H); δ_C ($CDCl_3$) 50.8, 56.0, 56.1, 59.2, 60.9, 110.2, 114.2, 123.3, 127.2, 127.6, 128.9, 149.4, 154.2, 160.3, 191.6; m/z (Electrospray)$^+$ Found 315.1231, $C_{18}H_{18}O_5$ requires 315.1227; m/z (Electrospray)$^+$ 315 ([M+H]$^+$, 100%); υ_{max} (KBr) /cm^{-1} 1780 (C=O).

1-(2, 4-dimethoxyphenyl)-2,3-epoxy-3-(4-methoxyphenyl)propan-1-one, DMU 10017

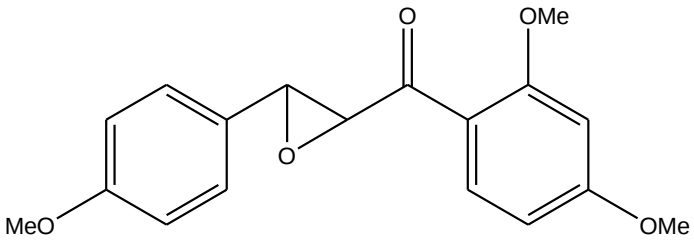

White crystals (2.74 g, 92%), mp 81-83ºC; δ_H ($CDCl_3$) 3.61 (3H, s, OCH_3), 3.85 (3H, s, OCH_3), 3.88 (3H, s, OCH_3), 3.94 (1H, d, CHO) 4.33 (1H, d, CHO), 6.43 (1H, d, Ar-H), 6.59 (1H,d d, Ar-H), 6.93 (2H, d, Ar-H), 7.30 (2H, d, Ar-H), 7.90 (1H, d, Ar-H); δ_C ($CDCl_3$) 55.4, 55.6, 59.5, 64.5, 98.1, 105.8, 114.0, 116.8, 127.2, 128.6, 132.8, 159.6, 161.6, 165.5, 192.9; m/z (Electrospray)$^+$ Found 315.1222, $C_{18}H_{18}O_5$ requires 315.1227; m/z (Electrospray)$^+$ 315 ($[M+H]^+$, 65%); υ_{max} (KBr) /cm^{-1} 1774 (C=O).

1-(2-methoxyphenyl)-2,3-epoxy-3-(2-methoxyphenyl)propan-1-one, DMU 10020

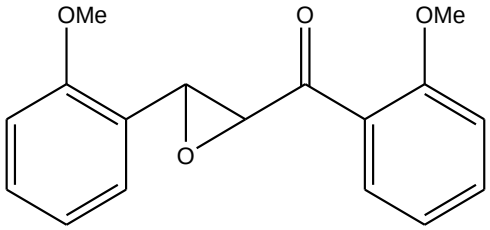

White crystals (2.74 g, 92%), mp 81-83ºC; δ_H ($CDCl_3$) 3.61 (3H, s, OCH_3), 3.85 (3H, s, OCH_3), 3.88 (3H, s, OCH_3), 3.94 (1H, d, CHO) 4.33 (1H, d, CHO), 6.43 (1H, d, Ar-H), 6.59 (1H,d d, Ar-H), 6.93 (2H, d, Ar-H), 7.30 (2H, d, Ar-H), 7.90 (1H, d, Ar-H); δ_C ($CDCl_3$) 55.4, 55.6, 59.5, 64.5, 98.1, 105.8, 114.0, 116.8, 127.2, 128.6, 132.8, 159.6, 161.6, 165.5, 192.9; m/z (Electrospray)$^+$ Found 315.1222, $C_{18}H_{18}O_5$ requires 315.1227; m/z (Electrospray)$^+$ 315 ($[M+H]^+$, 65%); υ_{max} (KBr) /cm^{-1} 1774 (C=O).

1-(2, 4-dimethoxyphenyl)-2,3-epoxy-3-(4-methoxyphenyl)propan-1-one, DMU 10021

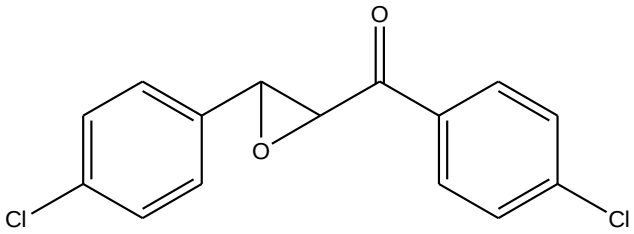

White crystals (2.08 g, 78%), mp 129-131ºC; δ_H ($CDCl_3$) 4.07 (1H, d, CHO) 4.18 (1H, d, CHO), 7.32 (2H, d, Ar-H), 7.40 (2H, d, Ar-H), 7.49 (2H, d, Ar-H), 7.98 (2H, d, Ar-H); δ_C ($CDCl_3$) 58.6, 61.0, 127.1, 129.3, 129.8, 133.6, 135.1, 140.8, 191.7; m/z (Electrospray)$^+$ Found 293.0136, $C_{15}H_{10}O_2Cl_2$ requires 293.0131; m/z (Electrospray)$^+$ 293 ([M+H]$^+$, 100%); υ_{max} (KBr) /cm^{-1} 1803 (C=O).

1-(3, 4-dimethoxyphenyl)-2,3-epoxy-3-(4-propoxyphenyl)propan-1-one, DMU 10023

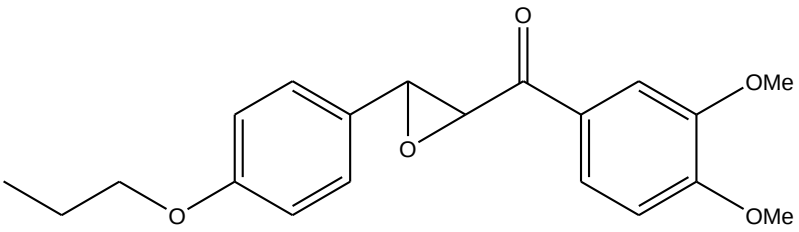

White crystals (2.11 g, 65%), mp 123-125ºC; δ_H ($CDCl_3$) 1.04 (3H, t, CH_3), 1.77-1.86 (2H, m, CH_2), 3.92-3.96 (8H, m, CH_2, OCH_3), 4.01 (1H, d, CHO), 4.24 (1H, d, CHO), 6.87-6.93 (3H, m, Ar-H), 7.27 (1H, d, Ar-H), 7.58 (1H, s, Ar-H), 7.67 (1H, d, Ar-H); m/z (Electrospray)$^+$ 356 ([M+H]$^+$, 100%); υ_{max} (KBr) /cm^{-1} 1687 (C=O).

9.4 General Procedure for the Synthesis of Substituted Pyrazoles

Hydrazine hydrate (0.18 cm^3, 5.7 mmol) was added drop-wise to a refluxing solution of the epoxide (3.8 mmol) in ethanol (40 cm^3). After 6 h at reflux the solution was allowed to cool to room temperature and the solvent removed *in vacuo*. The residue was dissolved in glacial acetic acid (30 cm^3). Concentrated sulphuric acid (0.25 cm^3) was added and the solution heated at reflux for 0.5 h. After cooling (ice bath) the solution was neutralised with concentrated ammonia solution and poured onto ice. The resulting brown precipitate was isolated by vacuum filtration. The pyrazole was purified by either recrystalisation from ethanol, or flash chromatography on silica gel using ethyl acetate − hexane (7:3) as eluent.

3-(3, 4-dimethoxyphenyl)-5-(3,4-dimethoxyphenyl)pyrazole, DMU 10101

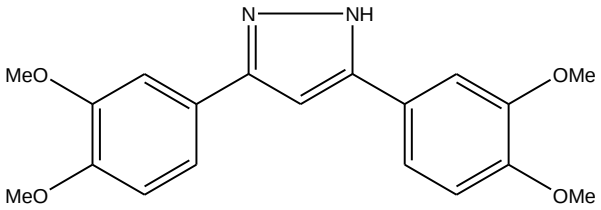

Brown crystals (1.12g, 87%), mp 84-86ºC; δ_H ($CDCl_3$) 3.94 (6H, s, 2 x OCH_3), 3.97 (6H, s, 2 x OCH_3), 6.71 (1H, s, Ar-H, C4-H), 6.94 (2H, d, Ar-H), 7.25-7.28 (4H, m, Ar-H); δ_C ($CDCl_3$) 55.7, 55.9, 98.8, 108.6, 111.2, 118.1, 124.2, 148.6, 149.0, 149.1; m/z (CI, NH_3)$^+$ Found 341.1499, $C_{19}H_{22}N_2O_4$ requires 341.1499; m/z (CI, NH_3)$^+$ 341 ($[M+H]^+$, 100%); υ_{max} (KBr) /cm^{-1} 3330 (N-H).

3-(4-methoxyphenyl)-5-(3,4,5-trimethoxyphenyl)pyrazole, DMU 10102

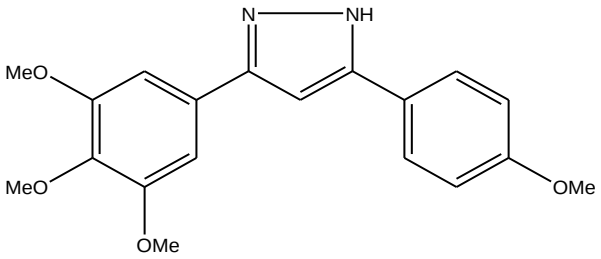

Brown crystals (1.05g, 81%), mp 80-82ºC; δ_H ($CDCl_3$) 3.84 (3H, s, OCH_3), 3.84-3.88 (3H, s, OCH_3), 3.88-3.90 (6H, s, 2 x OCH_3), 6.70 (1H, s, Ar-H, C4-H), 6.86-6.89 (4H, m, Ar-H),

7.60 (2H, d, Ar-H); δ_C ($CDCl_3$) 55.2, 55.8, 60.9, 98.9, 102.7, 114.2, 123.1, 126.8, 127.7, 137.8, 153.4, 159.6; m/z (CI, NH_3)$^+$ 341 ([M+H]$^+$, 100%); υ_{max} (KBr) /cm^{-1} 3150 (N-H).

3-(4-methoxyphenyl)-5-(4-methoxyphenyl)pyrazole, DMU 10103

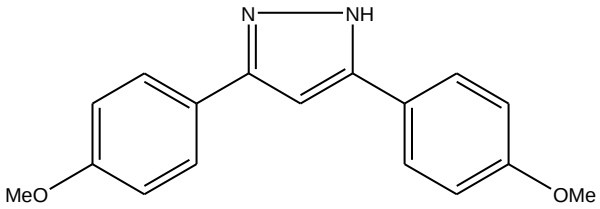

Brown crystals (0.99g, 93%), mp 77-79ºC; δ_H ($CDCl_3$) 3.85 (6H, s, 2 x OCH_3), 6.69 (1H, s, Ar-H, C4-H), 6.98 (4H, d, Ar-H), 7.65 (4H, d, Ar-H); m/z (CI, NH_3)$^+$ 281 ([M+H]$^+$, 100%); υ_{max} (KBr) /cm^{-1} 3300 (N-H).

3-(3,4,5-trimethoxyphenyl)-5-(3,4-methylenedioxyphenyl)pyrazole, DMU 10104

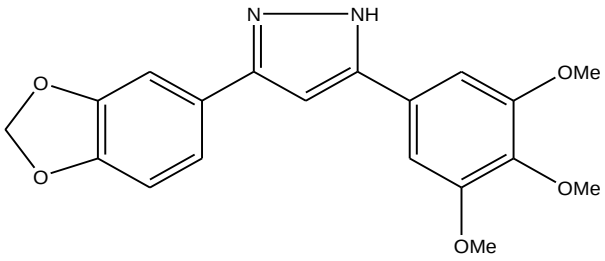

Brown crystals (0.99g, 73%), mp 101-103ºC; δ_H ($CDCl_3$) 3.90 (3H, s, OCH_3), 3.94 (6H, s, 2 x OCH_3), 6.02 (2H, s, OCH_2O), 6.70 (1H, s, Ar-H, C4-H) 6.89 (1H, d, Ar-H), 6.97 (2H, s, Ar-H), 7.15-7.20 (2H, m, Ar-H); δ_C ($CDCl_3$) 29.7, 55.9, 60.9, 99.1, 101.3, 102.6, 106.0, 108.5, 119.2, 127.1, 137.9, 147.6, 148.0, 153.4; m/z (CI, NH_3)$^+$ 355 ([M+H]$^+$, 100%); υ_{max} (KBr) /cm^{-1} 3250 (N-H).

3-(3,4-dimethoxyphenyl)-5-(3,4-methylenedioxyphenyl)pyrazole, DMU 10106

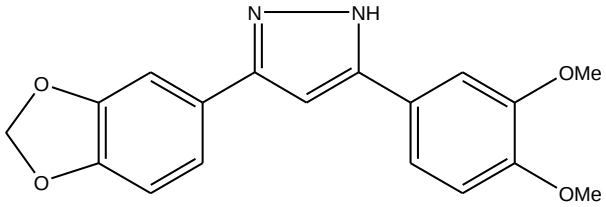

Brown crystals (0.81g, 66%), mp 109-111ºC; δ_H ($CDCl_3$) 3.85 (3H, s, OCH_3), 3.95 (3H, s, OCH_3), 6.00 (2H, s, OCH_2O), 6.68 (1H, s, Ar-H, C4-H), 6.80 (1H, d, Ar-H), 6.88 (1H, d, Ar-H), 7.10-7.19 (2H, m, Ar-H), 7.22 (2H, d, Ar-H); δ_C ($CDCl_3$) 55.9, 56.0, 99.4, 101.3, 106.3, 108.6, 109.0, 111.5, 118.2, 119.4, 148.2, 149.3; m/z (CI, NH_3)$^+$ Found 325.1181, $C_{18}H_{16}N_2O_4$ requires 325.1183; m/z (CI, NH_3)$^+$ 325 ([M+H]$^+$, 100%); υ_{max} (KBr) /cm^{-1} 3325 (N-H).

3-(2,3,4-trimethoxyphenyl)-5-(3,4-methylenedioxyphenyl)pyrazole, DMU 10107

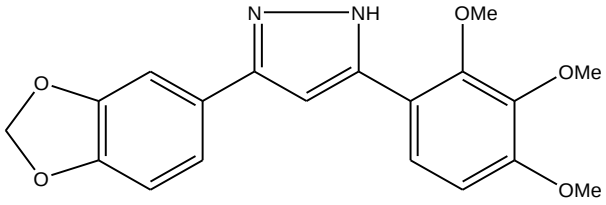

Brown solid (0.95g, 70%), mp 140-142ºC; δ_H ($CDCl_3$) 3.91 (3H, s, OCH_3), 3.92 (3H, s, OCH_3), 3.97 (3H, s, OCH_3), 6.00 (2H, s, CH_2O_2), 6.74 (1H, s, Ar-H), 6.78 (1H, d, Ar-H), 6.88 (1H, d, Ar-H), 7.33-7.39 (3H, m, Ar-H); δ_C ($CDCl_3$) 56.1, 61.0, 61.2, 99.3, 101.1, 106.3, 108.2, 108.4, 108.5, 115.8, 119.3, 122.3, 127.8, 141.8, 142.5, 147.3, 148.0, 150.8, 153.8; m/z [Electrospray]$^+$ 355 ([M+H]$^+$, 100%); υ_{max} (KBr) /cm^{-1} 3420 (N-H).

3-(2,4-dimethoxyphenyl)-5-(3,4-methylenedioxyphenyl)pyrazole, DMU 10108

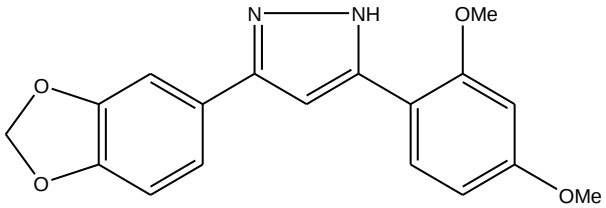

Brown crystals (0.89g, 72%), mp 169-171ºC; δ_H ($CDCl_3$) 3.87 (3H, s, OCH_3), 3.98 (3H, s, OCH_3), 6.00 (2H, s, CH_2O_2), 6.57-6.63 (2H, m, Ar-H), 6.73 (1H, s, Ar-H), 6.88 (1H, d, Ar-H), 7.32-7.39 (2H, m, Ar-H), 7.62 (1H, d, Ar-H); δ_C ($CDCl_3$) 55.5, 55.8, 98.6, 99.0, 101.0, 105.7, 106.3, 108.4, 110.9, 119.3, 128.0, 128.8, 142.0, 147.2, 147.9, 152.0, 157.1, 160.8; m/z (CI, NH_3)$^+$ Found 325.1183, $C_{18}H_{17}N_40_2$ requires 325.1183; (CI, NH_3)$^+$ 325 ([M+H]$^+$, 100%); υ_{max} (KBr) /cm^{-1} 3380 (N-H).

3-(2,5-dimethoxyphenyl)-5-(3,4-methylenedioxyphenyl)pyrazole, DMU 10109

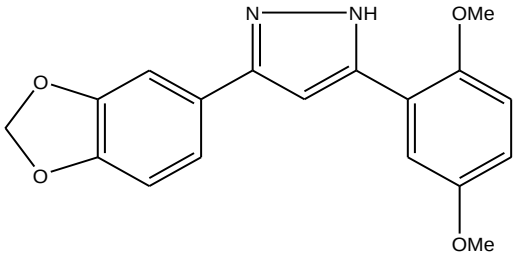

Brown crystals (0.90g, 73%), mp 154-156ºC; δ_H ($CDCl_3$) 3.85 (3H, s, OCH_3), 3.96 (3H, s, OCH_3), 6.00 (2H, s, CH_2O_2), 6.82 (1H, s, Ar-H), 6.84-6.89 (1H, m, Ar-H), 6.97 (1H, d, Ar-H), 7.24 (1H, d, Ar-H), 7.35 (1H, dd, Ar-H), 7.38 (1H, s, Ar-H); δ_C ($CDCl_3$) 55.8, 56.3, 99.6, 101.1, 106.3, 108.5, 112.8, 113.2, 114.2, 118.3, 119.3, 127.8, 141.9, 147.3, 148.0, 150.3, 154.0; m/z (CI, NH_3)$^+$ 325 ([M+H]$^+$, 100%); υ_{max} (KBr) /cm^{-1} 3425 (N-H).

3-(2,5-dimethoxyphenyl)-5-(2,5-dimethoxyphenyl)pyrazole, DMU 10110

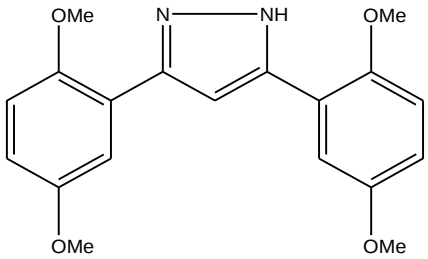

Brown crystals (0.90g, 70%), mp 135-137ºC; δ_H ($CDCl_3$) 3.85 (3H, s, OCH_3), 3.94 (3H, s, OCH_3), 6.86 (1H, d, Ar-H), 6.88 (1H, d, Ar-H), 6.96 (2H, d, Ar-H), 7.19 (1H, s, Ar-H), 7.45 (2H, d, Ar-H); δ_C ($CDCl_3$) 55.9, 56.4, 58.4, 103.9, 113.0, 113.4, 114.3, 120.9, 144.7, 150.9,

153.9; m/z (CI, NH_3)$^+$ Found 341.1493, $C_{19}H_{21}N_2O_4$ requires 341.1139; (CI, NH_3)$^+$ 341 ([M+H]$^+$, 100%); υ_{max} (KBr) /cm^{-1} 3425 (N-H).

3-(4-methoxyphenyl)-5-(2,5-dimethoxyphenyl)pyrazole, DMU 10111

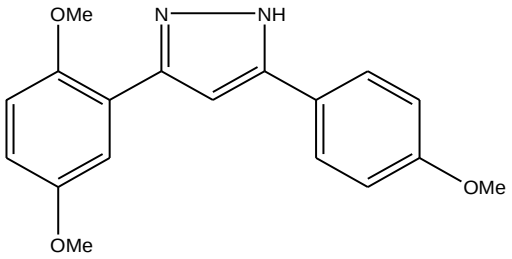

Brown oily residue (0.66g, 67%); δ_H ($CDCl_3$) 3.84 (3H, s, OCH_3), 3.86 (3H, s, OCH_3), 3.96 (3H, s, OCH_3), 6.85-6.88 (2H, m, Ar-H), 6.97 (3H, d, Ar-H), 7.27 (1H, s, Ar-H), 7.75 (2H, d, Ar-H); δ_C ($CDCl_3$) 55.3, 55.8, 56.3, 99.5, 112.8, 113.2, 114.0, 114.1, 118.5, 126.2, 126.9, 142.0, 150.3, 151.1, 154.0, 159.4; m/z (Electrospray)$^+$ Found 311.1389, $C_{18}H_{18}N_2O_3$ requires 311.1390; m/z (Electrospray)$^+$ 311 ([M+H]$^+$, 100%); υ_{max} (neat) /cm^{-1} 3298 (N-H).

3-(4-methoxyphenyl)-5-(3,5-dimethoxyphenyl)pyrazole, DMU 10112

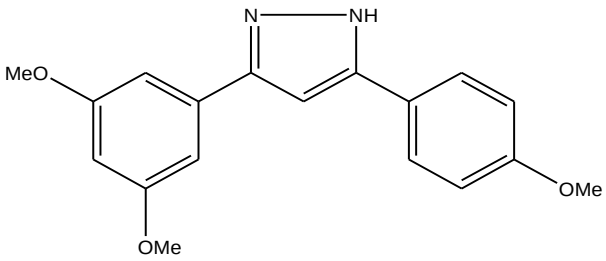

Brown crystals (0.85g, 87%), mp 71-73^{o}C; δ_H ($CDCl_3$) 3.75 (6H, s, OCH_3), 3.81 (3H, s, OCH_3), 6.41 (1H, s, Ar-H), 6.67 (1H, s, Ar-H), 6.86-6.89 (4H, m, Ar-H), 7.58 (2H, s, Ar-H); δ_C ($CDCl_3$) 55.3, 99.6, 100.5, 103.7, 114.3, 123.6, 126.9, 133.6, 159.7, 161.1; m/z (Electrospray)$^+$ Found 311.1390, $C_{18}H_{18}N_2O_3$ requires 311.1390; m/z (Electrospray)$^+$ 311 ([M+H]$^+$, 100%); υ_{max} (KBr) /cm^{-1} 3132 (N-H).

3-(4-methoxyphenyl)-5-(3,5-dimethoxyphenyl)pyrazole, DMU 10113

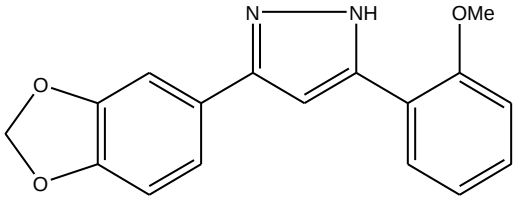

Brown crystals (0.78g, 70%), mp 136-138ºC; δ_H ($CDCl_3$) 3.90 (3H, s, OCH_3), 5.98 (2H, s, OCH_2O), 6.68 (1H, s, Ar-H, C4-H), 6.80 (1H, d, Ar-H), 6.88 (1H, d, Ar-H), 7.10-7.19 (2H, m, Ar-H), 7.22 (2H, d, Ar-H); m/z (Electrospray)$^+$ Found 325.1181, $C_{18}H_{16}N_2O_4$ requires 325.1183; m/z (Electrospray)$^+$ 325 ([M+H]$^+$, 100%); υ_{max} (KBr) /cm^{-1} 3325 (N-H).

3-(3, 4-dimethoxyphenyl)-5-(4-butoxyphenyl)pyrazole, DMU 10114

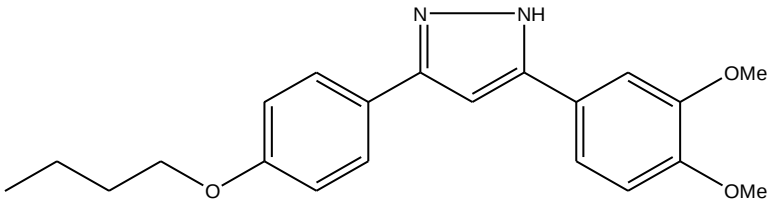

Brown crystals (0.87g, 65%), mp 74-76ºC; δ_H ($CDCl_3$) 1.00 (3H, t, CH_3), 1.52 (2H, q, CH_2), 1.74-1.83 (2H, m, CH_2), 3.90 (3H, s, OCH_3), 3.92 (3H, s, OCH_3), 4.0 (2H, t, CH_2), 6.70 (1H, s, Ar-H), 6.89-6.98 (3H, m, Ar-H), 7.39 (2H, d, Ar-H), 7.60 (2H, d, Ar-H); δ_C ($CDCl_3$) 13.9, 19.3, 31.3, 55.6, 55.8, 67.7, 98.6, 108.6, 111.1, 114.5, 118.2, 123.5, 124.7, 126.8, 147.8, 148.8, 149.0, 149.2, 159.1; m/z (Electrospray)$^+$ Found 353.1854, $C_{18}H_{18}N_2O_3$ requires 353.1851; m/z (Electrospray)$^+$ 353 ([M+H]$^+$, 100%)υ_{max} (KBr) /cm^{-1} 3328 (N-H).

3-(3,4-dimethoxyphenyl)-5-(4-methoxyphenyl)pyrazole, DMU 10116

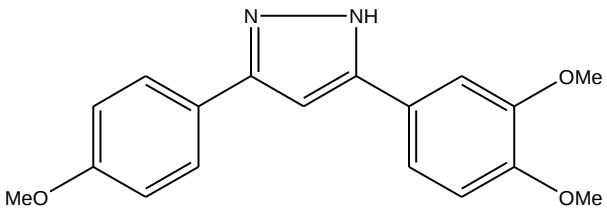

Brown crystals (0.78g, 66%), mp 75-77°C; δ_H ($CDCl_3$) 3.86 (3H, s, OCH_3), 3.92 (3H, s, OCH_3), 3.96 (3H, s, OCH_3), 6.70 (1H, s, Ar-H), 6.90-7.00 (3H, m, Ar-H), 7.30 (2H, d, Ar-H), 7.63 (2H, d, Ar-H); δ_C ($CDCl_3$) 55.3, 55.8, 55.9, 99.0, 108.9, 111.4, 114.3, 118.3, 123.6, 124.6, 126.9, 149.2, 159.8, 175.4; m/z (Electrospray)$^+$ 311 ($[M+H]^+$, 100%); υ_{max} (KBr) /cm^{-1} 3328 (N-H).

3-(2,4-dimethoxyphenyl)-5-(4-methoxyphenyl)pyrazole, DMU 10117

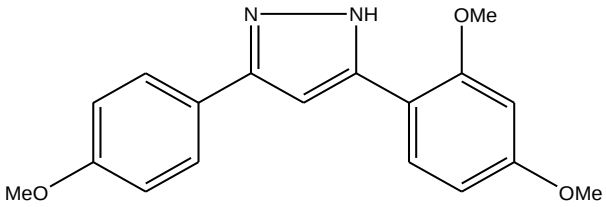

Brown crystals (1.06g, 90%), mp 126-128°C; δ_H ($CDCl_3$) 3.87 (3H, s, OCH_3), 3.88 (3H, s, OCH_3), 4.04 (3H, s, OCH_3), 6.60-6.64 (2H, m, Ar-H), 6.79 (1H, s, Ar-H, C4-H), 6.97 (2H, d, Ar-H), 7.65 (1H, d, Ar-H), 7.75 (2H, d, Ar-H); δ_C ($CDCl_3$) 55.3, 55.5, 55.7, 98.7, 98.9, 105.6, 110.8, 114.1, 125.7, 126.9, 128.8, 141.9, 150.2, 157.3, 159.5, 160.9, 175.5; m/z (Electrospray)$^+$ 311 ($[M+H]^+$, 100%); υ_{max} (KBr) /cm^{-1} 3315 (N-H).

3-(2-methoxyphenyl)-5-(2-methoxyphenyl)pyrazole, DMU 10120

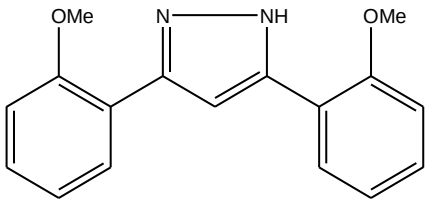

Brown oily residue (0.69g, 73%), δ_H ($CDCl_3$) 3.90 (6H, s, OCH_3), 7.00-7.09 (4H, m, Ar-H), 7.18 (1H, s, Ar-H, C4-H), 7.28-7.34 (2H, m, Ar-H), 7.99 (2H, d, Ar-H); δ_C ($CDCl_3$) 55.7, 103.8, 111.5, 121.2, 128.4, 128.9, 156.4; m/z (Electrospray)$^+$ 281 ($[M+H]^+$, 100%); υ_{max} (neat) /cm^{-1} 3250 (N-H).

3-(4-chloromethoxyphenyl)-5-(4-chloromethoxyphenyl)pyrazole, DMU 10121

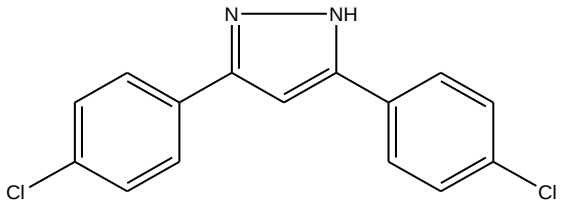

Light brown crystals (0.80g, 73%), mp 240-242°C; δ_H ($CDCl_3$) 6.82 (1H, s, Ar-H), 7.44 (4H, d, Ar-H), 7.66 (4H, d, Ar-H); δ_C ($CDCl_3$) 55.6, 103.8, 111.6, 119.7, 121.2, 128.3, 129.2, 143.9, 156.5, 176.0; m/z (Electrospray)$^+$ 289 ($[M+ H]^+$, 100, Cl-35), 291 ($[M+H]^+$, 60%, Cl-37); υ_{max} (KBr) /cm^{-1} 3124 (N-H).

3-(3,4-dimethoxyphenyl)-5-(4-propoxyphenyl)pyrazole, DMU 10123

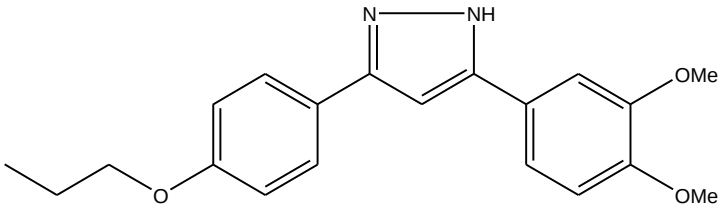

Brown oily residue (0.81g, 63%); δ_H ($CDCl_3$) 1.04 (3H, t, CH_3), 1.84 (2H, q, CH_2), 3.90 (6H, s, OCH_3), 3.93 (2H, t, CH_2), 6.70 (1H, s, Ar-H), 6.88-6.94 (3H, m, Ar-H), 7.27 (2H, s, Ar-H), 7.59 (2H, d, Ar-H); δ_C ($CDCl_3$) 10.5, 18.4, 22.6, 56.0, 58.5, 69.7, 99.2, 109.0, 111.5, 115.0, 118.3, 123.4, 124.7, 126.9, 147.7, 149.3, 159.5; m/z (Electrospray)$^+$ 339 ($[M+H]^+$, 100%); υ_{max} (neat) /cm^{-1} 3215 (N-H).

9.5 General Procedure for the Synthesis of Substituted Amino-Pyrimidines

A solution of the chalcone (9 mmol), guanidine hydrochloride (1.29 g, 13.5 mmol) and aqueous potassium hydroxide (4.94 cm^3, 50% w/v, 36 mmol) in ethanol (30 cm^3) was heated at reflux for 6 h. Hydrogen peroxide solution (1.84 cm^3, 50% w/v, 27 mmol) was added drop-wise to the solution and reflux continued for 1 h. The reaction was quenched with water (40 cm^3) and the resulting mixture extracted with dichloromethane (3 x 50 cm^3). The combined

organic extracts were dried ($MgSO_4$) and the solvent removed *in vacuo*. The pyrimidine was purified by either recrystalisation from methanol or ethanol, or by flash chromatography on silica gel using ethyl acetate − hexane (6:4) as eluent.

2-amino-4,6-diphenylpyrimidine, DMU 10200

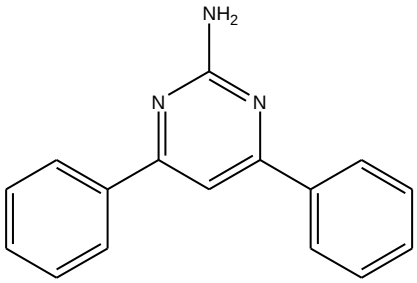

Beige crystals (0.67g, 30%), mp 119-121°C; δ_H ($CDCl_3$) 5.20 (2H, s, NH_2), 7.44-7.54 (7H, m, Ar-H), 8.00-8.09 (4H, m, Ar-H); δ_C ($CDCl_3$) 104.4, 127.1, 128.8, 130.5, 137.8, 163.6, 166.3, m/z $(CI)^+$ 248 ($[M+H]^+$ 100%); υ_{max} (KBr) /cm^{-1} 3320 (N-H).

2-amino-4-(4-methoxyphenyl)-6-(3,4,5-trimethoxyphenyl)pyrimidine, DMU 10201

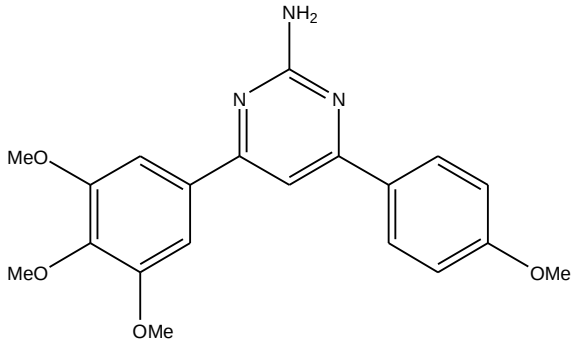

Beige crystals (1.02 g, 31%), mp 142-144°C; δ_H ($CDCl_3$) 3.88 (3H, s, OCH_3), 3.91 (3H, s, OCH_3), 3.98 (3H, s, OCH_3), 5.10 (2H, s, NH_2), 7.00 (2H, d, Ar-H), 7.30 (2H, s, Ar-H), 7.34 (1H, s, Ar-H, C5), 8.04 (2H, d, Ar-H); δ_C ($CDCl_3$) 55.4, 56.3, 61.0, 103.3, 103.8, 104.4, 114.1, 128.6, 130.1, 133.4, 140.2, 153.5, 161.7, 163.4, 165.7; m/z $(CI)^+$ 368 ($[M+H]^+$ 100%), υ_{max} (KBr) /cm^{-1} 3380 (N-H).

2-amino-6-(3,4-methylenedioxyphenyl)-4-(3,4,5-trimethoxyphenyl)pyrimidine, DMU 10202

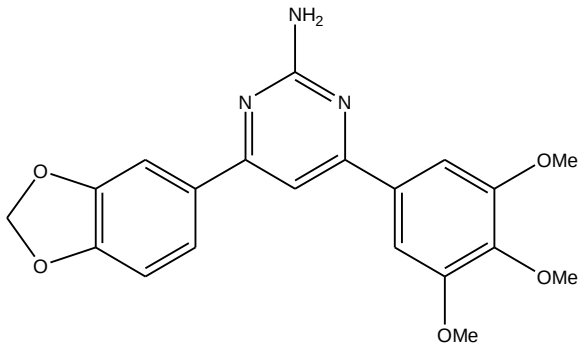

Light brown crystals (0.31g, 9%), mp 192-193ºC; δ_H ($CDCl_3$) 3.91 (3H, s, OCH_3), 3.98 (6H, s, OCH_3), 5.08 (2H, s, NH_2), 6.05 (2H, s, OCH_2O), 6.90 (2H, d, Ar-H), 7.30 (3H, d, Ar-H), 7.59 (1H, s, Ar-H, C5), 7.62 (1H, d, Ar-H); m/z (Electrospray)$^+$ 382 ($[M+H]^+$ 100%); υ_{max} (KBr) /cm^{-1} 3360 (N-H).

2-amino-4-(3,4-methylenedioxyphenyl)-6-(3,4-methylenedioxyphenyl)-pyrimidine, DMU 10203

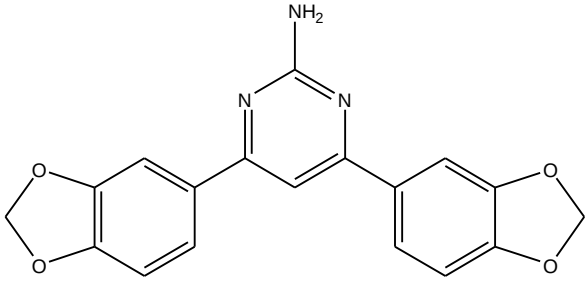

Off white crystals (0.99g, 33%), mp 222-224ºC; δ_H (DMSO-d_6) 5.46 (2H, s, NH_2), 6.04 (4H, s, 2 x OCH_2O), 6.90 (2H, d, Ar-H), 7.51 (2H, s, Ar-H), 7.58-7.67 (3H, m, Ar-H); δ_C (DMSO-d_6) 55.0, 56.0, 60.3, 97.7, 104.7, 113.9, 128.9, 152.9, 159.0, 162.1; m/z (Cl, NH_3)$^+$ 336 ($[M+H]^+$ 100%); υ_{max} (KBr) /cm^{-1} 3300 (N-H).

2-amino-4-(3,4-dimethoxyphenyl)-6-(3,4-methylenedioxyphenyl)pyrimidine, DMU 10214

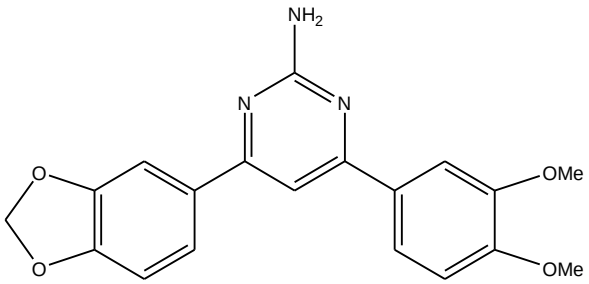

Beige crystals (0.79g, 25%), mp 180-182ºC; δ_H ($CDCl_3$) 3.94 (3H, s, OCH_3), 4.00(3H, s, OCH_3), 5.09 (2H, s, NH_2), 6.03 (2H, s, OCH_2O), 6.90 (1H, d, Ar-H), 6.94 (1H, d, Ar-H), 7.32 (1H, s, Ar-H, C5), 7.58 (1H, s, Ar-H), 7.61 (2H, d, Ar-H), 7.69 (1H, s, Ar-H); δ_C ($CDCl_3$) 56.1, 101.5, 103.0, 107.4, 108.4, 110.1, 111.0, 120.1, 121.69, 130.5, 132.2, 148.3, 149.3, 151.2, 163.4, 165.3; m/z (Cl, NH_3)$^+$ 352 ([M+H]$^+$ 100%); υ_{max} (KBr) /cm^{-1} 3390 (N-H).

2-amino-6-(3,4-methylenedioxyphenyl)-4-(2,3,4-trimethoxyphenyl)pyrimidine, DMU 10204

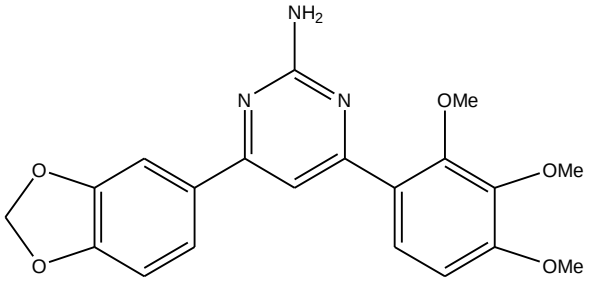

Light brown crystals (0.58g, 17%), mp 181-183ºC; δ_H ($CDCl_3$) 3.83 (3H, s, OCH_3), 3.91 (3H, s, OCH_3), 3.93 (3H, s, OCH_3), 5.04 (2H, s, NH_2), 6.04 (2H, s, CH_2O_2), 6.80 (1H, d, Ar-H), 6.90 (1H, d, Ar-H), 7.56-7.65 (4H, m, Ar-H); δ_C ($CDCl_3$) 56.1, 61.1, 61.5, 101.5, 107.4, 107.5, 107.7, 108.4, 121.7, 125.1, 132.2, 142.5, 148.2, 149.6, 152.9, 155.2, 163.3, 164.3, 164.7; m/z (Electrospray)$^+$ 382 ([M+H]$^+$ 100%); υ_{max} (KBr) /cm^{-1} 3440 (N-H).

2-amino-4-(2,4-dimethoxyphenyl)-6-(3,4-methylenedioxyphenyl)pyrimidine, DMU 10212

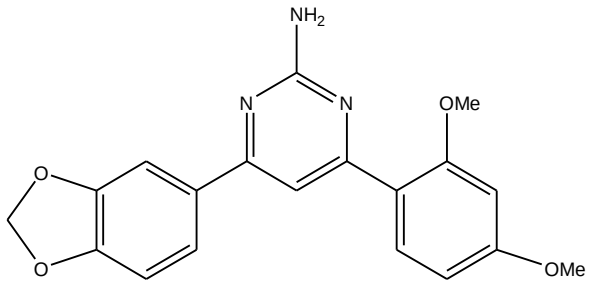

Beige crystals (0.98g, 31%), mp 133-135ºC; δ_H ($CDCl_3$) 3.87 (3H, s, OCH_3), 3.90 (3H, s, OCH_3), 5.02 (2H, s, NH_2), 6.03 (2H, s, CH_2O_2), 6.55 (1H, d, Ar-H), 6.61 (1H, d, Ar-H), 6.90 (1H, d, Ar-H), 7.53-7.61 (3H, m, Ar-H), 7.90 (1H, d, Ar-H); δ_C ($CDCl_3$) 55.7, 99.0, 101.4, 105.3, 107.5, 108.0, 108.4, 121.6, 131.8, 159.2, 164.3; m/z $(CI)^+$ 352 ($[M+H]^+$ 100%); υ_{max} (KBr) /cm^{-1} 3340 (N-H).

2-amino-4-(2,5-dimethoxyphenyl)-6-(3,4-methylenedioxyphenyl)pyrimidine, DMU 10205

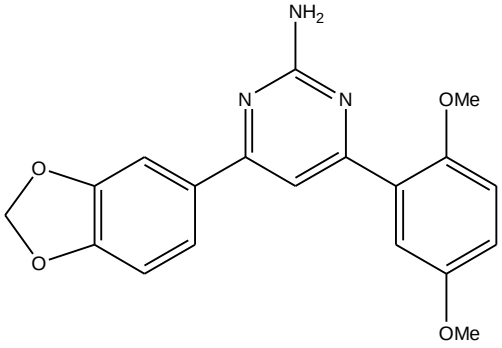

Beige crystals (0.35g, 11%), mp 133-135ºC; δ_H ($CDCl_3$) 3.84 (6H, s, 2 x OCH_3), 5.05 (2H, s, NH_2), 6.02 (2H, s, CH_2O_2), 6.89 (1H, d, Ar-H), 6.95 (2H, s, Ar-H), 7.43 (1H, s, Ar-H, C5), 7.53-7.60 (3H, m, Ar-H); m/z (Electrospray)$^+$ 352 ($[M+H]^+$ 100%).

2-amino-4-(4-methoxyphenyl)-6-(3,5-dimethoxyphenyl)pyrimidine, DMU 10206

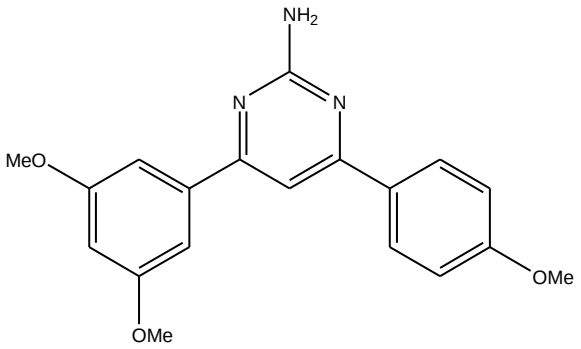

Pale yellow crystals (0.61g, 20%), mp 172-174ºC; δ_H ($CDCl_3$) 3.89 (9H, s, 3 x OCH_3), 5.12 (2H, s, NH_2), 6.60 (1H, s, Ar-H), 7.00 (2H, d, Ar-H), 7.20 (2H, s, Ar-H), 7.38 (1H, s, Ar-H, C5), 8.03 (2H, d, Ar-H); δ_C ($CDCl_3$) 60.3, 60.4, 106.9, 107.2, 110.0, 118.8, 133.6, 134.7, 144.9, 165.8, 166.4, 169.8; m/z (Electrospray)$^+$ 338 ([M+H]$^+$ 100%); υ_{max} (KBr) /cm^{-1} 3320 (N-H).

2-amino-4-(2-methoxyphenyl)-6-(3,4-methylenedioxyphenyl)pyrimidine, DMU 10213

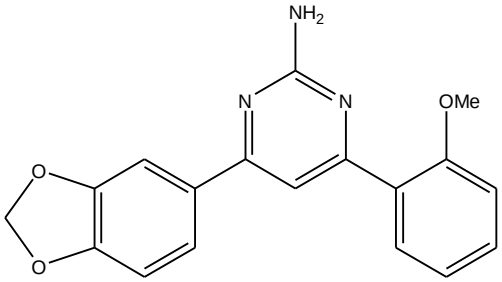

Light yellow crystals (0.92g, 32%), mp 142-144ºC; δ_H ($CDCl_3$) 3.90 (3H, s, OCH_3), 5.06 (2H, s, NH_2), 6.04 (2H, s, CH_2O_2), 6.90 (1H, d, Ar-H), 7.02 (1H, d, Ar-H), 7.08 (1H, t, Ar-H), 7.42 (1H, t, Ar-H), 7.52 (1H, s, Ar-H, C5), 7.54-7.61 (2H, m, Ar-H), 7.82 (1H, d, Ar-H); δ_C ($CDCl_3$) 55.8, 101.5, 107.5, 108.4, 108.5, 111.6, 121.0, 121.7, 127.5, 130.7, 131.0, 132.3, 148.2, 149.5, 157.6, 163.3, 164.4, 164.9; m/z (Electrospray)$^+$ Found 322.1189, $C_{18}H_{15}N_30_3$ requires 322.1186; m/z (Electrospray)$^+$ 322 ([M+H]$^+$, 100); υ_{max} (KBr) /cm^{-1} 3320 (N-H).

2-amino-4-(3,4-dimethoxyphenyl)-6-(4-methoxyphenyl)pyrimidine, DMU 10207

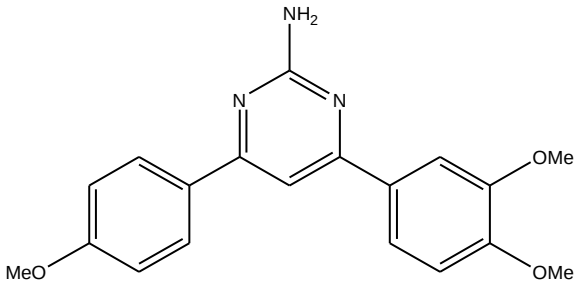

Off white crystals (0.67g, 22%), mp 145-147ºC; δ_H ($CDCl_3$) 3.88 (3H, s, OCH_3), 3.96 (3H, s, OCH_3), 4.00 (3H, s, OCH_3), 5.10 (2H, s, NH_2), 6.96 (1H, d, Ar-H), 7.01 (2H, d, Ar-H), 7.39 (1H, s, Ar-H, C5), 7.63 (1H, d, Ar-H), 7.70 (1H, s, Ar-H), 8.05 (2H, d, Ar-H); δ_C ($CDCl_3$) 55.4, 55.9, 56.0, 102.8, 109.9, 110.2, 114.1, 120.1, 128.4, 128.6, 130.2, 130.6, 149.1, 151.1, 161.6, 163.5, 165.4; m/z (Electrospray)$^+$ 338 ($[M+H]^+$, 100); υ_{max} (KBr) /cm^{-1} 3320 (N-H).

2-amino-4-(2,4-dimethoxyphenyl)-6-(4-methoxyphenyl)pyrimidine, DMU 10208

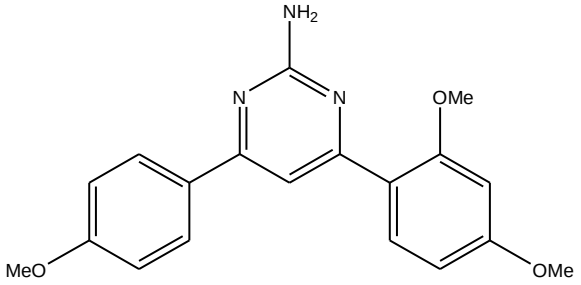

Light yellow crystals (0.45g, 15%), mp 119-121ºC; δ_H ($CDCl_3$) 3.88 (6H, s, 2 x OCH_3), 3.90 (3H, s, OCH_3), 5.00 (2H, s, NH_2), 6.56 (1H, s, Ar-H), 6.62 (1H, d, Ar-H), 6.99 (2H, d, Ar-H), 7.60 (1H, s, Ar-H, C5), 7.90 (1H, d, Ar-H), 8.00 (2H, d, Ar-H); δ_C ($CDCl_3$) 55.4, 55.5, 55.7, 99.0, 105.1, 107.9, 114.0, 120.2, 128.6, 130.6, 131.8, 159.1, 161.4, 162.3, 163.3, 164.2, 164.5; m/z (Electrospray)$^+$ 338 ($[M+H]^+$, 100); υ_{max} (KBr) /cm^{-1} 3300 (N-H).

2-amino-4-(4-methoxyphenyl)-6-(3,4-methylenedioxyphenyl)pyrimidine, DMU 10209

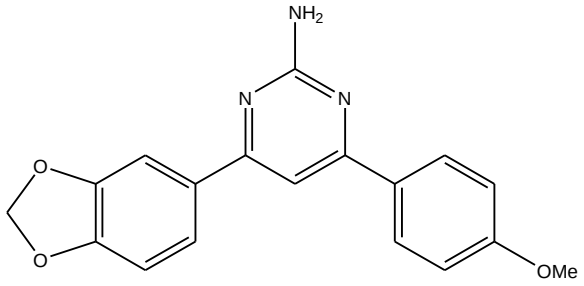

Beige crystals (0.84g, 29%), mp 132-134ºC; δ_H (DMSO-d_6) 3.84 (3H, s, OCH_3), 6.12 (2H, s, CH_2O_2), 6.59 (2H, s, NH_2), 7.02-7.10 (3H, m, Ar-H), 7.60 (1H, s, Ar-H, C5), 7.77-7.86 (2H, m, Ar-H), 8.20 (2H, d, Ar-H); δ_C (DMSO-d_6) 55.3, 94.5, 100.4, 101.5, 106.9, 108.2, 113.8, 121.5, 128.5, 129.7, 131.6, 147.8, 149.1, 161.1, 163.8, 164.2; m/z (Electrospray)$^+$ 322 ($[M+H]^+$, 100); υ_{max} (KBr) /cm^{-1} 3360 (N-H).

2-amino-4-(3, 5-dimethoxyphenyl)-6-(3,4-methylenedioxyphenyl)pyrimidine, DMU 10210

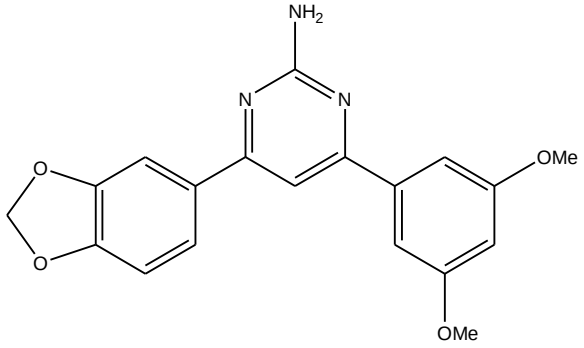

Beige crystals (1.01g, 32%), mp 125-127ºC; δ_H ($CDCl_3$) 3.89 (6H, s, 2 x OCH_3), 5.10 (2H, s, NH_2), 6.05 (2H, s, CH_2O_2), 6.60 (1H, s, Ar-H), 6.91 (1H, d, Ar-H), 7.19 (2H, s, Ar-H), 7.33 (1H, s, Ar-H, C5), 7.58-7.64 (2H, m, Ar-H); m/z (Electrospray)$^+$ 352 ($[M+H]^+$ 100%); υ_{max} (KBr) /cm^{-1} 3340 (N-H).

4-(3-methoxyphenyl)-6-(3,4-methylenedioxyphenyl)-2-amino-pyrimidine, DMU 10211

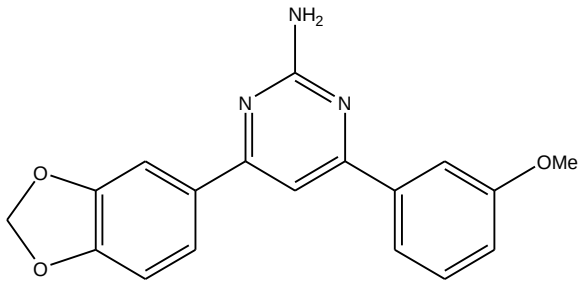

Yellow crystals (0.93g, 32%), mp 134-136ºC; δ_H ($CDCl_3$) 3.88 (3H, s, OCH_3), 5.17 (2H, s, NH_2), 6.03 (2H, s, OCH_2O), 6.90 (1H, d, Ar-H), 6.99 (2H, d, Ar-H), 7.31 (1H, d, Ar-H, C5), 7.58 (1H, s, Ar-H), 7.60 (1H, d, Ar-H), 8.03 (2H, d, Ar-H); δ_C ($CDCl_3$) 55.4, 101.6, 103.8, 107.4, 108.2, 112.2, 116.4, 119.5, 121.7, 129.8, 131.9, 139.3, 148.3, 149.7, 160.0, 163.5, 165.5, 165.9; m/z (Electrospray)$^+$ 322 ($[M+H]^+$, 100); υ_{max} (KBr) /cm^{-1} 3310 (N-H).

9.6 General Procedure for the Synthesis of Substituted Pyrimidones

Sodium nitrite solution (1.08 cm^3, 50% w/v, 7.8 mmol) was added to a refluxing solution of the amino-pyrimidine (1.31 mmol) in glacial acetic acid (50 cm^3). After 3 h at reflux the solution was allowed to cool and the solvent removed *in vacuo*. The crude product was recrystallised from ethanol.

4, 6-diphenylpyrimidin-2-one, DMU 10300

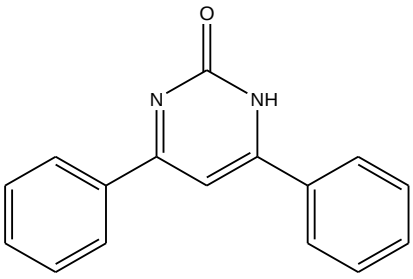

Off white crystals (0.24g, 75%), mp 221-223^{o}C; δ_H (DMSO-d_6) 7.40 (1H, s, Ar-H, C5), 7.48-7.56 (6H, m, Ar-H), 8.13-8.18 (4H, m, Ar-H); m/z (Electrospray)$^{+}$ 249 ([M+H]$^{+}$ 90%); υ_{max} (KBr) /cm^{-1} 1750 (C=O), 3440 (N-H).

4-(4-methoxyphenyl)-6-(3,4,5-trimethoxyphenyl)pyrimidin-2-one, DMU 10301

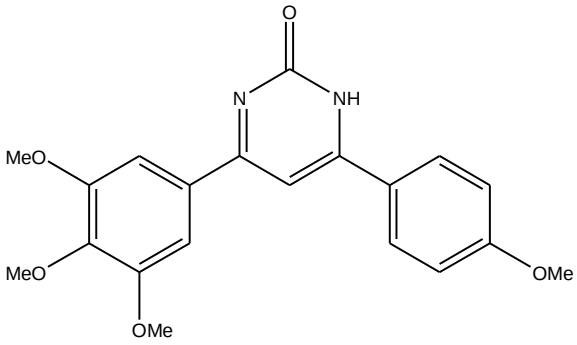

Light yellow crystals (0.42g, 85%), mp 275-277^{o}C; δ_H ($CDCl_3$) 3.92 (3H, s, OCH_3), 3.94 (3H, s, OCH_3), 4.00 (6H, s, 2 x OCH_3), 7.01 (1H, s, Ar-H, C5), 7.08 (2H, d, Ar-H), 7.30 (2H, s, Ar-H), 8.03 (2H, d, Ar-H); m/z (Electrospray)$^{+}$ 369 ([M+H]$^{+}$ 100%).

6-(3,4-methylenedioxyphenyl)-4-(3,4,5-trimethoxyphenyl)pyrimidin-2-one, DMU 10302

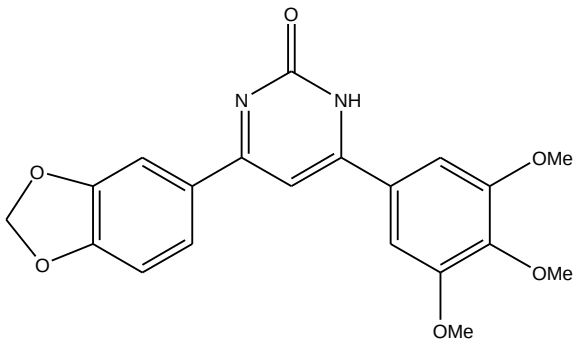

Dark orange crystals (0.015g, 3%), mp 271-273^{o}C; δ_H (DMSO-d_6) 3.74 (3H, s, OCH_3), 3.90 (6H, s, 2 x OCH_3), 6.15 (2H, s, OCH_2O), 7.10 (1H, d, Ar-H), 7.43 (3H, s, Ar-H), 7.76-7.85 (2H, m, Ar-H); m/z (CI, NH_3)$^{+}$ Found 383.1235, $C_{20}H_{19}N_2O_6$ requires 383.1238; m/z (CI, NH_3)$^{+}$ 383 ([M+H]$^{+}$, 100%).

4-(3,4-methylenedioxyphenyl)-6-(3,4-methylenedioxyphenyl)pyrimidin-2-one, DMU 10303

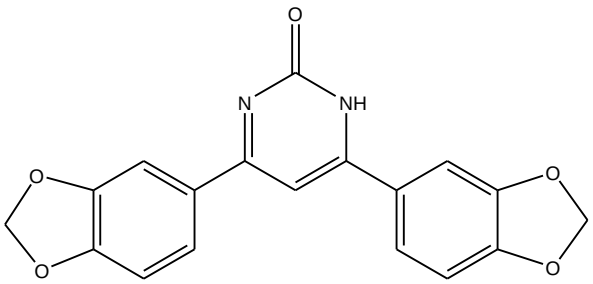

Light brown crystals (0.29g, 65%), mp 296-298^{o}C; δ_H (DMSO-d_6) 6.15 (2H, s, 2 x OCH_2O), 7.08 (2H, d, Ar-H), 7.45 (1H, s, Ar-H, C5), 7.74-7.82 (4H, m, Ar-H); m/z (CI, NH_3)$^+$ 337 ([M+H]$^+$, 100%); υ_{max} (KBr) /cm^{-1} 1640 (C=O), 3440 (N-H).

4-(3,4-dimethoxyphenyl)-6-(3,4-methylenedioxyphenyl)pyrimidin-2-one, DMU 10314

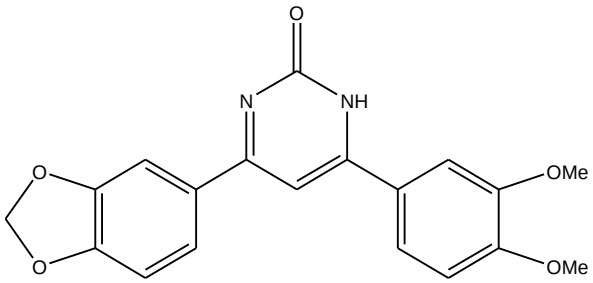

Light brown crystals (0..33g, 72%), mp 290-292^{o}C; δ_H (DMSO-d_6) 3.87 (3H, s, OCH_3), 3.90 (3H, s, OCH_3), 6.15 (2H, s, OCH_2O), 7.10 (2H, t, Ar-H), 7.42 (1H, s, Ar-H, C5), 7.70 (1H, s, Ar-H), 7.74-7.83 (3H, m, Ar-H); m/z [electrospray]$^+$ 353 ([M+H]$^+$, 79%); υ_{max} (KBr) /cm^{-1} 1630 (C=O), 3440 (N-H).

6-(3,4-methylenedioxyphenyl)-4-(2,3,4-trimethoxyphenyl)pyrimidin-2-one, DMU 10304

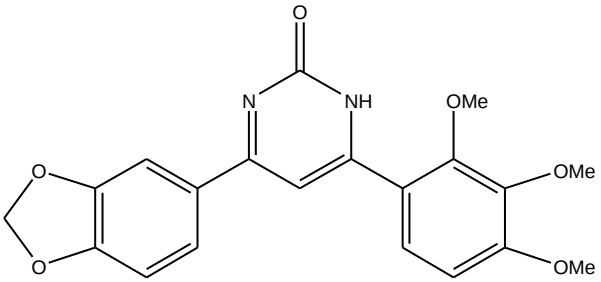

Pale yellow crystals (0.42g, 84%), mp 261-263ºC; δ_H (DMSO-d_6) 3.80 (6H, s, 2 x OCH_3), 3.90 (3H, s, OCH_3), 6.13 (2H, s, OCH_2O), 6.96 (1H, d, Ar-H), 7.05 (1H, d, Ar-H), 7.12 (1H, s, Ar-H, C5), 7.42 (1H, d, Ar-H), 7.65 (1H, d, Ar-H), 7.69 (1H, dd, Ar-H); δ_C (DMSO-d_6) 56.1, 60.6, 61.3, 107.2, 108.4, 124.9, 148.0, 155.6; m/z (Electrospray)$^+$ Found 383.1234, $C_{20}H_{18}N_2O_6$ requires 383.1236; m/z (Electrospray)$^+$ 353 ([M+H]$^+$, 100%); υ_{max} (KBr) /cm^{-1} 1685 (C=O).

4-(2,4-dimethoxyphenyl)-6-(3,4-methylenedioxyphenyl)pyrimidin-2-one, DMU 10312

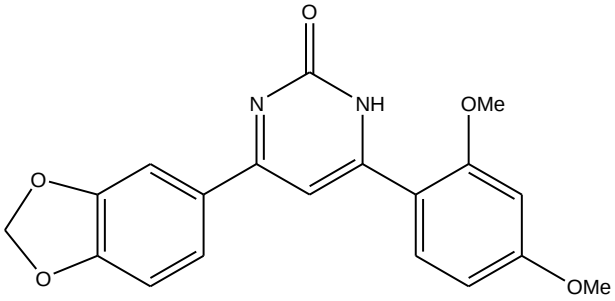

Orange crystals (0.39g, 84%), mp 198-200ºC; δ_H ($CDCl_3$) 3.90 (3H, s, OCH_3), 3.98 (3H, s, OCH_3), 6.05 (2H, s, OCH_2O), 6.59 (1H, d, Ar-H), 6.66 (1H, d, Ar-H), 6.87-6.94 (2H, m, Ar-H), 7.64-7.71 (3H, m, Ar-H); δ_C ($CDCl_3$) 55.7, 56.1, 99.4, 101.8, 106.5, 108.1, 108.3, 123.0, 131.1, 148.4, 150.9, 159.2, 164.1; m/z (Cl, NH_3)$^+$ Found 353.1137, $C_{19}H_{17}N_2O_5$ requires 353.1132; m/z (Cl, NH_3)$^+$ 353 ([M+H]$^+$, 53%); υ_{max} (KBr) /cm^{-1} 1680 (C=O).

4-(2,5-dimethoxyphenyl)-6-(3,4-methylenedioxyphenyl)pyrimidin-2-one, DMU 10305

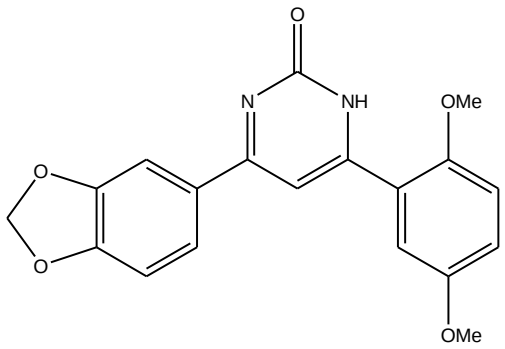

Pale yellow crystals (0.33g, 72%), mp 244-246ºC; δ_H (DMSO-d_6) 4.78 (3H, s, OCH_3), 4.80 (3H, s, OCH_3), 6.65 (2H, s, OCH_2O), 7.05 (1H, d, Ar-H), 7.10 (1H, d, Ar-H), 7.18-7.11 (2H, m, Ar-H), 7.20 (1H, d, Ar-H), 7.78 (1H, s, Ar-H), 7.83 (1H, d, Ar-H); m/z (Cl, NH_3)$^+$ Found 353.1135, $C_{19}H_{17}N_2O_5$ requires 353.1132; m/z (Cl, NH_3)$^+$ 353 ([M+H]$^+$, 56%); υ_{max} (KBr) /cm^{-1} 1680 (C=O).

6-(3,5-dimethoxyphenyl)-4-(4-methoxyphenyl)pyrimidin-2-one, DMU 10306

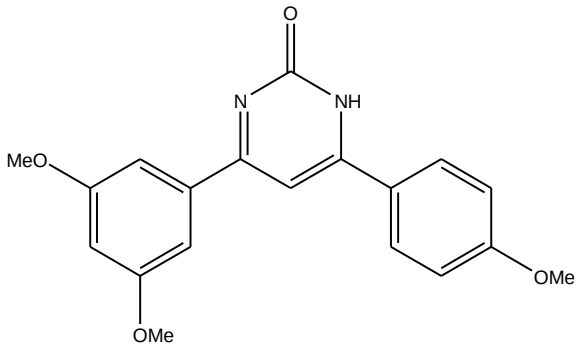

Pale yellow crystals (0.25g, 56%), mp 231-233ºC; δ_H (DMSO-d_6) 3.85 (9H, s, 3 x OCH_3), 6.70 (1H, t, Ar-H), 7.09 (2H, d, Ar-H), 7.29 (2H, d, Ar-H), 7.48 (1H, s, Ar-H, C5), 8.18 (2H, d, Ar-H); δ_C (DMSO-d_6) 55.5, 103.4, 105.4, 114.1, 129.5, 160.7, 162.1; m/z (CI, NH_3)$^+$ 339 ([M+H]$^+$, 100%); υ_{max} (KBr) /cm^{-1} 1770 (C=O), 3460 (N-H).

4-(2-methoxyphenyl)-6-(3,4-methylenedioxyphenyl)pyrimidin-2-one, DMU 10313

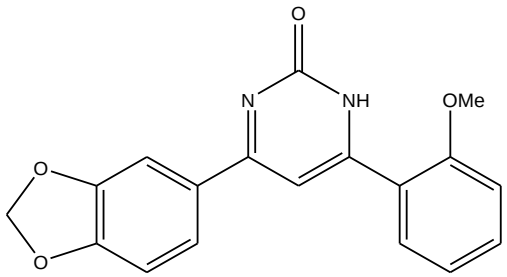

Yellow crystals (0.36g, 85%), m.p. 166-167ºC; δ_H (DMSO-d_6) 3.90 (3H, s, OMe), 6.10 (2H, s, OCH_2O), 6.90-7.10 (3H, m, Ar-H), 7.25(1H, d, Ar-H), 7.50-7.60 (1H, m, Ar-H), 7.65-7.70 (1H, m, Ar-H), 7.8 (1H, s, Ar-H); δc (DMSO-d_6) 56.1, 101.6, 102.2, 107.7, 108.8, 112.3, 120.9, 122.6, 123.2, 130.6, 132.7, 148.3, 150.6, 157.4, 158.2, 172.3; m/z [MALDI$^+$] 322 ($[M]^+$); υ_{max} (KBr) /cm^{-1}1663 (C=O).

4-(3,4-dimethoxyphenyl)-6-(4-methoxyphenyl)pyrimidin-2-one, DMU 10307

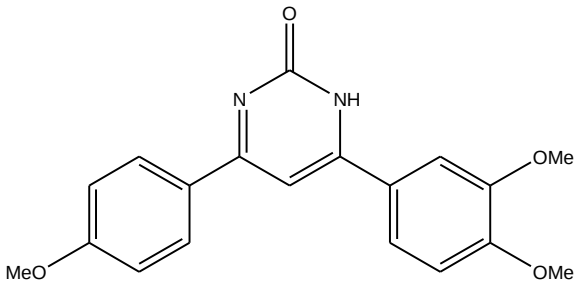

Light brown crystals (0.35g, 78%), mp 253-255ºC; δ_H ($CDCl_3$) 3.90 (3H, s, OCH_3), 3.98 (3H, s, OCH_3), 4.06 (3H, s, OCH_3), 7.00 (1H, d, Ar-H), 7.03-7.13 (3H, m, Ar-H), 7.63 (1H, dd, Ar-H), 7.77 (1H, s, Ar-H, C5), 8.06 (1H, d, Ar-H); m/z (CI, NH_3)$^+$ 339 ($[M+H]^+$, 100%); υ_{max} (KBr) /cm^{-1} 1650 (C=O), 3460 (N-H).

4-(2,4-dimethoxyphenyl)-6-methoxyphenyl)pyrimidin-2-one, DMU 10309

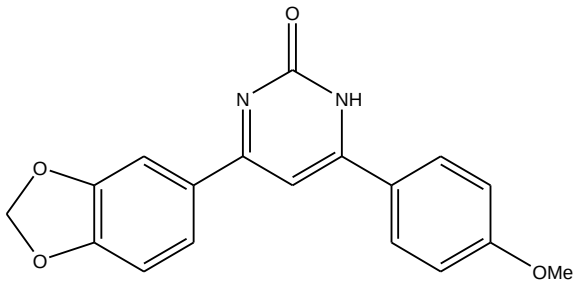

Light yellow crystals (0.20g, 47%), mp 300-302ºC; δ_H (DMSO-d_6) 3.85 (3H, s, OCH_3), 6.18 (2H, s, OCH_2O), 7.06 (1H, d, Ar-H), 7.10 (2H, d, Ar-H), 7.43 (1H, s, Ar-H, C5), 7.74-7.80 (2H, m, Ar-H), 8.18 (2H, d, Ar-H); δ_C (DMSO-d_6) 55.4, 56.0, 101.8, 107.4, 108.4, 114.1, 122.7, 129.3, 147.9, 150.1, 162.0; m/z (Cl, NH_3)$^+$ Found 323.1028, $C_{18}H_{15}N_2O4$ requires 323.1026; m/z (Cl, NH_3)$^+$ 323 ([M+H]$^+$, 59%).

4-(3,5-dimethoxyphenyl)-6-(3,4-methylenedioxyphenyl)pyrimidin-2-one, DMU 10310

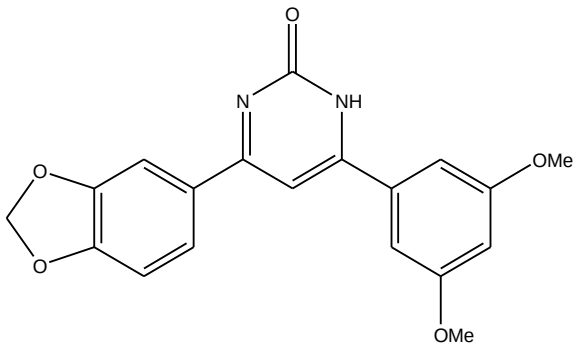

Pale yellow crystals (0.37g, 73%), mp 272-274ºC; δ_H (DMSO-d_6) 3.88 (6H, s, 2 x OCH_3), 6.13 (2H, s, OCH_2O), 6.67 (1H, d, Ar-H), 7.02 (1H, d, Ar-H), 7.27 (2H, s, Ar-H), 7.42 (1H, s, Ar-H), 7.75-7.85 (2H, m, Ar-H); δ_C (DMSO-d_6) 55.5, 101.8, 103.5, 105.4, 107.5, 108.4, 122.9, 148.0, 150.2, 160.7; m/z (Electrospray)$^+$ Found 353.1135, $C_{19}H_{17}N_2O_6$ requires 353.1136; m/z (Electrospray)$^+$ 353 ([M+H]$^+$, 100%); υ_{max} (KBr) /cm^{-1} 1645 (C=O).

4-(3,5-dimethoxyphenyl)-6-(3,4-methylenedioxyphenyl)pyrimidin-2-one, DMU 10311

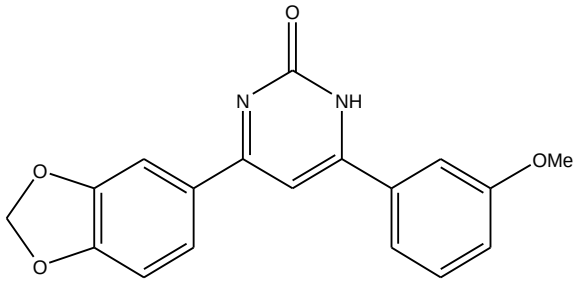

Pale yellow crystals (0.32g, 76%), mp 269-271°C; δ_H (DMSO-d_6) 3.86 (3H, s, OCH_3), 6.15 (2H, s, OCH_2O), 7.08 (1H, d, Ar-H), 7.15 (1H, dd, Ar-H), 7.42-7.48 (2H, m, Ar-H), 7.68 (1H, s, Ar-H, C5), 7.72 (1H, d, Ar-H), 7.77-7.85 (2H, m, Ar-H); δ_C (DMSO-d_6) 55.4, 101.8, 107.4, 108.4, 112.4, 117.5, 119.9, 122.8, 129.9, 148.0, 150.2, 159.6; m/z (CI, NH_3)$^+$ 323 ($[M+H]^+$, 56%);

9.7 General Procedure for the Synthesis of Substituted Morpholino-Pyrimidines

A solution of the chalcone (1.60 mmol), 4-amidinomorpholine hydrobromide (0.50 g, 2.38 mmol) and aqueous sodium hydroxide (0.50 cm^3, 50% w/v, 6.40 mmol) in ethanol (20 cm^3) was heated at reflux for 6h. Hydrogen peroxide solution (0.33 cm^3, 50% w/v, 4.80 mmol) was added drop-wise to the solution and reflux continued for 1 h. The reaction was quenched with water (40 cm^3) and the resulting mixture extracted with dichloromethane (3 x 60 cm^3). The combined organic extracts were dried ($MgSO_4$) and the solvent removed *in vacuo*. The morpholino-pyrimidine was purified by either recrystalisation from methanol or ethanol, or by flash chromatography on silica gel using ethyl acetate − hexane (4:6) as eluent.

4-(3,4-dimethoxyphenyl)-6-(3,4-dimethoxyphenyl)-2-morpholinopyrimidine, DMU 10400

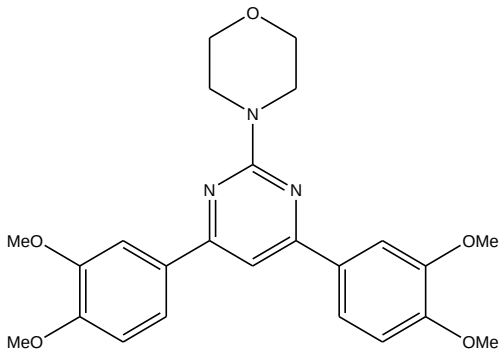

Yellow crystals (0.14g, 20%), mp 194-196ºC; δ_H ($CDCl_3$) 3.86 (4H, t, 2 x CH_2), 3.96 (6H, s, 2 x OCH_3), 3.98-4.04 (12H, m, 2 x OCH_3, 2 x CH_2), 6.80 (2H, d, Ar-H), 7.33 (1H, s, C-5), 7.68 (2H, d, Ar-H), 7.72 (2H, d, Ar-H); δ_C ($CDCl_3$) 44.5, 56.0, 56.1, 67.1, 101.3, 110.1, 110.9, 120.2, 131.0, 149.2, 151.2, 162.2, 164.6; m/z $(CI)^+$ 438 ($[M+H]^+$, 83%).

4-(3,4-methylenedioxyphenyl)-6-(3,4-methylenedioxyphenyl)-2-morpholinopyrimidine, DMU 10401

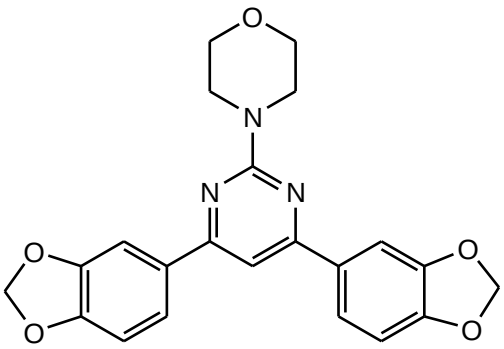

Yellow crystals (0.28g, 20%), mp 213-215ºC; δ_H ($CDCl_3$) 3.83 (4H, t, 2 x CH_2), 3.98 (4H, t, 2 x CH_2), 6.04 (2H, s, 2 x OCH_2O), 6.90 (2H, d, Ar-H), 7.24 (1H, s, C-5), 7.62 (3H, s, Ar-H), 7.64 (1H, d, Ar-H); δ_C ($CDCl_3$) 44.4, 67.0, 101.2, 101.5, 107.4, 108.3, 121.5, 132.5, 148.2, 149.6, 164.2; m/z (Electrospray)$^+$ 405 ($[M^+]$, 56%).

4-(4-methoxyphenyl)-6-(3,4,5-trimethoxyphenyl)-2-morpholinopyrimidine, DMU 10402

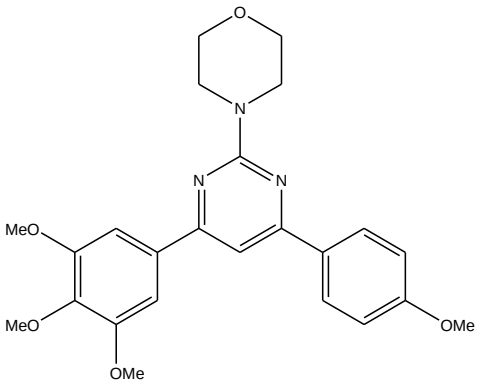

Beige crystals (0.16g, 31%), mp 135-137ºC; δ_H ($CDCl_3$) 3.75 (4H, t, 2 x CH_2), 3.82 (3H, s, OCH_3), 3.95 (3H, s, OCH_3), 3.88-3.96 (10H, m, 2 x OCH_3, 2 x CH_2), 6.93 (2H, d, Ar-H), 7.19 (2H, s, Ar-H), 7.22 (1H, s, C-5), 8.00 (2H, d, Ar-H); δ_C ($CDCl_3$) ; m/z $(CI)^+$ 408 ($[M+H]^+$, 87%).

4-(2-methoxyphenyl)-6-(3,4-methylenedioxyphenyl)-2-morpholinopyrimidine, DMU 10403

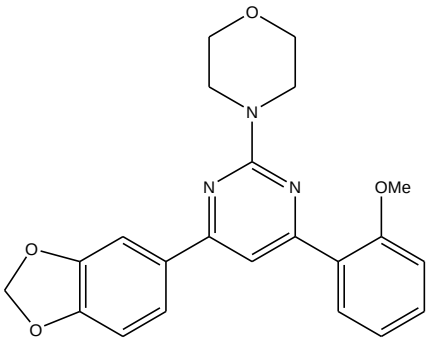

Oily residue (0.11g, 24%); δ_H ($CDCl_3$) 3.81 (4H, t, 2 x CH_2), 3.89 (3H, s, OCH_3), 3.95 (4H, t, 2 x CH_2), 6.01 (2H, s, OCH_2O), 6.89 (1H, d, Ar-H), 7.00 (1H, d, Ar-H), 7.07 (1H, t, Ar-H), 7.39 (1H, t, Ar-H), 7.56 (1H, s, Ar-H, C-5), 7.63 (2H, d, Ar-H), 7.95 (1H, d, Ar-H); δ_C ($CDCl_3$); m/z (Electrospray$^+$) Found 392.1605, $C_{22}H_{21}N_3O_4$ requires 392.1605; m/z (Electrospray$^+$) 392 ($[M+H]^+$, 100%).

4-(3,4-dimethoxyphenyl)-6-(4-methoxyphenyl)-2-morpholinopyrimidine, DMU 10404

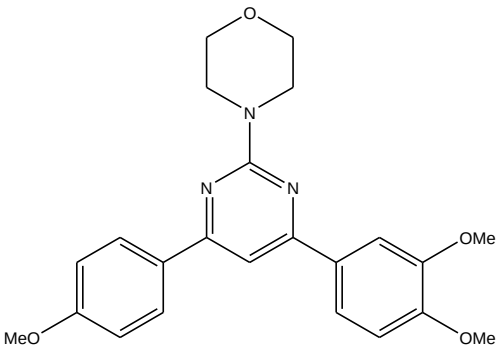

Yellow crystals (0.14g, 29%), mp 146-148ºC; δ_H ($CDCl_3$) 3.83 (4H, t, 2 x CH_2), 3.85 (3H, s, OCH_3), 3.95 (3H, s, OCH_3), 3.96-4.20 (7H, m, OCH_3, 2 x CH_2), 6.97 (1H, d, Ar-H), 7.00 (2H, d, Ar-H), 7.41 (1H, s, C-5), 7.70 (2H, d, Ar-H), 8.09 (2H, d, Ar-H); δ_C ($CDCl_3$) 44.5, 55.4, 56.1, 67.1, 101.1, 110.0, 110.9, 113.8, 120.2, 128.6, 130.7, 131.1, 149.1, 151.1, 161.6, 162.2, 164.5; m/z $(CI)^+$ 408 ([M+H], 100%).

4-(2,4-dimethoxyphenyl)-6-(4-methoxyphenyl)-2-morpholinopyrimidine, DMU 10405

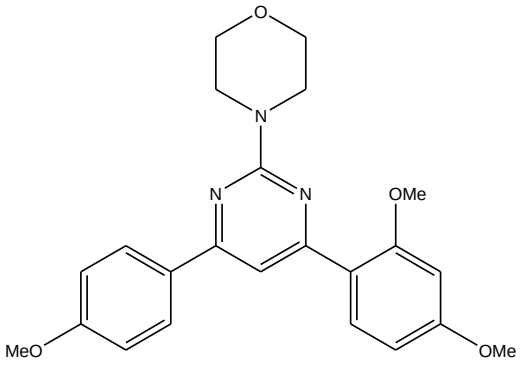

Light yellow crystals (0.13g, 26%), mp 145-147ºC; δ_H ($CDCl_3$) 3.82 (4H, t, 2 x CH_2), 3.87 (3H, s, 2 x OCH_3), 3.90 (3H, s, OCH_3), 3.96 (4H, t, 2 x CH_2), 6.56 (1H, d, Ar-H), 6.62 (1H, dd, Ar-H), 6.98 (2H, d, Ar-H), 7.63 (1H, s, C-5), 8.02 (1H, d, Ar-H), 8.05 (2H, d, Ar-H); δ_C ($CDCl_3$) 44.5, 55.4, 55.5, 55.8, 67.1, 99.0, 105.2, 106.3, 113.7, 120.6, 128.6, 131.1, 132.0, 159.4, 161.3, 162.1, 162.3, 163.2, 163.6; m/z $(CI)^+$ 408 ([M+H], 100%).

4-(3,5-dimethoxyphenyl)-6-(4-methoxyphenyl)-2-morpholinopyrimidine, DMU 10406

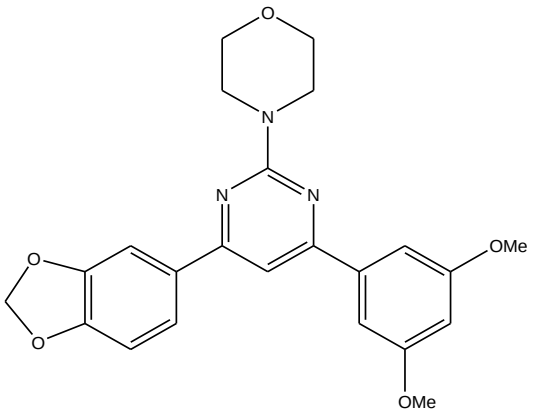

Light yellow crystals (0.13g, 23%), mp 181-183ºC; δ_H ($CDCl_3$) 3.82 (4H, t, 2 x CH_2), 3.88 (6H, s, 2 x OCH_3), 3.99 (4H, t, 2 x CH_2), 6.04 (2H, s, OCH_2O), 6.58 (1H, t, Ar-H), 6.90 (1H, d, Ar-H), 7.23 (2H, d, Ar-H), 7.28 (1H, s, C-5), 7.65 (2H, d, Ar-H); δ_C ($CDCl_3$) 44.5, 55.5, 67.0, 101.5, 101.9, 102.2, 105.4, 107.4, 108.3, 121.6, 140.4, 148.2, 149.7, 161.1, 162.1, 164.6, 164.9; m/z (Electrospray)$^+$ 422.1709, $C_{23}H_{23}N_3O_5$ requires 422.1710 m/z (Electrospray)$^+$ 422 ([M+H], 100%).

2-morpholino-4,6-diphenylpyrimidine, DMU 10408

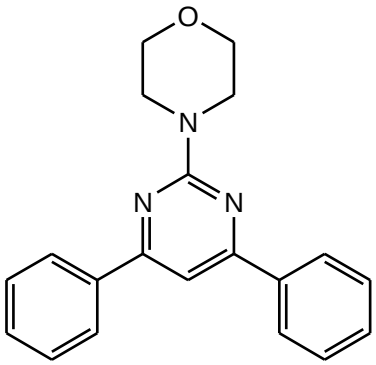

Light yellow crystals (0.12g, 36%), mp 121-123ºC; δ_H ($CDCl_3$) 3.84 (4H, t, CH_2), 4.02 (4H, t, CH_2), 7.44 (1H, s, C-5), 7.46-7.52 (6H, m, Ar-H), 8.08-8.15 (4H, m, Ar-H); δ_C ($CDCl_3$); m/z (Electrospray)$^+$ Found 318.1604, $C_{20}H_{19}N_3O$ requires 318.1601; m/z (Electrospray)$^+$ 318 ([M+H], 100%).

9.8 General Procedure for the Synthesis of Morpholino-Hydrochloride

S-methylisothiourea sulphate (5 g, 0.018 mol) and morpholine (3.14 ml, 0.036 mol) was stirred in water under reflux for 5 mins. A solution of aqueous barium chloride (11.24 cm^3, 50% w/v, 0.027 mol) was added and the reaction continued to stir under reflux for 1h. Once cool, the mixture was filtered through kieselguhr giving a colourless solution. The solvent was removed *in vacuo* leaving a white gum which was recrystallised from a mixture of ethanol and acetone (50:50). The product was obtained as white crystals which were collected by filtration.

Morpholino-Hydrochloride, DMU 10900

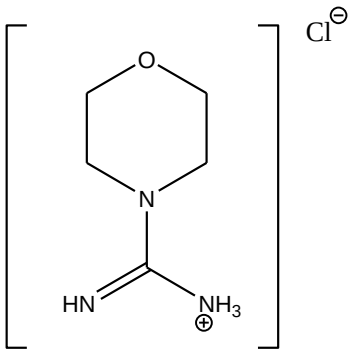

White crystals (0.15g, 5%), mp 190-192^oC; δ_H (DMSO-d_6) 3.52 (4H, t, 2 x CH_2), 3.83 (4H, t, 2 x CH_2); δ_C (DMSO-d_6); m/z (Electrospray)$^+$ 165 ($[M]^+$, 100%).

9.9 General Procedure for the Synthesis of Dimethylethylenediamino-Guanidine Hydrochloride

S-methylisothiourea sulphate (5 g, 0.018 mol) and *N*,*N*-dimethylethylenediamine (3.93 ml, 0.036 mols) was stirred in water under reflux for 5 minutes. A solution of aqueous barium chloride (11.24 cm^3, 50% w/v, 0.027 mol) was added and the reaction continued to stir under reflux for 1h. Once cool, the mixture was filtered through kieselguhr giving a colourless

solution. The solvent was removed *in vacuo* leaving a white gum which was recrystallised from a mixture of ethanol and acetone (50:50). The product was obtained as white crystals which were collected by filtration.

Dimethylethylenediamino-Guanidine Hydrochloride, DMU 10901

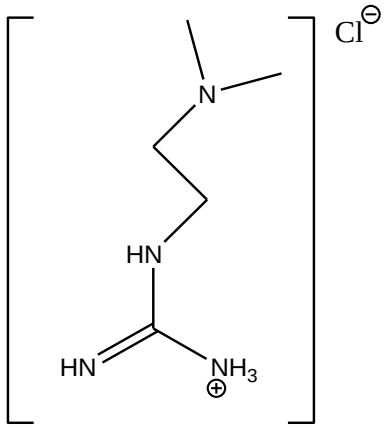

White crystals (0.21g, 7%), mp 221-223ºC; δ_H (DMSO-d_6) 2.39 (6H, s, 2 x CH_3), 2.78 (2H, t, CH_2), 3.39 (2H, t, CH_2); δ_C (D_2O) 36.5, 43.3, 55.6; m/z (Electrospray)$^+$ 166 ($[M]^+$, 29%); υ_{max} (KBr) /cm^{-1} 1600, 3470 (1º N-H), 3300 (2º N-H).

9.10 General procedure for the synthesis of substituted dimethylethylenediamino-pyrimidines

A solution of the chalcone (1.6 mmol), guanidinium-dimethylethyleneamine chloride (2.4 mmol) and aqueous sodium hydroxide (0.51 cm^3, 50% w/v, 6.4 mmol) in ethanol (10 cm^3) was heated at reflux for 24 h. The reaction was quenched with water (40 cm^3) and the organic mixture extracted with dichloromethane (3 x 50 cm^3). The combined organic extracts were dried ($MgSO_4$) and the solvent removed *in vacuo*. The morpholino-pyrimidine was purified by flash chromatography on silica gel using methanol-dichloromethane (1:9) as eluent.

4-(2,4-dimethoxyphenyl)-6-(3,4-methylenedioxyphenyl)-2-dimethylethylenediaminopyrimidine, DMU 10600

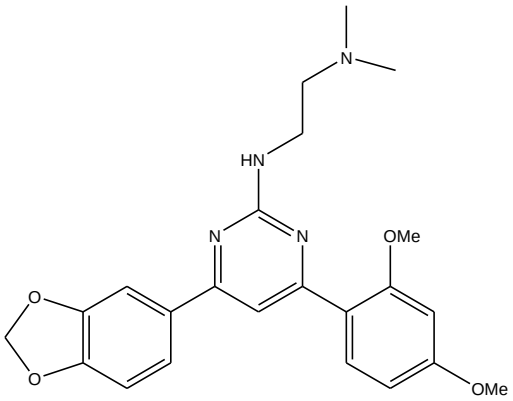

Light brown oil (0.26g, 39%), δ_H ($CDCl_3$) 2.66 (6H, s, 2 x CH_3), 3.07 (2H, t, CH_2), 3.82-3.92 (8H, m, CH_2, 2 x OCH_3), 5.87 (1H, s, broad, NH), 6.03 (2H, s, OCH_2O), 6.56 (1H, d, Ar-H), 6.62 (1H, dd, Ar-H), 6.89 (1H, d, Ar-H), 7.57-7.60 (3H, m, Ar-H, C5-H), 7.95 (1H, d, Ar-H); δ_C ($CDCl_3$) 29.4, 29.7, 31.9, 38.0, 55.5, 55.8, 57.8, 98.9, 101.4, 105.2, 107.4, 108.3, 120.1, 121.6, 131.2, 132.5, 148.1, 149.4, 159.3, 162.4; m/z (Electrospray)$^+$ 423.2026; m/z (Electrospray)$^+$ 423 ($[M+H]^+$, 100%).

2- dimethylethylenediamino-4,6-diphenylpyrimidine, DMU 10601

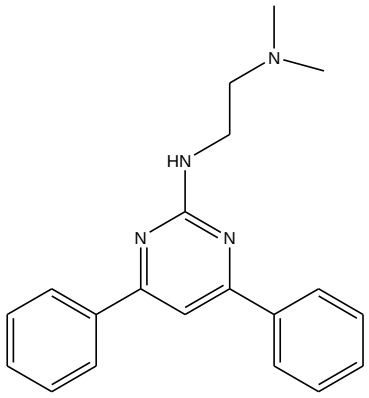

Light brown oil (0.14g, 42%), δ_H ($CDCl_3$) 2.41 (6H, s, 2 x CH_3), 2.74 (2H, t, CH_2), 3.77 (2H, q, CH_2), 5.77 (1H, s, broad, NH), 7.43 (1H, s, C5-H), 7.47-7.53 (6H, m, Ar-H), 8.05-8.14 (4H, m, Ar-H); δ_C ($CDCl_3$) 38.9, 45.1, 58.3, 102.9, 127.1, 128.7, 130.3, 138.1, 162.9; m/z (Electrospray)$^+$ Found 319.1921, $C_{20}H_{22}N_4$ requires 319.1917; m/z (Electrospray)$^+$ 319 ($[M+H]^+$, 100%).

4-(2-methoxyphenyl)-6-(3,4-methylenedioxyphenyl)-2-dimethylethylenediaminopyrimidine, DMU 10602

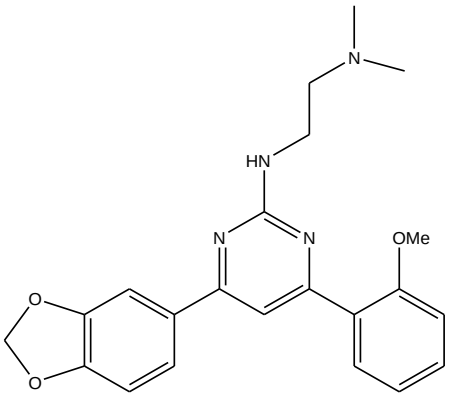

Brown oil (0.15g, 29%), δ_H ($CDCl_3$) 2.38 (6H, s, 2 x CH_3), 2.70 (2H, t, CH_2), 3.70 (2H, q, CH_2), 3.90 (3H, s, OCH_3), 5.64 (1H, s, broad, NH), 6.03 (2H, s, OCH_2O), 6.89 (1H, d, Ar-H), 7.01 (1H, d, Ar-H), 7.08 (1H, t, Ar-H), 7.40 (1H, t, Ar-H), 7.50 (1H, s, C5-H), 7.63 (2H, d, Ar-H), 7.90 (1H, d, Ar-H); m/z (Electrospray)$^+$ Found 393.1923, $C_{22}H_{24}N_4O_3$ requires 393.1921; m/z (Electrospray)$^+$ 393 ($[M+H]^+$, 100%).

9.11 General Procedure for the Synthesis of 2-Methyl-4-(2,4-Dimethoxyphenyl)-6-(3,4-Methylenedioxyphenyl)Pyrimidine

A solution of DMU 407 (6.4 mmol), acetamidine hydrochloride (9.6 mmol) and aqueous potassium hydroxide (2.90 cm^3, 50% w/v, 25.6 mmol) in ethanol (25 cm^3) was heated at reflux for 6 h. Hydrogen peroxide solution (1.31 cm^3, 50% w/v, 19.2 mmol) was added drop-wise to the solution and reflux continued for 1 h. The reaction was quenched with water (40 cm^3) and the resulting mixture extracted with dichloromethane (3 x 50 cm^3). The combined organic extracts were dried ($MgSO_4$) and the solvent removed *in vacuo*. The methyl-pyrimidine was purified by recrystalisation from ethanol.

2-methyl-4-(2, 4-dimethoxyphenyl)-6-(3, 4-methylenedioxyphenyl)pyrimidine, DMU 10700

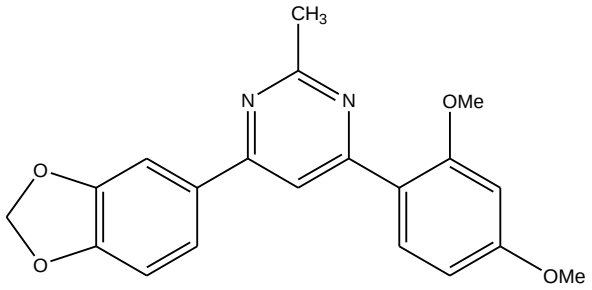

Yellow crystals (0.09g, 10%), mp 127-129ºC; δ_H ($CDCl_3$) 2.80 (3H, s, CH_3), 3.88 (3H, s, OCH_3), 3.90 (3H, s, OCH_3), 6.05 (2H, s, CH_2O_2), 6.60 (1H, d, Ar-H), 6.67 (1H, dd, Ar-H), 6.95 (1H, d, Ar-H), 7.60-7.69 (2H, m, Ar-H), 8.01 (2H, d, Ar-H); δ_C ($CDCl_3$) 55.5, 55.7, 99.0, 101.5, 105.4, 107.6, 108.5, 110.9, 113.5, 119.9, 121.8, 132.2, 132.4, 148.3, 149.6, 159.3, 162.5, 162.9, 167.7; m/z (Electrospray)$^+$ Found 351.1333, $C_{20}H_{18}N_2O_4$ requires 351.1339; m/z (Electrospray)$^+$ 351 ($[M+H]^+$, 100).

9.12 General Procedure for the Synthesis of 4-(2,4-Dimethoxyphenyl)-6-(3,4-Methylenedioxyphenyl)Pyrimidine

A solution of DMU 407 (9.62 mmol), formamidine hydrochloride (14.4 mmol) and aqueous potassium hydroxide (4.31 cm^3, 50% w/v, 38.5 mmol) in ethanol (30 cm^3) was heated at reflux for 6 h. Hydrogen peroxide solution (1.96 cm^3, 50% w/v, 28.9 mmol) was added drop-wise to the solution and reflux continued for 1 h. The reaction was quenched with water (40 cm^3) and the resulting mixture extracted with dichloromethane (3 x 50 cm^3). The combined organic extracts were dried ($MgSO_4$) and the solvent removed *in vacuo*. The pyrimidine was purified by recrystalisation from ethanol.

4-(2,4-dimethoxyphenyl)-6-(3,4-methylenedioxyphenyl)pyrimidine, DMU 10800

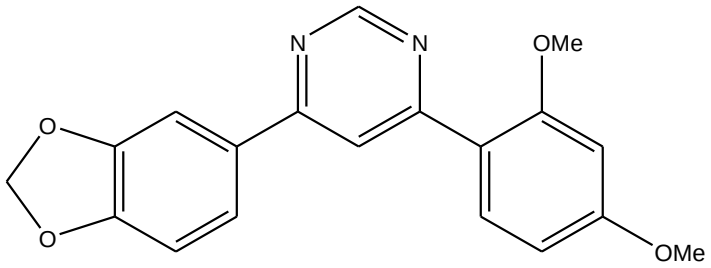

Brown crystals (0.32g, 10%), mp 132-134ºC; δ_H ($CDCl_3$) 3.88 (3H, s, OCH_3), 3.95 (3H, s, OCH_3), 6.08 (2H, s, CH_2O_2), 6.58 (1H, d, Ar-H), 6.68 (1H, dd, Ar-H), 6.94 (1H, d, Ar-H), 7.64 (1H, d, Ar-H), 7.69 (1H, d, Ar-H), 8.08 (1H, d, Ar-H), 8.25 (1H, s, Ar-H), 9.20 (1H, s, Ar-H); δ_C ($CDCl_3$) 55.5, 55.7, 99.0, 101.5, 105.4, 107.6, 108.5, 110.9, 113.5, 121.8, 132.4, 149.6, 159.3, 162.9, 167.7; m/z (Electrospray)$^+$ Found 337.1184, $C_{19}H_{16}N_2O_4$ requires 337.1183; m/z (Electrospray)$^+$ 337 ($[M+H]^+$, 100).

9.13 General procedure for the synthesis of 4-(2, 4-dimethoxyphenyl)-6-(3, 4-dihydroxyphenyl)-2-amino-pyrimidine

A solution of the pyrimidine (0.57 mmol) and boron trichloride (1.71 mmol) in dichloromethane (60 cm^3) was stirred at -5ºC under nitrogen for 24 h. The reaction was quenched with water (50 cm^3) and the resulting mixture extracted with ethyl acetate (3 x 50 cm^3). The combined organic extracts were dried ($MgSO_4$) and the solvent removed *in vacuo*. The dihydroxy-pyrimidine was purified by flash chromatography on silica gel using methanol-dichloromethane (1:9) as eluent.

4-(2,4-dimethoxyphenyl)-6-(3,4-dihydroxyphenyl)-2-amino-pyrimidine, DMU 10503

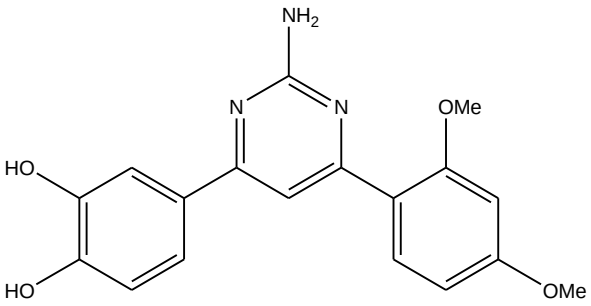

Brown oil (0.033g, 17%), δ_H ($CDCl_3$) 3.84 (3H, s, OCH_3), 3.90 (3H, s, OCH_3), 6.40 (2H, s, NH_2), 6.65 (1H, dd, Ar-H), 6.68 (1H, d, Ar-H), 6.85 (1H, d, Ar-H), 7.37-7.61 (1H, dd, Ar-H), 7.46 (1H, d, C5-H), 7.53 (1H, d, Ar-H), 7.89 (1H, d, Ar-H), 9.25 (1H, s, broad, OH), 9.44 (1H, s, broad, OH); m/z (Electrospray$^+$) 340.1290, $C_{18}H_{17}N_3O_4$ requires 340.1292; m/z (Electrospray$^+$) 340 ($[M+H]^+$, 100).

9.14 General procedure for the Synthesis of DMU 10500

A solution of 4-hydroxy-2-methoxybenzaldehyde (16 mmol) and pyridinium ρ-toluene sulfonate (0.38 mmol) in dichloromethane (30 ml) was stirred at room temperature for 0.5 h. This was followed by drop-wise addition of 3,4-dihydro-2*H*-pyran (4.08 ml) in dichloromethane (15 ml) and stirring continued for 24 h. The reaction was quenched with water (30 cm^3) and the resulting mixture extracted with dichloromethane (3 x 50 cm^3). The combined organic extracts were dried ($MgSO_4$) and the solvent removed *in vacuo*. The protected benzaldehyde was purified by flash chromatography on silica gel using dichloromethane – methanol as eluent.

2-(methoxy-4-tetrahydropyran-2-yloxy)benzaldehyde, DMU 10500

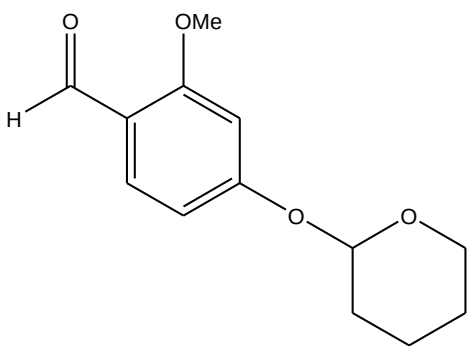

Yellow oil (1.83g, 49%), δ_H ($CDCl_3$) 3.90 (3H, s, OCH_3), 5.55 (1H, t, cyclic-H), 6.63 (1H, s, Ar-H), 6.70 (1H, d, Ar-H), 7.80 (1H, d, Ar-H), 10.30 (1H, s, CH); δ_C ($CDCl_3$); m/z (electrospray)$^+$ Found 237.1119, $C_{13}H_{16}O_4$ requires 237.1121; m/z (electrospray)$^+$ 237 ([M+ H]$^+$, 38%).

9.15 General procedure for the synthesis of the DMU 10501

A solution of 2-(methoxy-4-tetrahydropyran-2-yloxy)-benzaldehyde (7.8 mmol), 3, 4-(methylenedioxy)-acetophenone (7.8 mmol) and aqueous sodium hydroxide (2.50 cm^3, 50% w/v, 31.2 mmol) in methanol (30 ml) was stirred at room temperature for 24 h. Once complete (as indicated by TLC) the reaction was quenched with water (50 cm^3) and the resulting mixture was extracted with dichloromethane (3 x 40 cm^3). The organic extracts were dried ($MgSO_4$) and the solvent removed *in vacuo.* The crude was purified by flash chromatography on silica gel using ethyl acetate – hexane as eluent.

(E)-1-(3,4-methylenedioxyphenyl)-3-(2-methoxy-4-tetrahydropyran-2-yloxyphenyl)-2-propen-1-one, DMU 10501

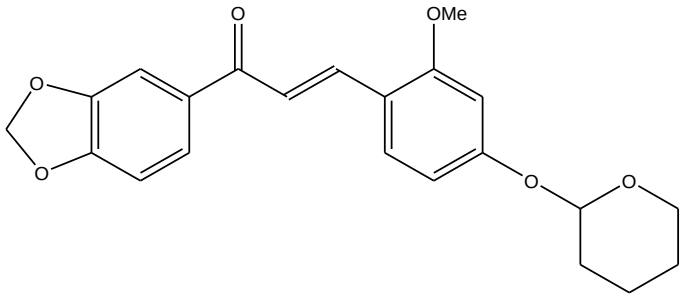

Yellow oil (2.30g, 77%), δ_H ($CDCl_3$) 3.90 (3H, s, OCH_3), 5.50 (1H, t, cyclic-H), 6.05 (2H, s, OCH_2O), 6.64 (1H, d, Ar-H), 6.70 (1H, dd, Ar-H), 6.89 (1H, d, J=12, C=C-H), 7.48 (1H, s, Ar-H), 7.53 (1H, d, Ar-H), 7.54 (1H, d, J=12, C=C-H), 7.63 (1H, dd, Ar-H), 8.03 (1H, d, Ar-H); δ_C ($CDCl_3$) 18.3, 18.5, 25.1, 30.2, 50.7, 55.6, 58.3, 62.0, 96.3, 100.3, 101.7, 107.8, 108.0, 108.2, 117.8, 120.3, 124.5, 130.7, 133.6, 140.1, 148.1, 151.3, 160.3, 189.1; m/z (Electrospray)$^+$ 383 ([M+H]$^+$, 100).

9.16 General Procedure for the Synthesis of DMU 10502

A solution of the protected chalcone (3.4 mmol), guanidine hydrochloride (5.1 mmol) and aqueous sodium hydroxide (1.08 cm^3, 50% w/v, 13.6 mmol) in ethanol (15 cm^3) was heated at reflux for 24 h. The reaction was quenched with water (40 cm^3) and the resulting mixture extracted with dichloromethane (3 x 50 cm^3). The combined organic extracts were dried ($MgSO_4$) and the solvent removed *in vacuo*. The protected pyrimidine was purified by flash chromatography on silica gel using ethyl acetate − hexane (4:6) as eluent.

2-amino-4-(3,4-methylenedioxyphenyl)-6-(2-methoxy-4-tetrahydropyran-2-yloxyphenyl)-pyrimidine, DMU 10502

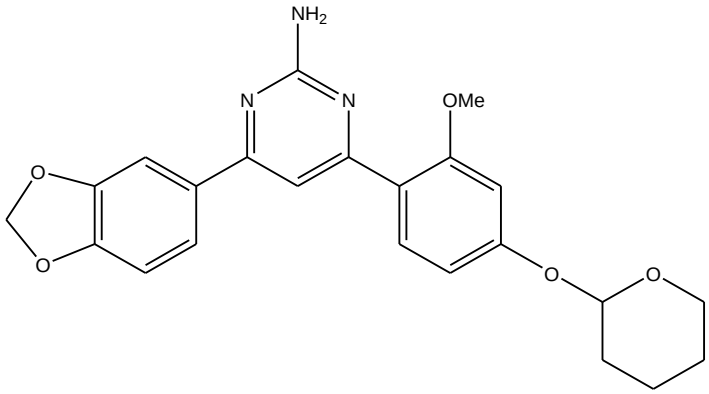

Yellow oil (0.025g, 3%), δ_H ($CDCl_3$) 3.90 (3H, s, OCH_3), 5.00 (2H, s, broad, NH_2), 5.52 (1H, t, Cyclic-H), 6.03 (2H, s, OCH_2O), 6.72 (1H, d, Ar-H), 6.78 (1H, dd, Ar-H), 6.90 (1H, d, Ar-H), 7.55 (1H, d, Ar-H), 7.5 (1H, d, Ar-H), 7.58 (1H, dd, Ar-H), 7.87 (1H, d, Ar-H); δ_C ($CDCl_3$); m/z (Electrospray)$^+$ Found 422.1710, $C_{22}H_{22}N_3O_5$ requires 422.1710; m/z (Electrospray)$^+$ 422 ($[M+H]^+$, 100).

10.0 Appendix

10.1 MTT Assay

To harvest the adhered cells, medium was aspirated and 1mL of a 1% trypsin-EDTA solution was added and the cells were gently agitated for 30 seconds. The trypsin-EDTA solution was removed and immediately replaced by a further 1mL aliquot of trypsin-EDTA solution. The cells were incubated at 37°C for approximately 5 minutes or until the cells were visibly non-adherent. The resultant cell suspension was placed in a sterile container with 5mL of fresh medium. To determine the density of the cell suspension, 100µL was added to 100µL of a trypan-blue solution (0.4%) and the number of viable cells was determined using a Neubauer haemocytometer (depth 0.1mm, 1/400mm^2). The cell suspension was diluted with medium to produce a cell count of $2x10^3$ cells.mL^{-1} and 100µL aliquots were dispensed into sterile, 96-well microtitre plates. With the exception of the MCF7 cells, all plates were incubated for 24 hours prior to the addition of the compounds of interest.

For the MCF7 cells, after allowing approximately 4 hours for cells to adhere, 100µL of medium containing TCDD (from 100mM stock in DMSO) or medium with 0.2% (v/v) DMSO only as a control was added to each well containing cells to give a final concentration of 10nM TCDD and 0.1% (v/v) DMSO, for 24 hours to induce CYP expression. The medium was then aspirated and 100µL of fresh medium was subsequently added.

Compounds requiring screening were added to the cells in ten-fold serial dilutions in warm medium (37°C), under subdued light, from an appropriate stock (in DMSO). Final concentrations were of 100, 30, 10, 3, 1, 0.3, 0.1, 0.03, 0.01, 0.003, 0.001 and 0.0003µM (in quadruplicate). The final concentration of DMSO did not exceed 0.1% (v/v). The cells were then allowed to grow on for 96 hours to attain 80-90% confluence in the control wells.

After 96 hours, 50µL of 2mg.mL^{-1} MTT (3-(4,5-Dimethylthiazol-2-yl)-2,5-diphenyl tetrazolium bromide in sterile phosphate buffer) was added to each well and incubated at 37°C for 2 hours. All medium was then aspirated and the product (reduced purple formazan) was solubilized with 150µL DMSO. Plates were vortexed and the absorbance at 540nm determined using a Molecular Devices SpectraMax M5 plate reader with SoftMax® Pro software, version 4.8.

Relative toxicities of each compound within each cell line were evaluated by determining IC_{50} values (50% of growth inhibition). Results were expressed as a percentage of the control value versus the negative logarithm of the molar drug concentration range using GraphPad Prism version 3.00 for Windows.

11.0 References

[1] Rang, H. P., Dale, M. M., Ritter, J. M., Moore, P. K., *Pharmacology*. 5th edition, Churchill Livingstone, **2003**.

[2] Sledge, G. W., Miller, K. D., *Exploiting the hallmarks of cancer: the future conquest of breast cancer*. European Journal of Cancer, **2003**, 39, 1668-1675.

[3] www.cancerresearchuk.org

[4] Ekholm, S. V., Reed, S. I., *Regulation of G1 cyclin-dependent kinases in the mammalian cell cycle.* Current Opinion in Cell Biology, **2000**, 12, 676-684.

[5] Sanchez, I., Dynlacht, B. D., *New insights into cyclins, CDKs, and cell cycle control. Seminars in Cell and Developmental Biology*, **2005**, 16, 311-321.

[6] Warmerdam, D. O., Kanaar, R., *Dealing with DNA damage: Relationships between checkpoint and repair pathways*. Mutation Research, **2010**, 704, 2-11.

[7] Rogers, K., *The Cell*. Britannica Educational Publishing, **2011**.

[8] Vermeulen, K., Dirk, R., Bockstaele, V., Berneman, Z. N., *The cell cycle: a review of regulation, deregulation and therapeutic targets in cancer*. Cell Proliferation, **2003**, 36, 131-149.

[9] Wang, Y., Ji, P., Liu, J., Broaddus, R. R., Xue, F., Zhang, W., *Centrosome-associated regulators of the G_2/M checkpoint as targets for cancer therapy*. Molecular Cancer, **2009**, 1-13.

[10] Duprez, L., Wirawan, E., Vanden Berghe, T., Vandenabeele, P., *The cell cycle: a review of regulation, deregulation and therapeutic targets in cancer*. Cell Proliferation, **2003**, 36, 131-149.

[11] Elmore, S., *Apoptosis: A Review of Programmed Cell Death*. *Toxicologic Pathology*, **2007**, 35, 4, 495-516.

[12] Pitot, H. C., *Pathways of progression in hepatocarcinogenesis*. The Lancet, **2001**, 358, 859-860.

[13] Geiger, T. R., Peeper, D. S., *Metastasis mechanisms*. International Journal of Biochemistry, Biophysics and Molecular Biology, **2009**, 1796, 293-308.

[14] Millau, J., Bastien, N., Drouin, R., *P53 transcriptional activities: A general overview and some thoughts*. Mutation Research, **2009**, 681, 118-133.

[15] Ryan, K. M., Phillips, A. C., Vousden, K. H., *Regulation and function of the p53 tumor suppressor protein*. Current Opinion in Cell Biology, **2001**, 13, 332-337.

[16] Zhu, L., *Tumour suppressor retinoblastoma protein Rb: A transcriptional regulator*. European Journal of Cancer, **2005**, 41, 2415-2427.

[17] Ross, J. F., Liu, X., Dynlacht, B. D., *Mechanism of Transcriptional Repression of E2F by the Retinoblastoma Tumor Suppressor Protein*. Molecular Cell, **1999**, 3, 195-205.

[18] A.S. Lundberg and R.A. Weinberg, *Control of the Cell Cycle and Apoptosis*. European Journal of Cancer, **1999**, 35, 4, 531-539.

[19] Liu, H., Dibling, B., Spike, B., Dirlam, A., Macleod, K., *New roles for the RB tumor suppressor protein*. Current Opinion in Genetics and Development, **2004**, 14, 55-64.

[20] DeGregori, J., *The Rb network*. Journal of Cell Science, **2004**, 117, 3411-3413.

[21] Zieske, J. D., Francesconi, C. M., Guo, X., *Cell cycle regulators at the ocular surface*. Experimental Eye Research, **2004**, 78, 447-456.

[22] Lain, S., Lane, D., *Improving cancer therapy by non-genotoxic activation of p53*. European Journal of Cancer, **2003**, 39, 1053-1060.

[23] Meek, D., *The p53 response to DNA damage*. DNA Repair, **2004**, 3, 1049-1056.

[24] Borrello, M. G., Degl'Innocenti, D., Pierotti, M. A., *Inflammation and cancer: The oncogene-driven connection*. Cancer Letters, **2008**, 267, 262-270.

[25]. Tsantoulis, P.K., Kastrinakis, N. G., Tourvas, A. D., Laskaris, G., Gorgoulis, V. G., *Advances in the biology of oral cancer*. Oral Oncology, **2007**, 43, 523-534.

[26] Miyakura, Y., Sugano, K., Fukayama, N., Konishi. F., Nagai, H., *Concurrent mutations of K-ras oncogene at codons 12 and 22 in colon cancer*. Japanese Journal of Clinical Oncology, **2002**, 32, 6, 219-221.

[27] Cerbinskaite, A., Mukhopadhyay, A., Plummer, E. R., Edmondson, R. J., *Defective Homologous Recombination in Human Cancers*. Cancer Treatment Reviews, **2011**.

[28] Braem, M. G. M., Schouton, L. J., Peeters, P. H. M., Brandt, P. A., Onland-Moret, N. C., *Genetic Susceptibility to Sporadic Ovarian Cancer: A Systematic Review*. Biochimica et Biophysica Acta, **2011**, 132-146.

[29] Thompson, P.A., Seyedi, F., Lang, N. P., MacLeod, S. L., Wogan, G. N., Anderson, K. E., Tang, Y., Coles, B., Kadlubar, F. F., *Comparison of DNA adduct levels associated with exogenous and endogenous exposures in human pancreas in relation to metabolic genotype*. Mutation Research, **1999**, 424, 263-274.

[30] Sagiv, S. K., Gaudet, M. M., Eng, S. M., Abrahamson, P. E., Shantakumar, S., Teitelbaum, S. L., Bell, P., Thomas, J. T., Neugut, A. I., Santella, R. M., Gammona, M. D., *Polycyclic aromatic hydrocarbon–DNA adducts and survival among women with breast cancer*. Environmental Research, **2009**, 109, 287-291.

[31] Rundle, A., *Carcinogen-DNA adducts as a biomarker for cancer risk*. Mutation Research, **2006**, 600, 23-36.

[32] Perlow, A. R., Broyde, S., *Evading the Proofreading Machinery of a Replicative DNA Polymerase: Induction of a Mutation by an Environmental Carcinogen*. Journal of Molecular Biology, **2001**, 309, 519-536.

[33] Takemura, H., Nagayoshic, H., Matsudac, T., Sakakibara, H., Moritad, M., Matsuid, A., Ohura, T., Shimoi, K., *Inhibitory effects of chrysoeriol on DNA adduct formation with benzo[a]pyrene in MCF-7 breast cancer cells*. Toxicology, **2010**, 274, 42-48.

[34] Sarid, R., Gao, S., *Viruses and human cancer: From detection to causality*. Cancer Letters, **2010**.

[35] Montesano, R., Hall, J., *Environmental causes of human cancers*. European Journal of Cancer, **2001**, 37, 67-87.

[36] Corrie, P. G., *Cytotoxic chemotherapy: clinical aspects*. Medicine, **2007**, 36, 1, 24-28.

[37] Sanderson, B. J. S., Shield, A. J., *Mutagenic damage to mammalian cells by therapeutic alkylating agents.* Mutation Research, **1996**, 355, 41-57.

[38] Lawley, P.D., Phillips, D.H., *DNA adducts from chemotherapeutic agents*. Mutation Research, **1996**, 355, 13-40.

[39] Allan, J. M., *The molecular mechanisms of alkylating agent-related acute myeloid leukaemia*. Haematologica Reports, **2006**, 2, 15, 28-29.

[40] Guest, I., Uetrecht, J., *Drugs toxic to the bone marrow that target the stromal cells*. Immunopharmacology, **2000**, 46, 103-112.

[41] Lind, M. J., *Principles of cytotoxic chemotherapy*. Medicine, **2007**, 36, 1, 19-23.

[42] Verweij, J., Jonge, M. J. A., *Achievements and future of chemotherapy*. European Journal of Cancer, **2000**, 36, 1479-1487.

[43] Marzanoa, C., Trevisanb, A., Giovagninic, L., Fregona, D., *Synthesis of a new platinum(II) complex: anticancer activity and nephrotoxicity in vitro.* Toxicology in Vitro, **2002**, 16, 413-419.

[44] Corrie, P. G., *Cytotoxic chemotherapy: clinical aspects*. Medicine, **2004**, 25-29.

[45] Shukla, P.K., Mishra, P.C., Suhai, S., *Reactions of DNA bases with the anti-cancer nitrogen mustard mechlorethamine: A quantum chemical study*. Chemical Physics Letters, **2007**, 449, 323-328.

[46] Mallet, G., Lematre, J., Vasilescu, D., *Interaction of the Alkylating Agent Mechlorethamine with DNA in Presence and in Absence of the Radioprotector WR-1065: A Transient Electric Birefringence Study*. Journal of Biological Physics, **1996**, 22, 1-14.

[47] Hurley, L. H., *DNA and its associated processes as targets for cancer therapy*. Nature Reviews, **2002**, 2, 188-200.

[48] Ferguson, L. R., Liu, A. P., Denny, W. A., Cullinane, C., Talarico, T., Phillips, D. R., *Transcriptional blockages in a cell-free system by sequence-selective DNA alkylating agents*. Chemico-Biological Interactions, **2000**, 126, 15-31.

[49] Giuliani, I., Baeza-Squiban , A. B., Marano, F., *Early cytotoxic effects of mechlorethamine, a nitrogen mustard, on mammalian airway epithelium*. Toxicology in Vitro, **1997**, 11, 695-702.

[50] Decatrisa, M.P., Sundarb, S., O'Byrne, K. J., *Platinum-based chemotherapy in metastatic breast cancer: current status*. Cancer Treatment Reviews, **2004**, 4, 53-81.

[51] Maria Kartalou, John M. Essigmann, *Mechanisms of resistance to cisplatin*. Mutation Research, **2001**, 478, 23-43.

[52] Desoize, B., Madoulet, C., *Particular aspects of platinum compounds used at present in cancer treatment*. Critical Reviews in Oncology/Hematology, **2002**, 42, 317–325.

[53] Pizarro, A. M., Sadler, P. J., *Unusual DNA binding modes for metal anticancer complexes*. Biochimie, **2009**, 91, 1198-1211.

[54] Rollins, K. D., Lindley, C., *Pemetrexed: A Multitargeted Antifolate*. Clinical Therapeutics, **2005**, 27, 1343-1382.

[55] Duthie, S. J., Narayanan, S., Brand, G. M., Pirie, L., Grant, G., *Impact of Folate Deficiency on DNA Stability*. The Journal of Nutrition, **2002**, 132, 2444-2449.

[56] Rampersaud, G. C., Kauwell, G. P. A., Hutson, A. D., Cerda, J. J., Bailey, L. B., *Genomic DNA methylation decreases in response to moderate folate depletion in elderly women*. American Journal for Clinical Nutrition, **2000**, 72, 998-1003.

[57] Linden, I. J. M., Nguyen, U., Heil, S. G., Franke, B., Vloet, S., Gellekink, H., Heijer, M., Blom, H. J., *Variation and expression of dihydrofolate reductase (DHFR) in relation to spina bifida.* Molecular Genetics and Metabolism, **2007**, 91, 98-103.

[58] Mazur, A. J., Nowak, D., Mannherz, H. G., Malicka-Błaszkiewicz, M., *Methotrexate induces apoptosis in CaSki and NRK cells and influences the organization of their actin cytoskeleton*. European Journal of Pharmacology, **2009**, 613, 24-33.

[59] Zagotto, G., Gatto, B., Moro, S., Sissi, C., Palumbo, M., *Anthracyclines: recent developments in their separation and quantitation*. Journal of Chromatography, **2001**, 764, 161-171.

[60] Verrill, M., *Anthracyclines in breast cancer: therapy and issues of toxicity*. *The Breast* Supplement, **2001**, 2, 8-15.

[61] Mizutania, H., Tada-Oikawaa, S., Hirakua, Y., Kojimab, M., Kawanishi, S., *Mechanism of apoptosis induced by doxorubicin through the generation of hydrogen peroxide*. Life Sciences, **2005**, 76, 1439-1453.

[62] Cho, H., Jung, M., Woo, S., Kim, J., Lee, E., Kwon, Y., Na, Y., *New benzoxanthone derivatives as topoisomerase inhibitors and DNA cross-linkers*. Bioorganic and Medicinal Chemistry, **2010**, 18, 1010-1017.

[63] Bachur, N. R., Gordon, S. L., Gee, M. V., Kon, H., *NADPH cytochrome P-450 reductase activation of quinone anticancer agents to free radicals*. Medical Sciences, **1979**, 76, 2, 954-957.

[64] Chen, K., Huzil, J. T., Freedman, H., Ramachandran, P., Antoniou, A., Tuszynski, J. A., Kurgan, L., *Identification of tubulin drug binding sites and prediction of relative differences in binding affinities to tubulin isotypes using digital signal processing*. Journal of Molecular Graphics and Modelling, **2008**, 27, 497-505.

[65] McGrogan, B. T., Gilmartin, B., Carney, D. N., McCann, A., *Taxanes, microtubules and chemoresistant breast cancer*. Biochimica et Biophysica Acta, **2008**, 1785, 96–132.

[66] Altmann, K., *Microtubule-stabilizing agents: a growing class of important anticancer drugs*. Current Opinion in Chemical Biology, **2001**, 5, 424-431.

[67] Ducki, S., Mackenzie, G., Greedy, B., Armitage, S., Chabert, J., Bennett, E., Nettles, J., Snyder, J. P., Lawrence, N. J., *Combretastatin-like chalcones as inhibitors of microtubule*

polymerisation. Part 2: Structure-based discovery of alpha-aryl chalcones. Bioorganic & Medicinal Chemistry, **2009**, 17, 7711-7722.

[68] Risinger, A. L., Giles, F. J., Mooberry, S. L., *Microtubule dynamics as a target in oncology*. Cancer Treatment Reviews, **2009**, 35, 255–261.

[69] Guo, B. H., Kai, G. Y., Jin, H. B., Tang, K. X., *Taxol synthesis*. African Journal of Biotechnology, **2006**, 5, 1, 15-20.

[70] Buey, R. M., Barasoain, I., Jackson, E., Meyer, A., Giannakakou, P., Paterson, I., Mooberry, S., Andreu, J. M., Diaz, J. F., *Microtubule Interactions with Chemically Diverse Stabilizing Agents: Thermodynamics of Binding to the Paclitaxel Site Predicts Cytotoxicity*. Chemistry and Biology, **2005**, 12, 1269-1279.

[71] Malika, S., Cusidó, R. M., Mirjalili, M. H., Moyanod, E., Palazón, J., Bonfill, M., *Production of the anticancer drug taxol in Taxus baccata suspension cultures: A review*. Process Biochemistry, **2011**, 46, 23-34.

[72] Iqbal, J., Sarti, F., Perera, G., Bernkop-Schnürch, A., *Development and in vivo evaluation of an oral drug delivery system for paclitaxel*. Biomaterials, **2011**, 32, 170-175.

[73] Mulzer, J., Altmann, K., Hofle, G., Muller, R., Prantz, K., *Epothilones- A fascinating family of microtubule stabilizing antitumor agents*. C. R. Chimie, **2008**, 11, 1336-1368.

[74] Lee, F. Y. F., Borzilleri, R., Fairchild, C. R., Kamath, A., Smykla, R., Kramer, R., Vite, G., *Preclinical discovery of ixabepilone, a highly active antineoplastic agent.* Cancer Chemotherapy and Pharmacology, **2008**, 63, 1, 157-66.

[75] Ducki, S., Rennison, D., Wooa, M., Kendall, A., Chabert, J., McGownb, A. T., Lawrence, N. J., *Combretastatin-like chalcones as inhibitors of microtubule polymerization. Part 1: Synthesis and biological evaluation of antivascular activity*. Bioorganic and Medicinal Chemistry, **2009**, 17, 7698–7710.

[76] Brown, T., Holt, H., Lee, M., *Synthesis of Biologically Active Heterocyclic Stilbene and Chalcone Analogs of Combretastatin*. Topics in Heterocyclic Chemistry, **2006**.

[77] Pettit, R. K., Pettit, G. R., Hamel, E., Hogan, F., Moser, B. R., Wolf, S., Pon, S., Chapuis, J. C., Schmidt, J. M., *E-Combretastatin and E-resveratrol structural modifications: Antimicrobial and cancer cell growth inhibitory b-E-nitrostyrenes*. Bioorganic and Medicinal Chemistry, **2009**, 17, 6606-6612.

[78] Levitzki, A., *Tyrosine kinases as targets for cancer therapy*. European Journal of Cancer, **2002**, 38, 5, 11-18.

[79] Sherman, S. I., *Tyrosine kinase inhibitors and the thyroid*. Best Practice and Research Clinical Endocrinology and Metabolism, **2009**, 23, 713–722.

[80] Madhusudan, S., Ganesan, T. S., *Tyrosine kinase inhibitors in cancer therapy*. Clinical Biochemistry, **2004**, 37, 618– 635.

[81] Patani, N., Mokbel, K., Herceptin *and breast cancer: An overview for surgeons*. Surgical Oncology, **2010**, 19, 11-21.

[82] Tai, W., Mahato, R., Cheng, K., *The role of HER2 in cancer therapy and targeted drug delivery*. Journal of Controlled Release, **2010**, 146, 264–275.

[83] Bennasroune, A., Gardin, A., Aunis, D., Crémel, G., Hubert, P., *Tyrosine kinase receptors as attractive targets of cancer therapy*. Critical Reviews in Oncology/Hematology, **2004**, 50, 23-38.

[84] Kruser, T. J., Wheeler, D. L., *Mechanisms of resistance to HER family targeting antibodies.* Experimental Cell Research, **2010**, 316, 1083-1100.

[85] Zhanga, D. Y., Lia, Y., Rizvia, S. M. A., Qua, C., Kearsleya, J., Allen, B. J., *Cytotoxicity of breast cancer cells overexpressing HER2/neu by ^{213}Bi-Herceptin radioimmunoconjugate*. Cancer Letters, **2005**, 218, 181–190.

[86] Kim, J. A., *Targeted therapies for the treatment of cancer*. The American Journal of Surgery, **2003**, 186, 264-268.

[87] Hsiao, H., Liu, Y., Tsai, H., Hsu, J., Yang, W., Chang, C., Lin, S., *Additional chromosome abnormalities in chronic myeloid leukemia*. Kaohsiung Journal of Medical Sciences, **2011**, 27, 49-54.

[88] Pliarchopoulou, K., Pectasides, D., *Late complications of chemotherapy in testicular cancer*. Cancer Treatment Reviews, **2010**, 36, 262–267.

[89] Zagonel, V., Rupolo, M., Pinto, A., *Active protection from chemotherapy toxicity*. Critical Reviews in Oncology:Hematology, **1998**, 27, 125–127.

[90] Sridhar, T., Symonds, R. P., *Principles of chemotherapy*. Obstetrics, Gynaecology and Reproductive Medicine, **2009**, 19, 3, 61-67.

[91] Fiore, F., Cutsem, E., *Acute and long-term gastrointestinal consequences of chemotherapy*. Best Practice and Research Clinical Gastroenterology, **2009**, 23, 113–124.

[92] Nakashima-Kamimura, N., Nishimaki, K., Mori, T., Asoh, S., Ohta, S., *Prevention of chemotherapy-induced alopecia by the anti-death FNK protein.* Life Sciences, **2008**, 82, 218-225.

[93] Boddy, A. V., English, M., Pearson, A. D. J., Idle J. R., Skinner, R., *Ifosfamide Nephrotoxicity: Limited Influence of Metabolism and Mode of Administration During Repeated Therapy in Paediatrics*. European Journal of Cancer, **1996**, 32A, 7, 1179-l184.

[94] Sehirli, O., Sakarcan, A., Velioglu-Ogunc, A., Cetinel, S., Gedik, N., Yegen, B. C., Sener, G., *Resveratrol improves ifosfamide-induced Fanconi syndrome in rats*. Toxicology and Applied Pharmacology, **2007**, 222, 33-41.

[95] Aleksa, K., Halachmi, N., Ito, S., Koren, G., *Renal ontogeny of ifosfamide nephrotoxicity*. The Journal of Laboratory and Clinical Medicine, **2004**, 144, 6, 285-293.

[96] Ginsberg, J. P., Womer, R. B., *Preventing organ-specific chemotherapy toxicity*. European Journal of Cancer, **2005**, 41, 2690-2700.

[97] Jeyaseelan, R., Poizat, C., Wu, H., Kedes, L., *Molecular Mechanisms of Doxorubicin-induced Cardiomyopathy*. The Journal of Biological Chemistry, **1997**, 272, 9, 5828-5832.

[98] Sanchez-Soria, P., Camenisch, T. D., *ErbB signaling in cardiac development and disease*. Seminars in Cell and Developmental Biology, **2010**, 21, 929-935.

[99] Soussain, C., Ricard, D., Fike, J. R., Mazeron, J., Psimaras, D., Delattre, J., *CNS complications of radiotherapy and chemotherapy*. The Lancet, **2009**, 374, 1639-1651.

[100] Minisini, A. M., Pauletto, G., Andreetta, C., Bergonzi, P., Fasola, G., *Anticancer drugs and central nervous system: Clinical issues for patients and physicians*. Cancer Letters, **2008**, 267, 1-9.

[101] DeVita, V. T., Hellman, S., Rosenberg, S. A., *Cancer, Principles and Practice of Oncology*. Lippincott, Williams and Wilkins, **2001**.

[102] Calabro. P., Yeh, E. T. H., *Cancer and the Heart*. B. C. Decker Inc, **2006**.

[103] Sinhababu, A. K., Thakker, D. R., *Prodrugs of anticancer agents*. Advanced Drug Delivery Reviews, **1996**, 19, 241-273.

[104] Testa, B., *Prodrugs: bridging pharmacodynamic/pharmacokinetic gaps*. Current Opinion in Chemical Biology, **2009**, 13, 338-344.

[105] Testa, B., *Prodrug research: futile or fertile?* Biochemical Pharmacology, **2004**, 68, 2097-2106.

[106] Denny, W., *Prodrug strategies in cancer therapy*. European Journal of Medicinal Chemistry, **2001**, 36, 577-595.

[107] Raleigh, S. M., Wanogho, E., Burke, M. D., McKeown, S. R., Patterson, L. H., *Involvement of human cytochromes P450 (CYP) in the reductive metabolism of AQ4N, a hypoxia activated anthraquinone di-N-oxide prodrug*. International Journal of Radiation Oncology • Biology • Physics, **1998**, 42, 4, 763-767.

[108] Niculescu-Duvaz, I., Springer, C.J., *Antibody-directed enzyme prodrug therapy (ADEPT): a review*. Advanced Drug Delivery Reviews, **1997**, 26, 151–172.

[109] Yu, Y., Fang, L., Sun, D., *Biodistribution of HuCC49ΔCH2-β-galactosidase in colorectal cancer xenograft model.* International Journal of Pharmaceutics, **2010**, 386, 208-215.

[110] Phelan, R. M., Ostermeier, M., Townsend, C. A., *Design and synthesis of a β-lactamase activated 5-fluorouracil prodrug*. Bioorganic and Medicinal Chemistry Letters, **2009**, 19, 1261-1263.

[111] Xu, G., McLeod, H. L., *Strategies for Enzyme/Prodrug Cancer Therapy*. Clinical Cancer Research, **2001**, 7, 3314-3324.

[112] Springer, C. J., Niculescu-Duvaz, I., *Prodrug-activating systems in suicide gene therapy*. The Journal of Clinical Investigation, **2000**, 105, 9, 1161-1167.

[113] McNeish, I. A., Searle, P. F., Young, L. S., Kerr, D. J., *Gene directed enzyme prodrug therapy for cancer*. Advanced Drug Delivery Reviews, **1997**, 26, 173-184.

[114] Altaner, C., *Prodrug cancer gene therapy*. Cancer Letters, **2008**, 270, 191-201.

[115] Portsmouth, D., Hlavaty, J., Renner, M., *Suicide genes for cancer therapy*. Molecular Aspects of Medicine, **2007**, 28, 4-41.

[116] Prosser, G. A., Copp, J. N., Syddall, S. P., Williams, E.M., Smaill, J. B., Wilson, W. R., Patterson, A. V., Ackerley, D. F., *Discovery and evaluation of Escherichia coli nitroreductases that activate the anti-cancer prodrug CB1954*. Biochemical Pharmacology, **2010**, 79, 678-687.

[117] McCarthy, H. O., Yakkundi, A., McErlane, V., Hughes, C. M., Keilty, G., Murray, M., Patterson, L. H., Hirst, D. G., McKeown, S. R., Robson, T., *Bioreductive GDEPT using cytochrome P450 3A4 in combination with AQ4N*. Cancer Gene Therapy, **2003**, 10, 40-48.

[118] Singh. P., Yam, M., Russell, P. J., Khatri, A., *Molecular and traditional chemotherapy: A united front against prostate cancer*. Cancer Letters, **2010**, 293, 1, 1-14.

[119] Jaberipour, M., Vass, S. O., Guise, C. P., Grove, J. I., Knox, R. J., Hud, L., Hyde, E. I., Searle, P. F., *Testing double mutants of the enzyme nitroreductase for enhanced cell sensitisation to prodrugs: Effects of combining beneficial single mutations*. Biochemical Pharmacology, **2010**, 79, 102-111.

[120] Hasler, J. A., Estabrook, R., Murray, M., Pikuleva, I., Waterman, M., Capdevila, J., Holla, V., Helvig, C., Falck, J. R., Farrell, G., Kaminsky, L. S., Spivack, S. D., Boitier, E., Beaune, P., *Human cytochromes P450*, Molecular Aspects of Medicine, **1999**, 20, 1-2, , 1-137.

[121] Omura, T., *Forty Years of Cytochrome P450*. Biochemical and Biophysical Research Communications, **1999**, 266, 690-698.

[122] Gottlieb, R., *Cytochrome P450: major player in reperfusion injury*. Archives of Biochemistry and Biophysics, **2003**, 420, 262-267.

[123] Wade, R. C., Motiejunas, D., Schleinkofer, K., Sudarko, Winn, P. J., Banerjee, A., Kariakin, A., Jung, C., *Multiple molecular recognition mechanisms*. Biochimica et Biophysica Acta, **2005**, 1754, 239-244.

[124] Lamb, D. C., Waterman, M. R., Kelly, S. L., Guengerich, F. P., *Cytochromes P450 and drug discovery*. Current Opinion in Biotechnology, **2007**, 18, 504-512.

[125] Arinc, E, *The role of polymorphic cytochrome P450 enzymes in drug design, development and drug interactions with a special emphasis on phenotyping*. Journal of Molecular Catalysis B: Enzymatic 64, **2010**, 120–122.

[126] Yim, S., Yun, S., Yun, C., *A Continuous Spectrophotometric Assay for NADPH-cytochrome P450 Reductase Activity Using 1,1-Diphenyl-2-Picrylhydrazyl*. Journal of Biochemistry and Molecular Biology, **2004**, 37, 5, 629-633.

[127] Gan, L., Moltke, L., Trepanier, L. A., Harmatz, J. S., Greenblatt, D. J., Court, M. H., *Role of NADPH-Cytochrome P450 Reductase and Cytochrome-b5/NADH-b5 Reductase in Variability of CYP3A Activity in Human Liver Microsomes*. The American Society for Pharmacology and Experimental Therapeutics, **2009**, 37, 1, 90-96.

[128] Backes, W. L., Kelley, R. W., *Organization of multiple cytochrome P450s with NADPH-cytochrome P450 reductase in membranes*. Pharmacology and Therapeutics, **2003**, 98, 221-233.

[129] Omura, T, *Heme–thiolate proteins*. Biochemical and Biophysical Research Communications, **2005**, 338, 404–409.

[130] Crewe, H. K., Ellis, S. W., Lennard, M. S., Tucker, G. T., *Variable Contribution of Cytochromes P450 2D6, 2C9 and 3A4 to the 4-Hydroxylation of Tamoxifen by Human Liver Microsomes*. Biochemical Pharmacology, **1997**, 53, 171-178.

[131] Iyer, K. R., Sinz, M. W., *Characterization of Phase I and Phase II hepatic drug metabolism activities in a panel of human liver preparations*. Chemico-Biological Interactions, **1999**, 118, 151-169.

[132] Singer, M. I., Shapiro, L. E., Shear, N. H., *Cytochrome P-450 3A: Interactions with dermatologic therapies*. Journal of the American Academy of Dermatology, **1997**, 37, 765-771.

[133] Purnapatre, K., Khattar, S. K., Saini, K. S., *Cytochrome P450s in the development of target-based anticancer drugs*. Cancer Letters, **2008**, 259, 1-15.

[134] Sutter, T. R., Tang, Y. M., Hayes, C. L., Won, Y. P., Jabsll, E. W., Lill, X., Yin, H., Cody, C. W., Greenlee, W. F., *Complete cDNA Sequence of a Human Dioxin-inducible mRNA Identifies a New Gene Subfamily of Cytochrome P450 That Maps to Chromosome 2**. The American Society for Biochemistry and Molecular Biology, **1994**, 269, 18, 13092-13099.

[135] Tsuchiya, Y., Nakajima, M., Kyo, S., Kanaya, T., Inoue, M., Yokoi, T., *Human CYP1B1 Is Regulated by Estradiol via Estrogen Receptor*. Cancer Research, **2004**, 64, 3119-3125.

[136] McFadyen, M. C. E., Melvin, W. T., Murray, G. I., *Cytochrome P450 CYP1B1 activity in renal cell carcinoma*. British Journal of Cancer, **2004**, 91, 966 -971.

[137] Murray, G. I., Taylor, M. C., McFadyen, M. C. E., McKay, J. A., Greenlee, W. F., Burke, M. D., Melvin, W. T., *Tumor-specific Expression of Cytochrome P450 CYP1B1*. Cancer Research, **1997**, 15, 3026-3031.

[138] M. C., McFadyen, Breeman, S., Payne, S., Stirk, C., Miller, I. D., Melvin, W. T., Murray, G. I., *Immunohistochemical Localization of Cytochrome P450 CYP1B1 in Breast Cancer with Monoclonal Antibodies Specific for CYP1B1*. The Journal of Histochemistry and Cytochemistry, **1999**, 47, 11, 145-1464.

[139] Gibson, P., Gill, J. H., Khan, P. A., Seargent, J. M., Martin, S. W., Batman, P. A., Griffith, J., Bradley, C., Double, J. A., Bibby, M. C., Loadman, P. M., *Cytochrome P450 1B1 (CYP1B1) Is Overexpressed in Human Colon Adenocarcinomas Relative to Normal Colon: Implications for Drug Development*. Molecular Cancer Therapeutics, **2003**, 2, 527-534.

[140] Lin. P., Chang, H., Ho, W. L., Wu, M. H., Su, J. M., *Association of aryl hydrocarbon receptor and cytochrome P4501B1 expressions in human non-small cell lung cancers*. Lung Cancer, **2003**, 42, 3, 255-261.

[141] Leclerc, J., Tournel, G., Courcot-Ngoubo Ngangue, E., Pottier, N., Lafitte, J. J., Jaillard, S., Mensier, E., Lhermitte, M., Broly, F., Lo-Guidice, J. M., *Profiling gene expression of whole cytochrome P450 superfamily in human bronchial and peripheral lung tissues: Differential expression in non-small cell lung cancers*. Biochimie, **2010**, 92, 3, 292-306.

[142] Carnell, D. M., Smith, R. E., Daley, F. M., Barber, P. R., Hoskin, P. J., Wilson, G. D., Murray, G. I., Everett, S. A., *Target validation of cytochrome P450 CYP1B1 in prostate carcinoma with protein expression in associated hyperplastic and premalignant tissue*. International Journal of Radiation Oncology • Biology • Physics, **2004**, 58, 2, 500-509.

[143] Androutsopoulos, V. P., Tsatsakis, A. M., Spandidos, D. A., *Cytochrome P450 CYP1A1: wider roles in cancer progression and prevention*. BioMed Central, **2009**, 9, 187, 1-17.

[144] Leung, Y., Lau, K., Mobley, J., Jiang, Z., Ho, S., *Overexpression of Cytochrome P450 1A1 and Its Novel Spliced Variant in Ovarian Cancer Cells: Alternative Subcellular Enzyme Compartmentation May Contribute to Carcinogenesis*. Cancer Research, **2005**, 65, 9, 3726-3734.

[145] Oyama, T., Kagawa, N., Kunugita, N., Kitagawa, K., Ogawa, M., Yamaguchi, T., Suzuki, R., Kinaga, T., Yashima, Y., Ozaki, S., Isse, T., Kim, Y., Kim, H., Kawamoto, T., *Expression of cytochrome P450 in tumor tissues and its association with cancer development.* Frontiers in Bioscience, **2004**, 9, 1967-1976.

[146] Tanaka, Y., Sasaki, M., Kaneuchi, M., Shiina, H., Igawa, M., Dahiya, R., *Polymorphisms of the CYP1B1 gene have higher risk for prostate cancer*. Biochemical and Biophysical Research Communications, **2002**, 296, 820-826.

[147] Rodrigues, I. S., Kuasne, H., Losi-Guembarovski, R., Fuganti, P. E., Gregório, E. P., Kishima, M. O., Kazuhiro, I., Freitas Rodrigues, M. A., Syllos Cólus, I. M., *Evaluation of the influence of polymorphic variants CYP1A1*2B, CYP1B1*2, CYP3A4*1B, GSTM1*0, and GSTT1*0 in prostate cancer*. Urologic Oncology: Seminars and Original Investigations, **2010**.

[148] Agundez, J. A. G, *Cytochrome P450 gene polymorphism and cancer*. Current Drug Metabolism, **2004**, 5, 211-224.

[149] McFadyen, M. C. E., Melvin, W. T., Murray, G. I., *Cytochrome P450 enzymes: Novel options for cancer therapeutics*. Molecular Cancer Therapeutics, **2003**, 363-371.

[150] Brunoa, R. D., Njar, V. C. O., *Targeting cytochrome P450 enzymes: A new approach in anti-cancer drug development*. Bioorganic and Medicinal Chemistry, **2007**, 15, 5047-5060.

[151] McFadyen, M. C. E., Murray, G. I., *Cytochrome P450 1B1: a novel anticancer therapeutic target*. Future Oncology, **2005**, 1, 2, 259-263.

[152] Roy, P., Waxman, D. J., *Activation of oxazaphosphorines by cytochrome P450: Application to gene-directed enzyme prodrug therapy for cancer*. Toxicology in Vitro, **2006**, 20, 176-186.

[153] Goldstein, M., Roos, W. P., Kaina, B., *Apoptotic death induced by the cyclophosphamide analogue mafosfamide in human lymphoblastoid cells: Contribution of DNA replication, transcription inhibition and Chk/p53 signaling*. Toxicology and Applied Pharmacology, **2008**, 229, 20-32.

[154] Xiea, H., Griskeviciusa, L., Stahlea, L., Hassan, Z., Yasara, U., Ranea, A., Brobergb, U., Kimby, E., Hassan, M., *Pharmacogenetics of cyclophosphamide in patients with hematological malignancies*. European Journal of Pharmaceutical Sciences, **2006**, 27, 54-61.

[155] Scripture, C. D., Sparreboom, A., Figg, W. D., *Modulation of cytochrome P450 activity: implications for cancer therapy*. Lancet Oncology, **2005,** 6, 780-89.

[156] Holland, J. F., Frei, E., *Cancer Medicine*. 5th Edition, B. C. Decker, **2000**.

[157] Ring, A., Dowsett, M., *Mechanisms of tamoxifen resistance*. Endocrine-Related Cancer, **2004**, 11, 643-658.

[158] Clemons, M., Danson, S., Howell, A., *Tamoxifen ('Nolvadex'): a review*. Cancer Treatment Reviews, **2002**, 28, 165-180.

[159] Kong, E. H., Pike, A. C. W., Hubbard, R. E., *Structure and mechanism of the oestrogen receptor*. Biochemical Society Transactions, **2003**, 31, 1, 56-59.

[160] Gauduchon, J., Gouilleux, F., Maillard, S., Marsaud, V., Renoir, J., Sola, B., *4-Hydroxytamoxifen Inhibits Proliferation of Multiple Myeloma Cells In vitro through Down-Regulation of c-Myc, Up-Regulation of p27Kip1, and Modulation of Bcl-2 Family Members*. Clinical Cancer Research, **2005**, 11, 2345-2354.

[161] Hertz, D. L., McLeod, H. L., Hoskins, J. M., *Pharmacogenetics of breast cancer therapies*. The Breast, **2009**, 18, 3, 59-63.

[162] Boocock, D. J., Brown, K., Gibbs, A. H., Sanchez, E., Turteltaub, K. W., White, I. N. H., *Identification of human CYP forms involved in the activation of tamoxifen and irreversible binding to DNA*. Carcinogenesis, **2002**, 23, 11, 1897-1901.

[163] Barcellos-Hoff, M. H., Ewan, K. B. R., *Transforming growth factor-β and breast cancer mammary gland development.* Breast Cancer Research, **2000**, 2, 92-99.

[164] Connor, C. E., Norris, J. D., Broadwater, G., Willson, T. M., Gottardis, M. M., Dewhirst, M. W., McDonnell, D. P., *Circumventing Tamoxifen Resistance in Breast Cancers Using Antiestrogens That Induce Unique Conformational Changes in the Estrogen Receptor*. Cancer Research, **2001**, 61, 2917-2922.

[165] Patterson, L. H., McKeown, S. R., *AQ4N: a new approach to hypoxia-activated cancer chemotherapy*. British Journal of Cancer, **2000**, 83, 12, 1589-1593.

[166] Rooseboom, M., Commandeur, J. M. N., Vermeulen, N. P. E., *Enzyme-catalyzed activation of anticancer prodrugs*. Pharmacological Reviews, **2004**, 56, 53-102.

[167] Lalani, A. S., Alters, S. E., Wong, A., Albertella, M. R., Cleland, J. L., Henner, W. D., *Selective Tumor Targeting by the Hypoxia-Activated Prodrug AQ4N BlocksTumor Growth and Metastasis in Preclinical Models of Pancreatic Cancer*. Clinical Cancer Research, **2007**, 13, 7, 2216-2225.

[168] Tredan, O., Garbens, A. B., Lalani, A. S., Tannock, I. F., *The Hypoxia-Activated ProDrug AQ4N Penetrates Deeply in Tumor Tissues and Complements the Limited Distribution of Mitoxantrone*. Cancer Research, **2009**, 69, 3, 940-947.

[169] Ali, M. M., Symons, M. C. R., Taiwo, F. A., Patterson, L. H., *Effects of AQ4N and its reduction product on adiation-mediated DNA strand breakage*. Chemico-Biological Interactions, **1999**, 123, 1-10.

[170] Patterson, L. H., McKeown, S. R., Ruparelia, K., Double, J. A., Bibby, M. C., Cole, S., Stratford, I. J., *Enhancement of chemotherapy and radiotherapy of murine tumours by AQ4N, a bioreductively activated anti-tumour agent*. British Journal of Cancer, **2000**, 82, 12, 1984-1990.

[171] McKeown, S. R., Coweny, R. L., Williams, K. J., *Bioreductive Drugs: from Concept to Clinic*. Clinical Oncology, **2007**, 19, 427-442.

[172] O'Rourke, M., Ward, C., Worthington, J., McKenna, J., Valentine, A., Robson, T., Hirst, D. G., McKeown, S. R., *Evaluation of the Antiangiogenic Potential of AQ4N*. Clinical Cancer Research, **2008**, 14, 5, 1502-1509.

[173] Bradshaw, T. D., Westwell, A. D., *The Development of the Antitumour Benzothiazole Prodrug, Phortress, as a Clinical Candidate*. Current Medicinal Chemistry, **2004**, 11, 1241-1253.

[174] Bradshaw, T. D., Bibby, M. C., Double, J. A., Fichtner, I., Cooper, P. A., Alley, M. C., Donohue, S., Stinson, S. F., Tomaszewjski, J. E., Sausville, E. A., Stevens, M. F. G., *Preclinical Evaluation of Amino Acid Prodrugs of Novel Antitumor 2-(4-Amino-3-ethylphenyl)Benzothiazoles*. Molecular Cancer Therapeutics, **2002**, 1, 239-246.

[175] Loaiza-perez, A. I., Trapani, V., Hose, C., Singh, S. S., Trepel, J. B., Stevens, M. F. G., Bradshaw, T. D., Sausville, E. A., *Aryl Hydrocarbon Receptor Mediates Sensitivity of MCF-7 Breast Cancer Cells to Antitumor Agent 2-(4-Amino-3-methylphenyl)Benzothiazole*. Molecular Pharmacology, **2002**, 61, 13-19.

[176] Brantley, E., Trapani, V., Alley, M. C., Hose, C. D., Bradshaw, T. D., Stevens, M. F. G., Sausville, E. A., Stinson, S. F., *Fluorinated 2-(4-Amino-3-Methylphenyl)Benzothiazoles Induce CYP1A1 Expression, Become Metabolized, and Bind to Macromolecules in Sensitive Human Cancer Cells*. Drug Metabolism and Disposition, **2004**, 32, 1392-1401.

[177] Leong, C. O., Suggitt, M., Swaine, D. J., Bibby, M. C., Stevens, M. F. G., Bradshaw, T. D., *In vitro, in vivo, and in silico analyses of the antitumor activity of 2-(4-amino-3-methylphenyl)-5-fluorobenzothiazoles*. Molecular Cancer Therapeutics, **2004**, 3, 12, 1565-1575.

[178] Leong, C. O., Gaskell, M., Martin, E. A., Heydon, R. T., Farmer, P. B., Bibby, M. C., Cooper, P. A., Double, J. A., Bradshaw, T. D., Stevens, M. F. G., *Antitumour 2-(4-aminophenyl)benzothiazoles generate DNA adducts in sensitive tumour cells in vitro and in vivo*. British Journal of Cancer, **2003**, 88, 470-477.

[179] Spink, D. C., Spink, B. C., Cao, J. Q., DePasquale, J. A., Pentecost, B. T., Fasco, M. J., Li, Y., Sutter, T. R., *Differential expression of CYP1A1 and CYP1B1 in human breast epithelial cells and breast tumor cells*. Carcinogenesis, **1998**, 19, 2, 291-298.

[180] Rahman, M., Sutter, C. H., Emmert, G. L., Sutter, T. R., *Regioselective 2-hydroxylation of 17β-estradiol by rat cytochrome P4501B1*. Toxicology and Applied Pharmacology, **2006**, 216, 469-478.

[181] Hayes, C. L., Spink, D. C., Spink, B. C., Caot, J. Q., Walker, N. J., Sutter, T. R., *17β-Estradiol Hydroxylation Catalyzed by Human Cytochrome P450lBl*. The Proceedings of the National Academy of Sciences, **1996**, 93, 9776-9781.

[182] Gao, N., Nester, R. A., Sarkar, M. A., *4-Hydroxy estradiol but not 2-hydroxy estradiol induces expression of hypoxia-inducible factor 1α and vascular endothelial growth factor A*

through phosphatidylinositol 3-kinase/Akt/FRAP pathway in OVCAR-3 and A2780-CP70 human ovarian carcinoma cells. Toxicology and Applied Pharmacology, **2004**, 196, 124-135.

[183] Androutsopoulos, V., Wilsher, N., Arroo, R. J., Potter, G. A., *Bioactivation of the phytoestrogen diosmetin by CYP1 cytochromes P450*. Cancer Letters, **2009**, 274, 54-60.

[184] Limer, J. L, Speirs, V., *Phyto-oestrogens and breast cancer chemoprevention*. Breast Cancer Research, **2004**, 6, 119-127.

[185] Kundu, J. K., Surh, Y., *Cancer chemopreventive and therapeutic potential of resveratrol: Mechanistic perspectives*. Cancer Letters, **2008**, 269, 243-261.

[186] Athar, M., Back, J. H., Kopelovich, L., Bickers, D. R, Kim, A. L., *Multiple molecular targets of resveratrol: Anti-carcinogenic mechanisms*. Archives of Biochemistry and Biophysics, **2009**, 486, 95-102.

[187] Ovesna, Z., Kozics, K., Bader, Y., Saiko, P., Handler, N., Erker, T., Szekeres, T., *Antioxidant activity of resveratrol, piceatannol and 3,3',4,4',5,5'-hexahydroxy-trans-stilbene in three leukemia cell lines*. Oncology Reports, **2006**, 16, 617-624.

[188] Wesolowska, O., Kuzdzal, M., Strancar J., Michalak, K., *Interaction of the chemopreventive agent resveratrol and its metabolite, piceatannol with model membranes*. Biochimica et Biophysica Acta, **2009**, 1788, 1851-1860.

[189] Signorelli, P., Ghidoni, R., *Resveratrol as an anticancer nutrient: molecular basis, open questions and promises*. Journal of Nutritional Biochemistry, **2005**, 16, 449-466.

[190] Potter, G. A., Patterson, L. H., Wanogho, E., Perry, P. J., Butler, P. C., Ijaz1, T., Ruparelia, K. C., Lamb, J. H., Farmer, P. B., Stanley, L. A., Burke, M. D., *The cancer preventative agent resveratrol is converted to the anticancer agent piceatannol by the cytochrome P450 enzyme CYP1B1*. British Journal of Cancer, **2002**, 86, 774-778.

[191] Potter et al., *U. S. Patent 7,598,294 B2*. United States, **2009**.

[192] Bhat, B. A., Dhar, K. L., Puri, S. C., Saxena, A. K., Shanmugavel, M., Qazi, G. N., *Synthesis and biological evaluation of chalcones and their derived pyrazoles as potential cytotoxic agents*. Bioorganic and Medicinal Chemistry Letters, **2005**, 15, 3177-3180.

[193] Sale, S., Tunstall, R. G., Ruparelia, K. C., Butler, P. C., Potter, G. A., Steward, W. P., Gescher, A. J., *Effects of the potential chemopreventive agent DMU-135 on adenoma development in the Apc^{Min+} mouse*. Invest New Drugs, **2006**, 24, 6, 459-464.

[194] Larsen, M., Kromann, M., Kharazmi, A., Nielsen, S. F., *Conformationally restricted anti-plasmodial chalcones*. Bioorganic and Medicinal Chemistry, **2005**, 15, 4858-4861.

[195] Coyle, J.D., Hill, R.R., Roberts, D.R., *Light, chemical change and life: a source book in photochemistry*. Milton Keynes, UK: Open University-Science, **1982**.

[196] Horspool, W., Armesto, D., *Organic Photochemistry: A Comprehensive Treatment*. Physical Chemistry Series, Horwood, **1992**.

[197] Ankrett, D., *Metabolic Bioactivation of Anticancer Chalcone Prodrugs by Human CYP1 Family Enzymes*. De Montfort University, **2008**.

[198] LeBlanc, R., Dickson, J., Brown, T., Stewart, M., Pati, H. N., VanDerveer, D., Arman, H., Harris, J., Pennington, W., Holt, H. L., Moses, L., *Synthesis and cytotoxicity of epoxide and pyrazole analogs of the combretastatins*. Bioorganic and Medicinal Chemistry, **2005**, 13, 6025–6034.

[199] Shaw, A. Y., Liau, H. H., Lu, P. J., Yang, C. N., Lee, C. H., Chen, J. Y., Xu, Z., Flynn, G., *3,5-Diaryl-1H-pyrazole as a molecular scaffold for the synthesis of apoptosis-inducing agents*. Bioorganic and Medicinal Chemistry, **2010**, 18, 3270–3278.

[200] Mihigo, O. S., Mammo, W., Bezabih, W., Andrae-Marobela, K., Abegaz, B. M., *Total synthesis, antiprotozoal and cytotoxicity activities of rhuschalcone VI and analogs*. Bioorganic and Medicinal Chemistry, **2010**, 18, 2464–2473.

[201] Narender, T., Reddy, K. P., *A simple and highly efficient method for the synthesis of chalcones by using borontrifluoride-etherate*. Tetrahedron Letters, **2007**, 48, 3177–3180.

[202] Won, S., Liu, C., Tsao, L., RuWeng, J., Ko, H., Wang, J., Lin, C., *Synthetic chalcones as potential anti-inflammatory and cancer chemopreventive agents*. European Journal of Medicinal Chemistry, **2005**, 40, 103–112.

[203] Sadeghi, B., Mirjalili, B. F., Hashemi, M. M., *$BF_3.SiO_2$: An Efficient Heterogeneous Alternative for Regio-Chemo and Stereoselective Claisen-Schmidt Condensation*. Journal of the Iranian Chemical Society, **2008**, 5, 694-698.

[204] Dong, F., Jian, C., Zhenghao, F., Kai, G., Zuliang, L., *Synthesis of chalcones via Claisen–Schmidt condensation reaction catalyzed by acyclic acidic ionic liquids*. Catalysis Communications, **2008**, 9, 1924–1927.

[205] Saravanamurugan, S., Palanichamy, M., Arabindoo, B., Murugesan, V., *Solvent free synthesis of chalcone and flavanone over zinc oxide supported metal oxide catalysts*. Catalysis Communications, **2005**, 6, 399–403.

[206]Thirunarayanan, G., Vanangamudi, G., *Synthesis of Some Aryl Chalcones Using Silica-Sulphuric Acid Reagent under Solvent Free Conditions*. E-Journal of Chemistry, **2007**, 4, 1, 90-96.

[207] Vollhardt, K. P. C., Schore, N. E., Organic Chemistry. 5th edition, W. H. Freeman, **2005**.

[208] Lauret, C., *Epoxy ketones as versatile building blocks in organic synthesis*. Tetrahedron: Asymmetry, **2001**, 12, 2359–2383.

[209] Trost, B. M., Fleming, I., Ley, S., *Comprehensive Organic Synthesis, Selectivity, Strategy and Efficiency in Modern Organic Chemistry*. Pergamon Press, Volume 7, **2005**.

[210] Clayden, J., Greeves, N., Warren, S., *Organic Chemistry*. Oxford University Press, **2001**.

[211] Zheng, C., Zhao, G., *Asymmetric epoxidation of α,β -unsaturated ketones using α,α-diarylprolinols as catalysts*. Chinese Science Bulletin, **2010**, 55, 17, 1712-1722.

[212] Hughes, D., Mehmet, H., *Cell Proliferation and Apoptosis*. BIOS Scientific, **2003**.

[213] Skupinska, K., Misiewicz-Krzeminska, I., Lubelska, K., Kasprzycka-Guttman, T., *The effect of isothiocyanates on CYP1A1 and CYP1A2 activities induced by polycyclic aromatic hydrocarbons in Mcf7 cells*. Toxicology in Vitro, **2009**, 23, 763–771.

[214] William, G., Angus, R., Larsen, M. C., Jefcoate, C. R., *Expression of CYP1A1 and CYP1B1 depends on cell-specific factors in human breast cancer cell lines: role of estrogen receptor status.* Carcinogenesis, **1999**, 20, 6, 947–955.

[215] Goodsell, D. S., *The Molecular Perspective: Tamoxifen and the Estrogen Receptor*. The Oncologist, **2002**, 7, 163-164.

[216] Androutsopoulos, V., Arroo, R., Hall, J. F., Surichan, S., Potter, G. A., *Antiproliferative and cytostatic effects of the natural product eupatorin on MDA-MB-468 human breast cancer cells due to CYP1-mediated metabolism*. Breast Cancer Research, **2008**, 10, 3, 1-12.

[217] Burdall, S. E., Hanby, A. M., Lansdown, M. R. J., Speirs, V., *Breast cancer cell lines: friend or foe?* Breast Cancer Research, **2003**, 5, 2, 89-95.

[218] Spink, B.C., Pang, S., Pentecost, B.T., Spink, D.C., *Induction of cytochrome P450 1B1 in MDA-MB-231 human breast cancer cells by non-ortho-substituted polychlorinated biphenyls*. Toxicology in Vitro, **2002**, 16, 695–704.

[219] Chen, Z., Hurh, Y., Na, H.,Kim, J., Chun, Y., Kim, D., Kang, K., Cho, M., Surh, Y., *Resveratrol Inhibits TCDD-Induced Expression of CYP1A1 and CYP1B1 and Catechol Estrogen-Mediated Oxidative DNA Damage in Cultured Human Mammary Epithelial Cells*. *Carcinogenesis*, **2004**, 25, 10, 2005-2013.

[220] Chun, Y., Lee, S., Kim, M. Y., *Modulation of Human Cytochrome P4501B1 Expression by 2,4,3',5'-Tetramethoxystilbene*. Drug Metabolism and Disposition, **2005**, 33, 12, 1771–1776.

[221] El-Hamouly, W. S., El-Khamry, A. A., Abbas, E. M. H., *Synthesis of new 4-aryl-isoxazolo[5,4-d]pyrimidin-6-one(thione) and 4-aryl-pyrazolo[3,4-d]-pyrimidin-6-one derivatives of potential antihypertensive activity*. Indian Journal of Chemistry, **2006**, 45B, 2091-2098.

[222] Deshmukh, M. B., Salunkhe, S. M., Patil, D. R., Anbhule, P. V., *A novel and efficient one step synthesis of 2-amino-5-cyano-6-hydroxy-4-arylpyrimidines and their anti-bacterial activity*. European Journal of Medicinal Chemistry, **2009**, 44, 2651–2654.

[223] Ma, J. G., Zhang, J. M., Jiang, H. H., Ma, W. Y., Zhou, J. H., *DFT study on mechanism of the classical Biginelli reaction*. Chinese Chemical Letters, **2008**, 19, 375–378.

[224] Varga, L., Nagy, T., Kovesdi, I., Benet-Buchholz, J., Dorman, G., Urge, L., Darvas, F., *Solution-phase parallel synthesis of 4,6-diaryl-pyrimidine-2-ylamines and 2-amino-5,5-disubstituted-3,5-dihydro-imidazol-4-ones via a rearrangement*. Tetrahedron, **2003**, 59, 655–662.

[225] Dewick, P. M., *Essentials of Organic Chemistry*. 1st edition, Wiley-Blackwell, **2006**.

[226] Agarwal, A., Srivastava, K., Puri, S. K., Prem, M., Chauhan, S., *Synthesis of 2,4,6-trisubstituted pyrimidines as antimalarial agents*. Bioorganic & Medicinal Chemistry, **2005**, 13, 4645–4650.

[227] Hu, M., Wu, M., Zhang, Y., Qiu, F., Yu, Y., *Synthesis of polysubstituted 5-aminopyrimidines from α-azidovinyl ketones and amidines*. Tetrahedron, **2011**, 67, 2676-2680.

[229] Lin, X., Murray, J. M., Rico, A. C., Wang, M. X., Chu, D. T., Zhou, Y., Rosario, M. D., Kaufman, S., Ma, S., Fang, E., Crawford, K., Jefferson, A. B., *Discovery of 2-pyrimidyl-5-amidothiophenes as potent inhibitors for AKT: Synthesis and SAR studies*. Bioorganic and Medicinal Chemistry Letters, **2006**, 16, 4163-4168.

[230] Fathalla, O. A., Awad, S. M., Mohamed, M. S., *Synthesis of New 2-Thiouracil-5-Sulphonamide Derivatives with Antibacterial and Antifungal Activity*. Archives of Pharmacal Research, **2005**, 28, 11, 1205-1212.

[231] Borovik, V. P., Shkurko, O. P., *Synthesis of functional 2_substituted 4-phenyl-9H-pyrimido[4,5-b]indoles*. Russian Chemical Bulletin, International Edition, **2002**, 51, 11, 2129-2133.

[232] Sammour, A., El-Deen, S. M. I. B., Nour, M. M., El-Halim, A. UAR Journal of Chemistry, **1970**, 13, 1.

[233] Agarwal, A., Srivastava, K., Puri, S. K., Chauhan, P. M. S., *Synthesis of 4-pyrido-6-aryl-2-substituted amino pyrimidines as a new class of antimalarial agents*. Bioorganic and Medicinal Chemistry, **2005**, 13, 6226-6232.

[234] Andrews, K. J. M., Anand, N., Todd, A. R., Topham, A. Journal of the Chemical Society. **1949**, 2490.

[235] Boek-Dohalska, L., Hodek, P., Sulc, M., Stiborova, M., *α-Naphthoflavone acts as activator and reversible or irreversible inhibitor of rabbit microsomal CYP3A6*. Chemico-Biological Interactions, **2001**, 138, 85–106.

[236] Lewis, D. F. V., Lake, G. G., George, S. G., Dickins, M., Eddershaw, P. J., Tarbit, M. H., Beresford, A. P., Goldfarb, P. S., Guengerich, F. P., *Molecular modelling of CYP1 family enzymes CYP1A1, CYP1A2, CYP1A6 and CYP1B1 based on sequence homology with CYP102*. Toxicology, **1999**, 139, 53–79.

[237] Surichan, S., *Bioactivation of Natural Dietary Prodrugs by Specific Cytochrome P450 Enzymes*. De Montfort University, **2008**.

[238] Castro, A., Miguel del Corral, J. M., Gordaliza, M., Grande, C., Gomez-Zurita, A., Garcia-Gravalos, D., San Feliciano, A., *Synthesis and cytotoxicity of podophyllotoxin analogues modified in the A ring*. European Journal of Medicinal Chemistry, **2003**, 38, 65-74.

[239] Jayapal, M. R., Sreedhar, N. Y., *Synthesis and characterization of 4-hydroxychalcones by aldol condensation using $SOCl_2$/EtOH*. International Journal of Current Pharmaceutical Research, **2010**, 2, 4, 60-62.

[240] Nguyen-Hai Nam, Yong Kim, Young-Jae You, Dong-Ho Hong, Hwan-Mook Kim, Byung-Zun Ahn, *Cytotoxic 2',5'-dihydroxychalcones with unexpected antiangiogenic activity*. European Journal of Medicinal Chemistry, **2003**, 38, 179-187.